

Object-oriented Modelling of Solar District Heating Grids with Underground Thermal Energy Storage

Dissertation

Doctoral thesis submitted in fulfillment of the requirements
for the degree of Doktor-Ingenieur (Dr.-Ing.)
at the
Department of Material and Earth Sciences,
Technical University of Darmstadt



TECHNISCHE
UNIVERSITÄT
DARMSTADT



Graduate School of
**Energy Science
and Engineering**

Submitted by

Julian Formhals, M.Sc.

Supervisor Prof. Dr. Ingo Sass
Co-supervisor Prof. Dr. Peter Stephan

Darmstadt, 23rd March 2022

Julian Philipp Formhals: Object-oriented Modelling of Solar District Heating Grids with
Underground Thermal Energy Storage

Darmstadt, Technical University of Darmstadt,

Year of publication on TUpriints: 2022

URN: urn:nbn:de:tuda-tuprints-215067

Day of the defense: 20.05.2022

Published under CC BY-SA 4.0 International

<https://creativecommons.org/licenses/>

Board of examiners

Supervisor: Prof. Dr. Ingo Sass

Co-supervisor: Prof. Dr. Peter Stephan

Examiner: Prof. Dr. Christoph Schüth

Examiner: Prof. Dr. Eva Schill



Declaration

I hereby declare that the presented dissertation is based on original research and is the result of my own work. I certify that this dissertation contains no material which has been accepted for the award of any other degree in my name, in any university or other tertiary institution and, to the best of my knowledge and belief, contains no material previously published or written by another person, except where due reference has been made in the text.

Darmstadt, 23rd March 2022



Abstract

The transformation of the heating sector towards renewable energy sources is a key element for the mitigation of man-made climate change. In this regard, solar thermal energy is a particularly well-suited solution, as it is a simple, cost-efficient and proven technology. A main barrier for a more widespread use, is the seasonal mismatch of heat demands and solar yields, which usually limits the solar share on the overall heat supply of district energy systems to about 20%. It is therefore necessary to store the abundant solar energy supply during summer for several months to be able to use it in winter. Underground thermal energy storage (UTES) is currently the most promising technology for such applications, as it shows a high maturity level in comparison to other technologies and facilitates storage of thermal energy on a district scale. Integration of UTES into solar district heating (SDH) systems is commonly accompanied by further technologies, such as geothermal energy, industrial waste heat or power-to-heat applications, resulting in complex energy systems. These SDH-UTES systems require a thorough design of component dimensions, system layouts and control strategies to ensure security of supply, while avoiding costly over-dimensioning of generation capacities. Therefore, dynamic system simulations are used for system design, as they consider the temporal distribution of heat supplies and demands as well as the strong interactions between components.

The modelling language Modelica constitutes a powerful conceptual approach for modelling and simulation of thermal energy systems and is therefore applied increasingly. However, to exploit Modelica's numerous advantages for the simulation of SDH-UTES systems and reach a large number of users, adequate model libraries are required. These should be accurate in their representation of physical components, easy to use and have a low numerical effort.

The presented cumulative dissertation and the corresponding publications in scientific journals demonstrate the development of such a model library called MoSDH (Modelica Solar District Heating). The library consists of components for the accurate, efficient, user friendly and robust simulation of such systems, including models for UTES technologies which were previously not implemented for Modelica. Selected models and aspects were already presented and demonstrated in case studies in the above-mentioned journal papers. The presented thesis contains a comprehensive description of the model components as well as the general system modelling concept. Furthermore, several case studies are used to highlight certain key functionalities and demonstrate the accurate representation of the physical systems in a numerically efficient way. The models can be used for extensive optimization studies as well as detailed investigations of certain specific aspects. In addition to that, the object-oriented modelling approach facilitates the easy adaption and reuse of model components. Finally, MoSDH is used to investigate the transition of a sub-grid of the TU Darmstadt university district heating (DH) system into a SDH-UTES system, demonstrating the possibility of those systems to satisfy the universities emission saving goals in a cost-efficient way.



Kurzfassung

Die Umstellung der Wärmeversorgung zu Heizzwecken auf erneuerbare Energiequellen ist ein zentraler Aspekt zur Eindämmung des menschengemachten Klimawandels. Solarthermie bietet sich dabei als einfache, kostengünstige und erprobte Technologie in besonderem Maße an. Hierbei besteht jedoch das naturgegebene Problem des saisonalen Versatzes des Wärmebedarfs und des solaren Angebots, wodurch Solarthermie in der Regel maximal 20 % des Wärmebedarfs von Fernwärmesystemen decken kann. Zur Erreichung höherer Deckungsraten ist es erforderlich das mannigfaltige solare Angebot im Sommer über mehrere Monate zu speichern und somit im Winter nutzbar zu machen. Untergrundwärmespeicher sind aktuell die vielversprechendste Technologie, da sie im Gegensatz zu alternativen Technologieansätzen bereits eine vergleichsweise hohe Marktreife aufweisen und Kapazitäten zur Speicherung des winterlichen Wärmebedarfs ganzer Quartiere umsetzbar sind. Die Kombination dieser Technologien zu solaren Wärmenetzen mit Untergrundwärmespeichern, die zusätzlich meist noch mit weiteren Wärmequellen wie Geothermie, industrieller Abwärme oder power-to-heat kombiniert werden, resultiert in komplexen Energiesystemen. Für diese ist eine genaue Auslegung der Komponentengrößen, Verschaltungsschemata und Betriebsweisen erforderlich, um sowohl die Versorgungssicherheit zu gewährleisten, als auch teure Überkapazitäten zu vermeiden. Zu diesem Zweck kommen in der Regel dynamische Systemsimulationen zum Einsatz, die den zeitlichen Verlauf von Wärmeangebot und -bedarf sowie die Wechselwirkungen der einzelnen Systemkomponenten berücksichtigen.

Die Modellierungssprache Modelica ist ein konzeptionell mächtiger Ansatz zur Modellierung und Simulation physikalischer Systeme und kommt bei der Simulation thermischer Energiesysteme vermehrt zum Einsatz. Um die zahlreichen Vorteile von Modelica jedoch für die Simulation solarer Wärmenetze mit Untergrundwärmespeichern nutzbar zu machen und ein breites Benutzerfeld zu erreichen, werden entsprechende Modellbibliotheken benötigt. Diese sollten das Verhalten der Systemkomponenten möglichst genau abbilden, einfach anzuwenden sein und einen geringen numerischen Rechenaufwand benötigen.

Im Rahmen dieser kumulativen Dissertation und den dazugehörigen Veröffentlichungen in wissenschaftlichen Fachzeitschriften wird die Entwicklung einer solchen Modellbibliothek erläutert. Diese MoSDH (Modelica Solar District Heating) genannte Modellbibliothek, umfasst Komponenten zur genauen, effizienten, benutzerfreundlichen und robusten Simulation solcher Systeme und beinhaltet Modelle für Untergrundwärmespeicher, die zuvor in der Modellierungssprache Modelica noch nicht implementiert waren. Vereinzelt Modelle und Aspekte von MoSDH wurden bereits in den besagten wissenschaftlichen Veröffentlichungen erläutert und für Fallstudien angewandt. Im Rahmen dieser Arbeit wird eine umfassendere Beschreibung der Komponenten sowie des allgemeinen Ansatzes zur Systemmodellierung gegeben. Anhand von Fallbeispielen werden verschiedene Funktionalitäten näher beleuchtet und die akkurate und numerisch effiziente Nachbildung realer Systeme demonstriert. Die Modelle eignen sich sowohl für groß angelegte Optimierungsstudien, als auch für die detaillierte Untersuchung einzelner Aspekte. Weiterhin wird aufgezeigt, wie der objekt-orientierte Ansatz zur einfachen Anpassung, Erweiterung und Wiederverwendung von Modellkomponenten genutzt werden kann. Letztendlich werden die Modelle verwendet um in einer Studie aufzuzeigen, wie die Transformation eines Teils des Fernwärmesystems der TU Darmstadt in ein solares Wärmenetz mit saisonalem Untergrundwärmespeicher kosteneffizient zur Erreichung der Emissionsziele der Universität beitragen könnte.



Acknowledgement

Firstly, I would like to thank my doctoral advisor Prof. Dr. Ingo Sass for his supervision and support. After he aroused my interest for the topic of geothermal energy by his lectures, he convinced me of joining his interdisciplinary team, which I never regretted. He trusted me to grow into my field of expertise independently and to take my personal path, but was always there with his valuable advice and ideas when they were needed. Without the trust, time and space he gave me, I wouldn't have been able to learn the many interesting new things that put me into my present position.

Next, I would like to thank my co-supervisor Prof. Dr. Peter Stephan, who provided his valuable input to this work. Moreover, as the holder of the chair of Technical Thermodynamics, he enabled me to collaborate with his research group of Analysis of Thermal Energy Systems, with whom I have had many constructive and friendly co-operations over the years. Particularly his students Johannes Oltmanns, Julia Eicke and Frederik Feike were a valuable and fruitful addition to my network of friends within the university.

A very special thanks goes to my colleagues Prof. Dr.-Ing. Bastian Welsch and Dr.-Ing. Daniel Schulte, who integrated me into their small sworn community and made my time at the university not only an educational one, but a very pleasant one as well. Daniel first introduced me to the topic of my dissertation and was later on a great motivator. Bastian always took his time to deeply engage in my works and provided me valuable advice, which helped me a lot in improving my works.

I also want to thank my colleague Hoofar Hemmatabady dearly for all the professional and personal discussions we had. In our strongly interdisciplinary environment, we talked the same technical language and shared a deep mutual understanding.

Furthermore, I would like to thank all the students that contributed to my works by their theses or sharpened my knowledge, by asking the right questions. As a representative of those, I would like to thank Xenia Kirschstein, who made a very valuable contribution to my work by developing initial versions of the tank and pit storage models within her thesis.

Many thanks go to Simone Roß-Krichbaum and Eva Ruffing, for their friendly, competent and reliable administrative support, which allowed me to keep my focus very much on my works. I would also like to thank Dr. Tanja Drobek, who managed the Graduate School of Excellence Energy Science and Engineering (GSC 1070) and organized it with great commitment, nourishing interdisciplinary exchange with fellow PhD students. In this context, funding of the Deutsche Forschungsgemeinschaft was very helpful and furthermore supported my stay in Denmark, which has been a key event for the development of my works.

My special thanks go to Morten Vang Bobach and his colleagues at Arcon-Sunmark, who hosted me in Skørping, Denmark. Morten provided me his vast knowledge in the field of solar district heating and underground thermal energy storage and inspired me to further specialize on this topic. His invitation to the late world's leading manufacturer of large-scale solar thermal collectors (STC) provided me with deep insights and memorable field trips. In this context, I also want to thank Jim Larsen of Brædstrup Fjernvarme and Lasse Kjærgaard Larsen of Marstal Fjernvarme for kindly sharing monitoring data of their plants and knowledge on their operation, which proved to be invaluable for my works.

My research was partly derived from the project DGE- Rollout (NWE 892), which was funded by the European Regional Development Fund (ERDF). Collaboration and exchange of knowledge with our international project partners provided me new insights on aspects of deep geothermal energy and simultaneously introduced me to many interesting and pleasant characters.

Last but not least, I want to thank my family for their support and love. Especially my uncle Gerald, who taught me his way of working and thereby opened up new ways to approach technical problems as well as Fiona and Felix, who proofread my manuscript, have to be mentioned.

Preface

The presented cumulative doctoral thesis is based on my work as a research assistant in the working group Geothermal Science and Technology at the Institute of Applied Geosciences, TU Darmstadt. A main focus of my work was put on the development of numerical models for dynamic simulation of solar district heating systems with underground thermal energy storage. These models were applied in several numerical studies to assess the efficient design of such systems. To complement these studies and conclude the model development process, the underlying work sets the focus on the thorough description of the model components and their functionalities.

My works are very much based on the works of my two colleagues Daniel Schulte and Bastian Welsch, who investigated the numerical modelling, simulation and characteristics of borehole thermal energy storage systems (Schulte, 2016; Welsch, 2019). In the context of a master thesis, I started to couple 3D finite element method (FEM) models of borehole thermal energy storages (BTES) (Schulte et al., 2016b) to solar district heating models in Modelica (Schwan and Unger, 2016). During my time as PhD candidate, the co-simulation approach (Welsch et al., 2017) was further developed and applied within several numerical case studies (Formhals et al., 2017b, 2017a). Initially, no suitable models for the simulation of BTES systems existed in Modelica, which motivated the development of a toolbox for modelling such systems called MoBTES (Formhals et al., 2020). Later on, the model was complemented by further components of SDH-UTES systems and ultimately resulted in the library MoSDH, which is presented in this thesis. Currently, the assessment of the different storage models contained in MoSDH is planned to take place as part of the IEA ECES Annex 39 Large Thermal Energy Storages for District Heating project, in which I participate as UTES expert.

In parallel with me, my colleague Hoofar Hemmatabady started working on system optimization of district heating and cooling (DHC) grids with BTES, by numerical simulations in TRNSYS (Hemmatabady et al., 2020, 2022). Since his dissertation was much more focused on the application of existing models, whereas I put a stronger focus on model development, we complemented each other well. Unfortunately, the timing of our works did not allow him to already use MoSDH for his studies. Therefore, our collaborations were strongly focused on technical aspects of the design and operation of SDH-UTES systems, while the tools we used differed.

A period which had a significant impact on my works and gave a lot of input, was my stay in Denmark at Arcon-Sunmark in 2018, a company which produced STC modules and pit thermal energy storage systems. The company did not only produce those components, but was constructing the systems as well and significantly contributed to the Danish SDH boom. The practical insights and operational data, that were kindly provided to me, were a great input to my works. Unfortunately, the company does not exist in its recent form anymore, but large parts of the team and facilities still contribute to SDH and UTES for different companies.

Over the duration of my works at the Geothermal Science and Technology group, I contributed to the planning and proposal process for the project SKEWS (Schulte et al., 2021), which aimed at the construction of a medium-deep borehole thermal energy storage (MD-BTES) pilot on the university campus. Unfortunately, approval of the project was only granted at the end of my engagement at the university. Nevertheless, I will curiously watch the progress of the project, which will hopefully result in the integration of the storage into the university DH system after

research activities are finished. My colleague Lukas Seib will continue the works on investigation of the integration of such an MD-BTES into the university grid and thereby apply our co-simulation methodology and Modelica models.

Table of Contents

| | |
|--|--------------|
| DECLARATION | V |
| ABSTRACT | VII |
| KURZFASSUNG | IX |
| ACKNOWLEDGEMENT | XI |
| PREFACE | XIII |
| TABLE OF CONTENTS | XV |
| LIST OF FIGURES | XVII |
| LIST OF TABLES | XIX |
| INDEX OF ABBREVIATIONS AND SYMBOLS | XX |
| CUMULATIVE DISSERTATION | XXIII |
| 1 INTRODUCTION | 1 |
| 2 STATE OF THE ART AND AIM OF THIS THESIS | 5 |
| 2.1 State of the art | 5 |
| 2.2 Aim of this thesis | 6 |
| 3 SOLAR DISTRICT HEATING WITH UNDERGROUND THERMAL ENERGY STORAGE | 7 |
| 3.1 Solar District Heating | 8 |
| 3.2 Underground Thermal Energy Storage | 10 |
| 3.3 System concepts and layouts | 13 |
| 4 OBJECT-ORIENTED MODELLING OF THERMAL ENERGY SYSTEMS | 15 |
| 4.1 Principles of modelling with Modelica | 15 |
| 4.2 Translation and simulation of Modelica models | 16 |
| 4.3 Modelling of Underground Thermal Energy Storage systems | 21 |
| 4.4 Co-simulation of UTES models | 22 |
| 5 MODELICA SOLAR DISTRICT HEATING MODEL LIBRARY | 23 |
| 5.1 Library interfaces and basic principles | 24 |
| 5.2 Modelling and control philosophy | 25 |
| 5.3 Structure and component overview | 27 |
| 5.3.1 Heat source components | 28 |
| 5.3.2 Thermal storage components | 31 |
| 5.3.3 Distribution components | 34 |
| 5.3.4 Ground components | 37 |
| 5.3.5 Weather data and heat demand components | 37 |
| 6 METHODS FOR MULTI-CRITERIAL ANALYSIS AND OPTIMIZATION OF SDH SYSTEMS | 39 |
| 6.1 Performance figures | 39 |
| 6.2 Analysis methods | 39 |
| 6.3 Optimization methods | 40 |
| 7 APPLICATION OF MOSDH | 41 |
| 7.1 Simulation of the Brødstrup Solar District Heating system | 41 |
| 7.2 Simulation of an SDH system with dynamic dimensions, layouts and boundary conditions | 46 |
| 7.3 Validation of the District Heating Pipes model | 47 |
| 7.4 Simulation of a DH grid ring network | 49 |

| | |
|---|------------|
| 7.5 Exergetic optimization of BHE design and operation of a medium-deep Borehole Thermal Energy Storage | 51 |
| 8 DISCUSSION AND CONCLUSION | 57 |
| 9 OUTLOOK | 61 |
| LITERATURE | 63 |
| APPENDIX A – CO-SIMULATION OF GEOTHERMAL APPLICATIONS AND HVAC SYSTEMS | 72 |
| APPENDIX B –A MODELICA TOOLBOX FOR THE SIMULATION OF BOREHOLE THERMAL ENERGY STORAGE SYSTEMS | 81 |
| APPENDIX C – OPTIMIZED LAYOUTS OF BOREHOLE THERMAL ENERGY STORAGE SYSTEMS IN 4TH GENERATION GRIDS | 105 |
| APPENDIX D – STRATEGIES FOR A TRANSITION TOWARDS A SOLAR DISTRICT HEATING GRID WITH INTEGRATED SEASONAL GEOTHERMAL ENERGY STORAGE | 132 |
| APPENDIX E – CO-SIMULATION OF DISTRICT HEATING SYSTEMS AND BOREHOLE HEAT EXCHANGER ARRAYS USING 3D FINITE ELEMENT METHOD SUBSURFACE MODELS | 145 |
| APPENDIX F – AI-BASED ENVIRO-ECONOMIC OPTIMIZATION OF SOLAR-COUPLED AND STANDALONE GEOTHERMAL SYSTEMS FOR HEATING AND COOLING | 168 |
| APPENDIX G – EXAMPLE MODEL SUMMARIES | 195 |

List of Figures

| | |
|--|----|
| Figure 1: Schematic structure of a Solar District Heating system with Underground Thermal Energy Storage..... | 7 |
| Figure 2: Solar thermal collector field of the SDH system in Marstal (DK)..... | 8 |
| Figure 3: Exemplary monthly load and solar yield profiles of SDH systems with a solar fraction of 20% and 100%..... | 9 |
| Figure 4: Common Underground Thermal Energy Storage types..... | 11 |
| Figure 5: Specific investment cost for large-scale thermal energy storages (including all necessary costs for building the storage device, without design, without connecting pipes and equipment in the heating plant and without VAT) (© Solites)..... | 12 |
| Figure 6: Typical translation process of a Modelica model. | 16 |
| Figure 7: Incidence array of an unsorted DAE before (left) and after (right) selection of states. Rows corresponding to equations and columns to variables. The total number of incidences is denoted as nz (adapted after (Dassault Systèmes, 2020b), © Taylor & Francis Group LLC)..... | 17 |
| Figure 8: Incidence array in Block Lower Triangular form before (left) and after (right) tearing. Rows corresponding to equations and columns to variables. The total number of incidences is denoted as nz (adapted after (Dassault Systèmes, 2020b), © Taylor & Francis Group LLC)..... | 19 |
| Figure 9: Example model MoSDH.Examples.ExampleGeoSolar..... | 20 |
| Figure 10: Combination of ground models with BHE and water pit models to form UTES models. | 22 |
| Figure 11: Pressure drop in a 100 m long DN32 pipe for water at 40 °C calculated with different methods and deviation of the simple friction model of the MSL to the exact calculated value. | 25 |
| Figure 12: Generic heat source and settings for the control variables in the context menu. | 26 |
| Figure 13: Avoiding over-determined hydraulic models in MoSDH..... | 27 |
| Figure 14: MoSDH library structure..... | 27 |
| Figure 15: Heat source component icons of the MoSDH library. | 28 |
| Figure 16: Diagram view of the internal structure of the thermal power plant model..... | 30 |
| Figure 17: Heat storage component icons of the MoSDH library. | 31 |
| Figure 18: Exemplary mesh of a BTES system of 32 BHEs connected in series of 4 and a different grouting in the upper section. | 32 |
| Figure 19: Structure of the TTES model and inputs of a single volume element model. | 33 |
| Figure 20: Exemplary mesh and main parameters of the PTES model..... | 34 |
| Figure 21: Heat distribution component icons of the MoSDH library. | 34 |
| Figure 22: Conceptual design of the DH pipe models. Left: two buried pipes. Right: buried twin pipe..... | 35 |
| Figure 23: Implementation of the district heating twin pipe model in MoSDH. | 36 |
| Figure 24: Structure diagram of the HeatExchanger model..... | 36 |
| Figure 25: Ground components icons of the MoSDH library. | 37 |

| | |
|---|----|
| Figure 26: Weather data and heat demand component icons of the MoSDH library. | 38 |
| Figure 27: System model of the Brødstrup SDH system for validation of the MoSDH model components..... | 42 |
| Figure 28: Monitoring data (blue) and generated performance maps for the heat pump power and COP. | 43 |
| Figure 29: Monitored and calculated values for the heat pump power and COP..... | 44 |
| Figure 30: Monitored and simulated energy budgets of the components of the Brødstrup SDH system for the period May 2012 to December 2016. | 44 |
| Figure 31: Model diagram for the transition strategy. | 46 |
| Figure 32: Model setup for the validation of the DH pipe model. | 47 |
| Figure 33: Specific heat losses for pre-insulated district heating pipes with a DN150 medium pipe and different diameters of the casing from simulations with MoSDH and manufacturer's data. | 48 |
| Figure 34: Specific heat losses for pre-insulated district heating pipes with a DN200 medium pipe and different diameters of the casing from simulations with MoSDH and manufacturer's data. | 48 |
| Figure 35: Specific heat losses for pre-insulated district heating pipes with a DN250 medium pipe and different diameters of the casing from simulations with MoSDH and manufacturer's data. | 48 |
| Figure 36: Diagram view of the rind grid example model. | 49 |
| Figure 37: Selected supply and return temperatures of heat demand components. | 50 |
| Figure 38: Thermal power of the power plant and heat demand components. | 50 |
| Figure 39: Volume flow rates of the thermal power plant and within selected pipe sections of the ring network..... | 51 |
| Figure 40: Schematic setup of the storage model for the optimization study. Left: cross section of the subsurface and the BHEs. Right: cross section of the BHE design. | 52 |
| Figure 41: Supply, return and exergy reference temperature as well as volume flow rate of the optimal system. | 53 |
| Figure 42: Evolution of the optimization variables and target function over the iterations of the optimization algorithm. | 54 |

List of Tables

| | |
|--|----|
| Table 1: Typical values of realized SDH systems with and without seasonal storage after (Mauthner and Herkel, 2016). | 7 |
| Table 2: Model statistics of the MoSDH.Examples.ExampleGeoSolar example model from the MoSDH library. | 20 |
| Table 3: Simulation statistics of the MoSDH.Examples.ExampleGeoSolar example model from the MoSDH library. | 21 |
| Table 4: Physical interfaces of the MoSDH library (Modelica Association, 2020). | 24 |
| Table 5: Annual monitoring (m) and simulaton (s) results for the Braedstrup SDH system in MWh, with deviations above 10% marked in red. | 45 |

Index of Abbreviations and Symbols

Abbreviations

| | | | |
|-------|---|------|--|
| 4GDH | 4 th generation district heating | LCOH | Levelized cost of heat |
| 5GDH | 5 th generation district heating | MD | Medium deep |
| ANN | Artificial neural network | MSL | Modelica standard library |
| ATES | Aquifer thermal energy storage | MTES | Mine thermal energy storage |
| BHE | Borehole heat exchanger | NE | North-East |
| BLT | Block lower triangular | NW | North-West |
| BTES | Borehole thermal energy storage | ODE | Ordinary differential equation |
| CHP | Combined heat and power | PI | Piping and instrumentation |
| COP | Coefficient of performance | PTES | Pit thermal energy storage |
| CSP | Concentrated solar power | PP | Poly Propylene |
| DAE | Differential algebraic equation | SDH | Solar district heating |
| DH | District heating | S | South |
| DHC | District heating and cooling | SE | South-East |
| DN | Diamètre nominal | SW | South-West |
| E | East | SPF | Seasonal performance factor |
| FEM | Finite element method | STC | Solar thermal collector |
| GC-HP | Ground coupled heat pump | TES | Thermal energy storage |
| GWP | Global warming potential | TCP | Transmission Control Protocol |
| HP | Heat pump | TRCM | Thermal resistance and capacitance model |
| IP | Internet Protocol | TTES | Tank thermal energy storage |
| LCA | Life cycle assessment | UTES | Underground thermal energy storage |

Formula symbols

| | | |
|------------------|---------------------|------------------------------------|
| A | [m ²] | Solar collector area |
| c | [J/(kg.K)] | Mass specific heat capacity |
| d | [m] | Diameter |
| f_s | [-] | Solar fraction |
| f_{shade} | [-] | Shading factor |
| I | [W/m ²] | Solar irradiation |
| h | [J/kg] | Mass specific enthalpy |
| \dot{H} | [W] | Enthalpy flow |
| $K_{\tau\alpha}$ | [-] | Incidence angle modifier |
| L | [-] | Lower triangular matrix |
| \dot{m} | [kg/s] | Mass flow rate |
| N_{cyc} | [-] | Storage cycles |
| n | [-] | Integer number |
| p | [Pa] | Pressure |
| \dot{Q} | [W] | Heat flow rate |
| r | [m] | Radius |
| R^2 | [-] | Coefficient of determination |
| R_l | [K/(W.m)] | Length specific thermal resistance |
| Re | [-] | Reynolds number |
| t | [s] | Time |

| | | |
|------------|---------------------------------------|---|
| T | [°C] | Temperature |
| u | [-] | System input |
| \dot{V} | [m ³ /s] | Volume flow rate |
| x | [-] | Unknown/variable/state |
| y | [-] | Algebraic/output variable |
| α | [-] | Absorption coefficient |
| α_1 | [W/(m ² .K)] | Linear thermal loss coefficient |
| α_2 | [W/(m ² .K ²)] | Quadratic thermal loss coefficient |
| β | [°] | Collector inclination angle |
| β_w | [1/K] | Thermal expansion coefficient of medium |
| Δ | [-] | Difference |
| η | [%] | Efficiency |
| η_0 | [%] | Optical collector efficiency |
| θ | [°] | Incidence angle of irradiation |
| κ | [-] | Kármán's constant |
| λ | [W/(m.K)] | Thermal conductivity |
| ρ_g | [-] | Ground reflectance factor |
| τ | [-] | Transmission coefficient |
| Ψ | [-] | Ratio of irradiation measured on horizontal and incidence |

Subscripts and superscripts

| | | | |
|--------------|------------------------|--------------|---------------------------|
| <i>b</i> | Beam irradiation | <i>port</i> | Storage element heat port |
| <i>bot</i> | Storage element bottom | <i>PP</i> | Poly propylene |
| <i>cap</i> | Storage capacity | <i>ref</i> | Reference |
| <i>ch</i> | Charged amount | <i>ret</i> | Return line |
| <i>d</i> | Diffuse irradiation | <i>rows</i> | Solar collector rows |
| <i>DH</i> | District heating line | <i>s</i> | Solar |
| <i>disch</i> | Discharged amount | <i>SE</i> | South-East |
| <i>E</i> | East | <i>shade</i> | Solar collector shading |
| <i>ex</i> | Exergetic | <i>st</i> | Storage |
| <i>g</i> | Ground | <i>STC</i> | Solar thermal collector |
| <i>gen</i> | Generation | <i>sup</i> | Supply line |
| <i>grout</i> | Borehole grouting | <i>surf</i> | Storage element surface |
| <i>i</i> | Inner | <i>T</i> | Total irradiation |
| <i>ins</i> | Insulation | <i>th</i> | Thermal |
| <i>m</i> | Mean | <i>top</i> | Storage element top |
| <i>net</i> | Net discharged exergy | <i>up</i> | Upper section |
| <i>o</i> | Outer | <i>wall</i> | Storage element wall |



Cumulative Dissertation

This cumulative dissertation comprises the following six journal publications, which are appended to the work.

Appendix A: Welsch, B., Rühaak, W., Schulte, D.O., **Formhals, J.**, Bär, K., and Sass, I., 2017, Co-Simulation of Geothermal Applications and HVAC Systems: *Energy Procedia*, v. 125, p. 345–352, <http://tubiblio.ulb.tu-darmstadt.de/89580/>.

Appendix B: **Formhals, J.**, Hemmatabady, H., Welsch, B., Schulte, D.O., and Sass, I., 2020, A Modelica toolbox for the simulation of borehole thermal energy storage systems: *Energies*, v. 13, doi:10.3390/en13092327.

Appendix C: Hemmatabady, H., **Formhals, J.**, Welsch, B., Schulte, D.O., and Sass, I., 2020, Optimized layouts of borehole thermal energy storage systems in 4th generation grids: *Energies*, v. 13, doi:10.3390/en13174405.

Appendix D: **Formhals, J.**, Feike, F., Hemmatabady, H., Welsch, B., and Sass, I., 2021, Strategies for a transition towards a solar district heating grid with integrated seasonal geothermal energy storage: *Energy*, v. 228, p. 120662, doi:10.1016/j.energy.2021.120662.

Appendix E: **Formhals, J.**, Welsch, B., Hemmatabady, H., Schulte, D.O., Seib, L., and Sass, I., 2021, Co-Simulation of District Heating Systems and Borehole Heat Exchanger Arrays using 3D Finite Element Method Subsurface Models. This is an Accepted Manuscript of an article published by Taylor & Francis in the *Journal of Building Performance Simulation*, accepted on 25.02.2022.

Appendix F: Hemmatabady, H., Welsch, B., **Formhals, J.**, and Sass, I., 2022, AI-based Enviro-economic Optimization of Solar-coupled and Standalone Geothermal Systems for Heating and Cooling. *Applied Energy*, doi:10.1016/j.apenergy.2022.118652.

Appendix A presents the initial methodology for the coupling of 3D FEM models in FEFLOW to above-ground system models for co-simulation. While the presented interface has been developed further significantly over time, the TCP/IP (Transmission Control Protocol/Internet Protocol) communication functionalities presented in this proceedings paper are still used today. Originally, FEFLOW was coupled to MATLAB-Simulink, using models of the Carnot toolbox for simulation of heating applications to consider interactions between BTES and the energy systems they are integrated into. The paper presents the implementation of the interface and demonstrates possible applications by an example study. In this example, a STC field is coupled to a BTES by a buffer tank and the size of the tank is varied in an optimization routine. Scope and simulated period of the study are limited deliberately, to be able to vary parameters of the co-simulation, such as the communication step size and discretization of the input data in a parameter study, for assessment of the developed interface.

Bastian Welsch was the first author of the article and carried out the main works, in particular development of the interface and execution of the simulation runs. Wolfram Rühaak had the idea of using the TCP/IP protocol for communication between FEFLOW and MATLAB and supervised the development. Daniel Schulte contributed to the preparation of the draft and to the implementation of the optimization routine. Kristian Bär and Ingo Sass were involved in discussion during the conceptual stage and supervised the research. My contribution to the work

was mainly the sharing of experiences on co-simulation schemes, as I had developed an interface for coupled simulation of a BTES model in MATLAB called BASIMO and SDH models in the Modelica environment SimulationX during my master thesis. All co-authors participated in the revision of the manuscript.

Appendix B presents a Modelica library for simulation of BTES systems called MoBTES, which was the starting point for MoSDH. Prior to this point, no dedicated BTES model existed in Modelica and simulation of such systems was carried out using co-simulation. However, as this approach is not suited for larger parameter studies, the desire for a simple BTES model within Modelica grew. The only available option for the simulation of borehole heat exchanger (BHE) arrays in Modelica at this time, was dedicated for heat extraction purposes and therefore the modelling approach aimed at the accurate representation of such systems, but lacked features like serially connected BHEs. The work presented in Appendix B elaborates the methodology for the modelling approaches which were implemented for the BTES model. The two-dimensional representation of the storage exploits the symmetry of BTES systems and has already been implemented for models in different modelling environments, where it has proven its good suitability for simulation of SDH-UTES systems (Pahud and Hellström, 1996; Franke, 1998a). However, the main modelling concept was added by further features, such as the consideration of the grout thermal capacity, partial insulation of BHEs and pressure calculation. For validation, the model was compared to 3D FEM models in FEFLOW for various BTES dimensions and layouts as well as to monitoring data of the first 500 days of operation of the Brødstrup BTES system. Overall, a good fit between the benchmark models and the MoBTES model could be proven. Especially the representation of the short-term dynamics of the monitoring data showed a very high accuracy. For the longer term, the model still resulted in deviations to the monitored data close to those of a 3D FEM model in FEFLOW, which was used for comparison.

As the first author of this paper I developed the Modelica model library, carried out the simulation runs in SimulationX/Modelica and FEFLOW, evaluated and visualized the results, drafted the manuscript and processed the monitoring data of the Brødstrup storage. Hoofar Hemmat-abady contributed during the early development stage of MoBTES by comparing simulation results to results of the DST model in TRNSYS for an initial validation and later on engaged in numerous discussions on the experimental design and analysis of the validation study. Bastian Welsch contributed the batch-file for automation of FEFLOW simulations, contributed his expertise on BTES modelling in FEFLOW, engaged in the discussion on the experimental design and analysis and supervised my work. Daniel Schulte contributed in discussions on the experimental design and analysis of results and Ingo Sass supervised the research and contributed valuable advice. All co-authors contributed to the revision of the manuscript.

Appendix C is a comprehensive study on different layouts for integration of borehole thermal energy storages into fourth generation district heating grids for heating and cooling. An exergo-economic approach for multi-objective optimization is applied to identify pareto-optimal systems. Four layouts are defined which differ in their cooling layout and the configuration of the BTES and an auxiliary gas boiler during heating season. Cooling is either supplied passively by the BTES or actively with an interconnected heat pump. During heating season, the buffer storage is either heated up to the supply temperature of the DH grid by a double stage heat pump to directly supply heat to the grid or to a lower temperature level by a single stage heat pump and the remaining temperature shift is covered by a gas boiler. The first case corresponds to a parallel operation of the geothermal system and the gas boiler and the second case to a serial operation. The results imply that passive cooling in combination with a serial combination of

the geothermal system and the gas boiler is favorable in terms of exergetic efficiency and leveled cost of energy. However, if highest exergetic efficiencies shall be achieved, a parallel integration layout is favorable. As an additional important result, a correlation between the exergetic efficiency of systems and the associated global warming potential (GWP) is identified, indicating lower GWPs for higher exergetic efficiencies.

First author of this work is Hoofar Hemmatabady who developed the methodology, carried out the simulations, evaluated and visualized the results of the study and prepared the initial draft. I contributed to the study by repeated discussions on the design of the used operation strategies, the design of experiments and the evaluation of results. Bastian Welsch contributed by his advice on the design of experiments, by contributing his life cycle assessment (LCA) methodology and analysis of results as well as supervision of the work. Daniel Schulte contributed to the design of experiments, analysis of results and supervision of the work. Ingo Sass supervised the research and contributed valuable advice.

Appendix D presents a notional case study on the transition of a campus DH system of the TU Darmstadt towards an SDH system with integrated MD-BTES. Five different strategies for the integration of STCs, an MD-BTES, integration of a waste heat source and the phase-out of combined heat and power (CHP) capacities are compared in regards to their ability to satisfy the university emission saving goals. The study investigates the time span from 2025 to 2050 and makes certain assumptions about the future development of energy prices, electricity emission factors and the DH grid temperature levels. The period is divided into three stages, for which different levels of construction and decommissioning of the components are defined for each of the five strategies. The case study is not comprehensive as it excludes certain aspects of the actual DH system under investigation, like the existing cooling grid or the connection of the grid to further campuses. However, by considering different times of construction, it includes an aspect which is commonly not investigated. It is the first application of the MoSDH library, which was developed further during the course of the works and adapted to the requirement of variable component dimensions to consider construction and deconstruction of components.

I was the first author of this study and developed the concept of the study as well as the used models. Furthermore, I carried out the simulation runs, visualized and evaluated the results and wrote the initial draft of the manuscript. Frederik Feike contributed his detailed knowledge and data of the DH system under investigation and provided central aspects of the scenario for its future development. He contributed projected heat load curves, which he generated by adapting measured load profiles to test reference year data. Furthermore, he contributed in the discussion of the results. Hoofar Hemmatabady contributed his valuable input to the design of experiments and discussion of results. Bastian Welsch developed the LCA framework which was used for calculation of costs and emissions attributed to the systems, gave valuable inputs during the joint discussion of results and supervised the work. Ingo Sass supervised the research. All authors contributed to the revision of the manuscript.

Appendix E is the author's original manuscript of an accepted paper and presents the latest developments of the co-simulation methodology. The interface was adapted to allow for the coupled simulation of SDH systems using the MoSDH library in Modelica and 3D FEM models of BHE arrays in FEFLOW. The interface presented in Appendix A is developed further and an additional coupling option is implemented which exchanges conductive process variables across the borehole wall instead of the convective BHE inlet and outlet variables. In comparison to the old approach, the new option allows for larger communication time steps and faster simulation

without a loss in accuracy. Moreover, the consideration of the BHEs in Modelica facilitates a more versatile operation of the storage, as it allows for arbitrary hydraulic connection schemes, pressure loss calculation or the reversal of the flow direction. In addition to the new interface option, the communication step size is changed dynamically by an adaptive control scheme, which reduces both communication error as well as computational effort. The co-simulation methodology is assessed by comparison of a single BHE co-simulation to a non-coupled simulation with regard to computational effort and accuracy. Furthermore, a notional SDH system with a small BTES is co-simulated, considering different groundwater flow velocities, to demonstrate the benefit of the proposed approach.

As the first author of this paper I developed the co-simulation methodology, by adaption of the FEFLOW plugin presented in Appendix A and implementation of a corresponding interface in Modelica. Furthermore, I carried out all simulations, evaluated and visualized the results and wrote the initial draft of the manuscript. Bastian Welsch strongly contributed to this work, by providing the initial version of the FEFLOW plug-in and his vast knowledge on plug-in development as well as modelling and simulation in FEFLOW. He engaged in regular discussions about the conceptual design of the communication scheme of the co-simulation, participated in the analysis of the study and supervised my work. Hoofar Hemmatabady and Daniel Schulte contributed to the analysis of the results and gave valuable advice. Lukas Seib was involved in the development of FEFLOW benchmark models and in the analysis of results. Ingo Sass closely supervised the research and was strongly involved in the original idea of developing a co-simulation methodology. All authors were involved in the revision of the manuscript.

Appendix F presents a comprehensive study on the optimization of solar-coupled and standalone geothermal systems for heating and cooling. Different scenarios are defined, to compare systems with active and passive operation of a BTES and integration of solar thermal energy. The high complexity of the approach is tackled by the use of an artificial neural network (ANN) proxy model for optimization, to reduce the computational effort and allow for a faster convergence of the optimization algorithm. The optimization searches for pareto-efficient systems with regards to the attributed emission factors and levelized cost of energy. The study concludes that an active charging and discharging of the BTES by a heat pump is the best solution for standalone geothermal systems and results in the lowest costs. The lowest emission factors are obtained by solar-coupled systems however.

Hoofar Hemmatabady is the first author of this work. He developed the optimization methodology and carried out all simulation runs. Furthermore, he evaluated the results and drafted the manuscript. Bastian Welsch supervised this work and was strongly involved in discussions about the design of experiments and analysis of the results. In addition to that, he provided his LCA framework for enviro-economic assessment. I contributed to this work by discussions on the overall design of the study and analysis of the results. Ingo Sass supervised the research and contributed valuable advice about the concept of the study. All authors contributed to the revision of the manuscript.

Further publications and presentations:

Sass I., Bär K., Schulte D.O., Welsch B., **Formhals J.**, Hornich W. and Homuth S. (2016): SKEWS (Solargekoppelter kristalliner Erdwärmesondenspeicher): Wärmespeicherprojekt der TU Darmstadt am Campus Lichtwiese, in 11. Tiefengeothermie-Forum, Darmstadt, Germany, 29 September 2016, <http://tubiblio.ulb.tu-darmstadt.de/84094/>.

-
- Formhals J.** (2016): Gekoppelte Simulation von Erdsonden-Wärmespeichern und solar unterstützten Nahwärmenetzen, *in* Geothermiekongress 2016, Science Bar, Essen, Germany, 29 November - 1 December 2016.
- Welsch B., Rühaak W., Schulte D.O., **Formhals J.**, Bär K. and Sass I. (2017): Co-Simulation of Geothermal Applications and HVAC Systems, *Energy Procedia*, v. 125, p. 345–352, <http://tubiblio.ulb.tu-darmstadt.de/89580/>.
- Formhals J.**, Schulte D.O., Welsch B. and Sass I. (2017): Coupled Simulation of Borehole Thermal Energy Storages and Solar District Heating Systems, *in* European Geosciences Union General Assembly 2017, Vienna, Austria, 23-28 April 2017, <http://tubiblio.ulb.tu-darmstadt.de/87114/>.
- Welsch B., Rühaak W., Schulte D.O., **Formhals J.**, Bär K. and Sass I. (2017): Optimization of Borehole Thermal Energy Storage System Design Using Comprehensive Coupled Simulation Models, *in* European Geosciences Union General Assembly 2017, Vienna, Austria, 23-28 April 2017, <http://tubiblio.ulb.tu-darmstadt.de/87115/>.
- Formhals J.**, Welsch B., Schulte D.O. and Sass I. (2017): Effects of the District Heating Supply Temperature on the Efficiency of Borehole Thermal Energy Storage Systems, *in* Proceedings 3rd International Conference on Smart Energy Systems and 4th Generation District Heating, Copenhagen, Denmark, 12-13 September 2017, <http://tubiblio.ulb.tu-darmstadt.de/89333/>.
- Schulte D.O., Welsch B., **Formhals J.** and Sass I. (2018): Der Schritt zum mitteltiefen Erdwärmesondenspeicher, *bbr - Leitungsbau | Brunnenbau | Geothermie*, v. 69, p. 70–75, <http://tubiblio.ulb.tu-darmstadt.de/108206/>.
- Formhals J.**, Welsch B. and Sass I. (2018): Co-simulation of solar district heating grids and borehole thermal energy storages using SimulationX, *in* ESI SimulationX Conference 2018, Dresden, Germany, 8-9 November 2018, <http://tubiblio.ulb.tu-darmstadt.de/118450/>.
- Formhals J.**, Welsch B. and Sass I. (2018): Multikriterielle Analyse von Erdwärmesondenspeichern und Wärmenetzen mittels gekoppelter Simulation, *in* Geothermiekongress 2018, Essen, Germany, 27-29 November 2018.
- Formhals J.**, Welsch B. and Sass I. (2019): Multi-criteria analysis of the integration of Solar Thermal Collectors and Borehole Thermal Energy Storage Systems into existing District Heating Grids, *in* European Geothermal PhD Day 2019, Potsdam, Germany, 25-27 February 2019.
- Sass I., Welsch B., Schedel M. and **Formhals J.** (2021): Verfahren zur Errichtung eines Rohrleitungsabschnittes eines Rohrsystems sowie Rohrleitungsabschnitt eines Rohrsystems in einem Wärmenetz, <http://tubiblio.ulb.tu-darmstadt.de/128097/>.
- Schulte D.O., **Formhals J.**, Welsch B. and Sass I. (2021): Medium Deep Borehole Thermal Energy Storage Pilot Plant, *in* World Geothermal Congress 2020, Reykjavik, Iceland, 24-27 October 2021.

1 Introduction

In an international agreement of historic dimensions, 195 nations signed the Paris Agreement in 2015, recognizing climate change as an urgent threat to humankind. The parties agreed on limiting the “increase in the global average temperature to well below 2 °C above pre-industrial levels and pursuing effort to limit the temperature increase to 1.5 °C above pre-industrial levels” (UN, 2015). While this text is written, several severe natural disasters have struck regions all over the world again. Statistics show that the occurrence of such events has nearly doubled over the past twenty years (CRED, 2020). While no single individual event is caused by climate change directly, an increased probability could be proven in numerous cases (Herring et al., 2021). Furthermore, the year of 2021 has seen natural gas prices surge to historic highs all over the world, but especially in Europe (Stapczynski, 2021). A combination of the recovery of industrial production activities from the COVID-19 crisis and geopolitical aspects have already led to an increase by almost 500% in Europe - the heating period of the winter still ahead. Several companies have reduced their production outputs due to this reason, with some having to file for insolvency (Flauger and Witsch, 2021). Even though this development is caused by several temporary factors and will most likely relax in the near future, it is a drastic demonstration of the dependence of most national economies from fossil fuel imports. The use of renewable energies significantly reduces this sensitivity of market and consumer prices to external political effects by nature. Consequently, there are historic examples, where past crisis’ have led to increased investments in renewable technologies for energy applications. A prime example being Denmark, which diversified its energy sectors, widely implemented district heating grids and heavily invested into research and development of renewable technologies as a consequence of the oil crisis in the seventies, to increase supply security (Bösch and Graf, 2014). In general, there seems to be a broad consensus about the targeted sustainable energy system of the future. However, the actual path and speed of this process is still under discussion, as it should be both economically efficient and socially acceptable. The sheer complexity of this global undertaking seems to overstress many actors, resulting in a paralyzing state where, in doubt, proven and well-known technologies are applied, even though the necessity of the transition to more sustainable approaches is almost undisputed. To provide guidelines for stakeholders of the transition process, several roadmaps have been developed on international and national levels (Möller et al., 2019; IEA, 2021; IRENA, 2021b). While these plans differ in ambition, scope and level of detail, all of them heavily rely on the replacement of fossil fuels by renewable energy sources in a much faster pace than what can be observed today.

In this context, the transition of the heating and cooling sector is generally considered much less in public discussion, especially compared to the power generation sector. However, in Europe heating and cooling accounts for half of the final energy demand, of which around three quarters are used for space heating and process heat. Only 22% of the demand is currently met by renewable energies (European Commission, 2021). Consequently, significant efforts will be necessary for a decarbonization of this sector. Since housing renovation rates are typically low, this transition will have to take place over a long period (European Commission, 2019). Quantity and quality of the measures which are implemented today, will define the profile of the domestic heating sector for the decades to come. Therefore, these measures should already fulfill the emission standards set for 2030 or even 2040. According to recent studies, it is still possible to fully decarbonize the European heating sector by 2050, by implementation of already existing and proven technologies (Susana et al., 2018). Obviously, the reduction of the final energy demand by energy saving measures, such as façade insulation, should contribute

the major part of the overall emission reductions. Nevertheless, the climate neutral supply of the remaining demand in heating will require a multiplication of renewable heat generation capacities (IEA, 2021; IRENA, 2021b). In this context, an increased deploy of District Heating (DH) in combination with geothermal and solar thermal energy, has been identified as an efficient solution (Möller et al., 2019) and consequently plays a key role in most energy system transformation plans (BMUB, 2016; IEA, 2021; IRENA, 2021b).

The combination of geothermal and solar thermal energy has proven to be fruitful in different ways. For example, shallow geothermal applications, which only utilize the first couple of meters below ground, obtain the main share of their energy supply from solar energy stored within the ground (Sass, 2016). Furthermore, energy from STCs can be used to regenerate the depletion of geothermal systems with predominant heat extraction and consequently improve their performance and ensure sustainable operation. In the case of solar thermal energy, the total annual supply of irradiation per square meter is typically much larger than the specific demand for space heating per square meter. While values of 1,000-2,000 kWh/(m².a) of annual global irradiation can be observed in European countries, the average heating demand of the existing stock amounts to less than 150 kWh/(m².a) (Pezzutto et al., 2015). Even though the actual technological exploitation of this potential will result in different numbers, this juxtaposition highlights the vast existing potential of solar thermal energy for heating. Furthermore, the collector technology for harvesting this renewable potential is exceptionally simple and consequently costs are low (IRENA, 2021a). Unfortunately, though, solar thermal energy has the inherent drawback of the seasonal mismatch between times of high supply and demand. Consequently, solar thermal alone can usually only supply around 20% of the annual demand, if a costly oversizing of the collectors is to be avoided (Trier et al., 2018a). In combination with (geothermal) underground thermal energy storage however, coverage rates of up to 100% can be realized (Mesquita et al., 2017). These systems store excess solar heat during summer in the subsurface and extract it in winter, when heat demand exceeds supply. Ultimately, this approach combines the abundant solar energy supply and the vast subsurface thermal capacities and can result in systems which are both more economic and environmentally friendly than each technology on its own (Elhashmi et al., 2020). One prerequisite of the favorability of such a system, especially in regards of economics, is its size, as both STC fields (IRENA, 2021a) and UTES (Pauschinger et al., 2018) show a strong economy of scale. Accordingly, integration into DH systems seems to be an auspicious option. These Solar District Heating (SDH) systems with seasonal UTES (SDH-UTES) have been applied increasingly in the past decade (Yang et al., 2021). However, they are yet far from being standard solutions, like small scale solar thermal or geothermal applications on their own, for which simple dimensioning guidelines and mass-produced solutions exist. The technological and economic efficiency of SDH systems with UTES still strongly varies for realized systems and research and development efforts have to be taken to support their broad commercial rollout.

While the performance of conventional fossil fired and decentralized heating systems is well understood and can be estimated quite accurate by simple relations in most cases, SDH-UTES systems pose a much bigger challenge. Their performance and economics are highly dependent on the operational temperature level as well as the temporal distributions of energy supply and demand (Tschopp et al., 2020). Consequently, the design process is usually carried out on a system level, taking all relevant parameters, processes, dynamics and interactions of the system components into account. Dynamic simulations with thermo-hydraulic system models can be used in this regard. However, to ensure the accurate assessment of the system performance

during the design stage and consequently an efficient and economic operation, suitable models of the system components are required. These models should be numerically efficient to allow for simulation of large systems, accurate in their representation of the component performance and relatively easy to use. Furthermore, the novelty of UTES technologies results in the introduction of a multitude of new design concepts and materials. Accordingly, models should be adaptable and extendable, to be able to assess the performance of these innovations. This work focusses on the modelling and simulation process of SDH-UTES systems, with the main emphasis being put on the modelling of the UTES systems, as these are more complex and have a higher requirement for further development compared to the other system components. A model library called “MoSDH – Modelica Solar District Heating” is presented and discussed. The library is implemented with the object-oriented modelling language Modelica, which is a conceptually powerful modelling language that is increasingly applied for the simulation of energy systems. However, Modelica models can inhibit a high level of complexity, which can result in less robust system models and has so far impaired a more widespread application by general engineers, limiting it mostly to the user field of modelling experts and scientists. Consequently, the main goal is to develop a dedicated library, that results in accurate, robust and easy to use models, that can be applied by both experts in modelling and experts in SDH-UTES system engineering.



2 State of the art and aim of this thesis

2.1 State of the art

Object-oriented modelling has been proposed repeatedly for the simulation of solar district heating systems. Franke (1997) illustrates a re-engineering of TRNSYS models (Solar Energy Laboratory, 2021) for STCs, a buffer storage and borehole thermal energy storage using an early version of Modelica (Franke, 1998b). He finds object-oriented modelling to reduce both model complexity and effort of the model development process. Furthermore, model order reduction and nonlinear optimization methods are applied on the state-space formulation of the system models, exploiting the equation-based approach of Modelica. Schrag (2001) also investigates object-oriented modelling of solar thermal applications, using the modelling language SMILE (Ernst et al., 1997), a predecessor of Modelica. He highlights the advantages of object-oriented modelling for optimization of system design on several application examples, including a solar district heating system with a deep BHE. Nevertheless, certain technical aspects of the approach are identified, which should be improved to increase the applicability. These aspects, that include compatibility to other model libraries, a graphical user interface and analytical derivatives, have been addressed by the development of the Modelica language standard (Modelica Association, 2021).

Development and prevalence of the Modelica modelling language led to a number of model libraries for DH and building performance simulation (Burhenne et al., 2013). While several libraries are not described in high detail, as they are commercially protected (Schwan and Unger, 2016) or have not been published (Giraud et al., 2015), a number of open-source libraries have been developed, using the IBPSA library as shared core (Wetter and Treeck, 2017). The IBPSA library was developed within the IEA Energy in Buildings and Communities Programme Annex 60 and uses the Fluid library from the Modelica Standard library (MSL) (Franke et al., 2009). Modelica was chosen due to its flexible multi-physics approach, which covers hydraulic, thermal and electrical components, as well as important features like bi-directional flow through pipes. The associated libraries are mostly focused on the detailed modelling of buildings (Nytsch-Geusen et al., 2013; Plessis et al., 2014; Wetter et al., 2014; Müller et al., 2016), but DH grids as well (Jorissen et al., 2018; Leitner, 2019). As a result of the shared effort, a large number of highly sophisticated and versatile model components are freely available. However, the underlying modelling approach of the MSL Fluid library incorporates a high level of complexity, which is not yet fully supported by all simulation environments. Regarding the modelling of SDH systems, most components are generally available, but the strong focus of the libraries on building performance simulation results in models which are not dedicated for the simulation of large systems.

Giraud et al. (2014) compare the modelling and simulation process of SDH systems using TRNSYS and the unpublished Modelica library DistrictHeating. They conclude that both approaches yield in similar results, if models of comparable detail are applied, with the Modelica models resulting in a generally higher computational effort. Furthermore, it is found that Modelica is favorable regarding model development effort, the modelling of hydraulic processes and practical aspects like interfaces for post-processing. A critical aspect for modelling of SDH systems in Modelica is the lack of suitable UTES models. A model which is commonly used for simulation of BTES systems is the Hybrid Step Response Model of the IBPSA library IDEAS (Jorissen et al., 2018). However, this model is dedicated for simulation of ground-coupled heat pump systems for heat extraction and consequently lacks certain key features of BTES systems and has a lower

accuracy for high temperature applications. A common misconception is the availability of serially connected BHEs, which is not supported, since it is only possible to connect the two shanks of an individual BHE in series. Concerning aquifer thermal energy storage systems in Modelica, a 1D modelling approach is proposed by Ribas Tugores et al. (2015) and validated against a 3D FEM model. However, the validation process is not described in detail and the model was not published. Even though several studies find Modelica to be favorable to TRNSYS for the modelling of SDH systems (Franke, 1998b; Giraud et al., 2014) or in general (Wetter and Haugstetter, 2006), a large number of studies and most likely the majority uses TRNSYS (Olsthoorn et al., 2016). The underlying reasons are diverse, but two very likely causes are the lack of suitable UTES models and the high level of complexity which is often associated to Modelica models.

2.2 Aim of this thesis

This cumulative thesis and the associated articles aim at the development, validation and demonstration of an object-oriented model library for the simulation of SDH-UTES systems. Specifically, the following tasks were addressed:

- Development of UTES models in Modelica for high temperature heat storage applications.
- Development of a co-simulation methodology to couple Modelica SDH system models to 3D FEM UTES models for detailed geological modelling.
- Development of a Modelica model library, which includes the most important components of SDH systems and allows an easy system model development as well as a robust simulation process.
- Application of the developed models in case studies, demonstrating their functionality by addressing relevant topics like the integration of SDH into existing DH structures, the consideration of groundwater and system design optimization.

To set the background, Chapter 3 gives an overview of the technologies SDH and UTES. The general concepts of these approaches are presented, a brief overview of the current market development is given and the main barriers for a further market penetration are addressed. Chapter 4 presents the object-oriented modelling language Modelica and gives an introduction into the main concepts and the basic process of the translation of models into computable code for simulation. Chapter 5 presents the developed model library MoSDH by giving an overview of the applied modelling concepts and the library content. Chapter 6 summarizes common methods for analysis and optimization of SDH systems. Chapter 7 focusses on application examples for the presented library, to demonstrate and assess certain functionalities. Finally, Chapter 8 and 9 draw a conclusion on the presented object-oriented modelling approach for SDH-UTES systems and an outlook on recommended developments. The underlying publications of this cumulative dissertation are appended in appendices A-F.

3 Solar District Heating with Underground Thermal Energy Storage

Figure 1 shows the basic concept of SDH-UTES systems. These systems integrate large STC fields and UTES for seasonal storage into DH networks. Prerequisite for the efficient operation of such a system are low grid temperature levels, which are commonly attributed to DH systems of the 4th generation (4GDH). The 4GDH concept is based on smart energy systems, that combine different energy sources and storage technologies, creating synergy effects. Consequently, SDH systems are not limited to solar thermal energy or UTES and multiple systems have been realized in combination with additional elements like power-to-heat technology, biomass boilers or wood-chip CHP.

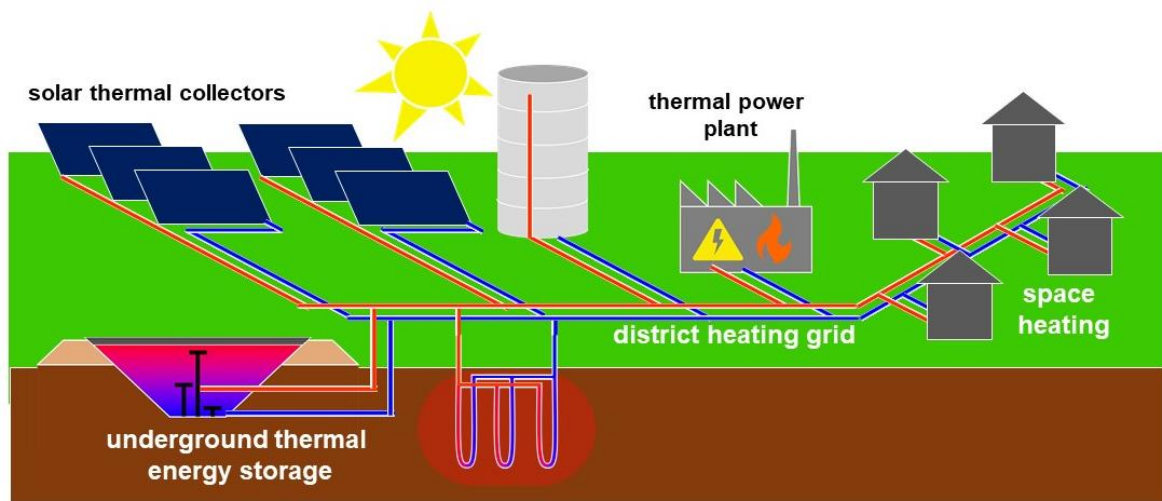


Figure 1: Schematic structure of a Solar District Heating system with Underground Thermal Energy Storage.

A classification of solar thermal systems for heating was defined within Task 52 of the IEA Solar Heating and Cooling program (Mauthner and Herkel, 2016). In this context 219 large-scale systems were analyzed to define the characteristics and economic performance of each category. Table 1 contains selected values for typical SDH systems with and without seasonal storage. As one can see, systems with seasonal storage usually result in a higher solar fraction, i.e. a higher share of solar energy on the total heat generation. This higher fraction however, results in lower solar yields and an increase in the levelized cost of heat (LCOH). The following chapters will give a brief overview of the technologies SDH and UTES and their current market situation.

Table 1: Typical values of realized SDH systems with and without seasonal storage after (Mauthner and Herkel, 2016).

| Thermal storage | Solar District Heating | |
|-----------------------------------|-------------------------------------|------------------------------------|
| | Diurnal storage | Seasonal storage |
| Solar fraction | 12% | 50% |
| Storage volume per collector area | 0.12 m ³ /m ² | 2.5 m ³ /m ² |
| Solar yield | 410 kWh/(m ² .a) | 365 kWh/(m ² .a) |
| LCOH | 4.1 €-ct/kWh | 5.5 €-ct/kWh |

3.1 Solar District Heating

Solar District Heating can be defined as a pipe network, connected to a collective of buildings for distribution of thermal energy for heating purposes, which is supplied by STCs with an aperture area of more than 500 m² (Weiss and Spörk-Dür, 2021). These collectors are usually implemented in large fields with flat plate collector modules of 12-14 m² and operating temperatures of 80-100 °C (Tschopp et al., 2020). In comparison to STCs for single-family houses, the use of large modules reduces the cost per square meter of aperture and results in lower losses through heat bridges and junctions. To obtain the required temperature shifts of up to 50 K, collector modules are connected in series of 5-10 modules per row and a distance of 4-6 m between rows (Figure 2).



Figure 2: Solar thermal collector field of the SDH system in Marstal (DK).

These fields, which can cover up to several hundreds of thousand square meters land, are often located in a close range to a DH network of small towns, where they are used to replace existing fossil fired heat generation capacities. Such a typical SDH system has between 5,000-15,000 m² aperture area with an annual solar yield of 400 kWh/(m².a) (Trier et al., 2018a). Due to the seasonal mismatch of the solar potential and the demand for space heating, systems without seasonal storage are limited in their size by the heat demand during summer. If the collected solar energy cannot be transported away from the collectors, stagnation occurs and temperatures may rise above the maximum operation temperatures of the collectors, ultimately resulting in their damage (Frank et al., 2015). Consequently, systems without seasonal storage are limited to solar fractions of around 20% for central European climates (Figure 3 left). A common practice to avoid stagnation during ongoing periods of excess solar energy are measures like the use of dry coolers or night cooling. In the latter case, hot fluid is circulated through the collector field and cooled down by the ambient, which can dispose around one third of the daily production (Trier et al., 2018a). The deliberate use of those measures for the compensation of solar excess heat during summer, however, is only feasible up to a small increase of the overall solar fraction. To achieve solar fractions of 50-100%, the use of seasonal thermal energy storage technology is required.

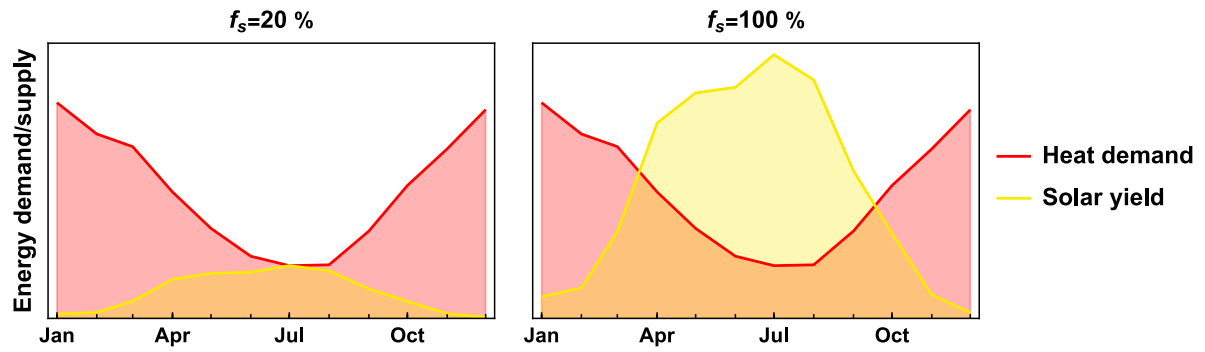


Figure 3: Exemplary monthly load and solar yield profiles of SDH systems with a solar fraction of 20% and 100%.

Construction of large STC fields started in the mid-eighties in Sweden and Denmark with the first systems of more than 1,000 m² aperture area (SDH, 2017). Since then, the total installed aperture area increased to more than two million square meters, of which around 80% are located in Denmark alone (Weiss and Spörk-Dür, 2021). This extraordinary leadership position was induced by very favorable technological and economic conditions, that resulted in a strong increase of installed systems since the 1990s. Firstly, about 63% of Danish households are connected to DH networks (Danish Energy Agency, 2017). These grids are often operated on low supply temperature levels of around 70 °C, which results in a large potential for systems that can be easily retrofitted with STC fields. Secondly, local utilities are mostly owned by consumers and municipalities and obligated by law to sell energy by a cost-of-service principle, which results in a more pronounced long-term view on investments (Trier et al., 2018b). As an additional effect, the non-profit approach results in a noticeable sharing of experience by operators (Trier et al., 2018a) and consequently the main data base of this thesis was provided by Danish plant operators. And third, SDH faced very favorable economic boundary conditions in Denmark, where taxes on natural gas are significantly higher in comparison to other European countries. In addition to that, a trading scheme for energy savings was installed, which allowed local utilities to count the production of solar thermal systems during their first year of operation as energy savings. Revenues for the trade of these certificates greatly improved the economics of solar thermal systems, resulting in the installation of ever more and ever larger plants (Tschopp et al., 2020). In 2016 the so far largest collector field was constructed in the city of Silkeborg, with an aperture area of 156,000 m² and a peak power of 110 MW_{th}.

As a consequence of the SDH boom, significant development effort was put into collector technology and production lines were automated and streamlined. In combination with a strong economy of scale, the LCOH for solar thermal energy fell from 0.066 USD/kWh in 2010 to 0.045 USD/kWh in 2019 (IRENA, 2021a). However, when the Danish trading scheme was suspended first in 2016 and ended in 2019, the Danish SDH market saw a rapid decline and consolidation process. Since then, about half of the newly constructed collector area is located in China, where the technology is being increasingly applied (Weiss and Spörk-Dür, 2021). Other countries have implemented different funding schemes to support the construction of innovative heating technologies like SDH systems and create a market momentum comparable to Denmark. In Germany for example, a funding line for innovative DH systems (“Wärmenetze 4.0” (BMWi, 2019)) is supporting the construction of low-temperature DH grids with large renewable shares. The funding line supports the development of concept studies and the construction of complete grids by up to 50% of the investment costs, as the high share of the initial investment costs on the total LCOH has been identified to be a main barrier for a further deployment of such grids (Pehnt, 2017).

A substantial barrier for broad implementation of SDH is land availability. Recent studies concluded that it is favorable to construct single large fields further away from the DH grid, rather than small roof-mounted systems. The strong economy of scale outweighs additional costs for transmission lines and availability of land is generally better. In theory, availability of suitable and available land should be sufficient in European countries (Trier et al., 2018a). Unfortunately, competing applications and slow procurement processes can pose additional problems and impede many projects in practice (Epp, 2021). Consequently, policy measures should address these issues to speed up the procurement process and the development of SDH technology should focus on a maximized exploitation of available land by shared usage (cf. Figure 2) or highly efficient technology such as concentrated solar power (CSP).

3.2 Underground Thermal Energy Storage

Integration of thermal energy storage technologies (TES) into DH systems has several benefits, such as the utilization of intermittent heat sources, reduction of peak capacities or the maximization of heat generation operating hours. These advantages are confronted with drawbacks like high investment costs or an increased complexity of the design process (Guelpa and Verda, 2019). Currently, tank thermal energy storage (TTES) is the most used TES technology in DH, where it is mainly used for load balancing and peak shaving. Besides TTES, around 105 GWh of additional TES capacity is installed in DH systems, of which half is realized as seasonal TES. These capacities are mainly realized by UTES systems. Alternatives, such as latent or thermochemical TES technologies, are currently still in prototype stadium. (IRENA, 2020)

UTES systems are defined by sensible storage of thermal energy below ground level and can use the ground itself, groundwater or industrial water as heat storage medium. Figure 4 gives an overview of the most common UTES types. Borehole TES (BTES) use soil as heat storage medium and charge and discharge the storage by pumping fluid which is above or below the temperature of the surrounding soil through a closed-loop system within boreholes. Heat transport outside the closed pipe system is mainly conductive and consequently the temperature level of the stored heat decreases both during charging and discharging. Furthermore, underground heat transport is relatively slow, which is an advantage for long storage periods, but limits the maximum charging and discharging rates. Construction wise, BTES differ only little from conventional BHE arrays for ground-coupled heat pump systems (GC-HP) and no clear distinction between those systems exists. This work defines BTES systems as BHE arrays which are used to increase the ground temperature to a level above undisturbed ground temperatures during charging and have a utilization ratio of ≤ 1 , i.e. the amount of extracted energy does not exceed the injected amount. Furthermore, BTES systems usually have a smaller spacing between BHEs than GC-HP systems and incorporate some kind of insulation layer on the ground surface, to reduce losses to the ambient air. While a significant flow of groundwater is desirable for GC-HP systems to regenerate the cooled down ground around BHEs, it is an unwanted process for BTES systems, where it transports stored heat out of the storage volume. Consequently, moderate groundwater flow rates constitute an important prerequisite for BTES locations.

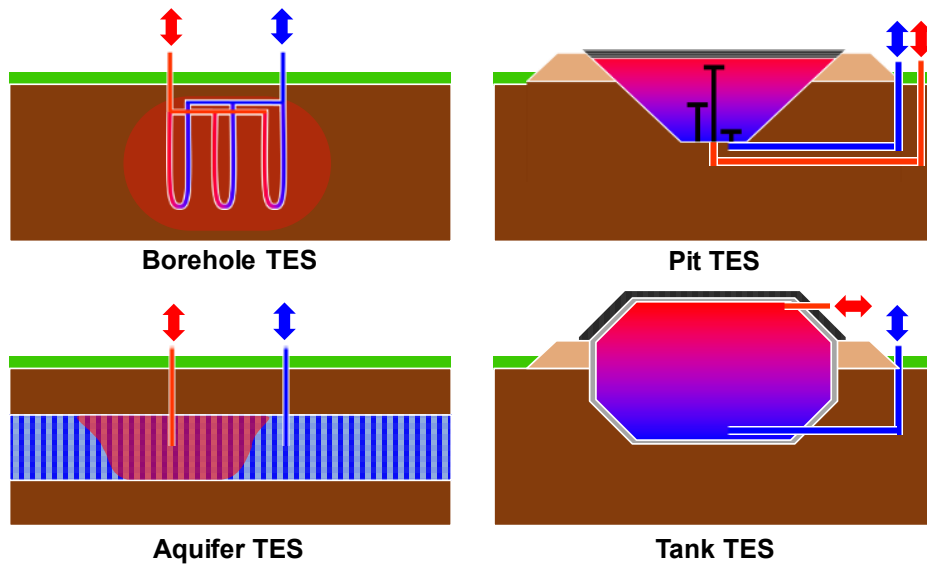


Figure 4: Common Underground Thermal Energy Storage types.

Another UTES technology which, has been installed increasingly in recent years is Pit TES (PTES). These systems use artificial pits which are filled with water as heat storage medium and covered by a floating lid for insulation (Jensen, 2014). The pit walls are sealed by a liner, but usually have no additional insulation. Charging and discharging of the PTES is done by injecting and extracting fluid and consequently high peak powers can be realized. So far, these systems have been built predominantly in Denmark, where volumes of 200,000 m³ have been realized. While the overall concept of PTES is quite simple, several of the installed systems showed problems with the durability of the top-cover. Thermal stratification within the storage results in the highest temperatures just below the lid and consequently exposure to temperatures of 80-90 °C for periods of several months. Under these conditions, vapor diffuses through the covering lid, soaks into the above insulation material and impairs the insulating effect (Errboe, 2018). Additionally, precipitation accumulates on top of the lid and squeezes the insulation material, if not removed. Several of the early PTES demonstrators suffered from these problems and are currently retrofitted with a “reversed open roof” concept lid, which is expected to have a higher durability (Bobach, 2020).

Aquifer TES (ATES) use groundwater as storage medium. Charging and discharging of these systems is done by injection and extraction of groundwater through wells. Suitable construction sites are hence limited to areas with a groundwater reservoir in a feasible depth, a low flow rate, no conflicts of use and a suitable hydro-chemistry. Latter one being very important for a low maintenance effort, since scaling and corrosion effects within wells and heat exchangers can substantially impair performance and economy of such systems. However, if these conditions are met, ATES systems constitute highly efficient and economic seasonal storages. Such conditions could be found in the Netherlands, where currently more than 2,500 systems have been installed, which amounts to 85% of the overall number of systems. (Fleuchaus et al., 2018)

Tank TES (TTES) differ from PTES systems by their solid shell construction. They are usually designed in a cylinder shape and can be erected above-ground, below-ground or partly buried. While most SDH systems incorporate TTES systems for diurnal storage, only very few have been designed for seasonal storage purposes. Major drawbacks of TTES for seasonal storage are their high heat losses to the surrounding and large space demands, which is why research efforts

have focused on advanced insulation concepts (Dahash et al., 2021) and partly buried TTES (Guelpa and Verda, 2019). Several additional UTES concepts or variants of the presented concepts have been proposed, such as storage of heat in abandoned mines (MTES) or medium-deep BTES (Welsch, 2019). While these concepts seem very promising, they are not yet on the same level of technological readiness.

Figure 5 gives an overview of the storage volume and specific investment costs of several realized UTES projects. The storage volume is given in water equivalents to facilitate the direct comparison of different UTES technologies and the orange lines indicate the overall corridor of specific costs in which most systems are located. It can be seen that the largest capacities so far were realized by PTES projects, whereas TTES were limited to smaller scales. Sizes of the shown ATES and BTES systems were located in the mid of the shown range. Generally, these two technologies are located completely in the subsurface and can be upscaled further. (Gabrielli et al., 2020). In the case of the “other” UTES system in Attenkirchen, a combination of a buried TTES and a surrounding BTES was tested. The presented choice of UTES systems, however, is far from complete and larger systems have already been constructed

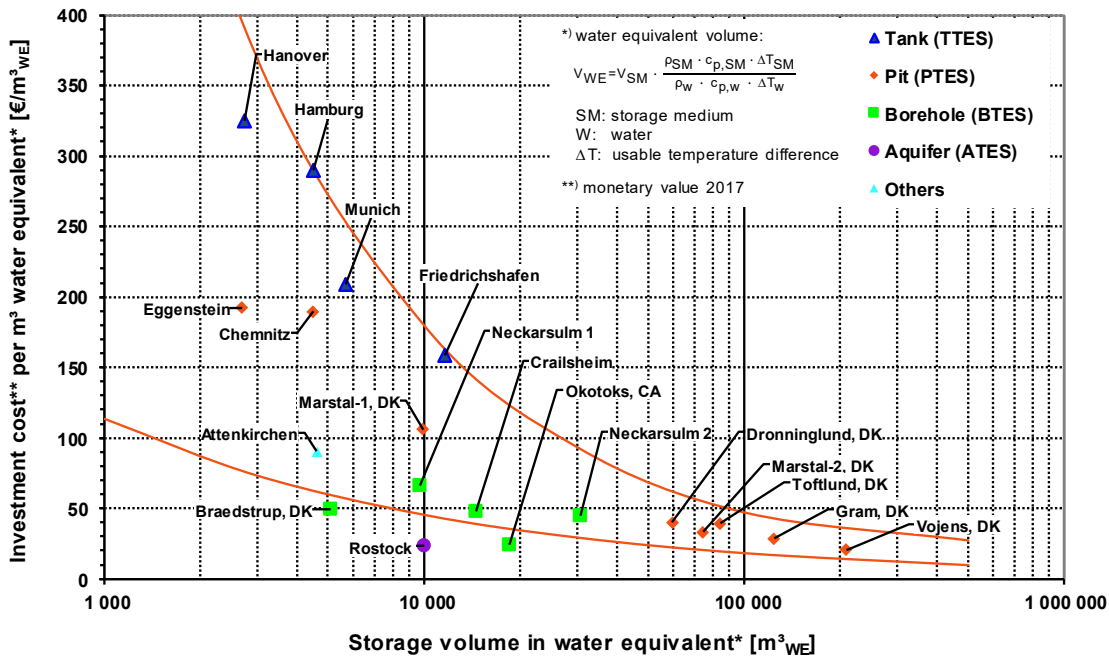


Figure 5: Specific investment cost for large-scale thermal energy storages (including all necessary costs for building the storage device, without design, without connecting pipes and equipment in the heating plant and without VAT) (© Solites)

Based on the presented figures, ATES systems result in the lowest specific investment costs. Since the storage volume is naturally given for those systems, construction costs are mainly caused by drilling of the wells. However, these systems have very specific site requirements and maintenance costs are usually higher compared to other UTES technologies. The highest investment costs can be observed for TTES systems, which, in combination with their large space requirements, limits them to smaller realized capacities. Overall, a strong economy of scales can be observed. In addition to that, larger UTES usually result in lower heat losses due to their

smaller ratio of surface to volume¹. As a result, larger and larger projects are being planned, to further reduce costs. Depending on the respective technology and region of application, cost reductions by factor 2-4 are required to achieve commercial competitiveness without subsidies (Reed et al., 2018; Yang et al., 2021).

3.3 System concepts and layouts

Several concepts for the design of SDH systems and the integration of individual components exist. While no general classification is defined, systems can be distinguished by certain characteristics, such as:

- DH grid concept: 1st-5th generation (1GDH-5GDH)
- Heat generation: Centralized and decentralized
- Combination with auxiliary heat sources: serial and parallel use of SDH and conventional heat sources
- Thermal storage: diurnal, seasonal, combined, hybrid/cascading
- Active and passive discharging of the UTES
- Heating only or heating and cooling

Choosing the right concept for a specific application is not straight forward, as the advantages of certain approaches are not always obvious and depend on the overall system. For example, 4GDH systems are considered to be favorable in comparison to the preceding generations, as they are generally more efficient and allow for the integration of low-temperature renewable heat sources. However, in the case of 5GDH grids, which are operated below the supply temperature level of the building heating systems, a heated discussion is still ongoing, elaborating the advantages and separating line of those concepts (Buffa et al., 2019; Lund et al., 2021). Nevertheless, certain general statements on the advantageousness of design concepts and layouts can be made for reasonable assumptions and common cases. An exemplary study on different layouts for district heating and cooling is presented in Appendix C.

¹ The volume of BTES systems is usually defined as the product of the number of BHEs, their length and the specific area around a single BHE in the grid, which is defined by the BHE spacing.



4 Object-oriented modelling of thermal energy systems

A fundamental and thorough introduction to the modelling language of Modelica would exceed the scope of the underlying work and excellent alternatives already exist (Fritzson, 2014; Tiller, 2021). Consequently, the following chapters will focus on specifics of the modelling of thermo-hydraulic energy systems and UTES in Modelica as well as the subsequent translation of such models into an executable form. In general, the acausal modelling approach of Modelica is meant to automatize this translation process and reduce the necessary effort for creating a model for the definition of the physical behavior of objects by equations. The deduction of how such a symbolically defined model can be translated into a form which can be efficiently handled by numerical solvers is supposed to be hidden from the general user. Nevertheless, a basic understanding of the steps taken by a Modelica tool during translation is beneficial for the development of efficient models.

4.1 Principles of modelling with Modelica

Modelica is a non-proprietary language for the modelling of physical systems developed by the Modelica Association since 1996. It arose from the desire to unify several existing approaches for the object-oriented modelling of physical systems and to create a standardized modelling format (Elmqvist, 1978). This tool independent approach supports a high reusability and exchange of developed models. The basic principles of the Modelica language, such as an equation-based approach and the object-oriented structuring concept, make it a versatile tool for modelling in many different domains. Consequently, a multitude of commercial and non-commercial Modelica model libraries have been developed so far. (Modelica Association, 2021)

The term object-oriented modelling is often used to summarize a set of properties under a single term (Otter, 1999a): It constitutes a concept of modularized and hierarchical structuring of models, but includes the concept of physical modelling as well. Latter one meaning the representation of system components by models, which correspond to actual objects and are defined independent of specific applications, i.e. acausal. Hence, the physical behavior of these objects is specified by symbolic equations rather than assignments, keeping the causality of whether a variable is an input or an output of the model unspecified. Consequently, single components can be modeled and tested independently from the overall system context, reducing the complexity of the process and facilitating the reuse of components for various applications. Solving such symbolically defined systems with numerical methods however, incorporates several additional challenges in comparison to causal models, which are described by explicit algorithmic expressions. An overview of the methods for tackling these challenges is given in the following chapter.

Models in Modelica are described in code defined by the Modelica Language Specification (Modelica Association, 2021). In general, this allows for a completely text-based modelling process, but components usually have a graphical view defined as well, which facilitates drag-and-drop modelling. Predefined interfaces are used to connect components to each other, corresponding to their physical interactions. These connections can be directed or undirected, i.e. acausal. The component behavior itself is described by locally defined variables and equations, incorporated sub-components and the interface variables. For acausal connectors, three types of interface variables exist: Potential variables are set equal for connected interfaces, generating equations of the form $x_1 = x_2 = x_3$. Flow variables of a connection set sum up to zero, resulting in the form $x_1 + x_2 + x_3 = 0$. The third kind, are stream variables. These are for transport

processes in which potential variables propagate downstream with a flow variable. An example is the temperature propagation of fluid transport in a pipe. (Otter, 1999a)

4.2 Translation and simulation of Modelica models

Modelica models are representations of physical systems, defined by mathematical equations, i.e. in an acausal way. Hence, any sort of operation and analysis can generally be applied. However, the most common application is dynamic simulation. Other typical applications would be steady state simulation for determination of a system equilibrium state, calculation of natural frequencies, system identification (input-output-analysis), model linearization or sensitivity analysis (ESI ITI, 2021). Consequently, the methods used to fulfill these tasks differ and even for the same task, methods differ from one simulation environment to another. In the case of SDH systems, dynamic multi-year simulation is by far the most common application and in the following the principals of a typical process for the translation and simulation of such a model in Modelica is described.

As Modelica is not a simulation environment, but a modelling language, no general rule for the simulation process of models exists. However, most software tools follow the same general steps for the translation of model code into an executable form for simulation. A typical process is depicted in Figure 6. It starts with the model in Modelica source code, that is generated by a user over the graphical user interface of a modelling environment. This can be done by drag-and-drop of model components to create an object diagram of the model, or by explicit writing of the source code. Once the model is specified, it is converted into an internal representation of the modelling environment for further processing (Fritzson, 2020).

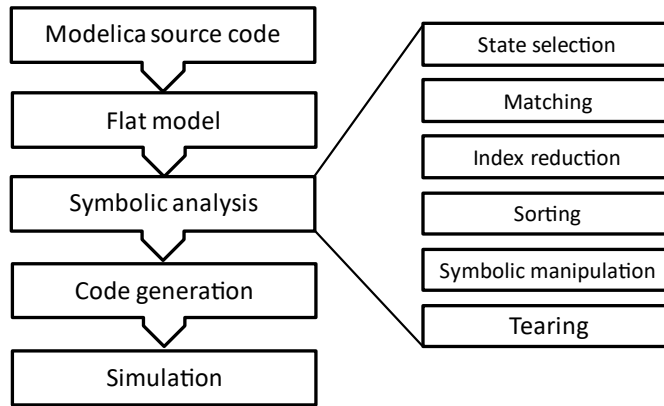


Figure 6: Typical translation process of a Modelica model.

In a first translation step, the object-oriented structure is dissolved by conversion of the hierarchical model into a flat model. During this step, instantiated and inherited classes are expanded, equations defined implicitly by connections between components are derived and complex constructs like algorithms or loops are executed. Resulting from this process, an unsorted set of differential-algebraic equations (DAE) in the form of Equation (1) is obtained (Otter, 1999b), where x is a vector containing all variables appearing in differentiated form, y contains all algebraic variables, u contains all system inputs and p contains all parameters.

$$0 = f(\dot{x}, x, y, u, p, t) \quad (1)$$

Numerical solving of such an unsorted DAE system is usually inefficient and solvers tend to be not robust (Fish and Harrison, 2017). Therefore, the general aim is to transform it into a set of

explicit ordinary-differential-equations (ODE) of minimum size, which is then passed on to the solver. If such a transformation is impossible or inefficient however, DAE solvers can be used as well (Liu et al., 2010; Fritzson, 2014). The manipulation methods, which are used for optimization of the system of equations, are summed up under the term symbolic analysis and can differ for Modelica environments, problem structures and user settings.

A main task of the symbolic analysis is the selection of states, to determine which of the variables generated from the Modelica code are state variables of the physical system, i.e. required for an unambiguous definition of the system state at any instant in time. All other variables are considered outputs and can be derived from the calculated state variables (Fritzson, 2014). The structure of the initially unsorted DAE can be described by an incidence array, where each row corresponds to an equation and each column to a variable (or a derivative of such). Non-zero entries of the array indicate the occurrence of a variable in the corresponding equation. On the left side of Figure 7 an example of such an initial incidence array (often called structure Jacobian) is shown. It has 1,200 equations and 1,200 variables, which are directly deduced from the Modelica code of the model. In the upper section, a diagonal band can be observed, that corresponds to the equations defined locally within components. The lower part of the array originates from connection equations coupling these local variables to each other. Most of these connector variables merely serve as aliases during modelling and are not required for solving of the actual problem. Consequently, these equations and their corresponding variables can be eliminated from the set of equations by the state selection process without loss of information. Furthermore, many variables are actually constant over time and can therefore be eliminated as well (Figure 7 right). (Dassault Systèmes, 2020b)

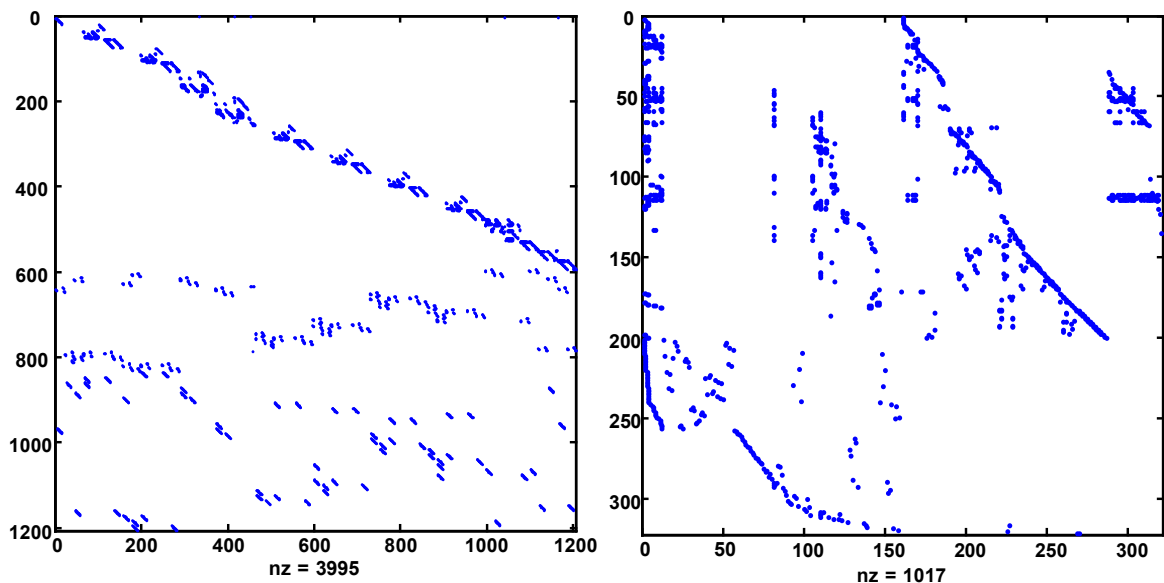


Figure 7: Incidence array of an unsorted DAE before (left) and after (right) selection of states. Rows corresponding to equations and columns to variables. The total number of incidences is denoted as *nz* (adapted after (Dassault Systèmes, 2020b), © Taylor & Francis Group LLC)

After state selection, sorting and transformation algorithms are applied to transform the DAE into an ODE in explicit state space form as given by Equation (2) (Braun et al., 2017). If the original DAE has derivatives of higher order than one, index reduction methods, such as the method of dummy derivatives (Elmqvist, 1993; Mattsson and Söderlind, 1993), have to be used. Note that only the upper part of Equation (2) has to be calculated to solve the model, while the

algebraic variables y only need to be computed at times where their values should be protocolled.

$$\begin{bmatrix} \dot{x} \\ y \end{bmatrix} = \begin{bmatrix} g(x, u, p, t) \\ h(x, u, p, t) \end{bmatrix} \quad (2)$$

In the next step, the set of equations is sorted after the flow of data, so states can be solved sequentially (Fritzson, 2014), which can be regarded as the causalization of the model. Therefore, each state is matched with an equation it occurs in and permutation is used to transform the system into block lower triangular (BLT) form, as shown on the left side of Figure 8. A complete lower triangular form would correspond to a purely explicit system of equations, in which each state could be determined directly, by recursive solving of the equations. However, in physical models this is usually not possible for all states, since acausal interconnections exist, that result in algebraic loops. These loops constitute small linear or non-linear implicit sets of equations, which correspond to the block elements of the BLT array (Figure 8 left, brown blocks). They are solved during the calculation of the right-hand side of the ODE. In many cases however, linear blocks of the form $Ax = b$ can be solved prior to the simulation. For some blocks however, iterative methods, such as the Newton Iteration, are required (ESI ITI, 2021). In this case, the Jacobian matrix is used to update predicted values for each iteration step. The equation-based approach of Modelica allows for the use of symbolic Jacobians in most cases, which is far more efficient, as these are calculated during the translation process, while numerical Jacobians have to be calculated repeatedly for each iteration step.

As the numerical effort of iterative solving of implicit sets of equations is significant, additional techniques are applied to reduce the size of the implicit blocks. In some cases, symbolic solutions exist and can be used to replace parts of the block elements. Another important method is “tearing” of the algebraic loops (Elmqvist and Otter, 1994). In this process the loop is broken up in such a way that a set of equations $\hat{f}(x)$ which forms a loop (Equation (3)) is substituted by two smaller sets of Equations (4) and (5), where x_1 , x_2 , \hat{f}_1 and \hat{f}_2 are the resulting subsets of states and equations and L is a lower triangular matrix. Starting with an initial guess value for x_2 , \hat{f}_1 can be used to directly calculate x_1 . Consequently, only the smaller subset \hat{f}_2 has to be solved by an iterative method. The process is repeated until x_2 converges. Since the computational effort of the applied iterative methods usually increases proportional to the cube of the system’s size, this step can reduce calculation times significantly (Wetter and Treeck, 2017).

$$0 = \hat{f}(x) \quad (3)$$

$$L x_1 = \hat{f}_1(x_2) \quad (4)$$

$$0 = \hat{f}_2(x_1, x_2) \quad (5)$$

Figure 8 (right) shows the small implicit systems of equation in dark grey and the explicit subset in green.

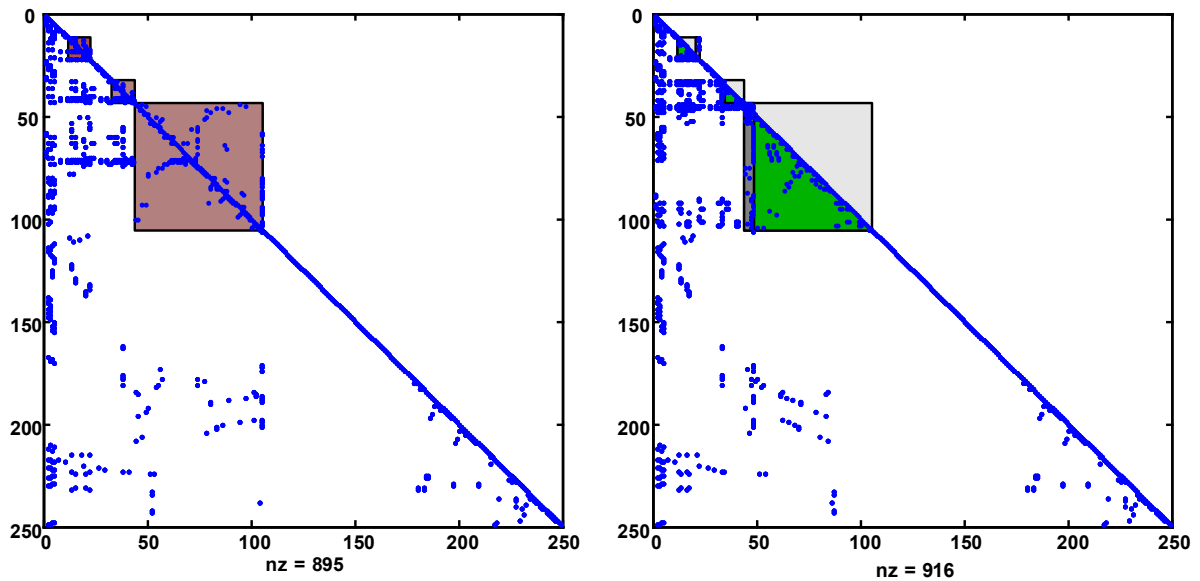


Figure 8: Incidence array in Block Lower Triangular form before (left) and after (right) tearing. Rows corresponding to equations and columns to variables. The total number of incidences is denoted as nz (adapted after (Dassault Systèmes, 2020b), © Taylor & Francis Group LLC).

In the final step, the translated model is usually compiled into the programming language C and linked to numeric solvers.

One aspect of Modelica models, which was excluded from the considerations up to this point, are the discrete parts of models. These are logical or integer values, which are not continuously and change their values at certain points in time, so called events. In between events, they are treated as constants and consequently ignored by the solver. If an event occurs, an iterative process is started, which solves the continuous model part and the discrete part in turn until the discrete variables do not change between subsequent iteration steps. Depending on the impact of the changed variables, the effort for reinitialization can be significant. In most cases however, this is not the case. The time instant of events can either be defined by a time relation (time events) or by crossing of defined threshold values of state variables (state event). In the first case, the exact time instant of the event is known in advance and the solver can directly steer to the point in time. In the latter case of state events, an iterative process has to be used to get within a defined small window close to the actual time (unless explicitly stated otherwise by the modeler). Accordingly, the occurrence of events can significantly slow down simulation of Modelica models and modelers should avoid triggering too many events, especially in the case of state events.

To illustrate some of the aspects of the discussed process, an example model from the MoSDH library is used (Figure 9). It contains a STC field and a BTES as seasonal storage, which is discharged by a heat pump. If the solar-geothermal system cannot cover the whole heat demand, a gas boiler is used as auxiliary heat source. A description of all shown components is given in Chapter 4.3. Simulation is carried out over one year and Dymola (Dassault Systèmes, 2020a) is used as simulation environment.

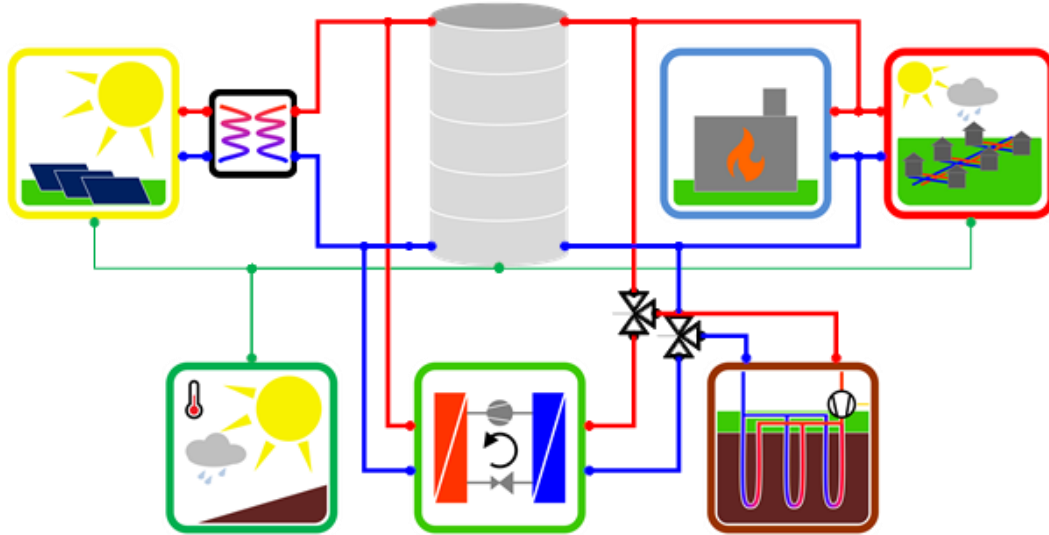


Figure 9: Example model MoSDH.Examples.ExampleGeoSolar.

Table 2 shows a summary of the model statistics before and after translation. For the given model and default settings, the number of parameters can be reduced from 12,654 to 175, while the number of constants increases from 33 to 18,033, indicating that many variables defined as parameters are actually constant. Accordingly, the number of unknowns is reduced from 22,946 to 6,301 of which only 669 are selected as state variables, whereas the remaining variables are algebraic. Finally, it can be seen that the number of linear and non-linear block elements can be reduced significantly, both in number as well as in size. Since the iterative calculation of the non-linear blocks constitutes a major share of the overall effort, their reduction in size is especially important.

Table 2: Model statistics of the MoSDH.Examples.ExampleGeoSolar example model from the MoSDH library.

| Original model | |
|---|--|
| Type | Number |
| Constants | 33 |
| Parameters | 12,654 |
| Unknowns | 22,946 |
| Differentiated unknowns | 669 |
| Translated model | |
| Type | Number |
| Constant | 18,033 |
| Parameters | 175 |
| Time-varying variables | 6,301 |
| Continuous time-states | 669 |
| Block elements | Size x number |
| Linear systems of equations | 7 x 36, 6 x 1, 4 x 711, 3 x 26, 2 x 11 |
| Linear systems of equations after manipulation | 2 x 36 |
| Nonlinear systems of equations | 27 x 1, 24 x 1, 9 x 1, 7 x 1, 5 x 1, 9 x 4 |
| Nonlinear systems of equations after manipulation | 4 x 1, 2 x 2, 1 x 11 |

Table 3 shows the summary of the simulation statistics. CVODE (Cohen and Hindmarsh, 1996) was chosen for integration, as it is a very efficient and robust solver, which is implemented in

many simulation environments. Since systems of equation resulting from Modelica models are usually quite sparse (cf. Figure 7 and Figure 8), application of sparse solvers can result in a significant speed-up of the simulation. The simulation finished after 43 s, of which less than one second was needed for initialization. The overall share of the iterative solving of the non-linear blocks, amounts to 7.3% of the computational effort.

Enabling of detailed logging settings allows for the detection of the share of each block on the overall time required for simulation. Which can be used to identify critical model parts. Knowing the assigned ID of a respective block, it is possible to access simulation analysis features and search for the block equations, to identify the critical algebraic loop in the model. For the chosen example model however, all nonlinear blocks result in comparable efforts and no further model adaptations, such as the manual breaking of the loop by introduction of a filter (Ensbury, 2019), are required. Furthermore, many tools support a feature in which states that slow down simulation are identified directly by comparison of the residuals during calculation.

Table 3: Simulation statistics of the MoSDH.Examples.ExampleGeoSolar example model from the MoSDH library.

| Simulation | |
|---------------------------------------|--------------------------|
| Settings | Value |
| Solver | CVODE SparseLU on 1 core |
| Tolerance | 1e-04 |
| Statistics | Value |
| CPU-time total | 43.006 s |
| CPU-time initialization | 0.022 s |
| Number of accepted time steps | 45,134 |
| Number of rejected time steps | 1078 |
| Number of time events | 365 |
| Number of state events | 3,144 |
| Number of non-linear block iterations | 71,522 |
| Number of Jacobian-evaluations | 7,186 |

Another aspect that slows down the simulation is the occurrence of many events. For thermo-hydraulic systems, these are often associated with a mal design of the control strategy, resulting in excessive switching of states and consequently turn on and off processes of components. For the presented example a total of 365 time events are triggered by the weather component for counting the number of simulated days. As time events are generally less critical, since they can be detected without event iteration and the increase of the counter for days does not affect the rest of the model significantly, the effort is negligible in this case. The state event which occurs most often is triggered by the internal control of the STC. Whenever solar irradiation exceeds a defined threshold value, operation of the circulation pumps is enabled. The conditional expression changes about twice a day in this case, which is reasonable for STCs and consequently does not constitute an issue.

4.3 Modelling of Underground Thermal Energy Storage systems

UTES systems are commonly built in a compact design to lower their surface to volume ratio and ultimately reduce thermal losses (Gehlin, 2016). This compact design allows for an accurate representation of the UTES system by 2D models for many cases (Dahash et al., 2020). Consequently, the numerical effort is reduced significantly for those models of reduced complexity, which is an important factor for system design simulation studies.

The object-oriented modelling approach of Modelica facilitates a high level of reusability. Figure 10 depicts the general concept of how a generic model for the simulation of conductive underground heat transport can be combined with different model components to create UTES models. The shown examples conceptually demonstrate the combination with a water pit model for creation of a PTES and BHE models for a BTES system. A detailed description of a BTES model is given in Appendix B and a PTES model is presented in Chapter 4.3.2.

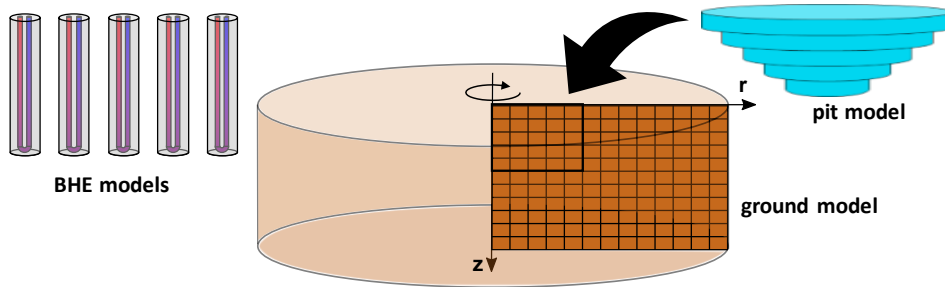


Figure 10: Combination of ground models with BHE and water pit models to form UTES models.

4.4 Co-simulation of UTES models

For many common applications, UTES models of reduced complexity can be utilized, which allows for the direct integration into system models. However, for certain applications and boundary conditions, those simplified models are unable to accurately describe the performance of the UTES. Examples for this could be the inability of 2D models to consider three dimensional asymmetric processes, such as groundwater flow or irregular BHE arrangements. In those cases, co-simulation of detailed 3D UTES models and Modelica system models can be a viable option. A methodology for co-simulation of DH models using MoSDH and FEM models of BHE arrays is demonstrated in Appendix E. The study compares two different interface options, of which one couples both models by the BHE inlet and outlet fluid streams (convective) and one at the borehole walls (conductive). In general, the presented methodology could be applied to different UTES technologies as well. Dahash et al. presents a similar methodology for co-simulation of PTES, coupling a stratified fluid volume model in Modelica to a FEM model of the subsurface in COMSOL using a conductive interface (Dahash et al., 2019). An example for the consideration of detailed hydro-thermal processes in BHE array models is given by Doughty et al. (Doughty et al., 2021). A major drawback of co-simulation, however, is a significantly increased numerical effort, making large studies like system optimization impracticable. The method is therefore mostly limited to detailed case studies with a sufficient data basis.

5 Modelica Solar District Heating Model Library

This chapter will provide an overview of the MoSDH library. As a complete description would exceed the limits of this work, only the basic concepts and conventions are outlined and a brief description of the main components is given.

The development of MoSDH, the Modelica Solar District Heating library, was kickstarted by the desire for an object-oriented BTES model. The only available eligible model at that time was the Hybrid Step Response Model of the Modelica IDEAS library (Jorissen et al., 2018). However, as this model is not focused on storage applications, but rather BHE arrays for heat extraction and therefore lacks certain important features, a new model called MoBTES was developed (Formhals et al., 2020). It is specifically designed for storage applications and follows modelling approaches which are known from the famous DST model in TRNSYS (Pahud and Hellström, 1996). The flexibility which comes along with the object-oriented and physical modelling approach of Modelica, made it easy to implement additional features, such as partially insulated BHEs, individual operation of BHE array zones or coupled calculation of pressure drop.

Initially MoBTES was meant to be used with component models from existing commercial or non-commercial libraries. These libraries however, mostly originate from building performance simulation and are therefore not optimized for simulation of DH systems (Wetter et al., 2014; Schwan and Unger, 2016). Apart from UTES models, these libraries include a multitude of sophisticated component models, that can be used for a wide range of applications. However, due to the following reasons, the initial MoBTES model was developed further and supplemented by additional models, resulting in the MoSDH library:

- 1) Complexity: A major difference to the aforementioned existing libraries is the implemented level of detail and consideration of short-time dynamics. MoSDH is dedicated for DH system design and analysis. For this purpose, dynamic behavior of components on a scale of seconds is irrelevant, as long as the components show a physically and technologically correct performance on an hourly scale and upwards. In contrary, including these features introduces an added complexity to the system model, which is irrelevant for multi-year analysis, but constitutes an additional source for modelling errors and thus impedes the overall model robustness.
- 2) UTES models: As mentioned above, the lack of a suited BTES model was the initial motivation for starting the development of MoSDH. Furthermore, there was no Modelica PTES model available.
- 3) Protection: Commercial libraries incorporate some degree of protection by nature, which makes adaptations of the models difficult or even impossible. Besides this, license fees impede broad application of the models for purposes such as teaching.
- 4) Tool independency: Modelica is generally a tool independent modelling language. However, commercial simulation environments often interpret certain aspects of the Modelica standard specification slightly different or support additional features, which go beyond the standard. Consequently, tool independency is a difficult task, especially for more sophisticated models. Furthermore, commercial libraries are often coupled to a specific simulation environment, restricting their applicability.


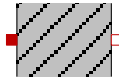
Based on these requirements, the MoSDH library was developed for simulation of SDH systems with UTES. The components follow a simple modular approach to facilitate the easy development of system models. By following a few simple rules, the modeler shall be able to create

system models, which have a well constrained thermo-hydraulic network. Consequently, the modelling effort, which is usually required to develop thermo-hydraulic models that are neither under- nor over-determined, can be put into aspects on a higher level, such as system control strategies.

5.1 Library interfaces and basic principles

Components of the MoSDH library are based on low level components from the Thermal library of the MSL (Tiller, 2000) for simulation of one-dimensional incompressible thermo-fluid and conductive heat transfer models. An overview of the two sub-libraries is given in Table 4.

Table 4: Physical interfaces of the MoSDH library (Modelica Association, 2020).

| |  |  |
|----------------------------|--|---|
| Domain | Thermo-fluids | Conductive heat transfer |
| Sub-library | Modelica.Thermal.FluidHeatFlow | Modelica.Thermal.HeatTransfer |
| Potential variables | Pressure p Specific enthalpy h | Temperature T |
| Flow variables | Mass flow rate \dot{m} Enthalpy flow rate \dot{H} | Heat flow rate \dot{Q} |
| Assumptions | <ul style="list-style-type: none"> • Reversal of flow is possible • Incompressible media with constant properties • No change of phase and no mixing of different media • Neglection of kinetic energy | Lumped capacities |

The Thermal library was deliberately chosen for its simplicity, as it facilitates the modelling of all physical phenomena which were considered central for the defined application. However, it should be mentioned that the majority of the existing open source libraries are based on the MSL Fluid library, which allows for a modelling on a higher level of detail, but consequently includes many additional settings and parameters. So far, the choice of the Thermal library has proven to be very practicable, as it results in robust and fast simulations, while keeping the modelling effort low. Nevertheless, the option of changing the library base components could be worthwhile, as it would simplify the combination of MoSDH with existing libraries.

Since colors of interface ports define the resulting colors of connection lines in Modelica model diagrams, the fluid ports used in MoSDH are colored blue, purple, red and black, to indicate the nominal temperature level of a connection. These ports have the same base class as the ports used in the MSL FluidHeatFlow library, which allows the connection of MSL and MoSDH models.

The MSL FluidHeatFlow library considers the coupling of volume flow rates and pressure drop by friction. Calculation of the pressure drop in pipe components is approximated by a linear function of the flow rate in the laminar regime and a quadratic relation within the turbulent regime. A smooth transition between both regimes is assumed, as this decreases the computational effort significantly and results in more robust models. Reference points for pressure drop

at transition from laminar to turbulent regime as well as for a nominal point have to be defined by parameters and are used to derive the pressure drop relation of the pipe model. Figure 11 shows the comparison of the pressure drop of the model to values calculated after Blasius (VDI, 2013). The nominal points for the MoSDH pipe models are located at Reynolds numbers of 2,320 and 25,000. However, the MSL pipe model calculates pressure drop by a quadratic function of the volume flow, whereas an exponent of 7/4 would be more exact. Consequently, the MSL model is only accurate close to the nominal points, but can differ significantly for operational points with smaller or larger Reynolds numbers. Since pipe flow regimes may differ substantially for applications such as DH networks or BHEs, the resulting error can be large. Consequently, an adapted version of the MSL pipe model with an exponent of 7/4 was used, which results in a much better fit to the calculated values (Figure 11). A comparison of the computational effort of MoSDH example models showed no significant difference.

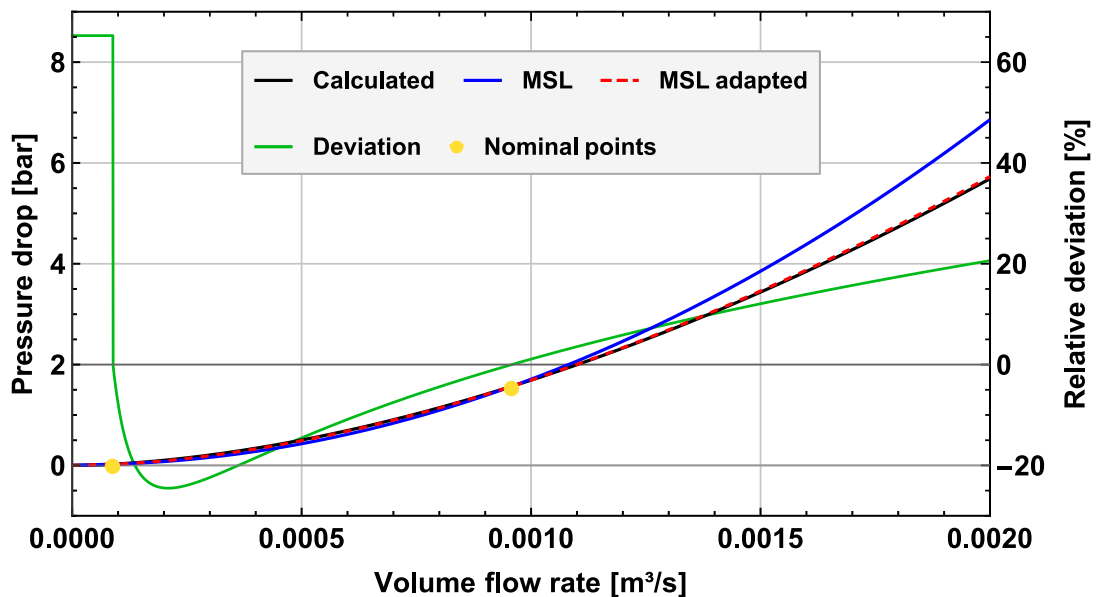


Figure 11: Pressure drop in a 100 m long DN32 pipe for water at 40 °C calculated with different methods and deviation of the simple friction model of the MSL to the exact calculated value.

In addition to the physical interfaces described in Table 4, an interface for the exchange of weather data is implemented in MoSDH (green ports). The interface has to be connected to a weather data component, which reads data for ambient temperature, solar irradiation and wind speed from text files. Furthermore, auxiliary variables like calendar data are calculated and can be accessed by connecting components to the weather data interface.

5.2 Modelling and control philosophy

The general modelling philosophy for high level components of the MoSDH library is to include as much as possible inside the components, to keep the system model tidy and easy to read for observers. Including components like circulation pumps and sensors within each model, certainly makes them less versatile. However, most model components almost exclusively reoccur in certain combinations with other components, so combining them from the beginning can reduce the final modelling effort and the risk of modelling errors. As MoSDH is primarily dedicated to system analysis, the effort of the individual control strategy of a component should be

kept at a minimum. Consequently, an approach was chosen, in which the system control strategy is primarily focused on activating and deactivating components and defining their operational set point.

Figure 12 shows the basic working principle of most heat source components in MoSDH. Depending on the chosen control mode, the user has to define two of the three input variables thermal power, supply temperature and volume flow rate. According to the nature of the actual heat source component and constraints defined by parameters, the internal control will try to match the defined inputs by controlling the heat input rate P_{th} and the volume flow rate \dot{V} . In the case of passive heat sources, like STCs or BHEs, only the volume flow rate or the reference supply temperature have to be defined, whereas certain components require additional inputs to define their operational point (e.g. heat pumps).

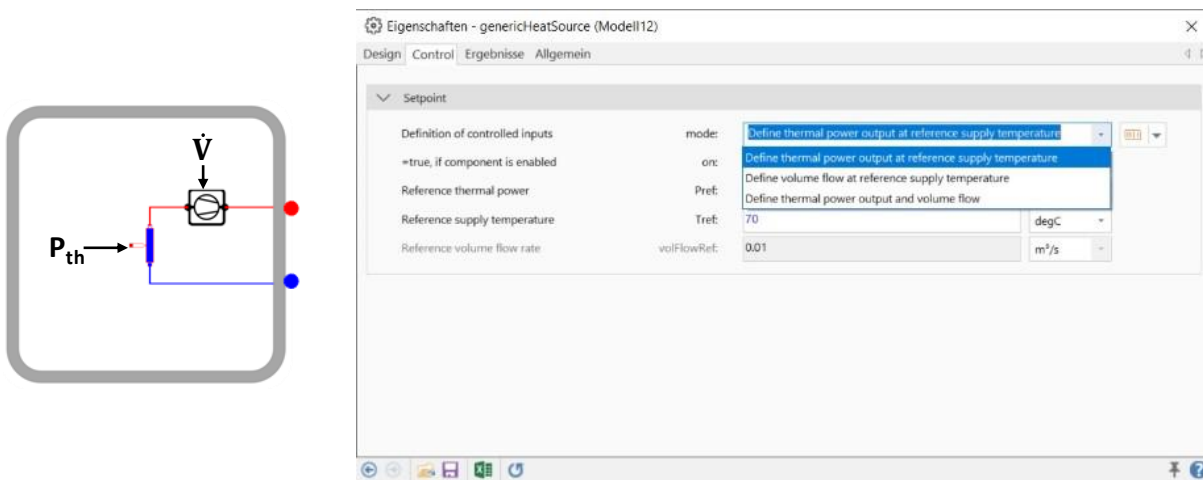


Figure 12: Generic heat source and settings for the control variables in the context menu.

An important and challenging aspect of object-oriented hydraulic network models is the avoidance of under- or overdetermined systems. For MoSDH heat sinks and sources the volume flow rate is generally defined explicitly by the pump, whereas the required pressure difference of the pump is calculated accordingly and practically handled as a result variable. Consequently, a direct connection of two such components to a closed loop (Figure 13 a), will result in an overdetermined system. In these cases, a shunt component can be used for hydraulic decoupling of the components (Figure 13 b). For system models, the required degree of freedom is usually introduced by a heat storage component (Figure 13 c). Additionally, the absolute pressure level has to be defined for closed hydraulic systems, as pressure relations in components only define pressure differences. In MoSDH these absolute pressure levels can be defined optionally in any component which can be used to introduce the degree of freedom mentioned above, like buffer storages, shunts or heat exchangers.

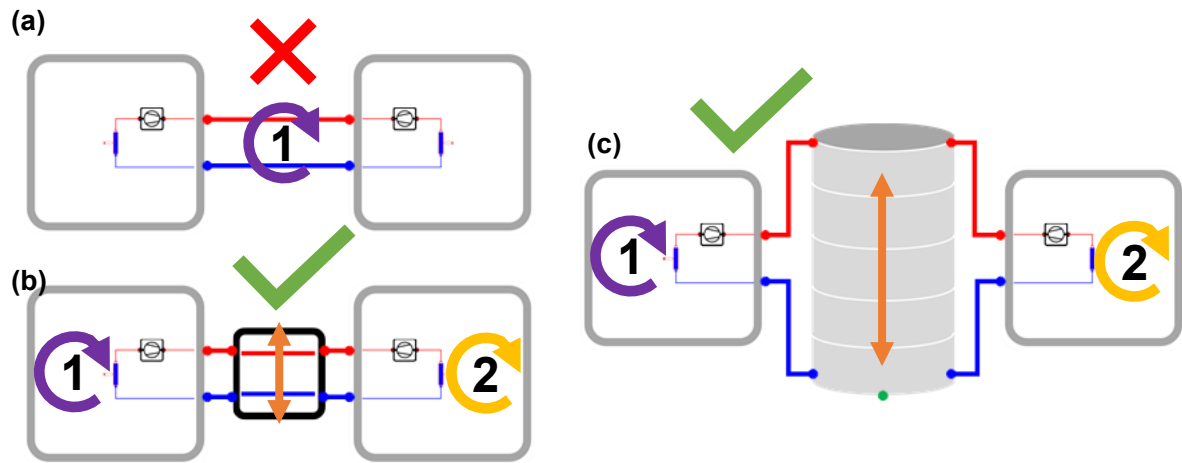


Figure 13: Avoiding over-determined hydraulic models in MoSDH.

5.3 Structure and component overview

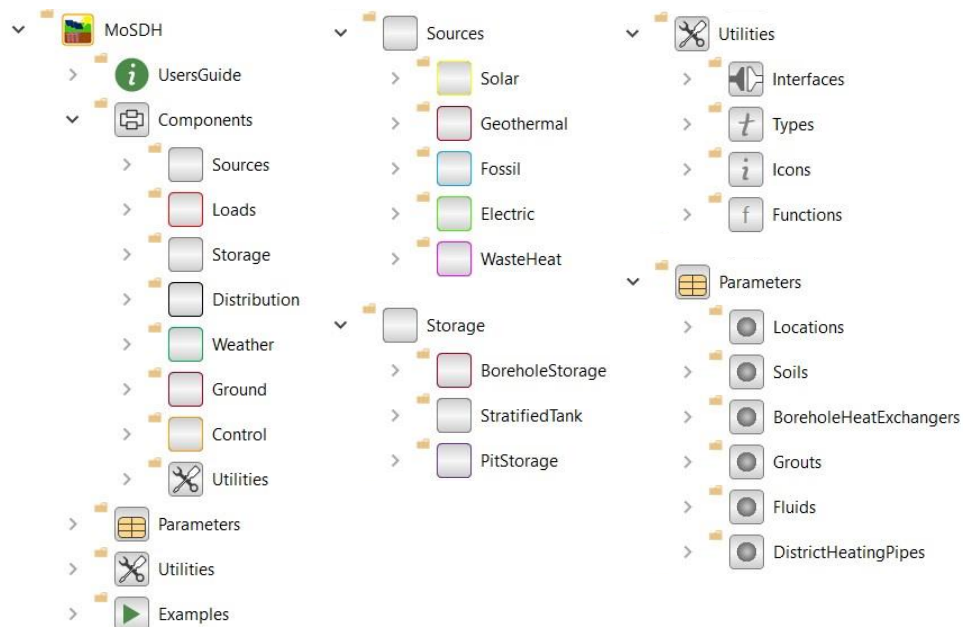


Figure 14: MoSDH library structure.

Figure 14 gives an overview about the top-level structure of the MoSDH library. The following content is included in the shown sub-packages:

UsersGuide: Brief documentation of the library, as well as release notes and copyright clauses. The main part of the documentation, is included in the respective model components.

Components: Includes the model components that will be described briefly in the following chapters.

Parameters: Collection of records with predefined parameter datasets for locations, soils, BHE designs, media and DH pipe designs.

Utilities: Includes the library interfaces presented in Chapter 4.1, a collection of icons and enumerations.

Examples: Collection of exemplary system models to demonstrate general modelling concepts. These are not optimized in any way, but include basic operation strategies and default parameters that result in robust simulations. Further small example models are located directly at each component to demonstrate their specific usage.

5.3.1 Heat source components

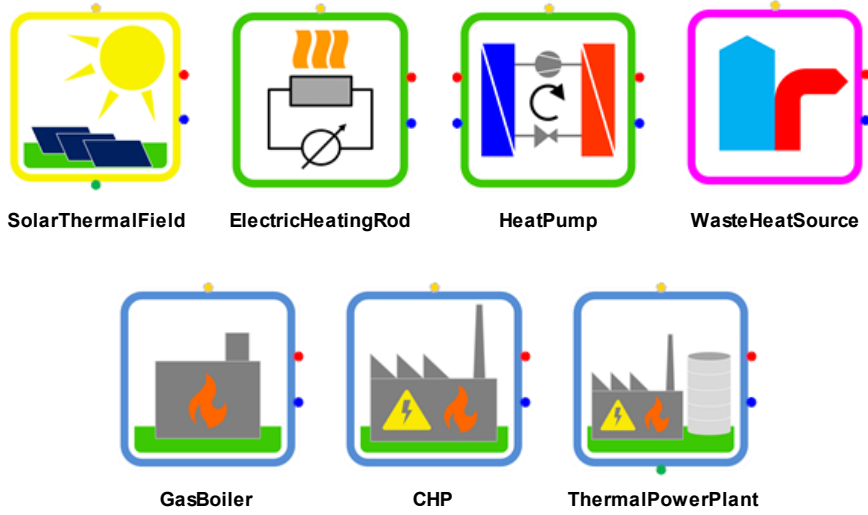


Figure 15: Heat source component icons of the MoSDH library.

SolarThermalField

The STC field model includes collector modules which can be connected in series and in parallel. The model gets a 3D vector for the direct irradiation and a scalar value for the diffuse irradiation through the ambient-connector (green) and calculates the total irradiation on the collector modules, considering shading between collector rows. Collector irradiation is calculated using the isotropic diffuse model after Liu and Jordan (1963). The total irradiation I_T on a collector tilted by the angle β is calculated after Equation (6), using measurements of the direct irradiation on a horizontal I_b and diffuse irradiation I_d (Duffie et al., 1994). The model considers three kinds of irradiation: direct beam irradiation, isotropic diffuse radiation from the sky and irradiation reflected from the ground. Conversion of beam irradiation measured on the horizontal to beam irradiation on the tilted collector is obtained by coefficient ψ , which is defined by the orientation of the collector and the position of the sun at time t . The fraction of the total irradiation on the ground which is reflected, is defined by the diffuse reflectance factor ρ_g .

$$I_T = I_b \psi(t) + \left(\frac{1 + \cos(\beta)}{2} \right) + (I_b + I_d) \rho_g \left(\frac{1 - \cos(\beta)}{2} \right) \quad (6)$$

To account for shading between collector rows of a collector field consisting of n_{rows} , the first term of Equation (6) is multiplied by a shading factor f_{shade} , which gives the fraction of the collector area, that is not covered from the sun by the previous collector row. However, since only one collector row is actually modeled in the SolarThermalField model and the first collector row is expected to have no shading, the average shading factor of all rows is used for calculation (Equation (7)). Furthermore, values for the transmission τ and absorption α of collector

modules under real conditions differ from values measured under test conditions, where the irradiation on the collector is normal to the collector plane. This effect is considered by the incidence angle modifier $K_{\tau\alpha}(\theta)$, which is a correction factor usually provided by data sheets in the form of table data or as a function in dependence of the incidence angle θ . Effective incidence angles for diffuse irradiation θ_d and for ground-reflected irradiation θ_g are given by Equation (8) and (9) (Brandemuehl and Beckman, 1980).

$$I_T = \psi K_{\tau\alpha}(\theta_b) \left(\frac{n_{rows} - 1}{n_{rows}} \right) f_{shade} I_b + K_{\tau\alpha}(\theta_d) \left(\frac{1 + \cos(\beta)}{2} \right) I_d \quad (7)$$

$$+ K_{\tau\alpha}(\theta_g) \rho_g \left(\frac{1 - \cos(\beta)}{2} \right) (I_b + I_d)$$

$$\theta_d = 59.7 - 0.1388 \beta + 0.001497 \beta^2 \quad (8)$$

$$\theta_g = 90 - 0.5788 \beta + 0.002693 \beta^2 \quad (9)$$

After calculating the amount of the total irradiation on a collector module, the useful energy output of the module is calculated by using an efficiency relation after Equation (10), where η is the overall efficiency, η_0 is the optical efficiency, α_1 is a linear loss coefficient, α_2 is a quadratic loss coefficient and ΔT_m is the temperature difference between the mean temperature of the fluid inside the collector module and the ambient temperature (Duffie et al., 1994).

$$\eta = \eta_0 - \alpha_1 \frac{\Delta T_m}{I_T} - \alpha_2 \frac{(\Delta T_m)^2}{I_T} \quad (10)$$

There are three available modes for controlling the SolarThermalField component. For the default mode, a reference supply temperature has to be given as input and the volume flow rate is regulated accordingly. For the second mode, the volume flow rate can be defined as input, if a custom control strategy should be applied. An experimental third mode was added to emulate night cooling by circulation of hot fluid through the collector. In this mode the volume flow rate is reversed and controlled to meet a defined return temperature. While the mode generally succeeds in the desired purpose of disposal of excess heat, it has not been validated so far.

CHP

This model of a CHP plant consists of several units, which can be modulated in power or switched on and off completely. Curves for the power-to-heat ratio and the fuel utilization in relation to the modulation of the unit have to be defined by parameters. Generated electricity and fuel consumption are calculated accordingly. The number of enabled units, their respective reference powers and supply temperatures can be defined in the control settings of the component. The internal control of the component will activate and modulate the CHP units according to the control signals, considering the restrictions for maximum power, temperatures and degree of modulation defined by model parameters.

GasBoiler, ElectricHeatingRod and WasteHeatSource

These three models constitute simple heat generation components, which only differ in their consumed fuel. The fuel efficiency in relation to the level of modulation has to be defined by a parameter. Generally, the heat supply of the components is defined by the supply temperature, the volume flow rate and the thermal power, of which two values have to be defined by control variables, depending on the current mode.

ThermalPowerPlant

The thermal power plant model combines CHP units, a natural gas boiler and a small buffer storage to maximize operating times of the CHP units. From an external view, the component is controlled similar to the gas boiler, defining two variables out of the supply temperature, the volume flow rate and the thermal power. Additionally, the number of enabled CHP units has to be defined. Control of the individual sub-components (Figure 16) from outside however, is not necessary. The internal control strategy of the plant, tries to maximize the share of CHP heat, while keeping the number of turn on and off processes low. To do so, CHP units are activated and deactivated according to the buffer storage's state of charge. The plant then supplies the requested thermal power at reference temperature, by direct feed from the CHP units, feed from the buffer storage and, if necessary, by the natural gas boiler.

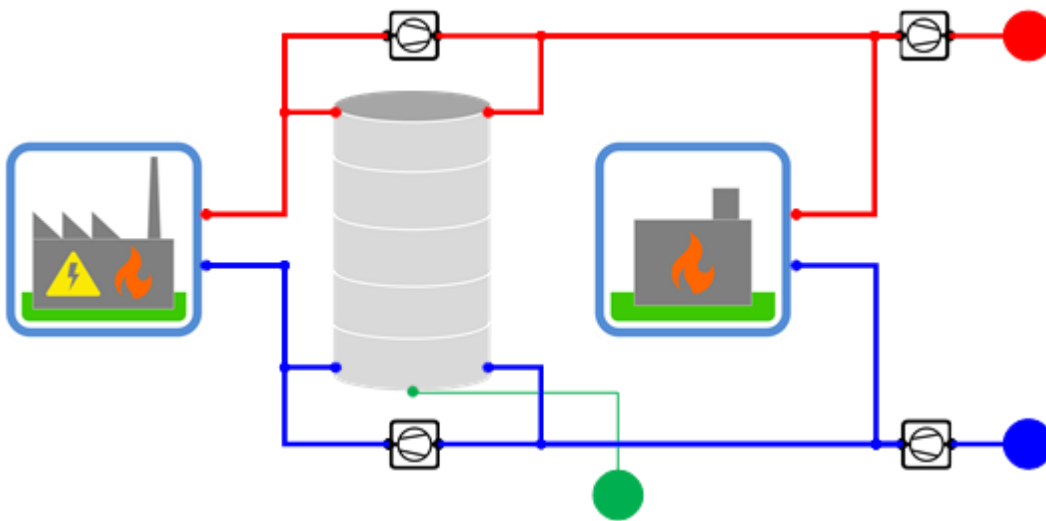


Figure 16: Diagram view of the internal structure of the thermal power plant model.

HeatPump

Model of an electric driven compression heat pump, for which the performance has to be defined by maps for the coefficient of performance (COP) and the heating power in relation to evaporator and condenser temperatures. Limits for the range of operation temperatures for evaporator and condenser have to be defined. If source side temperatures exceed the defined maximum, the fluid stream is automatically cooled down by mixing with the source return flow. Different operation modes are implemented, for which three of the control variables load side temperature and heating power as well as source side volume flow rate, temperature difference and cooling power have to be defined.

5.3.2 Thermal storage components

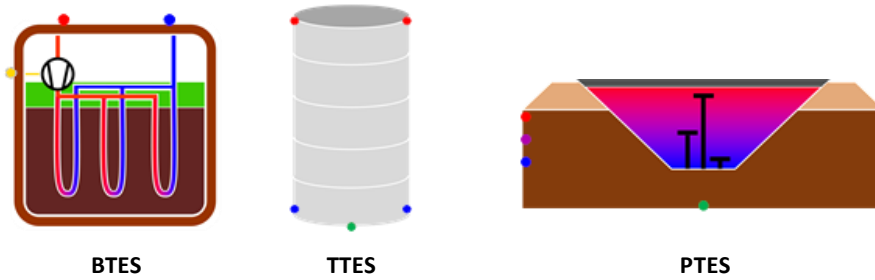


Figure 17: Heat storage component icons of the MoSDH library.

Borehole thermal energy storage

A detailed description of the BTES modelling concept is given in Appendix B and application examples are presented in Chapters 6.1, 6.2 and 6.4. The model was validated using simulation results of 3D FEM models and monitoring data from the Brødstrup BTES system. One aspect which was not presented so far however, is the generation of the model mesh, which can have a significant impact on the model's computational effort. Therefore, the process and main parameters will be illustrated by an example model in this chapter. The mesh generation process is carried out during the translation process or more precisely during the generation of the flat model for each storage layout individually (cf. Chapter 4.2). Figure 18 shows a generated mesh of a BTES system with 32 BHEs (parameter $nBHEs$) with each four connected in series ($nBHEsInSeries$). Consequently, only four BHEs are actually modelled, with each of them being representative for eight. The depth of the BHE heads is 1 m ($BHEstart$) and the total length is 50 m ($BHElength$). A different grout material was used for the upper 5 m of the boreholes ($useUpperGroutSection$, $lengthUpperGroutSection$).

A vertical supermesh is generated by combination of the depths of the geological layers ($location.layerThicknessVector$), the aforementioned BHE geometries and the total model depth, which is defined in relation to the length of the BHEs ($relativeDepth$). Subsequently, the supermesh is filled with smaller elements to form the actual mesh. The size of the smallest elements is restricted by the smallest supermesh element and a limiting parameter ($dZminMax$). Within each section of the supermesh, the size of the elements increases towards the center by a predefined factor ($growthFactor$), which was set to 2 in this case.

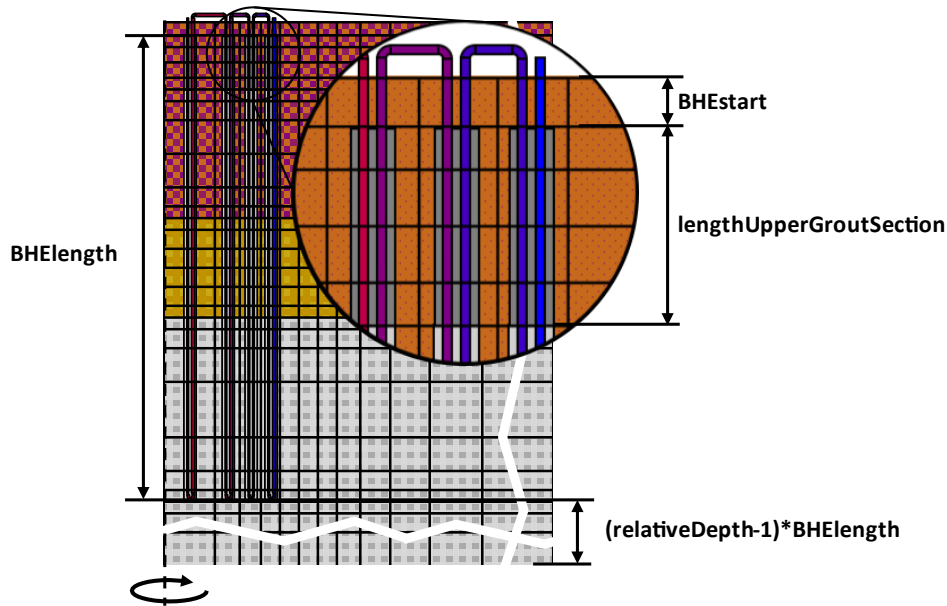


Figure 18: Exemplary mesh of a BTES system of 32 BHEs connected in series of 4 and a different grouting in the upper section.

The radial mesh within the storage region is defined by the spacing of the BHEs (*BHEspacing*) and the chosen layout. According to those settings, the radii of the axisymmetric cylinder model rings are calculated to meet the volume attributed to the BHEs of the corresponding storage region. Outside of the storage region, 3 elements of the thickness of the outermost BHE ring are appended, followed by elements with growing thicknesses (*nAdditionalElementsR*). The final meshing in vertical and radial direction as well as further statistics of the generated model, can be printed to the output area of simulation tools for debugging purposes (*printModelStructure*).

Tank thermal energy storage

The *TTES* model can be used for simulation of stratified fluid storage models. It contains the sub-model *StratifiedStorageVolume*, which divides a cylindrical fluid volume in several layers (Figure 19). Each layer has two fluid ports for injection and extraction on load and source side (black disk). Since the ports are implemented as an array, only one port is visible in the structure diagram though. In addition to the fluid ports, each layer has a conductive port to consider heat losses through the wall and additional ports are located at the top and bottom of the storage volume (red and white squares). Heat losses through the wall and the storage top are calculated either by using the dynamic ambient temperature defined by the ambient port (green) or a constant temperature defined by a parameter. Insulation of the storage top, wall and bottom can be defined by respective parameter values.

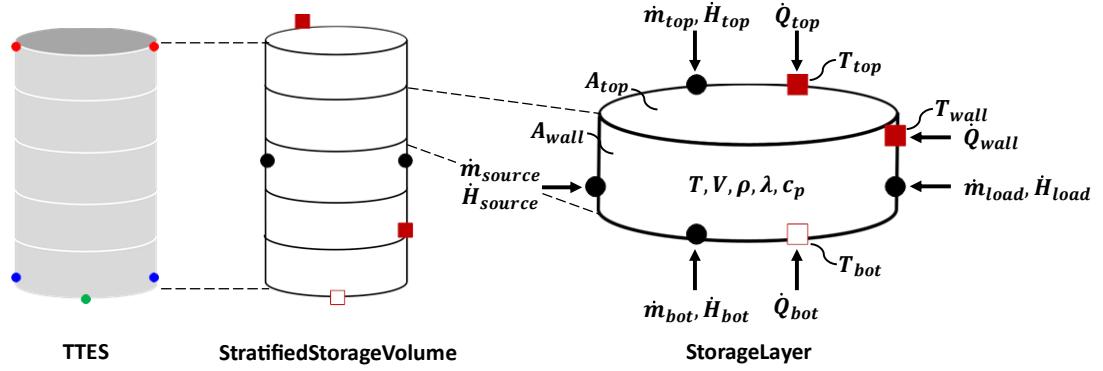


Figure 19: Structure of the TTES model and inputs of a single volume element model.

Heat losses to the ground are calculated by the steady state thermal resistance of a disk on a half infinite medium R_{gr} according to Equation (11), where λ_{gr} is the thermal conductivity of the ground and r the bottom radius (VDI, 2013).

$$R_{gr} = \frac{1}{4 \lambda_{gr} r} \quad (11)$$

Within each layer a constant temperature is assumed and the mass and energy balance are considered according to Equation (12) and (13) respectively. Conductive heat transport between adjoining storage layers is calculated after Equation (14), where \dot{Q}_{port} is either the heat flux to the below layer (bot), the above layer (top) or the shell surface (wall), A_{surf} the respective contact surface, λ is the thermal conductivity of the medium and h the height of the segment. In the case of thermal inversion, i.e. a lower temperature within the upper layer, the occurring natural convection is considered by an artificial increase of the thermal conductivity. The respective term $\lambda_{buoyancy}$ is calculated after Equation (15), where β_w is the thermal expansion coefficient of the storage medium and κ the Kármán constant (Zofer, 2019).

$$0 = \dot{m}_{top} + \dot{m}_{bot} + \dot{m}_{source} + \dot{m}_{load} \quad (12)$$

$$\rho V c \frac{\delta T}{\delta t} = \dot{H}_{top} + \dot{H}_{bot} + \dot{H}_{source} + \dot{H}_{load} + \dot{Q}_{top} + \dot{Q}_{bot} + \dot{Q}_{wall} \quad (13)$$

$$\dot{Q}_{port} = (T_{port} - T) \frac{2 A_{surf}}{h} (\lambda + \lambda_{buoyancy}) \quad (14)$$

$$\lambda_{buoyancy} \begin{cases} \frac{2}{3} \rho c \kappa h^2 \sqrt{\left| -g \beta_w \frac{(T_{port} - T)}{h} \right|}, & T_{up} < T_{low} \\ 0, & else \end{cases} \quad (15)$$

The presented modelling approaches of the stratified storage model have been validated in the original literature and consequently validation of the model, which was carried out in the course of a master thesis, focused on the correct implementation, by comparing the model results to results from existing buffer storage models (Kirschstein, 2020).

Pit thermal energy storage

The *PTES* model combines ground elements from the *BTES* model with the base class for stratified water volumes of the *TTES* model. Consequently, the model is an axisymmetric 2D representation of a pit storage, i.e. a truncated cone. The main geometry parameters of the model can be seen in Figure 20. The lid is modeled in greater detail, as it has proven to be a critical aspect for *PTES* systems (cf. Chapter 2.2). A user defined number of insulation layers is modeled by thermal resistances and capacities, using temperature dependent values for the thermal conductivity. Three fluid ports are connected to the top layer, the bottom layer and a user defined layer, to connect the *PTES* component to the system model.

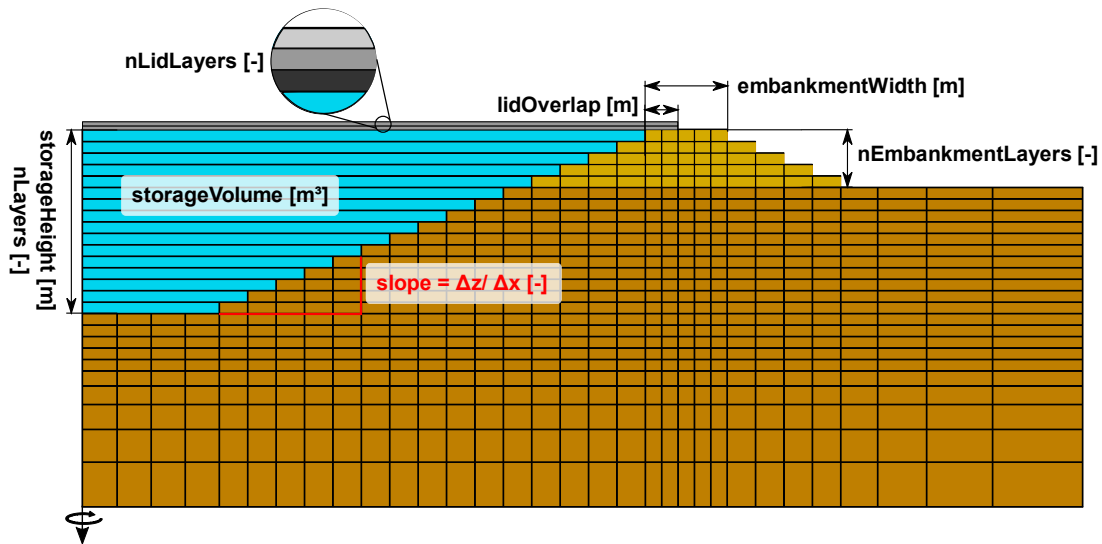


Figure 20: Exemplary mesh and main parameters of the *PTES* model.

One aspect which is very much simplified in the model, is the geometry of the pit wall. For simplicity, rectangular elements were used, resulting in the step shape shown in Figure 20. Heat transfer from the pit layer elements to the adjoining ground elements was only considered in radial direction. However, the actual slope and area of the truncated cone volume of the *StratifiedStorageVolume* model is considered for calculation of the heat transfer coefficients, which are calculated according to the *VDI Wärmeatlas* (VDI, 2013; Kirschstein, 2020). However, development and validation of the pit storage model is still in progress.

5.3.3 Distribution components

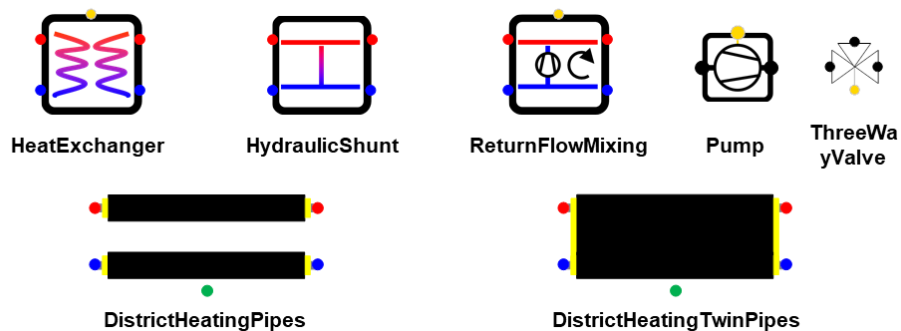


Figure 21: Heat distribution component icons of the *MoSDH* library.

District heating pipe models

District heating pipes are modeled using pipe segments and thermal resistance and capacitance models (TRCM) for the heat transport between the fluid, the composite pipes and the ground surface. One model for two buried pre-insulated DH pipes (*DistrictHeatingPipes*) and one model for a buried twin pipe (*DistrictHeatingTwinPipes*) are included (Figure 21). Both options reuse the TRCM model of the single-U BHE segments from the BTES model in MoSDH. In the case of the two pipes model, the composite of medium pipe, insulation layer and casing is aggregated into a single thermal resistance and represented by the BHE pipes. The grout region of the BHE model represents a virtual cylindrical region around the two pipes (Figure 22 left). In the case of the twin pipe model, the BHE model can be reused for modelling of the medium pipes, the insulation and the casing only (Figure 22 right). As the twin pipe model uses the thermal capacities of the grout material of the BHE model, it can consider short-term dynamics of the DH pipes more accurately than the model for the two buried DH pipes.

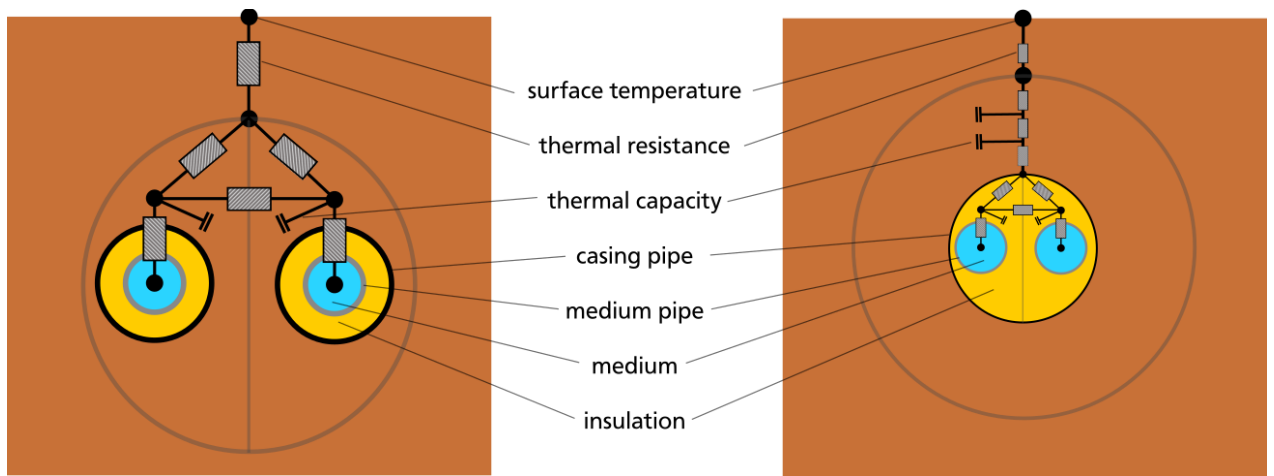


Figure 22: Conceptual design of the DH pipe models. Left: two buried pipes. Right: buried twin pipe.

The heat transport between the virtual circular region of the two pipes model and the ground surface is represented by a steady state thermal resistance. The surface temperature is filtered by a first order transfer function with a time constant of 10 days as ground temperatures changes are attenuated and delayed in comparison to the ambient air temperature (Verschaffel-Drefke et al., 2021). The steady state resistance per length unit is calculated after Equation (16), where λ is the ground thermal conductivity, d is the pipe center depth below surface and r is the radius of the virtual region (VDI, 2013).

$$R_l = \frac{\text{arcosh}(d/r)}{2 \pi \lambda} \quad (16)$$

In contrast to the two pipes model, the twin pipe model has a cylindrical finite-differences model added between the BHE segment model and the steady state thermal resistance to the ground surface, to cover the short-term dynamics around the pipe. The implementation of the twin pipe model in MoSDH is shown in Figure 23. Only one element each for the pipe segment, finite-differences model and thermal resistance arrays are shown in the structure view. Coefficients for the heat transmission between fluid and pipe walls as well as pressure losses are calculated after VDI Wärmearatlas (VDI, 2013).

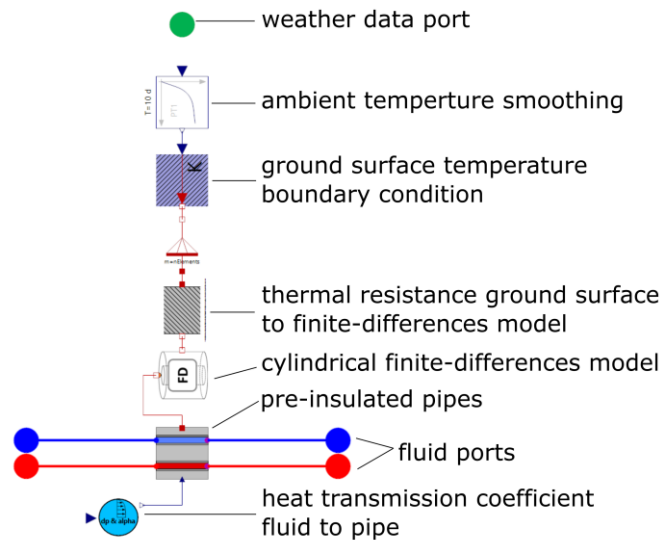


Figure 23: Implementation of the district heating twin pipe model in MoSDH.

Heat exchanger model

The HeatExchanger model uses a discretized approach, in which the source and load side volume as well as the heat transfer surface are divided in segments. Heat transfer coefficient and surface have to be defined as parameters. The included pumps and absolute pressure components are only included conditionally and are generated according to the chosen control mode and settings, which allows for a versatile combination of the heat exchanger with other system components.

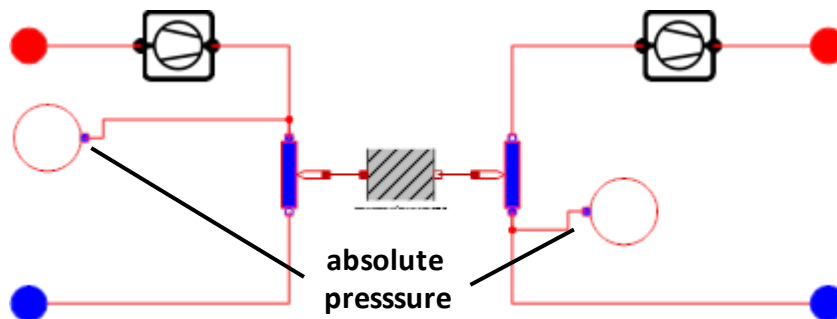


Figure 24: Structure diagram of the HeatExchanger model.

Hydraulic shunt and return flow mixing models

These components can be used to model a connection between supply and return line. In the case of the hydraulic shunt, a passive connection is used, which introduces an additional degree of freedom to the hydraulic network. Application of the component is demonstrated in Chapter 4.2. The return flow mixing component uses a pump between supply and return line, to control the volume flow rate to meet a defined load side supply temperature by mixing the supply line flow with cooler water from the return line. Such a component is usually used, if the supply temperature of heat sources exceeds the required or allowed supply temperature of the grid or individual consumers.

Pump model and three-way valve

The pump model, which is also included in most components, generates a defined volume flow rate and the associated pressure difference. An efficiency curve in relation to the nominal volume flow rate can be defined to calculate the required energy demand. The three-way valve component is either used for diverting a volume flow according to a defined input signal or to introduce an additional node in the hydraulic network for avoiding of unwanted mixing.

5.3.4 Ground components

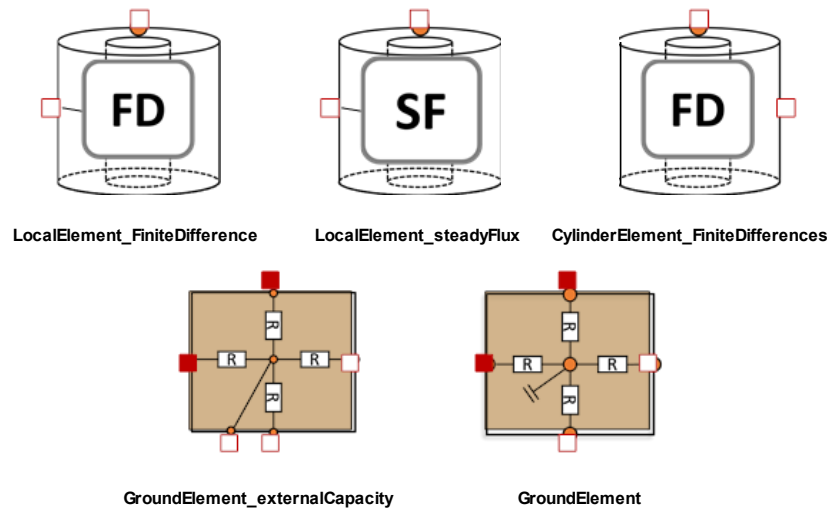


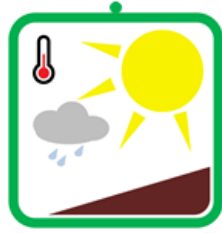
Figure 25: Ground components icons of the MoSDH library.

The ground models used in MoSDH consider conductive heat transport for axisymmetric applications using a finite differences approach. The generated 2D mesh is called the global underground model, as it is used for the modelling of the large-scale heat transport processes. For the combination of the BHE models and the global underground model, a relation between the average temperature in a ground element and the borehole wall temperature is required, which is given by the local ground elements (cf. Appendix B). Additionally, a regular cylindrical finite differences model was implemented, to calculate heat transport between the inner and outer surface of a cylindrical volume. This component is used for the DH pipe models (Chapter 4.3.3.).

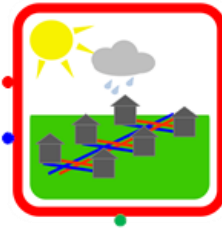
5.3.5 Weather data and heat demand components

The implemented heat demand component reads a load curve from a text file. A reference return temperature has to be defined, according to which the volume flow rate is regulated. In the case of insufficient supply temperatures, the actual extracted heat is reduced from the value defined by the load curve and a warning message is given.

The weather data component can be used to read ambient temperature as well as direct and diffuse solar irradiation time tables from text files and convert them into the format required by other model components. The direct irradiation data can be defined as data measured on a horizontal or inclined surface as well as data measured in beam direction, to allow for the easy integration of common data types. Calculation of the current position of the sun and the resulting inclination angles are carried out after Duffie and Beckmann (1994).



WeatherData



HeatDemand

Figure 26: Weather data and heat demand component icons of the MoSDH library.

6 Methods for multi-criterial analysis and optimization of SDH systems

6.1 Performance figures

A key performance figure for solar thermal energy systems is the solar fraction f_s (Equation (17)), which gives the ratio of the energy supplied by STCs Q_s to the overall heat generation Q_{gen} . In the case of UTES systems, the storage utilization rate η_{st} is defined as the ratio of discharged energy Q_{disch} to the charged amount Q_{ch} (Equation (18)). Since UTES systems like BTES or ATES have no defined system boundary and can utilize ambient energy, this ratio can show values above one. Another key figure is the number of annual storage cycles N_{cyc} , which sets the discharged energy in relation to the maximum capacity of the storage Q_{cap} (Equation (19)). A value above one indicates that a UTES system is not only used for seasonal storage, but for diurnal storage as well.

$$f_s = \frac{Q_s}{Q_{gen}} \quad (17)$$

$$\eta_{st} = \frac{Q_{disch}}{Q_{ch}} \quad (18)$$

$$N_{cyc} = \frac{Q_{disch}}{Q_{cap}} \quad (19)$$

6.2 Analysis methods

Multi-criteria assessment of DH systems is often carried out using performance indicators regarding economic, environmental and energetic efficiency. However, on a system level, often only the first two are actual target numbers for optimization. A common approach for a holistic analysis of those target numbers is the method of LCA, which considers costs and environmental effects of components from cradle to grave. Application of the LCA method for economic and environmental assessment of SDH systems with BTES is presented in Welsch et al. (2018) and further application examples for dynamic system simulations as well as details of the method are given in Appendix C and D.

A method, which can give additional insights into the performance of thermal energy systems, is the analysis of exergetic efficiency (Falk, 2018). In contrast to a conventional energetic analysis, it considers not only the amount of thermal energy flows of a system, but the temperature levels as well. This concept is especially useful in the case of SDH-UTES systems, as the efficiency of STCs and UTES technologies varies strongly with regard to the temperature level they are operated on. Accordingly, exergetic analysis can give a more detailed insight on the efficient contribution of each component to the final use for heating and localize potential for improvement. However, the exergy content of a thermal energy flow is a relative number, depending on a defined reference temperature and can therefore give no absolute answers. Consequently, exergetic efficiency can be regarded as a factor contributing to the actual numbers of interest, which are usually the specific costs and environmental burdens related to the supply of thermal energy. Examples for the application of exergetic analysis are given in Appendix C and Chapter 6.4.

6.3 Optimization methods

Optimization of SDH-UTES systems poses a challenging task, as it constitutes a non-linear optimization problem depending on a multitude of variables and constraints. Consequently, optimization of such dynamic systems usually starts with the definition of reasonable assumptions for many of those variables, reducing the problem to the key variables. A further reduction of the optimized variables can be achieved by dimensional analysis, identifying the actual core of the problem under investigation and utilizing similarities of the system (Spurk, 1992; Pelz, 2011). This method has been used excessively for the analysis of BTES systems in the past, where it is known under the name of “g-functions”, giving a dimensionless response function to a heat extraction/injection pulse for BHE arrays (Claesson and Eskilson, 1988). In the context of SDH-UTES however, this method has not been applied so far. In future research its application should be considered, as it has a significant potential to reduce the number of optimization variables and give results with a higher generality.

Another approach for tackling the high complexity of optimization of SDH systems, is the incorporation of proxy models, which serve as intermediate level between the dynamic system simulations used for the evaluation of the performance and the optimization algorithm (Schulte et al., 2016a). These proxy models are created, calibrated and validated by training simulation runs of the dynamic system model and give a relation between the optimization variable inputs and the target function value. For problems with a manageable number of inputs, these proxy models can be accurately defined by polynomial functions (Schulte et al., 2016a). For more complex problems with a less clear input-output correlation ANN can be used. The actual optimization algorithm is then applied on the ANN proxy models rather than the actual dynamic system model. Application of such an approach for SDH systems with UTES and demonstration of their ability to significantly reduce the computational effort is given in Appendix F.

7 Application of MoSDH

7.1 Simulation of the Brødstrup Solar District Heating system

The Brødstrup SDH system is operated by Brødstrup Fjernvarme and supplies around 1,450 households with 37 to 42 GWh of heat annually (Schmidt, 2019). Two STC fields of 8,000 m² and 10,600 m² supply around 20% of the annual heat which is delivered to the DH system. Daily imbalances of solar supply and heat demand are compensated by two buffer storages of 5,500 m³ and 2,000 m³, whereas a BTES is used for seasonal storage of solar heat. During summer, the two buffer tanks are operated in series and act as one big buffer. During winter, a 1.2 MW_{th} heat pump is operated between the two buffer tanks and heats up the larger one while cooling down the smaller buffer down to 10 °C, for discharging of the BTES. The BTES consists of 48 BHEs of 45 m each, connected in series to strings of 6 and taps into a storage volume of around 19,000 m³ of soil. The solar system is complemented by two CHP units with a thermal power of 4.1 MW each and an electric boiler of 10 MW_{th} (Jensen et al., 2016). Depending on the current solar production, heat demand and electricity market prices, the SDH system can feed electricity generated by the CHP units into the power grid or convert electricity from the grid to heat using the electric boiler. The remaining heat demand, which corresponds to 45-60% of the annual demand, is covered by heat from natural gas boilers (13 MW_{th} + 10 MW_{th}). Monitoring data from the commissioning of the system in May 2012 to the end of 2016 is used for the validation of the system model.

Model setup

The overall model of the SDH-UTES system in Brødstrup is shown in Figure 27. Model boundaries include generation, storage and distribution of the thermal energy, but exclude a detailed modelling of the consumer side. System layout and component dimensions were derived from literature, PI (piping and instrumentation) diagrams and information from the plant operators and designers. Wherever possible, models are parametrized using information which would be available during the stage of system design. However, for some components no such data existed and monitoring data was used to derive parametrization. An overview of the component parametrization and the used input data is given in Appendix G and a detailed description of the used BTES model is presented in Appendix B. For the cases where no literature data was available for parametrization, a short description of the process is given in the following. The raw monitoring data has a temporal discretization of 5 min, but was aggregated to hourly values.

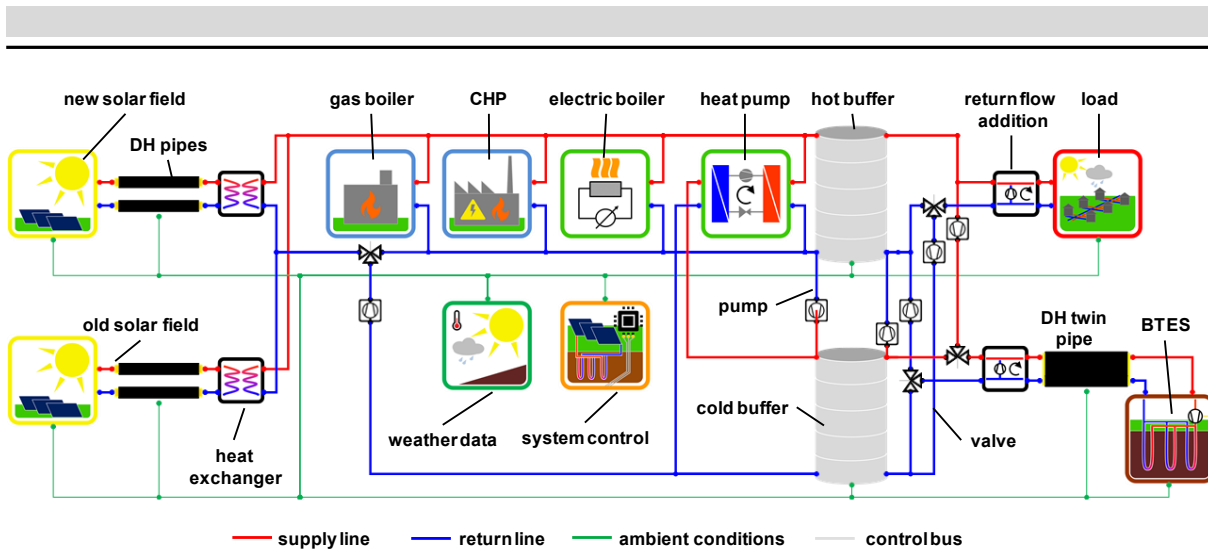


Figure 27: System model of the Brædstrup SDH system for validation of the MoSDH model components.

Since the selection of heat sources is not only defined by the state of the SDH system, but uses data from the power grid and weather forecasts as well, the actual system control strategy could not be reproduced. Therefore, operation times of the CHP and the electric boiler models were defined by the operating times from the monitoring data. Furthermore, it was not possible to deduce control strategies of the BTES and the heat pump, as those were operated variable to test different operation modes. Hence, the volume flow through the BTES model was defined by the monitoring data and the heat pump was controlled to cool down the cold buffer model down to the level of the monitored temperatures. However, during short periods of time, the heat pump was operated, even though the BTES was charged from the hot buffer and the DH return flow was fed into the cold buffer. As the DH grid return acts as the heat pump's source for such an operation and no ambient energy is obtained outside of the system boundaries, the heat pump basically acts as an electric heater. However, this mode of operation was difficult to reproduce as well, since the monitoring data includes no information about the state of valves or pumps and consequently the actual flow paths could not be deduced during all periods.

As there are two separate collector fields, for which monitoring data is given separately, two such components are used in the system model as well. They are connected to the system via pre-insulated DH pipes and heat exchangers. Based on map data, the length of the transmission lines was estimated to 160 m for the smaller field and to 650 m for the larger field. The models were parametrized according to DN200/355 (diamètre nominal) pre-insulated pipes. Actual sizes of the heat exchangers were not known and therefore estimated using the nominal operation points of the collector fields as well as a typical heat transfer coefficient for flat plate heat exchangers of $1,000 \text{ W}/(\text{m}^2 \cdot \text{K})$ (VDI, 2013). The MoSDH collector models usually take diffuse and direct irradiation as well as ambient temperature as input data from the weather component. From the current position of the sun and the collector field geometry, the fraction of the collectors which is shaded by a neighboring row can be calculated. This shading factor can be used to calculate the amount of direct irradiation on collectors, but has no effect on the diffuse irradiation (cf. Chapter 4.3.1.). Common weather datasets include direct irradiation measured on a horizontal surface or in beam direction (BBSR, 2017; NREL, 2020). However, as the Brædstrup monitoring data only includes measurements for the total irradiation on a tilted surface, i.e. no distinction between direct and diffuse parts, the STC field component and the weather data component had to be extended for the use of such input data. Calculation of the

impact of shading however, is impaired, as the shading factor was applied to the total irradiation, wrongly reducing the actual diffuse irradiation on the collectors. However, this approach is expected to be more accurate than neglecting the effect of shading overall.

The heat pump model takes performance curves for the load side thermal power and the COP in dependence of evaporator and condenser fluid temperatures as input data. Since no catalogue data of the required inputs is available, monitoring data was used to create performance maps for the heating power and COP of the heat pump by regression analysis (Figure 28). Data of the condenser outlet temperature, the evaporator inlet temperature, the heating power and the COP with a temporal discretization of 5 minutes was used. The maximum monitored heating power amounted to 1,000 kW and a large number of datapoints showed exactly this value, independent of the corresponding condenser and evaporator temperatures. Since this indicates a sensor error, those points were excluded from the data. After further filtering for values within the range of operation given by the manufacturer of the heat pump, the final size of the dataset amounted to 28,354 data points.

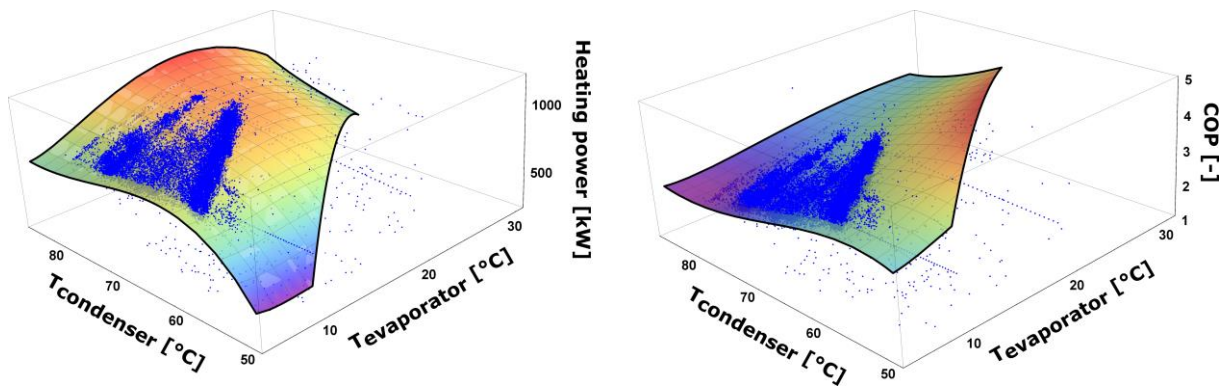


Figure 28: Monitoring data (blue) and generated performance maps for the heat pump power and COP.

Figure 29 shows the correlation of monitored values and values calculated by the regression models. Overall, the scattering of the monitored values is rather high, which is probably due to effects related to dynamic operation of the heat pump. However, the R^2 values of both regression models indicate an adequate representation of the heat pump performance by the generated performance maps.

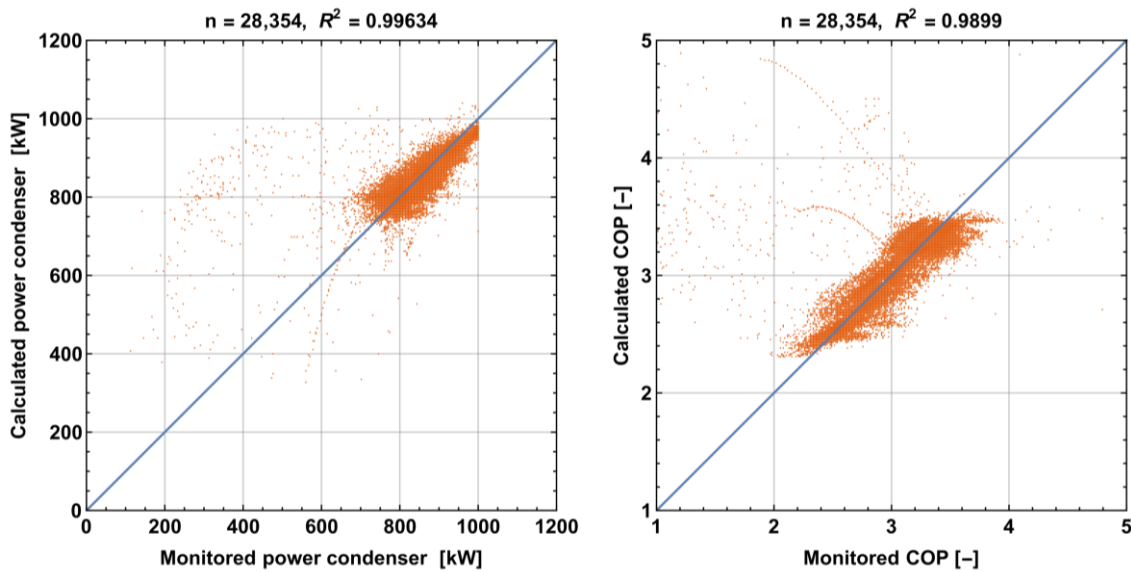


Figure 29: Monitored and calculated values for the heat pump power and COP.

Results

Figure 30 shows the overall energy budget of the system components. For monitoring, the sum of heat generation amounts to 146.5 GWh while the heat delivered to the DH grid amounts to 181.9 GWh. Consequently, the monitored heat generation is at least 35.4 GWh below the actual value. This is probably mainly caused by missing data from one of the gas boilers, which showed no operation during most of the monitored period. Accordingly, the simulated heat generation of the gas boilers is around 41.7 GWh higher than the monitored value. However, components for both solar thermal fields and the electric boiler show a good agreement between simulated and monitored values, resulting in deviations of -2%, -1.4% and -1.8% respectively. In contrast to that, heat generation of the CHP model component significantly deviated from monitoring data by -10.2%. Since the reference thermal power of the CHP model component was set to the monitored thermal power, but the component was deactivated if the hot buffer storage was completely filled, this deviation is expected to be caused by the overall system control, rather than the actual model component's accuracy.

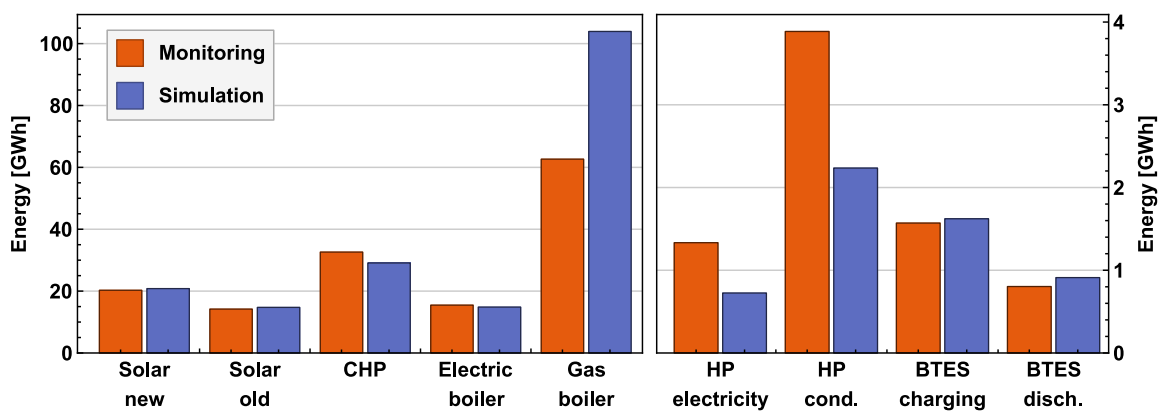


Figure 30: Monitored and simulated energy budgets of the components of the Brødstrup SDH system for the period May 2012 to December 2016.

The thermal budget of the BTES component shows a good agreement to the monitored values for charging with a deviation of 4%, whereas this value amounts to 14.1% for discharging. However, a comparison of the overall values is not very meaningful, since a closer look at the budget of each year of operation reveals a much different picture, with a maximum deviation of 44.4% for discharging in 2015 (Table 5). Parametrization of the model was carried out according to a parameter estimation study in which a 3D FEM model was parametrized to fit monitored ground temperatures within the first 500 day of operation (Tordrup et al., 2017). The overall deviation of the BTES energy budget amounted to 4.0% for the fitted model. Accordingly, the simulation results using the MoSDH model show very low deviations to the monitoring data for charging (2012: -1.6%, 2013: 2.9%) and discharging (1.9%, 0.8%) in the first two years. A good fit for the subsequent years could not be achieved, even with a 3D FEM model in FEFLOW, set up according to the above-mentioned parameter estimation study. A definite conclusion about the origin of these deviations is not possible, but probable causes are the neglect of natural convection in unsaturated soil, precipitation and groundwater flow processes, as the storage is located at a location with several sandy layers (Sørensen et al., 2013). Finally, a comparison of the heat pump simulation results to the monitoring data, reveals significant deviations, which is most likely caused by the previously mentioned operation of the heat pump as electric heater between DH return and supply, which could not be reproduced.

Table 5: Annual monitoring (m) and simulation (s) results for the Braedstrup SDH system in MWh, with deviations above 10% marked in red.

| | 2012 | 2013 | 2014 | 2015 | 2016 | |
|-------------------------|-----------------|-----------------|-----------------|-----------------|-----------------|---|
| DH supply | 22,963.1 | 41,722.7 | 36,969.3 | 39,258.9 | 40,965.2 | m |
| | 22,963.1 | 41,722.7 | 36,969.3 | 39,258.9 | 40,965.2 | s |
| Solar field (old) | 2,216.7 | 3,099.4 | 2,895.2 | 2,947.5 | 487.3 | m |
| | 2,243.4 | 3,172.8 | 3,068.6 | 3,193.7 | 3,056.5 | s |
| Solar field (new) | 3,385.7 | 4,583.4 | 4,770.2 | 4,688.9 | 4,340.3 | m |
| | 3,166.9 | 4,489.4 | 4,344.8 | 4,498.2 | 4,311.4 | s |
| CHP | 6,618.0 | 9,231.2 | 5,327.5 | 3,953.6 | 7,486.3 | m |
| | 5,559.7 | 8,370.6 | 4,844.0 | 3,623.1 | 6,697.7 | s |
| Electric boiler thermal | 1,822.5 | 1,787.8 | 1,899.5 | 6,417.7 | 3,538.8 | m |
| | 1,724.1 | 1,776.8 | 1,790.4 | 6,036.3 | 3,510.0 | s |
| Natural gas boiler | 23.0 | 8,246.0 | 18,979.1 | 16,845.0 | 18,561.0 | m |
| | 10,650.1 | 24,279.2 | 23,083.3 | 22,236.2 | 23,672.6 | s |
| BTES charging | 434.1 | 400.8 | 337.4 | 274.4 | 123.6 | m |
| | 426.5 | 412.3 | 347.0 | 314.7 | 121.8 | s |
| BTES discharging | 129.4 | 181.8 | 275.3 | 137.9 | 78.8 | m |
| | 131.3 | 195.5 | 284.6 | 196.8 | 102.9 | s |
| Heat pump thermal | 266.9 | 500.4 | 1,011.4 | 1,542.2 | 565.1 | m |
| | 291.6 | 466.4 | 751.6 | 467.7 | 258.0 | s |
| Heat pump electricity | 90.3 | 186.9 | 369.0 | 497.9 | 188.8 | m |
| | 95.6 | 157.9 | 256.3 | 137.9 | 77.0 | s |
| Heat pump SPF | 2.96 | 2.68 | 2.74 | 3.10 | 2.99 | m |
| | 3.05 | 2.95 | 2.93 | 3.39 | 3.35 | s |

It can be concluded, that reproduction of the Brødstrup monitoring data is a difficult task. To get a better picture on the actual accuracy of the system model, additional monitoring data about the operation of the plant would be required and data should be complete. Especially in the case of the natural gas boiler where data was missing over longer periods and the heat pump, where the power apparently exceeded the maximum value of the sensor, a meaningful comparison between simulated and monitored values is not possible. Consequently, simulation of these two components showed the largest deviations to monitoring data. In the case of the BTES, co-simulation with a detailed FEM model and consideration of convective processes could result in better results. However, this would require additional data about ground water conditions, precipitation and soil humidity. In contrast to those difficulties, validation of both STC fields turned out successful, with a maximum annual deviation to the monitoring data of -4.2% for both components. Considering the previously mentioned inaccuracies in calculation of the collector shading an underestimation of the solar yield seems reasonable and the model accuracy is considered to be sufficiently accurate.

7.2 Simulation of an SDH system with dynamic dimensions, layouts and boundary conditions

A numerical case study was carried out, to investigate the transition process of an existing DH grid towards an SDH system with medium-deep BTES (Appendix D). The time frame of the study ranged from 2025 to 2050 and consequently dynamic boundary conditions such as energy prices or power grid emission factors were considered. Different strategies regarding the construction and decommissioning of system components were compared. The dynamic nature of the study necessitated a system model with variable dimensions and layouts, which required adaptations to the models of the MoSDH library. However, due to the flexibility of Modelica models such an adaption was possible with little modelling effort. The number of STC rows in parallel, which is usually a parameter, was changed to a variable, to be able to adapt the size of the field at any time during simulation. Since the buffer storage volume was defined in relation to the STC, the corresponding parameter had to be changed to a variable as well. Furthermore, the BTES model was adapted to individually control the volume flow through each section of the BTES, facilitating the operation of 19 or 37 BHEs. Consequently, an expansion of the storage dimensions could be emulated during operation.

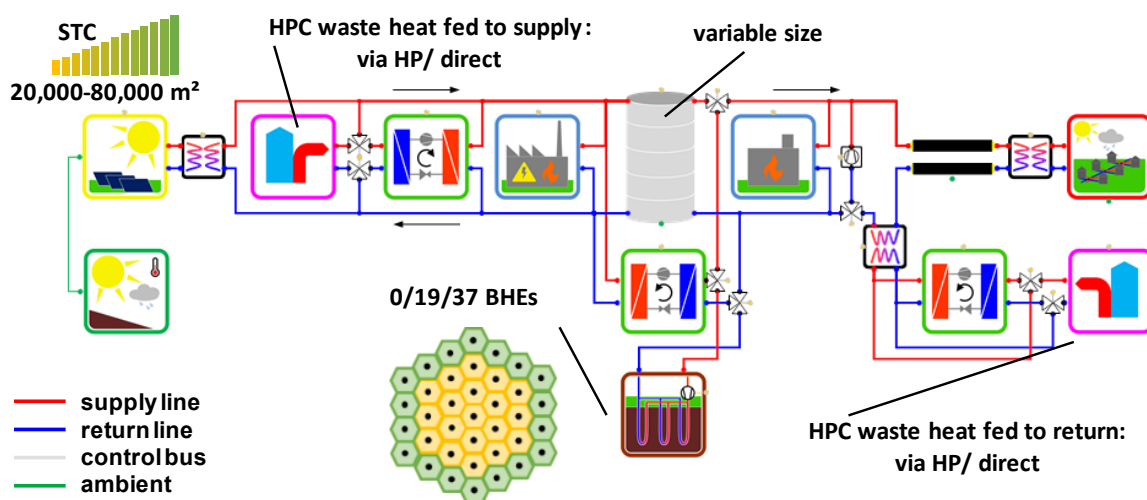


Figure 31: Model diagram for the transition strategy.

The study concluded that a gradual transition strategy can satisfy the targeted emission saving goals in the most economical way. A construction of the full-sized system in 2025 or 2030, resulted in overall higher costs, whereas none of the investigated systems which did not include solar thermal energy from 2025 onwards succeeded in satisfying the emission reduction targets.

Regarding the application of MoSDH, the study demonstrated the capabilities of adapting the existing components to meet very specific requirements. The object-oriented structure of the models and the equation-based concept of Modelica, simplified this process and enabled the non-standard approach of time-varying component dimensions.

7.3 Validation of the District Heating Pipes model

To verify the plausibility and correct implementation of the DH pipe models, specific heat losses and pressure losses are compared to values from manufacturer data (isoplus, 2020). First one being only available for the case of two buried pipes, but since the twin pipe model is conceptually more detailed, results are expected to be at least as accurate as for the two pipes model. A simple test model consisting of the *DistrictHeatingPipes* model, two pumps and a weather data component is set up (Figure 32) and simulated over one year to assess heat losses for steady state conditions. According to the boundary conditions mentioned in the manufacturer datasheet, the initial ground and surface temperatures are set to 10 °C. For the medium pipe dimensions DN150, DN200 and DN250 are considered, with three insulation thickness options each. Depth and axial distance of the pipes are varied for each option according to the recommended values from the datasheet. The volume flow rate is set to the mean value of the operational range which is recommended to result in a pressure drop of 60 – 80 Pa/m. Furthermore, the supply and return line temperatures are varied between 80 – 120 °C and 40 – 80 °C respectively.

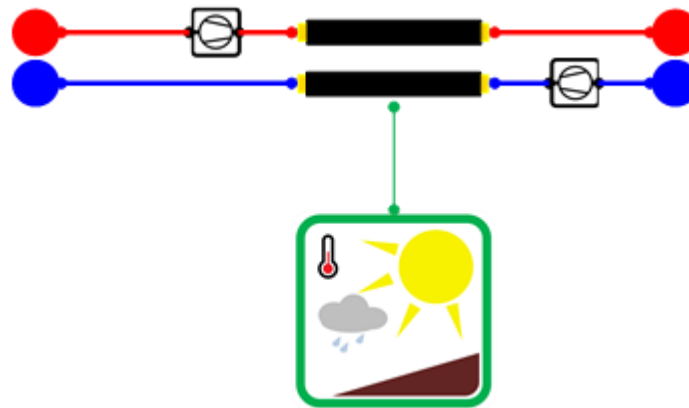


Figure 32: Model setup for the validation of the DH pipe model.

The resulting specific heat losses per meter of DH line (supply and return) are shown in Figure 33, Figure 34 and Figure 35. The maximum deviation between the simulated values and the values from manufacturer data can be observed for the DN150/315 pipes (double reinforced insulation) and amounts to 4.1%. The root mean square error for all options amounts to 2.44%, indicating plausible values regarding heat losses calculated by the *DistrictHeatingPipes* model.

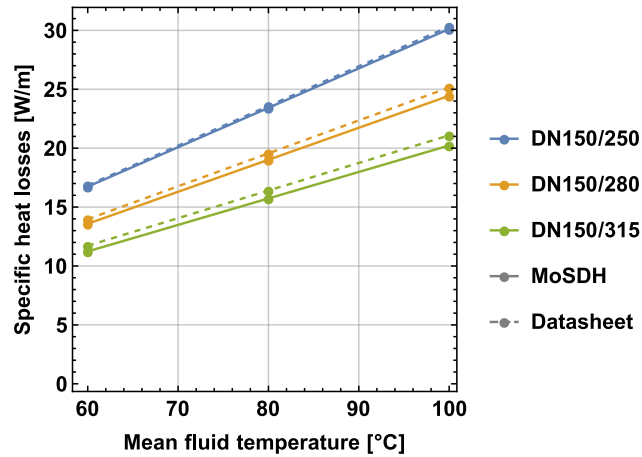


Figure 33: Specific heat losses for pre-insulated district heating pipes with a DN150 medium pipe and different diameters of the casing from simulations with MoSDH and manufacturer's data.

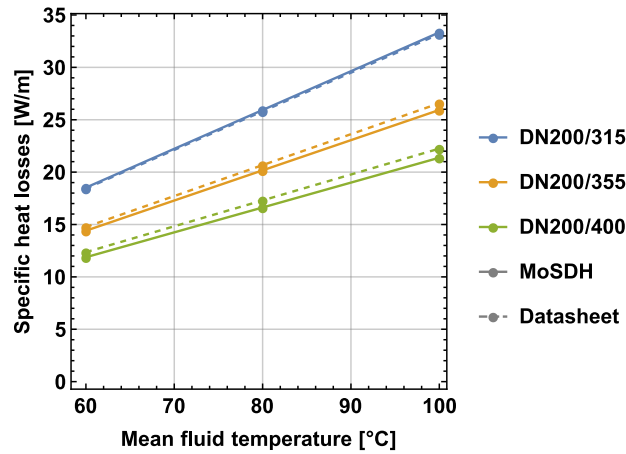


Figure 34: Specific heat losses for pre-insulated district heating pipes with a DN200 medium pipe and different diameters of the casing from simulations with MoSDH and manufacturer's data.

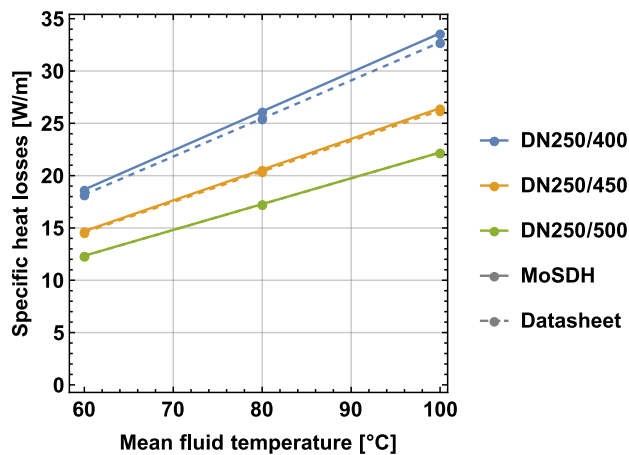


Figure 35: Specific heat losses for pre-insulated district heating pipes with a DN250 medium pipe and different diameters of the casing from simulations with MoSDH and manufacturer's data.

Pressure loss calculation of the DH pipe models is carried out according to Chapter 4.1. For volume flow rates within the recommended operational range, a pressure loss of 60-80 Pa/m is given by manufacturer data. For comparison, the mean value of the recommended flow range

was chosen for simulation, which resulted in pressure drops of 72.0 Pa/m, 72.8 Pa/m and 67.7 Pa/m for the DN150, DN200 and DN250 models respectively. Consequently, calculation of the DH pipe models is considered accurate.

7.4 Simulation of a DH grid ring network

A common layout of DH grids are ring networks. These have a main distribution ring from which sub-strings branch off to individual buildings and sub-networks. According to the current heat demand of the connected buildings, the flow direction can change in certain sections of the ring. One strength of acausal pipe models is their ability to consider such a reversal of flow. To test the DH pipe models from the MoSDH library in this regard, a generic model of a ring network was used (MoSDH.Examples.ExampleCHPgrid, Figure 36).

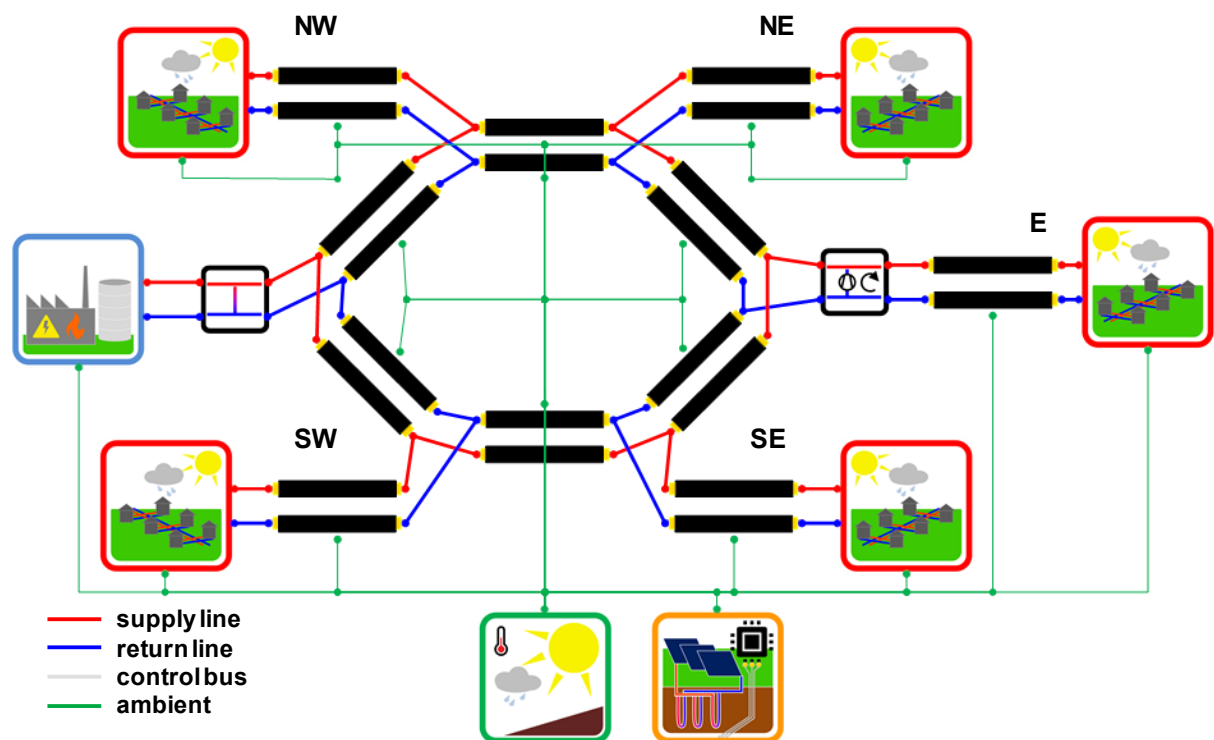


Figure 36: Diagram view of the ring grid example model.

The heat demand is supplied by a central thermal power plant (see Chapter 4.3), consisting of 3 CHP units with 2 MW_{th} each, a gas boiler with a peak power of 10 MW_{th} and a buffer storage of 500 m³ to increase run-times of the CHP units. Five load components are placed along the grid, four of them with an identical load curve with a total demand of 5 GWh/a and one with a demand of 25 GWh/a (NE = North-East). The supply temperature is varied according to the ambient temperature between 85-110 °C, with a return temperature of 65 °C. The supply temperature of the grid branch in the East is lowered by mixing of the return flow into the supply line to be 10 K below the overall supply temperature (Figure 37). Each load component draws fluid from the supply line to meet its demand and the reference return temperature. The ring has a total length of 6 km and consists of pre-insulated DH pipes with DN250 medium pipes, while each transmission line to individual load components has a length of 500 m using DN150 medium pipes. Each DH pipes model uses 5 pipe segments and all additional DH line parameters were set according to the example models from Chapter 6.3 using the smallest insulation thickness option. No overall system control strategy is necessary, as the control of the thermal plant

was defined to meet the volume flow rate drawn from the grid at the defined supply temperature. One year of operation was simulated, which took 68.7 s.

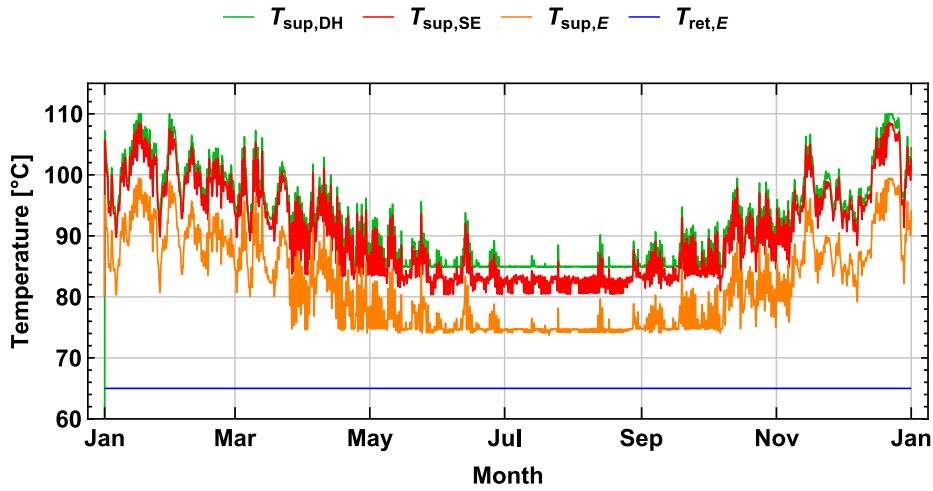


Figure 37: Selected supply and return temperatures of heat demand components.

The temporal distribution of heat demand and generation over the simulated year can be seen in Figure 38. As the heat load profile of the four components besides the north-eastern is identical, only one curve is plotted. While their combined heat demand of 20 GWh/a is lower than the heat demand of the NE load component in total, it is higher during summer. This was deliberately chosen, to provoke changing flow regimes over the duration of the simulation. Furthermore, it can be seen, that the CHP units can meet the total heat demand during summer, but have to be supported by the gas boiler from October to May. Overall, 77.4% of the heat demand is supplied by the CHP units and thermal losses from the grid amount to 8.3% of the total generated heat.

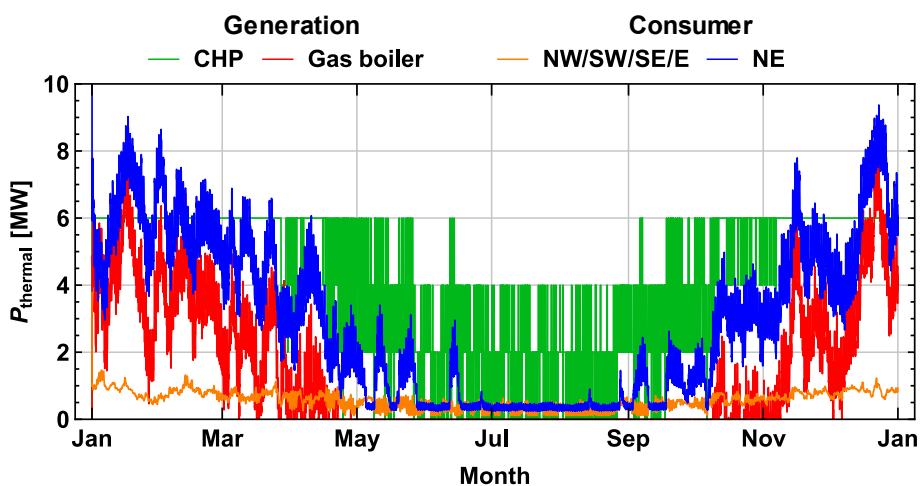


Figure 38: Thermal power of the power plant and heat demand components.

Figure 39 shows volume flow rates for selected sections of the DH network. It can be seen, that the direction of flow changes for the NE section of the ring grid, with negative values indicating a counter-clock flow direction in the supply line. Since all ring segments have the same dimensions and the load of the NE load is higher than the remaining loads combined during winter,

while it is lower during summer, the resulting flow direction in the NE ring segment is consistent.

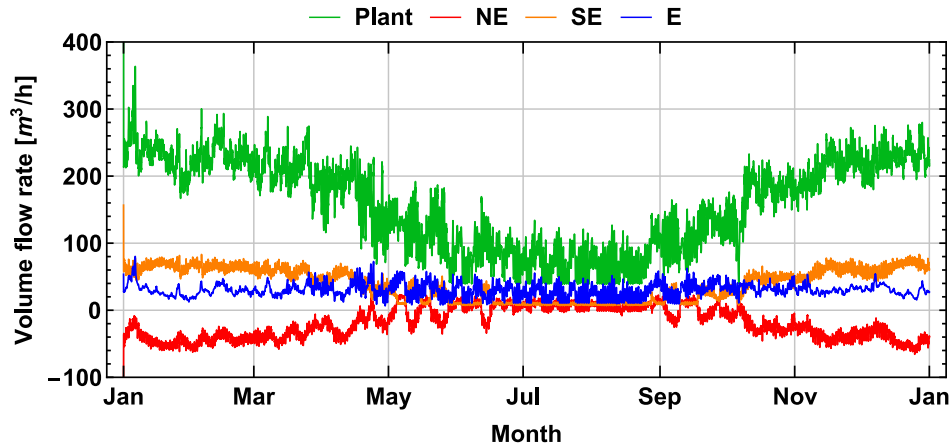


Figure 39: Volume flow rates of the thermal power plant and within selected pipe sections of the ring network.

The presented example demonstrates the capability of MoSDH to consider meshed DH grids. While more efficient DH models exist, which are dedicated to DH grid simulations (del Hoyo Arce et al., 2018), the time of 68.7 s for the simulation of one year implies that it is generally feasible to simulate more complex grid models as well.

7.5 Exergetic optimization of BHE design and operation of a medium-deep Borehole Thermal Energy Storage

Besides the dimensioning of the system components, their specific design and operation is another important objective of dynamic simulations. As the complexity of an optimization of the overall system in regards to dimensioning, operation and the specific components design on a high level of detail would exceed the capabilities of even sophisticated optimization methods such as ANN proxy methods (cf. Chapter 5), reasonable assumptions have to be made for certain parameters and inputs. However, if the overall design of the system has been optimized, certain aspects can be considered in greater detail to further improve performance. If large improvements can be achieved, it might be necessary to repeat the original system optimization with the updated configuration. As an example application of such a detail study using MoSDH, the BHE design and operation of a medium-deep BTES system is exergetically optimized. The overall dimensions, such as number and length of BHEs as well as charging temperature and volume flow rate, are considered as constant. Figure 40 (left) shows a schematic cross section through the medium-deep BTES system, which consists of 19 BHEs with a length of 750 m each. The upper lithological layer shall be soil with a thermal conductivity of 1.5 W/(m.K), while the lower layer represents the crystalline bedrock with a respective value of 2.65 W/(m.K). The storage of heat is supposed to be predominantly located in the crystalline to conserve groundwater resources in shallow aquifers (Welsch et al., 2016). Accordingly, the upper sections of the BHEs use a grout with a thermal conductivity which is reduced from 1.5 W/(m.K) to 0.5 W/(m.K). Charging of the storage is done with a constant temperature of 70 °C and a flow rate of 1 l/s per BHE, while discharging conditions are subject to optimization. Each phase takes 6 months and a total of 25 years are simulated. For further details of the study see Appendix G.

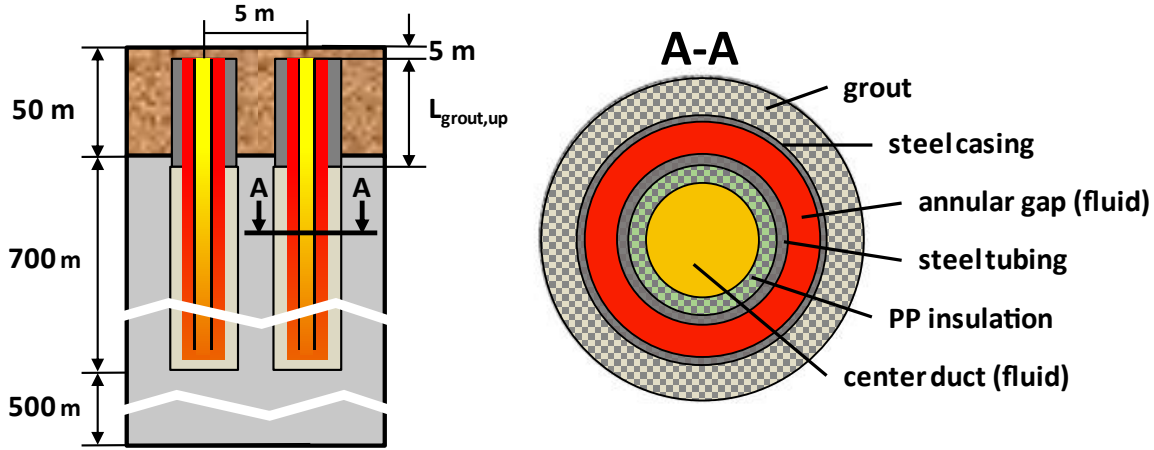


Figure 40: Schematic setup of the storage model for the optimization study. Left: cross section of the subsurface and the BHEs. Right: cross section of the BHE design.

A coaxial design of the BHEs is used (Figure 40 right), with an additional Poly Propylene insulation layer within the inner tubing, to reduce the thermal short-circuit between the inner and outer duct (Handke et al., 2019). This effect is rather small for shallow BHEs for heat extraction, as the temperature difference of the downward and upward duct is usually rather small. For the considered medium-deep BTES concept for high temperature storage however, a charging temperature of 70 °C is defined, which, in combination with the large contact surface, would result in a much stronger short-circuit effect. Accordingly, the insulation is crucial for transporting the high temperature heat to the desired depths of the storage, rather than transferring it to the return fluid stream of the BTES. As an opposing effect, however, an increased insulation layer will reduce the inner cross section and result in a higher pressure drop and ultimately an increased electricity demand of the circulation pump. As the BHE model from MoSDH only considers a single inner pipe, a thermal conductivity λ_{model} is calculated, corresponding to the serial connection of the thermal resistance of the steel tubing and the PP insulation. Equation (20) gives the resulting effective thermal conductivity of the model, which is obtained by addition of the resistance of two concentric cylinders, one with the dimensions of the tubing and one with the dimensions of the PP insulation.

$$\lambda_{model} = \frac{\lambda_{PP} \lambda_{steel} \log\left(\frac{r_{o,tubing}}{r_{i,tubing} - t_{PP}}\right)}{\lambda_{PP} \log\left(\frac{r_{o,tubing}}{r_{i,tubing}}\right) + \lambda_{steel} \log\left(\frac{r_{i,tubing}}{r_{i,tubing} - t_{PP}}\right)} \quad (20)$$

Recent studies suggest the use of grout with a reduced thermal conductivity in the upper section of BTES systems to lower thermal losses to the surface and maximize extracted energy (Schulte et al., 2016c). This approach however, results in a reduced useful borehole length as well as a smaller effective storage volume and therefore additional investigation is required to identify the optimal length of the insulated section. Furthermore, the amount of extracted energy is strongly influenced by the inlet temperature level and flow rate during discharging. In general, lower temperatures and higher flow rates will continuously increase this amount, but the extracted energy will be on a lower temperature level. Hence, an exergetic optimization approach is used in this example study, which considers the usefulness of the discharged energy as well as the demand for electricity in a single budget and consequently gives an optimum combination for the described trade-off problems. Calculation of exergy values is carried out after Appendix C

with the reference temperature $T_{\text{ref,ex}}$ being set to a sinusoidal signal with a mean value of 10 °C and an amplitude of 10 K (Figure 41).

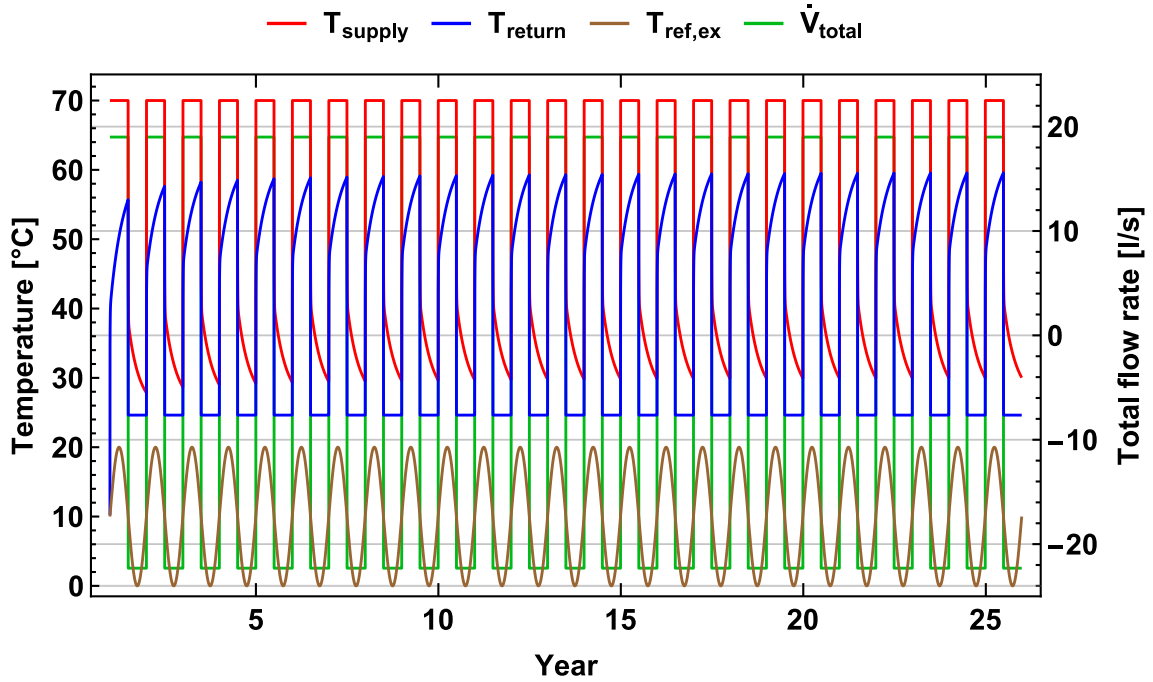


Figure 41: Supply, return and exergy reference temperature as well as volume flow rate of the optimal system.

The net discharged amount of exergy $Ex_{\text{disch,net}}$, i.e. the amount of discharged exergy subtracted by the required pump electricity, is defined as optimization target. The chosen constraints can be seen in Equations (22-25), where T_{disch} is the inlet temperature during discharging, \dot{V}_{disch} the respective volume flow rate per BHE, t_{ins} the thickness of the insulation layer and $L_{\text{grout,up}}$ the length of the upper grout section.

$$\max Ex_{\text{disch,net}}(T_{\text{disch}}, \dot{V}_{\text{disch}}, t_{\text{ins}}, L_{\text{grout,up}}) \quad (21)$$

$$\text{subject to } 1 \text{ } ^\circ\text{C} \leq T_{\text{disch}} \leq 45 \text{ } ^\circ\text{C} \quad (22)$$

$$0.1 \text{ l/s} \leq \dot{V}_{\text{disch}} \leq 4 \text{ l/s} \quad (23)$$

$$2 \text{ mm} \leq t_{\text{ins}} \leq 40 \text{ mm}, t_{\text{ins}} \in \mathbb{N} \quad (24)$$

$$10 \text{ m} \leq L_{\text{grout,up}} \leq 100 \text{ m}, L_{\text{grout,up}} \in \mathbb{N} \quad (25)$$

Optimization is carried out using the NMinimize function of Mathematica (Wolfram Research, 2021a). The Nelder-Mead Method is chosen (Nelder and Mead, 1965), a direct search method for nonlinear optimization, often called simplex-method. The optimization algorithm succeeds in locating a maximum after 3,576 s and a total of 50 simulation runs. The average time for a single run amounts to 70.1 s, of which 53.6 s are required for the translation and compilation process and 16.5 s for the actual simulation. A repeated translation process is necessary, since $L_{\text{grout,up}}$ is a structural parameter that affects the model's mesh. Changes of free parameters, such as T_{disch} and \dot{V}_{disch} , would not require a repeated translation process. While the relative amount of the translation process varies significantly between different models, the presented study demonstrates the important distinction between structural and free parameters.

Figure 42 shows the evolution of the target function and the input variables during execution of the optimization algorithm. The maximum discharged exergy after 50 iterations amounts to 311.1 MWh/a and is achieved by a discharging temperature of 24.6 °C, a respective flow rate of 1.17 l/s, an insulation thickness of 23 mm and a length of the upper grout section of 31 m. For certain combinations of parameters, negative values for the net extracted exergy are possible. In the case of the sixth iteration, the combination of a narrow hydraulic diameter of the inner duct (36.9 mm) and a high volume flow rate per BHE (2.84 l/s), the exergy required for operation of the circulation pump exceeds the extracted exergy. Under these circumstances, it would be favorable to convert the used electricity directly to heat using a heating rod, rather than operating the BTES.

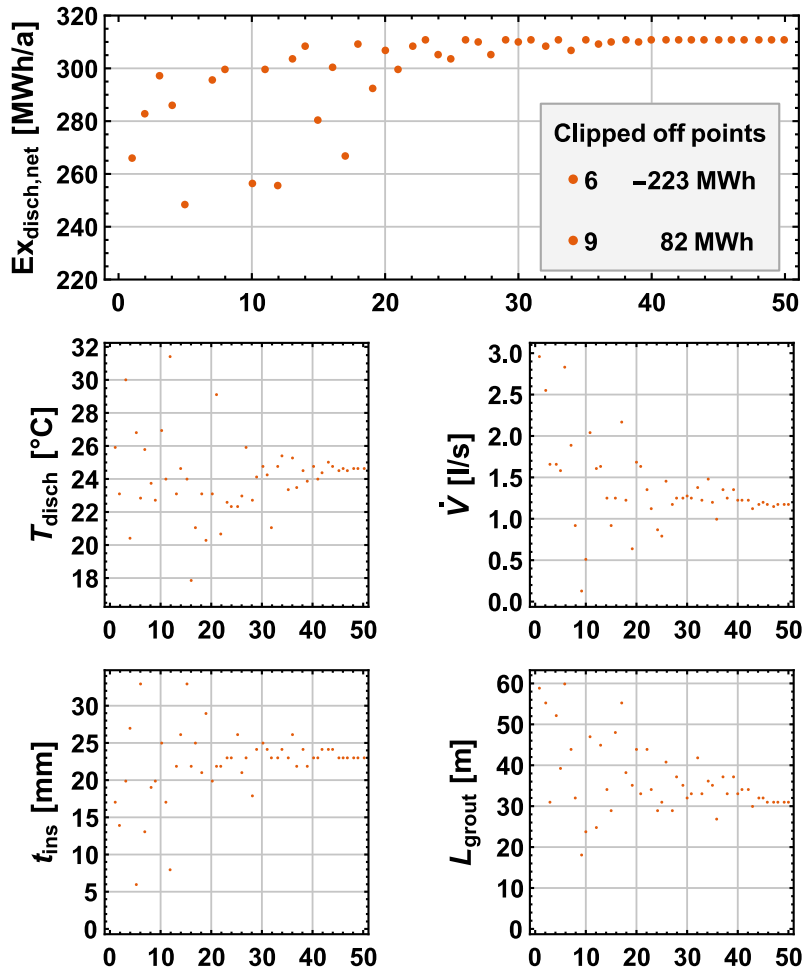


Figure 42: Evolution of the optimization variables and target function over the iterations of the optimization algorithm.

The presented optimization study serves as an example for the abilities of Modelica and MoSDH to carry out certain detail studies. The use of the physical multi-domain approach facilitates the joint consideration of interdependent aspects, like temperature levels, pressure loss and electricity demand.

In this specific case, further aspects should be considered for the design of actual systems. From an environmental point of view, it might be favorable to use an insulating grout over the whole length of the upper soil layer for protection of groundwater resources. A comprehensive study should furthermore consider the cost of exergy, as the used electricity might be associated with higher costs than the exergetic content of the thermal energy. Furthermore, the material price

of the insulation was not considered. For a comprehensive investigation, these aspects should be included in future studies.

Overall, the presented exergetic analysis approach allows for additional insight into the underlying trade-off problem of the case study in comparison to an energetic analysis. For optimization, the target variable was deliberately chosen to be the magnitude of the exergetic output, rather than the exergetic efficiency, as efficiency on its own is only an intermediate goal. Especially in the case of renewable exergy inputs to an energy system, efficiency further loses meaning, as inputs are virtually inexhaustible. Consequently, the low exergetic efficiency of e.g. converting solar irradiation into thermal energy is much less critical than conversion of electric energy into low temperature thermal energy. Therefore, exergetic analysis on a system level should be accompanied by further aspects like economic and environmental figures, as presented in Appendix C.



8 Discussion and Conclusion

Solar District Heating with Underground Thermal Energy Storage is an essential part of most pathways for the transition of the heating sector towards more sustainable energy systems, as it is a promising technology with a high level of maturity. While recently realized systems highlight these potentials, they also disclose existing barriers and necessary future developments. Therefore, the further rollout of this technology is not a straight forward process. Besides necessary developments on regulatory frameworks and material aspects, an accurate design process is key for their efficient and sustainable operation. As SDH-UTES systems constitute strongly interconnected energy networks, this design process should be carried out on a system level and sophisticated models are required to accurately predict component performances.

While the modelling language Modelica is already predominantly used in academia, as it is considered to be conceptually powerful and well suited to tackle the complexities of interconnected smart energy systems, it has not gained the same status for design engineers of SDH systems yet. A major cause for this disparity, is the level of detail, which is often too high, especially since many model libraries are dedicated for building performance simulations first and district energy systems only second. Application of these libraries consequently results in complex system models, which complicates the modelling process and impairs robustness. Furthermore, existing model libraries so far lack UTES models. Consequently, main goals behind the development of a dedicated SDH-UTES model library were to achieve a simple end-user modelling experience, while utilizing the functionalities of Modelica for flexible, physically well-founded and efficient models of such systems. For conceptual system modelling, efforts for creation of the physical model should be reduced to the required minimum, to free up capacities for the development of sophisticated control strategies or adaptations to the model components to incorporate new technological concepts.

The presented MoSDH library comprises such models for SDH-UTES systems by implementation of existing and proven model reduction approaches with the object-oriented modelling language Modelica, while aiming at a user experience as known from popular modelling environments, such as TRNSYS. Component models for system parts such as STCs, heat pumps or CHP plants are incorporated, using mostly simple and hence efficient and robust modelling approaches. The major novelty in comparison to existing libraries however, is constituted by the UTES components. These require a higher level of complexity for an accurate prediction of their performance and no equivalent models existed in Modelica so far. As specific UTES technologies, BTES and PTES components were implemented, as these are currently considered most often for SDH concepts and can be modeled more adequately in Modelica in comparison to ATES systems. However, this choice already limits the range of possible technologies and further UTES models should be added to support a more technology open system design process.

In several examples, the high reusability of Modelica models, which is achieved by the object-oriented or modular concept, could be demonstrated. Especially for the underground components, which require a higher development effort in comparison to the above-ground components, the use of ground elements for both BTES and PTES models or the reuse of BHE segments for modelling of the DH pipes, reduced the modelling effort significantly. In addition to that, the shared base classes for heat source components and the standardized component control structure proved to be practical. Firstly, the effort for initial model creation and adaptations to all models was reduced. Secondly, the homogeneous structure of the model control simplifies the use of the components, as they can be controlled in very similar ways. However, it should be

stated that the initial modelling effort for creation of consistent base classes and the assurance of tool independent models is significant. Especially latter one is an aspect in which the Modelica language standard should be improved. The fact that the language syntax is not defined in a too narrow way is an advantage, if only a single modelling and simulation environment is used, since several different ways exist, which result in the desired effect. However, these margins are not interpreted in the same way in every Modelica environment and consequently it is a difficult and sometimes impossible task to define a truly tool independent model. From the view point of tool developers, these differences might be interpreted as features. However, tool independent modelling is rightfully promoted as one of the major concepts and strengths of Modelica and should therefore be implemented without compromises. MoSDH was developed and successfully tested in SimulationX (ESI ITI, 2021), Dymola (Dassault Systèmes, 2020a) and OpenModelica (OpenModelica, 2021), but failed the test for Wolfram System Modeler (Wolfram Research, 2021b) so far. While it might be possible to find general tool independent ways of defining models, it is yet a tedious task and the language specification should be clarified concerning certain aspects to further promote robust tool independent modelling. However, since the Modelica language specification is still developed lively in a joint effort by tool vendors and users, it is possible, that this issue will be improved in the future.

An important aspect for the modelling of SDH-UTES systems is a good extendibility of models, since those systems are not standardized and often incorporate certain unique design features. The object-oriented modelling approach of Modelica proved to facilitate the easy adaption of models for certain innovative technological aspects or to specific requirements of a study and consequently so did MoSDH. The exergetic optimization study in Chapter 6.5 demonstrated the implementation of non-standard features, such as insulation of the inner BHE pipe or the use of different grouting materials within segments of the borehole. Further possibilities were demonstrated in Appendix D, where the definition of component dimensions was changed from parameters to discrete variables. The thereby gained possibility to adapt dimensions during runtime of the simulation was used to emulate construction and decommissioning of components. Such a feature would require for an introduction of separate model components for each construction stage within most simulation environments. In the case of the medium-deep BTES, certain regions of the BHE array were enabled or disabled according to the chosen dimensions. Consequently, the distribution of heat at the instant of an expansion of the BTES is not lost, since the underground model is not affected from the activation of additional BHEs. In the presented case, the described feature was used to emulate the construction of additional BHEs. However, the same approach could be used to facilitate the modelling of cascaded BTES systems, in which parts of the storage can be operated selectively - a feature which is repeatedly considered for smart BTES systems.

A further central concept of the modelling language Modelica is the acausal and equation-based definition of models, which is supposed to redirect the focus of the modelling process from numerical aspects towards the physical definition of the model behavior. Generally, Modelica tools incorporate a toolbox of sophisticated symbolic methods to automatically translate a model into efficient numerical code. Nevertheless, a basic understanding of this translation process, as described in Chapter 3.2, is highly recommended, as it can help to identify inefficiencies in the model and improve the model performance in certain cases. Although this understanding is highly recommended, it cannot be expected for the large majority of end-users and consequently model developers should focus on the development of easy to use and robust models. While MoSDH still shows several potentials for improvements, it has generally proven to be

well suited in this regard, as it has been successfully applied in teaching and student theses by students which were not familiar with Modelica.

A critical limitation of MoSDH for simulation of 4GDH systems is its set of implemented components. Even though it comprises the central components for simulation of SDH-UTES systems, it does not provide components which go beyond this very specific type of district energy systems. In general, the model components could be combined directly with components from other model libraries which are based on the MSL Thermal library or to virtually any Modelica model by the use of an interface. However, the MSL Thermal library is only used for a small number of libraries, whereas many libraries for thermal energy systems use the MSL Fluid library as basis. Consequently, a swap of the base models of MoSDH to the models from this library could facilitate an easier combination of MoSDH models with a large number of models from other libraries and significantly increase the number of potential users.

Simulation of the Brødstrup SDH system revealed, that the detailed reproduction of the operation of complex SDH systems is a difficult task, as a manifold of information is required, which is not always available. However, the example can be used to show that the modelling and simulation of such a system is possible with MoSDH and that the STC field model can reproduce the performance of real applications correctly. The long-time performance of the BTES system could not be reproduced accurately beyond the time-frame of the data used for parameter estimation. These deviations are expected to be caused by convective processes, that cannot be considered by the simplified modelling approach of the MoSDH BTES model. To consider the interaction of such UTES systems with significant convective processes and the DH system, the use of more detailed models is required.

A co-simulation methodology was presented, which allows for the coupled simulation of MoSDH models and FEM models in FEFLOW. The novel approach of positioning the coupling interface at the borehole wall and exchange of conductive process variables proved to be more robust compared to the previously applied convective approach. Furthermore, the consideration of the BHEs within Modelica allows for the use of physical pipe models and consequently facilitates the consideration of pressure drop calculation and arbitrary hydraulic connection schemes. While the methodology has already been applied for several case studies, the co-simulation of UTES FEM models and Modelica should be improved overall. Development of an interface for a specific combination of software tools is highly inefficient and should therefore be avoided. Instead, tool independent standards, such as the Functional Mockup Interface (Blockwitz et al., 2012) should be applied, as they can be used by a much wider range of simulation tools. Implementation of such an interface however, can only be done by tool developers directly and currently no such interface was implemented for 3D FEM tools for subsurface applications. The presented interface was therefore necessary to facilitate this kind of simulation, but the required programming effort should be viewed very critically.

As the use of co-simulation drastically increases the computational effort by the coupling of two separate solvers, the added effort should be compensated by an equally high gain of information. This is usually the case for systems with strong interactions between the UTES and SDH system, non-negligible convective processes and a sufficient data basis to model these processes. In many cases however, a detailed modelling of the subsurface is difficult due to a lack of sufficient geological and hydrogeological data. The computational effort of such a co-simulation approach is furthermore still too high to carry out extensive parameter studies, as required for

an initial dimensioning of SDH-UTES systems. Consequently, it is recommended to add co-simulations by a preceding standalone simulation study, to limit the range of parameters under investigation and subsequently use co-simulation for refinement, validation and assessment of environmental impacts.

In contrast to detailed studies, which are the recommended application for co-simulation, the conceptual design process of SDH-UTES systems requires a large number of simulations. Since many assumptions and boundary conditions of these systems are subject to considerable uncertainties, a too high level of detail is not useful during this stage, as the model can be expected to be “wrong” with a high certainty anyway. However, to increase the probability of an efficient operation of the system at the conceptual design stage, a system engineer should rather aim for a robust optimization, by a variation of input parameters to account for uncertainties. A method which can significantly reduce the computational effort of SDH-UTES design optimization is the application of ANN proxy models (Appendix F). The main effort of such a proxy-based optimization is caused by the generation of the proxy models through training simulations, whereas the effort of the actual optimization process is insignificant. Consequently, these proxy model optimizations are well suited to incorporate uncertainty into the design process and aim for robust system design optimization.

As an overall conclusion, it can be stated that the object-oriented modelling language Modelica is well suited for simulation of SDH-UTES systems, which could be substantiated by several application examples of different nature. The practical advantages of the powerful fundamental concepts of Modelica, like object-orientation or acausal equation-based modelling, might not be apparent on first sight, but undoubtedly prove their value during the model development process. However, as elaborated repeatedly, Modelica models can result in a high complexity, which hampers a more widespread application for system design applications. This very practical point has most likely a higher importance for the design process of SDH-UTES systems than the aim for highest accuracies and levels of detail. Despite all of this, the points of critique on the existing model library stock should not be misread, as there was no Modelica library dedicated to SDH-UTES systems in an extent comparable to TRNSYS and the focus of many libraries is rather put on building performance simulation. The presented work demonstrated a model development approach which tackles this problem and should be developed further.

9 Outlook

Object-oriented modelling and simulation shows a great potential for an efficient, flexible and accurate representation of SDH-UTES systems, as demonstrated with the MoSDH library. The presented example studies however, could only give a small overview of possible applications and features. Modelica proves to be a conceptual powerful tool, on which the scope of applications is merely limited by the imagination and work time of the user. As the lively community is steadily growing and the fundamental equation-based approach is generally adaptable to arbitrary future developments, the strong momentum of Modelica can be expected to be maintained. Consequently, model development in Modelica exhibits a higher sustainability in comparison to other approaches. In line with this fact, the small model library MoSDH shows still great potential for further developments, which can improve its significance.

A currently still ongoing topic is the comprehensive demonstration and validation of the PTES model, in an extent comparable to the BTES model. So far, the correctness of the model has only been verified by comparison to existing PTES models in TRNSYS. Results indicated a generally correct implementation, but did not allow for a thorough validation, as these models differ in certain central design features. Consequently, the PTES model will be validated in the near future by a thorough validation process.

So far, the implementation of control strategy functionalities does not meet the same level of maturity as the system component models show. The originally envisaged highly modularized control approach for the overall system could not be realized so far. Besides the example models of MoSDH, which are ready to use, the creation of new system models requires the complete development of a system control strategy by the. On the one hand, this is caused by the nature of SDH systems, which are usually unique and therefore require individual strategies. On the other hand though, the existing functionalities could still be improved to simplify this process. One aspect, which was very much limiting this development, were issues concerning the handling of array variables in expandable connectors, i.e. bus systems. As this issue was not limited to a single, but several simulation environments, implementation of a central bus system, connecting all components to a modularized system control component, were postponed until tool development has caught up with this feature.

A further aspect, which could provide a great benefit for the modelling of UTES systems in Modelica, is the development of an ATES model. Together with BTES and PTES systems, this technology covers most of UTES applications, but is still missing in MoSDH. While representation of ATES systems by models of reduced complexity is more complex than in the case of BTES and PTES systems, the addition of models with a rough representation of their performance would already generate a great benefit.

In addition to further storage components, a general extension by new components could improve the significance of MoSDH substantially. Exemplary, the addition of CSP collector components should be mentioned. Considering the aspect of land availability for SDH systems, which constitutes one of the major barriers for a more widespread implementation, the specific solar yield of collector systems can be expected to become of increasing importance. As most SDH systems currently use flat plate collectors, due to their superior cost-benefit ratio, only this technology was implemented so far. However, to increase the range of technologies, implementation of CSP collectors is planned for the near future.

The wish list for additional components is extensive, which is fueled by the general development towards smart energy systems, that combine a multitude of different energy sources and facilitate sector coupling. Since such development efforts go way beyond the intended scope of MoSDH and many of these components actually already exist within open-source model libraries, the aim should be to couple MoSDH with these. An obvious choice in this regard would be to switch the used base library of MoSDH. While hydraulic components currently use the MSL Thermal library, the use of the MSL Fluid library would instantaneously facilitate the combination with a vast number of highly sophisticated models. However, as MoSDH is intended to generally allow for a simple model development process, the high level of detail of the MSL Fluid models should be excluded from the top-level model components to stay true to the original modelling philosophy.

A further aspect which has not yet been handled properly, is the coupling of MoSDH to highly detailed 3D FEM models based on a geological survey. So far, the coupling methodology was applied to generic 3D FEM models to demonstrate the benefits. This issue is currently addressed within the context of two research projects. In the framework of the project DGE-Rollout, a detailed geological survey of a potential location for a medium-deep BTES demonstrator on campus Lichtwiese of the TU Darmstadt is carried out. The planned storage will be constructed within the just started project SKEWS (Schulte et al., 2021) and will consist of four BHEs with 750 m length each. Thermal storage is supposed to take place predominantly in the crystalline bedrock, which starts at approximately 50-100 m below ground surface, whereas the upper section of the BHEs will incorporate an insulating grout material to reduce thermal impacts on groundwater. The BTES and the university DH infrastructure will be modelled and simulated with the presented co-simulation approach in great detail and hopefully data from the operation of the demonstrator can be used to validate the approach for such applications.

Literature

- Bava F., Furbo S. and Perers B. (2015): Simulation of a Solar Collector Array Consisting of two Types of Solar Collectors, with and Without Convection Barrier, *in Energy Procedia*, v. 70, doi:10.1016/j.egypro.2015.02.091.
- BBSR (2017): Updated and enhanced test reference years (TRY) of Germany for medium and extreme weather conditions, Federal Office for Building and Regional Planning.
- Blockwitz T., Otter M., Akesson J., Arnold M., et al. (2012): Functional Mockup Interface 2.0: The Standard for Tool independent Exchange of Simulation Models, *in Proceedings of the 9th International Modelica Conference*, Munich, Germany, 3-5 September 2012, v. 76, doi:10.3384/ecp12076173.
- BMUB (2016): Climate Action Plan 2050 - Principles and goals of the German government's climate policy, Federal Ministry for the Environment, Nature Conservation, Building and Nuclear Safety (BMUB), https://ec.europa.eu/clima/sites/lts/lts_de_en.pdf (accessed 9 March 2022).
- BMWi (2019): Wärmenetze 4.0 – Bundesförderung effiziente Wärmenetze, Federal Ministry for Economic Affairs and Energy, <https://www.bundesanzeiger.de/pub/publication/iWrOAbNtQ7qTa0GkMrh?0> (accessed 9 March 2022).
- Bobach M.V. (2020): Scaling up Pit Thermal Energy Storages, *HOT|COOL - International magazine on district heating and cooling* 04/20, p. 8–9.
- Bösch F. and Graf R. (2014): Reacting to anticipations: Energy crises and energy policy in the 1970s - an introduction, *Historical Social Research*, v. 39, doi:10.12759/hsr.39.2014.4.7-21.
- Brandemuehl M.J. and Beckman W.A. (1980): Transmission of diffuse radiation through CPC and flat plate collector glazings, *Solar Energy*, v. 24, doi:10.1016/0038-092X(80)90320-5.
- Braun W., Casella F. and Bachmann B. (2017): Solving large-scale Modelica models: new approaches and experimental results using OpenModelica, *in Proceedings of the 12th International Modelica Conference*, Prague, Czech Republic, 15-17 May 2017, doi:10.3384/ecp17132557.
- Buffa S., Cozzini M., D'Antoni M., Baratieri M. and Fedrizzi R. (2019): 5th generation district heating and cooling systems: A review of existing cases in Europe, *Renewable and Sustainable Energy Reviews*, v. 104, doi:10.1016/j.rser.2018.12.059.
- Burhenne S., Wystrcil D., Elci M., Narmsara S. and Herkel S. (2013): Building performance simulation using Modelica: Analysis of the current state and application areas, *in 13th Conference of the International Building Performance Simulation Association*, Chambéry, France, 25-28 August 2013.
- Claesson J. and Eskilson P. (1988): Conductive heat extraction to a deep borehole: Thermal analyses and dimensioning rules, *Energy*, doi:10.1016/0360-5442(88)90005-9.
- Cohen S.D. and Hindmarsh A.C. (1996): CVODE, a stiff/nonstiff ODE solver in C, *Computers in physics*, v. 10, doi:10.1063/1.4822377.
- CRED (2020): The human cost of disasters: an overview of the last 20 years (2000-2019), Centre for Research on the Epidemiology of Disasters,

<https://www.preventionweb.net/publication/human-cost-disasters-overview-last-20-years-2000-2019> (accessed 9 March 2022).

- Dahash A., Ochs F. and Tosatto A. (2019): Co-Simulation of Dynamic Energy System Simulation and COMSOL Multiphysics, *in* Proceedings COMSOL Conference 2019, Cambridge, UK, 24–26 September 2019.
- Dahash A., Ochs F. and Tosatto A. (2021): Techno-economic and exergy analysis of tank and pit thermal energy storage for renewables district heating systems, *Renewable Energy*, v. 180, doi:10.1016/j.renene.2021.08.106.
- Dahash A., Ochs F., Tosatto A. and Streicher W. (2020): Toward efficient numerical modelling and analysis of large-scale thermal energy storage for renewable district heating, *Applied Energy*, v. 279, doi:10.1016/j.apenergy.2020.115840.
- Danish Energy Agency (2017): Regulation and planning of district heating in Denmark, https://ens.dk/sites/ens.dk/files/Globalcooperation/regulation_and_planning_of_district_heating_in_denmark.pdf (accessed 9 March 2022).
- Dassault Systèmes (2020a): Dymola - Dynamic Modelling Laboratory, Version 2021x, Dassault Systèmes SE.
- Dassault Systèmes (2020b): Dymola - Dynamic Modelling Laboratory - User Manual, Version 2021x, Dassault Systèmes SE.
- Doughty C., Hu J., Dobson P., Nico P. and Wetter M. (2021): Coupling subsurface and above-surface models for optimizing the design of borefields and district heating and cooling systems in the presence of varying water-table depth, *in* Proceedings of 46th Workshop on Geothermal Reservoir Engineering, Stanford, California, USA, 16-18 February 2021.
- Duffie J.A., Beckman W.A. and Worek W.M. (1994): Solar Engineering of Thermal Processes, 2nd ed., *Journal of Solar Energy Engineering*, v. 116, doi:10.1115/1.2930068.
- Elhashmi R., Hallinan K.P. and Chiasson A.D. (2020): Low-energy opportunity for multi-family residences: A review and simulation-based study of a solar borehole thermal energy storage system, *Energy*, v. 204, doi:10.1016/j.energy.2020.117870.
- Elmqvist H. (1978): A Structured Model Language for Large Continuous Systems, Dissertation, Lund Institute of Technology, 229 p.
- Elmqvist H. (1993): Automated Formula Manipulation Supports Object-Oriented Continuous-System Modelling, *IEEE Control Systems*, v. 13, doi:10.1109/37.206983.
- Elmqvist H. and Otter M. (1994): Methods for tearing systems of equations in object-oriented modelling, *in* ESM 94 European simulation multiconference, Barcelona, Spain, 1-3 June 1994.
- Ensbury T. (2019): Claytex Tech Blog - Reducing Non-Linear Systems with Filters, <https://www.claytex.com/tech-blog/reducing-non-linear-systems-with-filters/> (accessed 27 October 2021).
- Epp B. (2021): German SDH market could be bigger, if there was enough space, <https://www.solarthermalworld.org/news/german-sdh-market-could-be-bigger-if-there-was-enough-space> (accessed 14 October 2021).
- Ernst T., Jähnichen S. and Klose M. (1997): The Architecture of the Smile/M Simulation Environment, *in* Proceedings 15th IMACS World Congress on Scientific Computation, Modelling and Applied Mathematics, Berlin, Germany, August 1997.

-
- Errboe N. (2018): Fjernvarmelager for fuglene: Utætheder sender solvarmen og pengene op i det blå, <https://ing.dk/artikel/fjernvarmelager-fuglene-utaetheder-sender-solvarmen-pengene-blaa-212987> (accessed 19 October 2021).
- ESI ITI (2021): SimulationX 4.2 Documentation - Die Globale Symbolische Analyse, <http://doc.simulationx.com/4.2/1031/Content/Simulation/GlobalSymbolicAnalysis.htm> (accessed 23 August 2021).
- European Commission (2019): Comprehensive study of building energy renovation activities and the uptake of nearly zero-energy buildings in the EU, https://ec.europa.eu/energy/sites/ener/files/documents/1.final_report.pdf (accessed 9 March 2022).
- European Commission (2021): European Commission - Heating and Cooling, <https://ec.europa.eu/energy/en/topics/energy-efficiency/heating-and-cooling> (accessed 7 September 2021).
- Falk P.M. (2018): Evaluation of district heating systems based on exergy analysis, Dissertation, Technical University of Darmstadt, <http://tuprints.ulb.tu-darmstadt.de/7372/>.
- Fish G. and Harrison S. (2017): Introduction to the model translation and symbolic processing, <https://www.claytex.com/tech-blog/model-translation-and-symbolic-manipulation/> (accessed 9 July 2021).
- Flauger J. and Witsch K. (2021): Gaspreisexplosion: Erster deutscher Versorger stellt den Gasvertrieb ein, <https://www.handelsblatt.com/unternehmen/deutsche-energiepool-gaspreisexplosion-erster-deutscher-versorger-stellt-den-gasvertrieb-ein/27645040.html> (accessed 28 September 2021).
- Fleuchaus P., Godschalk B., Stober I. and Blum P. (2018): Worldwide application of aquifer thermal energy storage – A review, *Renewable and Sustainable Energy Reviews*, v. 94, doi:10.1016/j.rser.2018.06.057.
- Formhals J., Hemmatabady H., Welsch B., Schulte D.O. and Sass I. (2020): A Modelica toolbox for the simulation of borehole thermal energy storage systems, *Energies*, v. 13, doi:10.3390/en13092327.
- Formhals J., Schulte D.O., Welsch B. and Sass I. (2017a): Coupled Simulation of Borehole Thermal Energy Storages and Solar District Heating Systems, *in European Geosciences Union General Assembly 2017*, Vienna, Austria, 23-28 April 2017, <http://tubiblio.ulb.tu-darmstadt.de/87114/>.
- Formhals J., Welsch B., Schulte D.O. and Sass I. (2017b): Effects of the District Heating Supply Temperature on the Efficiency of Borehole Thermal Energy Storage Systems, *in Proceedings 3rd International Conference on Smart Energy Systems and 4th Generation District Heating*, Copenhagen, Denmark, 12-13 September 2017, <http://tubiblio.ulb.tu-darmstadt.de/89333/>.
- Frank E., Mauthner F. and Fischer S. (2015): Solar Heating and Cooling Programme Task 49 Solar Process Heat for Production and Advanced Applications - Technical Report A.1.2 Overheating prevention and stagnation handling in solar process heat applications, International Energy Agency.
- Franke R. (1998a): Integrierte dynamische Modellierung und Optimierung von Systemen mit saisonaler Wärmespeicherung, Düsseldorf, VDI-Verlag, Fortschrittberichte VDI : Reihe 6, Energietechnik Nr. 394, 156 p.

-
- Franke R. (1998b): Modelling and Optimal Design of a Central Solar Heating Plant with Heat Storage in the Ground Using Modelica, *in* Proceedings of the Eurosim '98 Simulation Congress, Espoo, Finland, 14-15 April 1998.
- Franke R. (1997): Object-oriented modelling of solar heating systems, *Solar Energy*, v. 60, doi:10.1016/S0038-092X(96)00156-9.
- Franke R., Casella F., Sielemann M., Proelss K. and Otter M. (2009): Standardization of Thermo-Fluid Modelling in Modelica.Fluid, *in* Proceedings of the 7 International Modelica Conference, Como, Italy, 20-22 September 2009, doi:10.3384/ecp09430077.
- Fritzson P. (2020): Modelica: Equation-Based, Object-Oriented Modelling of Physical Systems, *Foundations of Multi-Paradigm Modelling for Cyber-Physical Systems*, p. 45–96, doi:10.1007/978-3-030-43946-0_3.
- Fritzson P. (2014): Principles of Object Oriented Modelling and Simulation with Modelica 3.3: A Cyber-Physical Approach, Piscataway, NJ, USA, IEEE Press, doi:10.1002/9781118989166.
- Gabrielli P., Acquilino A., Siri S., Bracco S., Sansavini G. and Mazzotti M. (2020): Optimization of low-carbon multi-energy systems with seasonal geothermal energy storage: The Anergy Grid of ETH Zurich, *Energy Conversion and Management: X*, v. 8, doi:10.1016/j.ecmx.2020.100052.
- Gehlin S. (2016): Borehole thermal energy storage, *in* Advances in Ground-Source Heat Pump Systems, Elsevier, p. 295–327, doi:10.1016/b978-0-08-100311-4.00011-x.
- Giraud L., Baviere R., Vallée M. and Paulus C. (2015): Presentation, Validation and Application of the DistrictHeating Modelica Library, *in* Proceedings of the 11th International Modelica Conference, Versailles, France, 21-23 September 2015, doi:10.3384/ecp1511879.
- Giraud L., Paulus C. and Baviere R. (2014): Modelling of Solar District Heating: A Comparison Between TRNSYS and MODELICA, *in* Proceedings EuroSun 2014, Aix-les-Bains, France, 16-19 September 2014, doi:10.18086/eurosun.2014.19.06.
- Guelpa E. and Verda V. (2019): Thermal energy storage in district heating and cooling systems: A review, *Applied Energy*, v. 252, doi:10.1016/j.apenergy.2019.113474.
- Handke H., Reisig O., Düppre T., Zinke B. and Schulz S. (2019): Verrohrung für eine Erdwärmesonde zur Gewinnung geothermischer Energie, insbesondere tiefegeothermischer Energie, patent no. DE 10 2015 112 892.6, p. 28.
- Hemmatbady H., Formhals J., Welsch B., Schulte D.O. and Sass I. (2020): Optimized layouts of borehole thermal energy storage systems in 4th generation grids, *Energies*, v. 13, doi:10.3390/en13174405.
- Hemmatbady H., Welsch B., Formhals J. and Sass I. (2022): AI-based enviro-economic optimization of solar-coupled and standalone geothermal systems for heating and cooling, *Applied Energy*, v. 311, doi:10.1016/j.apenergy.2022.118652.
- Herring S.C., Christidis N., Hoell A., Hoerling M.P. and Stott P.A. (2021): Explaining Extreme Events of 2019 from a Climate Perspective, *Bulletin of the American Meteorological Society*, v. 102, doi:10.1175/bams-explainingextremeevents2019.1.
- del Hoyo Arce I., Herrero López S., López Perez S., Rămă M., Klobut K. and Febres J.A. (2018): Models for fast modelling of district heating and cooling networks, *Renewable and Sustainable Energy Reviews*, v. 82, doi:10.1016/j.rser.2017.06.109.

-
- IEA (2021): Net Zero by 2050: A Roadmap for the Global Energy Sector, International Energy Agency.
- IRENA (2020): Innovation Outlook: Thermal Energy Storage, International Renewable Energy Agency, <https://www.irena.org/publications/2020/Nov/Innovation-outlook-Thermal-energy-storage> (accessed 9 March 2022).
- IRENA (2021a): Renewable Power Generation Costs in 2020, International Renewable Energy Agency, <https://www.irena.org/publications/2021/Jun/Renewable-Power-Costs-in-2020> (accessed 9 March 2022).
- IRENA (2021b): World Energy Transitions Outlook: 1.5°C Pathway, International Renewable Energy Agency, <https://www.irena.org/publications/2021/Jun/World-Energy-Transitions-Outlook> (accessed 9 March 2022).
- isoplus (2020): Design manual rigid compound systems, isoplus Fernwärmetechnik GmbH, https://www.isoplus-pipes.com/fileadmin/data/downloads/documents/germany/manuals/chapter_2_web.pdf (accessed 9 March 2022).
- Jensen M.V. (2014): Solar Heating and Cooling Programme Task 45 Large scale solar heating and cooling - Seasonal pit heat storages - guidelines for materials & construction, International Energy Agency.
- Jensen L.L., Rutz D., Doczekal C., Gjorgievski V., Batas-Bjelic I., Kazagic A., Ademovic A., Sunko R., Duic N. and Puksec T. (2016): CoolHeating - Best Practice Examples of Renewable District Heating and Cooling, Project No: 691679,.
- Jorissen F., Reynders G., Baetens R., Picard D., Saelens D. and Helsen L. (2018): Implementation and verification of the ideas building energy simulation library, *Journal of Building Performance Simulation*, v. 11, doi:10.1080/19401493.2018.1428361.
- Kirschstein X. (2020): Modelling, simulation and analysis of the integration of seasonal underground thermal energy storages into Campus Lichtwiese district heating grid, Master thesis, Technical University of Darmstadt, XIV, p.49 p.
- Leitner B. (2019): Modelica DisHeatLib library, <https://github.com/AIT-IES/DisHeatLib> (accessed 10 February 2022).
- Liu L., Felgner F. and Frey G. (2010): Comparison of 4 numerical solvers for stiff and hybrid systems simulation, *in Proceedings of the 15th IEEE International Conference on Emerging Technologies and Factory Automation*, Bilbao, Spain, 13-16 September 2010, doi:10.1109/ETFA.2010.5641330.
- Liu B.Y.H. and Jordan R.C. (1963): The long-term average performance of flat-plate solar-energy collectors, *Solar Energy*, v. 7, doi:10.1016/0038-092x(63)90006-9.
- Lund H., Østergaard P.A., Nielsen T.B., Werner S., Thorsen J.E., Gudmundsson O., Arabkoohsar A. and Mathiesen B.V. (2021): Perspectives on fourth and fifth generation district heating, *Energy*, v. 227, doi:10.1016/j.energy.2021.120520.
- Mattsson S.E. and Söderlind G. (1993): Index Reduction in Differential-Algebraic Equations Using Dummy Derivatives, *SIAM Journal on Scientific Computing*, v. 14, doi:10.1137/0914043.
- Mauthner F. and Herkel S. (2016): Solar Heating and Cooling Programme Task 52 Solar Heat and Energy Economics in Urban Environments - Technical Report Subtask C1 - Technology

and demonstrators, International Energy Agency.

- Mesquita L., McClenahan D., Thornton J., Carriere J. and Wong B. (2017): Drake Landing solar community - 10 years of operation, *in* Proceedings ISES Solar World Congress 2017 - IEA SHC International Conference on Solar Heating and Cooling for Buildings and Industry 2017, Abu Dhabi, UAE, 29 October - 02 November 2017, doi:10.18086/swc.2017.06.09.
- Modelica Association (2020): Modelica.Thermal - Library of thermal system components to model heat transfer and simple thermo-fluid pipe flow, https://doc.modelica.org/Modelica4.0.0/Resources/helpDymola/Modelica_Thermal.html#Modelica.Thermal (accessed 6 October 2021).
- Modelica Association (2021): Modelica - A Unifed Object-Oriented Language for Systems Modelling, <https://modelica.org/modelicalanguage.html> (accessed 9 March 2022).
- Möller B., Wiechers E., Persson U., Grundahl L., Lund R.S. and Mathiesen B.V. (2019): Heat Roadmap Europe: Towards EU-Wide, local heat supply strategies, *Energy*, v. 177, doi:10.1016/j.energy.2019.04.098.
- Müller D., Lauster M., Constantin A., Fuchs M. and Remmen P. (2016): Aixlib - an Open-Source Modelica Library Within the IEA-EBC Annex 60 Framework, *in* Proceedings of Central European Symposium on Building Physics CESBP 2016, Dresden, Germany, 14-16 September 2016.
- Nelder J.A. and Mead R. (1965): A Simplex Method for Function Minimization, *The Computer Journal*, v. 7, doi:10.1093/comjnl/7.4.308.
- NREL (2020): EnergyPlus, Version 9.6.0, United States National Renewable Energy Laboratory, <https://energyplus.net/>.
- Nytsch-Geusen C., Huber J., Ljubijankic M. and Rädler J. (2013): Modelica BuildingSystems - eine Modellbibliothek zur Simulation komplexer energietechnischer Gebäudesysteme, *Bauphysik*, v. 35, doi:10.1002/bapi.201310045.
- Olsthoorn D., Haghghat F. and Mirzaei P.A. (2016): Integration of storage and renewable energy into district heating systems: A review of modelling and optimization, *Solar Energy*, v. 136, doi:10.1016/j.solener.2016.06.054.
- OpenModelica (2021): OpenModelica, Version 1.18.0, Open Source Modelica Consortium, <https://www.openmodelica.org>.
- Otter M. (1999a): Objektorientierte Modellierung Physikalischer Systeme, Teil 1: Übersicht, at *Automatisierungstechnik*, v. 47, p. A1--A4, <https://elib.dlr.de/3463/>.
- Otter M. (1999b): Objektorientierte Modellierung Physikalischer Systeme, Teil 4: Transformationsalgorithmen, at *Automatisierungstechnik*, v. 47, p. A13--A16, <https://elib.dlr.de/3510/>.
- Pahud D. and Hellström G. (1996): The new duct ground heat model for TRNSYS, *in* Proceedings Eurotherm Seminar n°49, Physical models for Thermal Energy Stores, Eindhoven, Netherlands, 25-27 March 1996.
- Pauschinger T., Schmidt T., Alex Soerensen P., Aart Snijders D., Djebbar R., Boulter R. and Jeff Thornton C. (2018): Integrated Cost-effective Large-scale Thermal Energy Storage for Smart District Heating and Cooling - Design Aspects for Large-Scale Aquifer and Pit Thermal Energy Storage for District Heating and Cooling, International Energy Agency

Technology Collaboration Programme on District Heating and Cooling including Combined Heat and Power, v. 2018.

- Pehnt M. (2017): Wärmenetze 4.0 - Endbericht - Kurzstudie zur Umsetzung der Maßnahme "Modellvorhaben erneuerbare Energien und hocheffizienten Niedertemperaturwärmenetzen," ifeu - Institut für Energie- und Umweltforschung, <https://www.bmwi.de/Redaktion/DE/Publikationen/Studien/endbericht-kurzstudie-waermenetzsysteme-4-0.html> (accessed 9 March 2022).
- Pelz P.F. (2011): Upper Limit for Hydropower in an Open-Channel Flow, *Journal of Hydraulic Engineering*, v. 137, doi:10.1061/(asce)hy.1943-7900.0000393.
- Pezzutto S., Toleikyte A. and de Felice M. (2015): Assessment of the Space Heating and Cooling Market in the EU28: A Comparison between EU15 and EU13 Member States, *International Journal of Contemporary ENERGY*, v. 1.
- Plessis G., Kaemmerlen A. and Lindsay A. (2014): BuildSysPro: a Modelica library for modelling buildings and energy systems, *in Proceedings of the 10th International Modelica Conference*, Lund, Sweden, 10-12 March 2014, doi:10.3384/ecp140961161.
- Reed A.L., Novelli A.P., Doran K.L., Ge S., Lu N. and McCartney J.S. (2018): Solar district heating with underground thermal energy storage: Pathways to commercial viability in North America, *Renewable Energy*, v. 126, p. 1–13, doi:10.1016/j.renene.2018.03.019.
- Ribas Tugores C., Francke H., Cudok F., Inderfurth A., Kranz S. and Nytsch-Geusen C. (2015): Coupled modelling of a District Heating System with Aquifer Thermal Energy Storage and Absorption Heat Transformer, *in Proceedings of the 11th International Modelica Conference*, Versailles, France, 21-13 September 2015, doi:10.3384/ecp15118197.
- Sass I. (Ed.) (2016): *Shallow Geothermal Systems - Recommendations on Design, Construction, Operation and Monitoring*, Berlin, Germany, Ernst & Sohn, a Wiley Brand, doi:10.1002/9783433606674.
- Schmidt T. (2019): Brædstrup district heating monitoring data evaluation for the years 2014-2017, Solites Steinbeis Research Institute for Solar and Sustainable Thermal Energy Systems.
- Schrag T. (2001): Modellierung, Simulation und Optimierung solarthermischer Anlagen in einer objektorientierten Simulationsumgebung, Dissertation, Technische Universität Berlin, doi:10.14279/depositonce-249.
- Schulte D.O. (2016): Simulation and optimization of medium deep borehole thermal energy storage systems, Dissertation, Technical University of Darmstadt, XXII, 132 p.
- Schulte D.O., Formhals J., Welsch B. and Sass I. (2021): Medium Deep Borehole Thermal Energy Storage Pilot Plant, *in World Geothermal Congress 2020*, Reykjavik, Iceland, 24-27 October 2021.
- Schulte D.O., Rühaak W., Oladyshkin S., Welsch B. and Sass I. (2016a): Optimization of Medium-Deep Borehole Thermal Energy Storage Systems, *Energy Technology*, v. 4, p. 104–113, <http://tubiblio.ulb.tu-darmstadt.de/77267/>.
- Schulte D.O., Rühaak W., Welsch B. and Sass I. (2016b): BASIMO – Borehole Heat Exchanger Array Simulation and Optimization Tool, *Energy Procedia*, v. 97, p. 210–217, <http://tubiblio.ulb.tu-darmstadt.de/85267/>.
- Schulte D.O., Welsch B., Boockmeyer A., Rühaak W., Bär K., Bauer S. and Sass I. (2016c):

Modelling insulated borehole heat exchangers, *Environmental Earth Sciences*, v. 75, doi:10.1007/s12665-016-5638-x.

Schwan T. and Unger R. (2016): Holistic district heating grid design with SimulationX / Green City, in *Proceedings ESI SimulationX User Forum 2016*, Dresden, Germany, 24-25 November 2016.

SDH (2017): Solar District Heating plant database, Solites Steinbeis Research Institute for Solar and Sustainable Thermal Energy Systems, <https://www.solar-district-heating.eu/en/plant-database/> (accessed 9 March 2022).

Solar Energy Laboratory (2021): TRNSYS, Version 18, Madison, WI, USA, Solar Energy Laboratory, University of Wisconsin.

Sørensen P.A., Larsen J., Thøgersen L., Dannemand Andersen J., Østergaard C. and Schmidt T. (2013): Boreholes in Brødstrup, Final report, ForskEL (project no. 2010 – 1 – 10498), EUDP (project no. 64012-0007-1), PlanEnergi.

Spurk J.H. (1992): *Dimensionsanalyse in der Strömungslehre*, Berlin, Springer-Verlag, doi:10.1007/978-3-662-01581-0.

Stapczynski S. (2021): Europe's Energy Crisis Is Coming for the Rest of the World, Too, <https://www.bloomberg.com/news/articles/2021-09-27/europe-s-energy-crisis-is-about-to-go-global-as-gas-prices-soar> (accessed 28 September 2021).

Susana P., Lund R.S., Mathiesen B.V., Miguel C., et al. (2018): Heat Roadmap Europe 4: Quantifying the Impact of Low-Carbon Heating and Cooling Roadmaps (No. 695989), Aalborg Universitet, www.heatroadmap.eu.

Tiller M. (2021): Modelica by Example - Modelica Standard Library, <https://mbe.modelica.university/components/packages/msl/> (accessed 24 August 2021).

Tiller M. (2000): Modelica Thermal Library, in *Modelica Workshop 2000 Proceedings*, Lund, Sweden, 23-24 October 2000, p. 137–144.

Tordrup K.W., Poulsen S.E. and Bjørn H. (2017): An improved method for upscaling borehole thermal energy storage using inverse finite element modelling, *Renewable Energy*, v. 105, p. 13–21, doi:10.1016/j.renene.2016.12.011.

Trier D., Bava F., Kok Skov C. and Sørensen S.S. (2018a): Solar Heating and Cooling Programme Task 52 Solar district heating - Trends and possibilities - Characteristics of ground-mounted systems for screening of land use requirements and feasibility. Technical report of Subtask B., International Energy Agency.

Trier D., Skov C.K., Sørensen S.S. and Bava F. (2018b): Solar Heating and Cooling Programme Task 52 Solar District Heating Trends and Possibilities - Technical Report Subtask B - Characteristics of Ground-Mounted Systems for Screening of Land Use Requirements and Feasibility, International Energy Agency.

Tschopp D., Tian Z., Berberich M., Fan J., Perers B. and Furbo S. (2020): Large-scale solar thermal systems in leading countries: A review and comparative study of Denmark, China, Germany and Austria, *Applied Energy*, v. 270, doi:10.1016/j.apenergy.2020.114997.

UN (2015): Paris Agreement United Nations Framework Convention on Climate Change, https://unfccc.int/sites/default/files/english_paris_agreement.pdf (accessed 9 March 2022).

VDI (2013): *VDI-Wärmeatlas*, Berlin, Heidelberg, Germany, VDI e.V., doi:10.1007/978-3-642-

19981-3.

- Verschaffel-Drefke C., Schedel M., Balzer C., Hinrichsen V. and Sass I. (2021): Heat Dissipation in Variable Underground Power Cable Beddings: Experiences from a Real Scale Field Experiment, *Energies*, v. 14, doi:10.3390/en14217189.
- Weiss W. and Spörk-Dür M. (2021): IEA Solar Heating & Cooling Programme - Solar Heat Worldwide - Global market development and trends 2020, International Energy Agency.
- Welsch B. (2019): Technical, Environmental and Economic Assessment of Medium Deep Borehole Thermal Energy Storage Systems, Dissertation, Technical University of Darmstadt, XXI, p191 p., <http://tubiblio.ulb.tu-darmstadt.de/111762/>.
- Welsch B., Göllner-Völker L., Schulte D.O., Bär K., Sass I. and Schebek L. (2018): Environmental and economic assessment of borehole thermal energy storage in district heating systems, *Applied Energy*, v. 216, p. 73–90, doi:10.1016/j.apenergy.2018.02.011.
- Welsch B., Rühaak W., Schulte D.O., Bär K. and Sass I. (2016): Characteristics of medium deep borehole thermal energy storage, *International Journal of Energy Research*, v. 40, p. 1855–1868, doi:10.1002/er.3570.
- Welsch B., Rühaak W., Schulte D.O., Formhals J., Bär K. and Sass I. (2017): Co-Simulation of Geothermal Applications and HVAC Systems, *Energy Procedia*, v. 125, p. 345–352, doi:10.1016/j.egypro.2017.08.040.
- Wetter M. and Haugstetter (2006): Modelica versus TRNSYS – A Comparison between an equation-based and a procedural modelling language for building energy simulation, *in* Proceedings of the SimBuild 2nd National Conference of the International Building Performance Simulation Association USA, Cambridge, MA, USA, 02-04 August 2006.
- Wetter M. and Treeck C. Van (2017): IEA Energy in Buildings and Communities Programme - Annex 60 Final Report - New generation computational tools for building and community energy systems, International Energy Agency.
- Wetter M., Zuo W., Nouidui T.S. and Pang X. (2014): Modelica Buildings library, *Journal of Building Performance Simulation*, v. 7, doi:10.1080/19401493.2013.765506.
- Wolfram Research (2021a): Mathematica, Version 12.3.1, Wolfram Research Inc., <https://www.wolfram.com/mathematica/>.
- Wolfram Research (2021b): Wolfram SystemModeler, Version 12.3.1, Wolfram Research Inc.
- Yang T., Liu W., Kramer G.J. and Sun Q. (2021): Seasonal thermal energy storage: A techno-economic literature review, *Renewable and Sustainable Energy Reviews*, v. 139, doi:10.1016/j.rser.2021.110732.
- Zofer P. (2019): Analyse und Vergleich von Modelica-Modellen thermischer Energiespeicher, Master thesis, Technische Universität München, XIII, p.81 p.

Appendix A – Co-Simulation of Geothermal Applications and HVAC Systems

Published as:

Welsch, B., Rühaak, W., Schulte, D.O., **Formhals, J.**, Bär, K., and Sass, I., 2017, Co-Simulation of Geothermal Applications and HVAC Systems: Energy Procedia, v. 125, p. 345–352, <http://tubiblio.ulb.tu-darmstadt.de/89580/>.



European Geosciences Union General Assembly 2017, EGU
Division Energy, Resources & Environment, ERE

Co-Simulation of Geothermal Applications and HVAC Systems

Bastian Welsch^{a,b,*}, Wolfram Rühaak^c, Daniel O. Schulte^{a,b}, Julian Formhals^{a,b},
Kristian Bär^a, Ingo Sass^{a,b}

^aTechnische Universität Darmstadt, Department of Geothermal Science and Technology, Schnittspahnstraße 9, 64287 Darmstadt, Germany

^bDarmstadt Graduate School of Excellence Energy Science and Engineering, Jovanka-Bontschits-Straße 2, 64287 Darmstadt, Germany

^cFederal Institute for Geosciences and Natural Resources, Stilleweg 2, 30655 Hannover, Germany

Abstract

An interface is developed to couple the finite element program FEFLOW with the MATLAB-SIMULINK software. The TCP/IP based data exchange routine allows for a co-simulation of borehole heat exchangers and of HVAC components, so that each subsystem can be modeled in its specialized simulation environment. Hereby, the interaction of the subsystems is taken into account, which leads to a more precise representation of the systems' dynamic behavior. Furthermore, the concept supports the application of mathematical optimization algorithms that can be utilized to automatically determine several design parameters for an overall improved system performance.

© 2017 The Authors. Published by Elsevier Ltd.

Peer-review under responsibility of the scientific committee of the European Geosciences Union (EGU) General Assembly 2017 – Division Energy, Resources and the Environment (ERE).

Keywords: Coupling; co-simulation; optimization; geothermal; HVAC; borehole heat exchanger; FEFLOW; MATLAB

1. Introduction

Large scale geothermal applications are eminently suitable for the substitution of fossil based energy sources, particularly in the district heating sector in combination with low supply temperatures. Furthermore, shallow and medium deep borehole thermal energy storage (BTES) systems are very promising technologies with regard to the seasonal storage of solar thermal energy [1-4]. However, these systems are most efficient if they are large enough, i.e. when the storage capacities lie in the range of several GWh of heat per year. Such a heat demand is only present

* Corresponding author. Tel.: +49-6151-16-22096; fax: +49-6151-16-23601.

E-mail address: welsch@geo.tu-darmstadt.de

in large district heating grids, which usually consist of several subsystems like heat sources (e.g. solarthermics or a combined heat and power plant), geothermal applications (e.g. a borehole thermal energy storage system), heat consumers (e.g. space heating systems), diurnal storages (i.e. water tanks), additional heat sources for peak load coverage (e.g. a heat pump or a gas boiler) and the distribution network. For the design and the optimization of an integrated system, numerical simulations of all subsystems are imperative. Borehole thermal energy storage systems are usually simulated with finite element programs under consideration of groundwater flow and heat transport in the subsurface. In contrast, the heating, ventilation and air conditioning (HVAC) installations are often analyzed with modular transient simulation software packages for modeling physical systems. The separate simulation of the borehole energy storage and HVAC installations is well-established, but represents a simplification. In reality, the subsystems interact dynamically with each other. The fluid temperatures of the heat generation system, the heating system and the underground storage are interdependent and affect the performance of each subsystem. Coupled simulation models, which co-simulate the subsystems are required, to take these interdependencies into account.

There are different program codes for the simulation of the interaction of borehole heat exchangers (BHEs) with the subsurface (e.g. BASIMO [5]). Here, the program FEFLOW [6, 7] is used to compute the subsurface heat transport including a one-dimensional solution for the BHEs [8, 9]. The Carnot Blockset [10] for MATLAB-SIMULINK [11] is deployed for the simulation of the HVAC components. This allows for a readily combination with the MATLAB optimization toolbox, which provides various powerful mathematical optimization algorithms.

2. Implementation

Simulation software packages from different developers usually do not contain pre-defined coupling interfaces and in addition to that, might be based on different program languages. Hence, a major challenge is to develop a robust and versatile communication architecture between them. We decided to use a client-server network connection based on the Transmission Control Protocol/Internet Protocol (TCP/IP). The TCP/IP protocol suite specifies how data has to be packetized, addressed, transmitted, routed and received at the destination. It assures that data loss is identified and corrected and it allows for a bidirectional communication. Furthermore, it offers the possibility to run the different simulation packages on separate computers (Fig. 1).

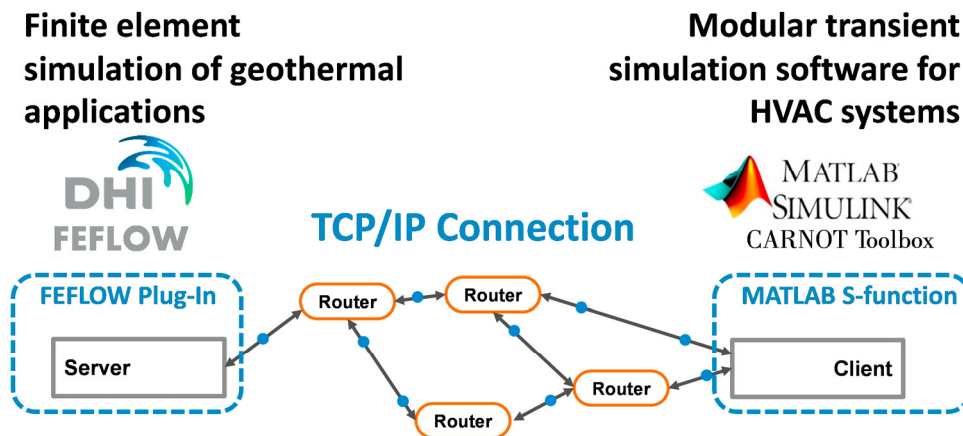


Fig. 1. Principle of the socket-client connection between FEFLOW and SIMULINK.

To establish such a connection, it is necessary that both software packages allow for the execution of proprietary source code. FEFLOW has a programming interface (IFM), which provides the possibility to read or change several model parameters during a simulation and also to execute C++ code. In SIMULINK, so called S-function blocks are available that can be integrated into the model and contain own MATLAB code or C++ code, as well.

The following routine is executed to establish the connection, send data via the interfaces and close the connection (cf. Fig. 2): FEFLOW operates as the server, which passively waits for a connection. Therefore, a TCP

socket is established and a port number is assigned to the socket. A socket is the endpoint of a network-based connection. The socket address is composed of the IP address of the host and the port number. SIMULINK is instructed to serve as the client. It also creates a socket, which then calls the address of the server socket. After the server has accepted the connection, data can be sent and received. Finally, after the connection is no longer needed, the sockets are closed to release the ports.

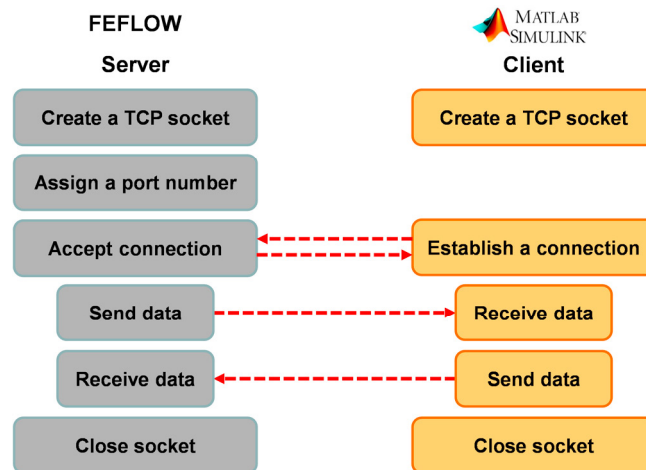


Fig. 2. Implementation scheme of the socket-client connection between FEFLOW and SIMULINK.

The connection is established shortly before the simulations are started. Subsequently, the transfer parameters are exchanged at distinct communication times. The communication time step size is constant and has to be defined in advance. Both programs generally maintain their own simulation time step control. However, it has to be ensured, that the simulation time steps coincide at the communication time steps.

3. Application example: optimal buffer storage size

3.1. System and model description

The following simplified BTES system is used to demonstrate the capability of the approach (cf. Fig. 3): A borehole storage of a specific size (37 BHE, 100 m each) is considered to be charged by a solar thermal collector system with a given collector area (15.000 m², corresponds to approx. 6 GWh of heat gain per year). A water tank between the collectors and the seasonal storage serves as a buffer storage, which cushions the daily peak loads that occur during the solar heat generation. Thus, the capacity of the buffer storage is expected to have a strong influence on the heat amount that can be transferred from the collectors into the BTES. Consequently, identifying the optimal volume of the water tank V_{buf} will maximize the heat $Q_{BTES,stor}$ that can be stored in the BTES. As this scenario only focuses on the charging process of the BTES, the representation of the heating system is not necessary.

Since there are two separated closed fluid circuits, both have to be actuated by circulation pumps. The operation of these pumps is temperature-controlled. As soon as a trigger temperature in the collectors of 60 °C is exceeded, the collector circuit is started. Accordingly, the circulation is stopped when the collectors' return temperature falls below a certain trigger temperature of 30 °C. A second operational constraint of the solar circulation pump is implemented: the collector outlet temperature has to be at least two degree centigrade above the collector inlet temperature. This shall prevent the occurrence of negative collector outputs. Likewise, the operation of the BTES fluid circuit is controlled in a similar manner: it starts operating as soon as the temperature at a sensor close to the top of the buffer storage tank exceeds a threshold of 70 °C and it stops when the sensor temperature drops beneath 42 °C. Furthermore, the pump is switched of, when the supply temperature of the BTES undercuts the return temperature. Thereby, the BTES operation is restricted to charging conditions only.

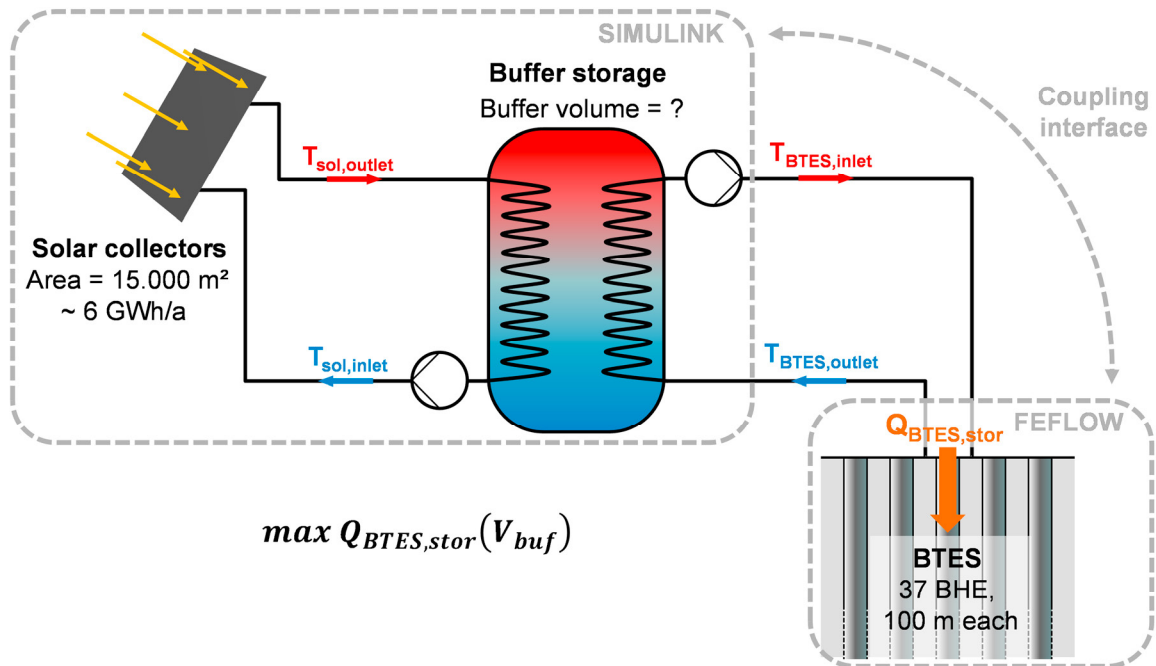


Fig. 3. Schematic of the application example setup.

While the HVAC-system components such as the solar collectors, the buffer storage tank, the circulation pumps and the control system are modeled in MATLAB-SIMULINK with the Carnot Blockset [10], the BTES is represented in a FEFLOW 3D finite element model. Both models are connected through TCP/IP and co-simulated using the approach presented herein. Therefore, the BTES supply temperature, as well as the volume flow rate in the BTES circuit are transferred from the HVAC model to the BTES model. Whereas, the BTES model only sends back the BTES return temperature. The values are exchanged at predefined communication intervals of five minutes of simulated time. Hourly solar radiation data and ambient temperature data from a test reference year dataset of Germany [12] (medium weather conditions, region 12) serve as input parameters for the solar collectors and the buffer storage tank.

3.2. Simulation results

Fig. 4 illustrates the simulation results for the first day of operation. In the morning hours, the sun raises and the solar insolation starts to increase. At about 9:50 the trigger temperature for the solar circulation pump is reached and the charging of the buffer storage starts. About one hour later, the trigger temperature of the BTES circuit is also exceeded. From that point on, heat is also transferred from the buffer storage to the BTES. In the afternoon, the solar yield decreases. Consequently, the temperature of the buffer storage decreases as well. At about 17:15 the solar yields are too low and the solar circuit pump is switched off. Since the buffer storage still contains enough heat, the charging of the BTES continues until the switch-off criterion for the BTES circulation pump is reached as well at about 2:15 in the night.

In summary, it can be stated that the simulation results are realistic and have a high level of detail. The co-simulation of the components allows for a very close inspection of the interaction processes of the components.

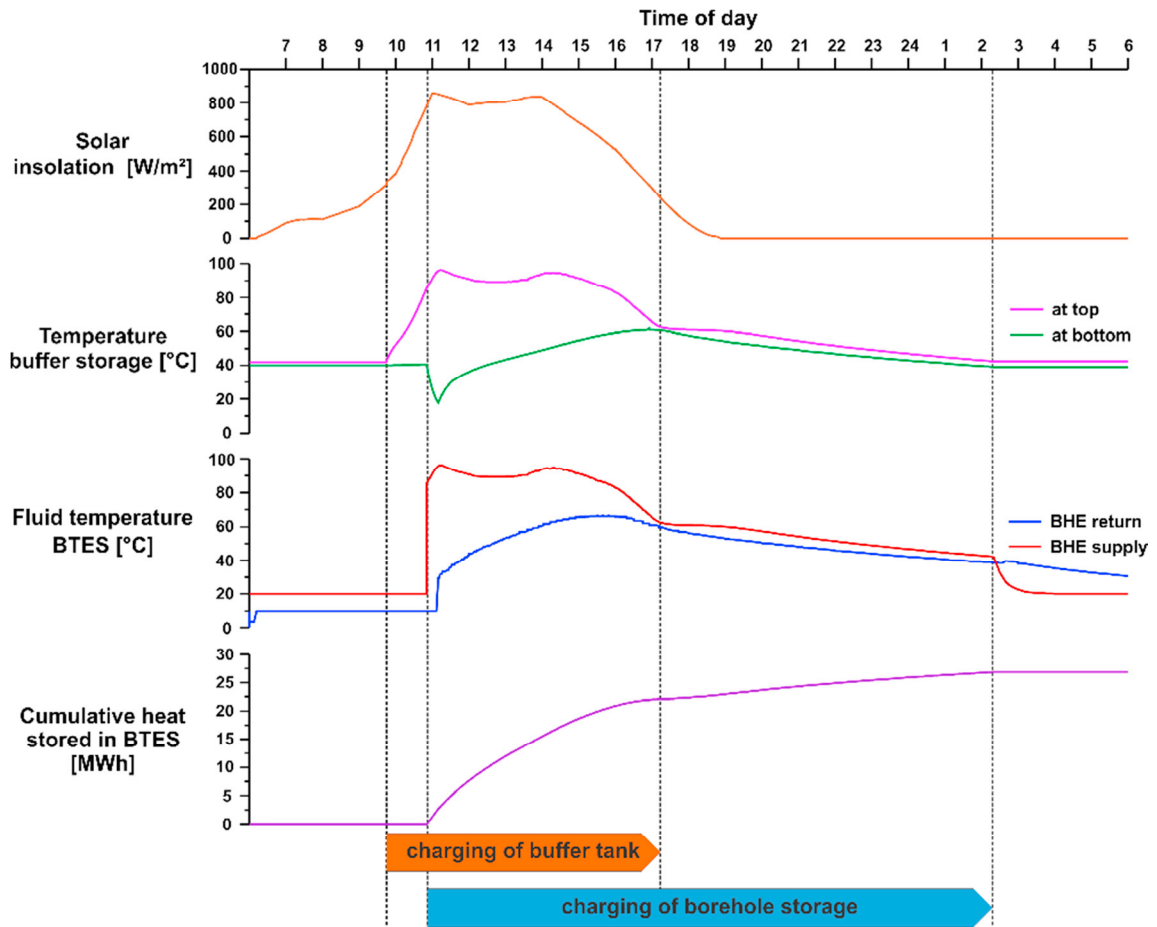


Fig. 4. Course of different system parameters during the first day of simulation.

3.3. Optimization procedure

Only with this very detailed inspection of the system's behavior resulting from the coupled simulation, it is possible to improve the system's performance by enhancing single or multiple components. In the presented scenario, an optimized buffer storage capacity can maximize the amount of solar heat that is stored in the BTES. This can be realized by applying a mathematical optimization algorithm, which automatically iterates the buffer storage volume until the optimum is found within a confidence interval.

In this example, the MATLAB function called *fminbnd* is deployed, which is part of the MATLAB Optimization Toolbox. It is based on Brent's algorithm as described in [13] and combines a golden-section search and a parabolic interpolation for finding a minimum on a fixed interval. Therefore, the objective function, which is the amount of stored heat at the optimal buffer storage capacity, has to be formulated as follows:

$$\max(Q_{BTES,stor}(V_{buf})) = -\min(-Q_{BTES,stor}(V_{buf})) \quad (1)$$

The principle of the optimization procedure is shown in Fig. 5. In every optimization iteration, the function *fminbnd* systematically chooses a buffer storage tank volume, which lies inside a predefined parameter range and passes this value to a MATLAB function called *StartSim*. This function in turn starts both, the FEFLOW model as well as the SIMULINK model and sets the buffer storage tank volume in the SIMULINK model to the chosen value. Subsequently, both models connect to each other via their TCP/IP interfaces and start to co-simulate.

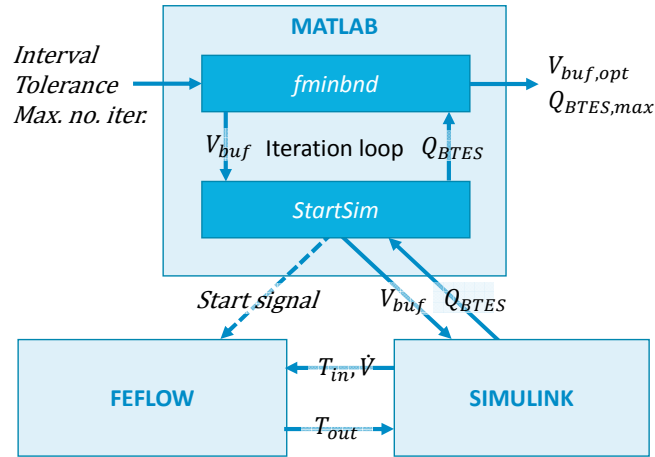


Fig. 5. Flowchart of the optimization process.

Due to the relatively small communication step size of 5 minutes, the simulation of one day takes up to one hour. For this reason, the simulation of three consecutive days is deemed to be sufficient. After this final simulation time is reached, the amount of heat that has been stored into the BTES is returned from the model to the *StartSim* function and from there to the optimization algorithm. The iteration procedure is repeated until a maximum is found for the amount of stored heat within a pre-set termination tolerance.

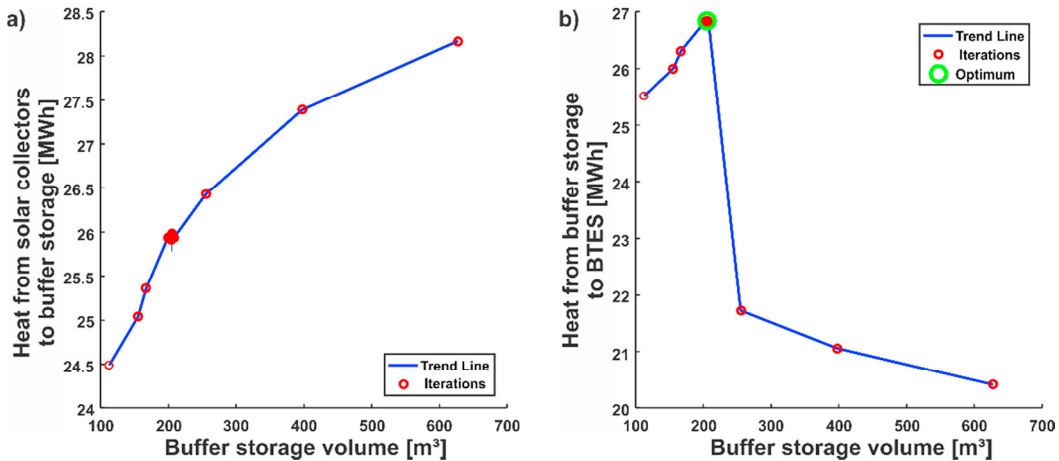


Fig. 6. Heat amount that is transferred (a) from the solar collectors to the buffer storage and (b) from the buffer storage to the BTES for the respective iteration of the buffer volume.

The optimization algorithm finds the optimum after 21 optimization iterations at a water tank volume of about 205 m³ and an error < 0.015%. It is obvious that from the seventh iteration on, the algorithm is already very close to the optimum value (error < 3.5%). Therefore, choosing a larger termination tolerance could decrease the iteration number significantly.

Fig. 6a illustrates the heat amount that is transferred from the solar thermal collectors to the buffer storage depending on the water tank size. Increasing the water tank volume leads to an increase in the buffer storage capacity. As a result, the efficiency of the collectors increases with the heat amount that is transferred from the collectors to the buffer storage.

The heat amount that is subsequently stored from the buffer storage to the BTES (Fig. 6b) increases with the water tank size as well, until a maximum is reached. Beyond this point, a significant decrease in the BTES load can

be observed. With increasing water tank size, the buffer storage temperature generally decreases. This leads to a shortened time span in which the trigger criterion for the pump operation in the BTES circuit is satisfied. As a consequence, the duration of the charging cycle decreases and the amount of stored heat diminishes. The water tank size resulting in a maximum BTES load can be considered ideal for the specific system setup and control strategy.

4. Transmission error

The applied coupling approach has to be regarded as a loose coupling, since no iteration process between the two simulation environments is implemented in the procedure. The values received from the respectively other model at a distinct communication step are kept constant until the subsequent communication step is reached. Accordingly, the accuracy of the co-simulation is very sensitive to the communication step size.

Therefore, a simple variation study is conducted, in which a 24 h synthetic thermal load profile is created through a constant flow of heat carried fluid with varying temperatures in MATLAB-SIMULINK. The synthetic load profile consists of several constant load steps with different magnitudes. Fluid flow rate and temperature are passed to a BHE model in FEFLOW via the coupling interface. Simultaneously, the thermal load that is applied by the analytical BHE solution to the FEFLOW finite element mesh is gathered and summed up to a total heat amount at the end of the simulation. Afterwards, the recorded heat amount in FEFLOW is compared to the heat amount that theoretically results from the synthetic load profile and a relative transmission error is calculated. Furthermore, the computation time for one load cycle is captured.

The co-simulation is repeated several times, varying the communication step size as well as the load profiles itself (profiles of two different days) and the duration of the particular load steps (1h, 2h, 4h). The transmission error generally depends on the ratio of the communication step size to the load step size. Therefore, a relative communication step size is defined as the communication step size normalized by the duration of the particular load steps. For instance, the relative step size is 1, when the communication step has the same length as the load steps and it is 0.1 when 10 communication steps are performed during one load step. Additionally, the computation speed-up related to the slowest model for each communication step size variation series is calculated.

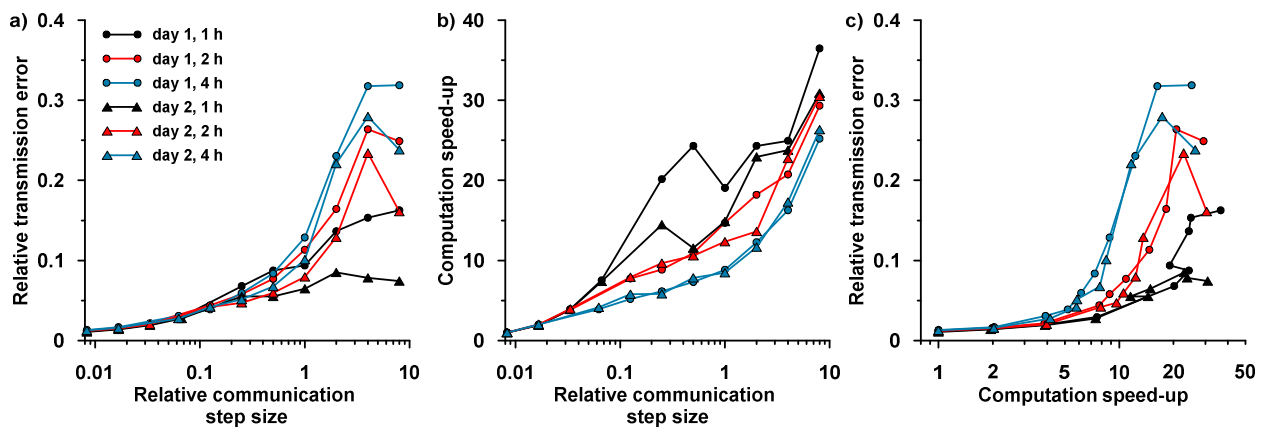


Fig. 7. a) Relative transmission error and b) computation speed-up against the relative communication step size, c) comparison of transmission error and computation speed-up.

The results of the time stepping study confirm that the relative communication step size is a major control parameter for the transmission error (Fig.7a). For relative communication time steps sizes up to 0.2, the transmission error increases independently from the specific load scenario. Larger communication time steps result in an increasing variance of the transmission error and the concurrence of communication time steps with load changes becomes more important. In summary, it can be stated that for communication time steps smaller than 0.2 the transmission error can be estimated quite well, whereas for larger communication time steps, the uncertainty increases. However, increasing the communication time steps leads to a strong improvement of the computational

performance (Fig.7b). Especially, FEFLOW's internal time stepping control can choose larger time steps and thus decrease the simulation time significantly. Tolerating an increase in the relative transmission error from about 1% to 3% allows for an increase in the computational performance by a factor of 4 (Fig.7c).

5. Discussion & conclusion

A TCP/IP interface has been developed, which connects the software package FEFLOW with MATLAB-SIMULINK and facilitates coupled simulations of subsurface processes and HVAC systems. The coupled simulations are particularly advantageous when considering large and complex heating systems, as the mutual interaction of the subsystems can be taken into account. In combination with mathematical optimization algorithms, the high detail of the coupled simulations allows for the appropriate design of system components and the maximization of the overall system performance.

As it is, the approach only provides a loose coupling of the subsystem simulations. This can result in relatively large transmission errors between the respective models and is strongly dependent on the communication time step size. Small communication time steps can limit the transmission error, but they come at a high computational cost. A priori knowledge of the system behavior is critical for the choice of the step size. Future research should focus on the implementation of iteration schemes and an adaptive communication time step control to tighten the coupling between sub-models. This will reduce the transmission errors and make the coupled simulations more robust, even at larger communication time steps that can speed up the simulations significantly.

Nevertheless, in a first example of a BTES system fed by solar thermal collectors, the coupling approach demonstrates its functionality. The coupling interface is, however, not restricted to scenarios considering BHEs, but can easily be applied to any other type of problem linking the subsurface to HVAC, like open-loop systems. This makes the presented approach a versatile tool for detailed simulations of geothermal energy supply systems.

Acknowledgements

We want to thank for the financial support by the DFG in the framework of the Excellence Initiative, Darmstadt Graduate School of Excellence Energy Science and Engineering (GSC 1070).

References

- [1] Schulte, D.O., Rühaak, W., Oladyshkin, S., Welsch, B., Sass, I. (2016) "Optimization of Medium-Deep Borehole Thermal Energy Storage Systems." *Energy Technology* 4.1: 104-113.
- [2] Schulte, D.O., Welsch, B., Boockmeyer, A., Rühaak, W., Bär, K., Bauer, S., Sass, I. (2016) "Modeling insulated borehole heat exchangers." *Environmental Earth Sciences* 75.10: 1-12.
- [3] Welsch, B., Rühaak, W., Schulte, D.O., Bär, K., Sass, I. (2016) "Characteristics of medium deep borehole thermal energy storage." *International Journal of Energy Research* 40.13: 1855-1868.
- [4] Bär, K., Rühaak, W., Welsch, B., Schulte, D., Homuth, S., Sass, I. (2015) "Seasonal High Temperature Heat Storage with Medium Deep Borehole Heat Exchangers." *Energy Procedia* 76: 351-360.
- [5] Schulte, D.O., Rühaak, W., Welsch, B., Sass, I. (2016) "BASIMO – Borehole Heat Exchanger Array Simulation and Optimization Tool." *Energy Procedia* 97: 210-217.
- [6] Diersch, H.-J.G. (2014) "Feflow - Finite Element Modeling of Flow, Mass and Heat Transport in Porous and Fractured Media." Springer Berlin Heidelberg.
- [7] DHI-WASY. (2014) "FEFLOW finite element subsurface flow and transport simulation system - Recent release 6.2."
- [8] Diersch, H.-J.G., Bauer, D., Heidemann, W., Rühaak, W., Schätzl, P. (2011) "Finite element modeling of borehole heat exchanger systems: Part 2. Numerical simulation." *Computers & Geosciences* 37.8: 1136-1147.
- [9] Eskilson, P., Claesson, J. (1988) "Simulation model for thermally interacting heat extraction boreholes." *Numerical Heat Transfer* 13.2: 149-165.
- [10] Solar-Institute Jülich. (2016) "CARNOT 6.0 for MATLAB 2013b."
- [11] The MathWorks Inc. (2016) "MATLAB 2016a."
- [12] BBR. (2011) "Updated and enhanced test reference years (TRY) of Germany for medium and extreme weather conditions." in Federal Office for Building and Regional Planning (BBR).
- [13] Forsythe, G.E., Malcolm, M.A., Moler, C.B. (1977) "Computer methods for mathematical computations." Prentice-Hall, Englewood Cliffs, NJ pp. XI, 259.


Appendix B –A Modelica Toolbox for the Simulation of Borehole Thermal Energy Storage Systems

Published as:

Formhals, J., Hemmatabady, H., Welsch, B., Schulte, D.O., and Sass, I., 2020, A Modelica toolbox for the simulation of borehole thermal energy storage systems: *Energies*, v. 13, doi:10.3390/en13092327.

Article

A Modelica Toolbox for the Simulation of Borehole Thermal Energy Storage Systems

Julian Formhals^{1,2,*}, Hoofar Hemmatabady^{1,2}, Bastian Welsch^{1,2} , Daniel Otto Schulte¹ and Ingo Sass^{1,2}

¹ Geothermal Science and Technology, Technical University of Darmstadt, Schnittspahnstraße 9, 64287 Darmstadt, Germany; hemmatabady@geo.tu-darmstadt.de (H.H.); welsch@geo.tu-darmstadt.de (B.W.); schulte@geo.tu-darmstadt.de (D.O.S.); sass@geo.tu-darmstadt.de (I.S.)

² Graduate School of Excellence Energy Science and Engineering, Technical University of Darmstadt, Otto-Berndt-Str. 3, 64287 Darmstadt, Germany

* Correspondence: formhals@geo.tu-darmstadt.de; Tel.: +49-6151-16-20443

Received: 31 March 2020; Accepted: 25 April 2020; Published: 7 May 2020



Abstract: Borehole thermal energy storage (BTES) systems facilitate the subsurface seasonal storage of thermal energy on district heating scales. These systems' performances are strongly dependent on operational conditions like temperature levels or hydraulic circuitry. Preliminary numerical system simulations improve comprehension of the storage performance and its interdependencies with other system components, but require both accurate and computationally efficient models. This study presents a toolbox for the simulation of borehole thermal energy storage systems in *Modelica*. The storage model is divided into a borehole heat exchanger (BHE), a local, and a global sub-model. For each sub-model, different modeling approaches can be deployed. To assess the overall performance of the model, two studies are carried out: One compares the model results to those of 3D finite element method (FEM) models to investigate the model's validity over a large range of parameters. In a second study, the accuracies of the implemented model variants are assessed by comparing their results to monitoring data from an existing BTES system. Both studies prove the validity of the modeling approaches under investigation. Although the differences in accuracy for the compared variants are small, the proper model choice can significantly reduce the computational effort.

Keywords: borehole thermal energy storage; Modelica; district heating; borehole heat exchanger; thermal resistance capacity model; model reduction

1. Introduction

Borehole thermal energy storage (BTES) systems are suitable for large-scale storage of thermal energy in the subsurface over periods of several months, thus facilitating seasonal storage of, e.g., solar thermal energy or waste heat [1–3]. The concept is principally based on storage of thermal energy in the subsurface, while the subsurface (i.e., soil or rock and pore water) serves as storage medium, the heat is injected and extracted with an array of borehole heat exchangers (BHE). For the construction of BHEs, a closed pipe loop is placed into a borehole and the remaining annular space between the piping and the borehole wall is backfilled to establish a good thermal contact between the pipes and the ground. Subsequently, heat can be injected or extracted by circulating a heat carrier fluid through the BHEs. The temperature difference between the heat carrier fluid and the rock determines the direction of heat transfer. For efficient operation of BTES systems, careful design based on a thorough understanding of its behavior is imperative. Operational conditions like the temperature and volume flow of the entering fluid have a strong impact on the storage performance. These conditions are defined by other components of the district heating system in which the BTES is embedded. Therefore,

a dynamic simulation of the whole system is necessary to account for all interactions and to achieve an accurate assessment of the heating system's performance. A language for the modeling and simulation of multi-domain physical systems is *Modelica* [4]. It uses an object-oriented equation-based approach facilitating state of the art modeling, simulation, and optimization of district heating systems [5–7]. While there are numerous analytical and numerical modeling approaches for the standalone assessment of BTES systems [8–10], only very few of those models are suited and implemented for dynamic system simulation software tools [11,12]. To overcome this and facilitate both accurate and efficient modeling and simulation of BTES systems in *Modelica*, a new model was developed. The model exploits typical characteristics of BTES systems for reducing the model complexity, while including the most important features of practical applications.

1.1. State-of-the-Art Modeling Approaches for BTES Systems

BTES systems are preferably built in areas with little to no groundwater flow to avoid larger dissipation of thermal energy by convective heat transport [13]. Thus, BTES models often disregard convective heat transport in the subsurface and focus on conductive processes [2,14]. However, the heat transport inside the BHE pipes is dominated by the circulation of the heat carrier fluid making convection the most important process. This difference in the prevailing heat transport processes inside and outside the BHE and their corresponding magnitudes have led to a variety of hybrid models [15–17]. These models usually consist of sub-models for the BHE and the surrounding ground. While the dimensions of the BHE models reach down to millimeters and seconds, the ground models focus primarily on scales from centimeters to dozens of meters and hours to years. This large range of magnitudes of the ground model has led to many approaches, which further divide the ground into a local and a global part. The local part covers the heat dissipation process around a single BHE and the global part considers only the heat transport between those local areas and the ground surrounding the storage [18]. Consequently, the division of the model decouples the different superposed heat diffusion processes of the storage system. When interactions with other model parts are disregarded, the underlying processes in all three models (the BHE model, the local, and the global model) exhibit distinct radial symmetric characteristics. This allows for a reduction of the model dimensions from 3D to 2D, which goes along with a significant reduction in the model's degrees of freedom (DoF). For each of the aforementioned sub-models, multiple analytical and numerical modeling approaches exist.

1.2. Existing BTES Models for Dynamic System Simulation

In general, there are many models for BHEs implemented into different software tools for dynamic system simulation. However, only a few take into account the thermal interactions between neighboring BHEs [16]. One of the first models—the Superposition Borehole Model (SBM)—was conceptualized by Eskilsson and Claesson [19]. It uses Thermal Resistance Models (TRM) for the representation of single BHEs. So-called “g-functions” are applied to factor in the interactions between neighboring BHEs in arrays with arbitrary geometric configurations. However, such functions have to be generated in advance by externally executed detailed numerical simulations. They solve the thermal response of a step-pulse for multiple line sources in a dimensionless form. Some methods have been developed to aggregate pulses further back in time, thus facilitating multi-year simulations with dynamic load conditions [20]. However, as transient storage operation conditions require sophisticated temporal superposition, the model is more suited for constant operation scenarios.

The most widespread BTES model is the duct ground storage model (DST) by Pahud and Hellström [11]. It reduces the global 3D thermal diffusion problem to a 2D problem assuming a radial symmetric storage geometry. As with the aforementioned SBM, the DST model also utilizes a TRM approach to represent single BHEs. The overall temperature inside the ground is obtained by the superposition of a local, a global, and a steady flux part. While the local and the global model are realized with finite difference models (FDM), the steady flux part is defined by analytical equations.

Both the SBM and the DST model have been implemented into *TRNSYS* [21], a software for dynamic simulations of thermal energy systems.

So far, the only BTES model that has been developed using the modeling language *Modelica*, is the Hybrid Step Response Model (HSRM) by Picard and Helsen [12]. For the representation of BHEs, the model uses a Thermal Resistance and Capacity Model (TRCM), as introduced by Bauer [22], increasing the short-time accuracy compared to TRM based models. Around each single BHE, a radial FDM is used for the local model. Moreover, the global temperature field is obtained using Javed's method [20], which is a simplified and more compact version of Claesson's approach. It analytically calculates the step response of multiple equal line sources. Temporal superposition of multiple pulses again renders the consideration of time-varying operation scenarios possible. As a result, the HSRM model facilitates accurate simulations of both short-term and long-term behavior of BTES systems with arbitrary designs. Nevertheless, the pre-calculation of the response functions for the global model are time-consuming. Consequently, the model is better suited for studies with a small number of different configurations. As a uniform temperature along all borehole walls is assumed, the applicability of the HSRM model is restricted to BTES systems with BHEs connected in parallel

Obviously, the existing models for simulation of BTES systems have certain drawbacks: Both the DST and SBM model disregard the thermal capacity of the backfilling inside the boreholes. Considering that the space between the pipes and the borehole wall—i.e., the backfilled space—yields the steepest thermal gradients, this imposes a serious limitation on the short-time accuracy of these models. Furthermore, there is no existing model that can simulate both the impact of different hydraulic circuitries as well as the resulting pressure losses. While parallel connection of BHEs is common for heat extraction boreholes, most BHE arrays for storage purposes show serial connection schemes. Therefore, disregarding serial connections as in the HSRM model poses a strong limitation for BTES applications. Moreover, the existing models assume homogeneous thermal properties inside the storage volume and do not allow for consideration of stratigraphic changes in these properties or of an upper BHE section with thermally insulating grout [23]. Additionally, there are some practical limitations of the models. For example, it is not possible to simulate two instances of the DST model simultaneously.

One general advantage of the modeling language *Modelica* is the possibility to create tool-independent models that can be used in different modeling and simulation environments. Even though *Modelica* standard conformity poses a challenging task for complex models, developers should try not to restrain the use of their model to a single software. Unfortunately, the HSRM does only work in the *Modelica* environment it was developed with.

To overcome these issues, a new open source *Modelica* toolbox for the Simulation of BTES systems, the *MoBTES* component library, has been developed. It is not restricted to a single simulation environment and has a modular structure, enabling modification of component type and modeling approaches. Important design features of BTES systems, like serial and parallel BHE connections, reversal of flow direction, pressure loss calculation, consideration of stratigraphic subsurface models, and partly insulated BHEs, are implemented.

2. Methods

2.1. *MoBTES* Modeling Approaches

To enable the efficient simulation of BTES systems in *Modelica* for both dynamic system simulations and large parameter studies, the component library *MoBTES* was created. It extensively utilizes object-orientation to allow for a high reusability of the BTES model components and an easy extensibility. It comprises components for the simulation of BHEs and BTES systems and uses components and interfaces from the *Modelica* standard libraries *Fluid Heat Flow* and *Heat Transfer* [4]. Generally, all models are built in accordance with the *Modelica Language Specification* version 3.4 [4], avoiding syntax and scripts specific to individual *Modelica* environments. Nevertheless, problems may occur since each environment handles the implementation of the *Modelica* language slightly different. The library

has been developed and optimized for user experience using *SimulationX* [24], but other software tools have been successfully tested as well. A short description of the library structure and the tested simulation environments can be found in Appendix A.

Analogous to the previously mentioned BTES modeling approaches, the model is subdivided into a global part, a local part, and a BHE part. In contrast to the actual shape of the storage under investigation, circular global, and local models are used, allowing for a reduction from 3D to 2D, by exploiting their symmetries. However, *MoBTES* offers the option to choose from circular, rectangular, and hexagonal layouts. The radii of the global and local models are calculated to result in volumes equivalent to those of the actual layout. The hypothesis that the size of the model volume is of higher importance than its shape is in line with Hellström [18] who concluded a detailed study on this matter.

Figure 1 shows the discretization of the modeled region into smaller volume elements that form the global model. The global model calculates heat flows on a large scale and therefore only considers the average temperature inside each volume element. Each global element, which is located inside the actual storage region, is connected to an element of the local model. This local element, in turn, is connected to a corresponding BHE element, such that it interconnects the BHE element with the global element. This setup of interfaces between the different sub-models links the borehole wall temperature and the average temperature inside the respective storage volume, i.e., the global element temperature. Exploiting the equation-based nature of *Modelica*, this allows for an independent mathematical description of the thermal processes within each sub-model.

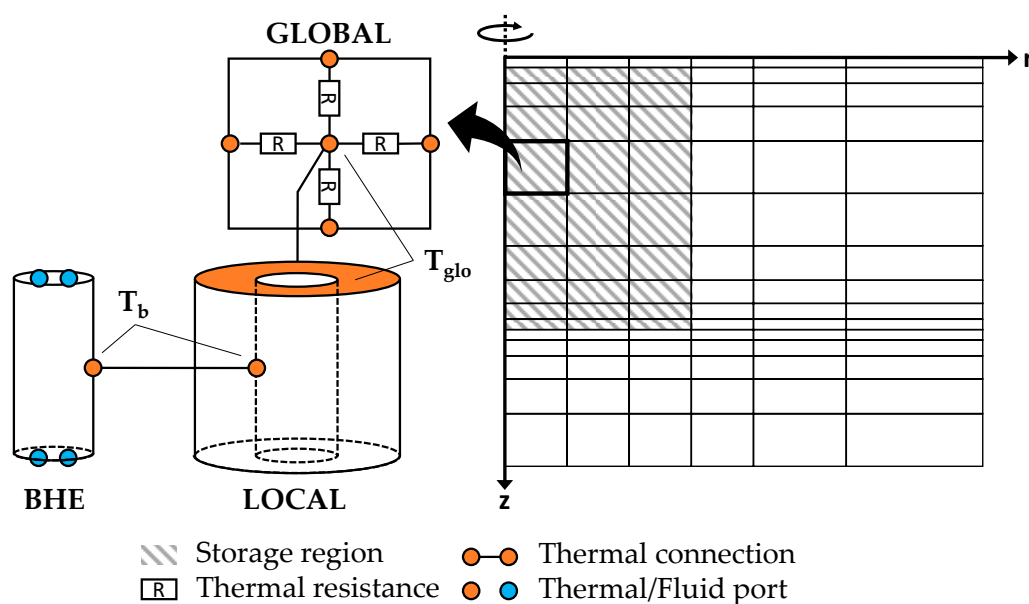


Figure 1. Mesh of a MoBTES model (right) and the fundamental connection scheme of the sub-models (left). The local element interconnects the global elements to their associated borehole heat exchanger (BHE) elements by giving a relation between the borehole wall temperature (T_b) and the mean volume temperature (T_{glo}).

The definition of interfaces between the sub-models together with *Modelica's* object-oriented approach render the replacement of each sub-model possible and facilitate the utilization of different modeling approaches or component types. This enables the adaption of the model to the requirements of each application in terms of short- or long-term accuracy and computational effort. All currently available variants will be outlined in the following chapters.

2.1.1. Borehole Heat Exchanger Models

The BHEs are divided vertically into segments that are connected by flow ports. *MoBTES* offers two interchangeable approaches to solve the heat transport problem inside the BHEs, both of which

have their advantages and disadvantages. As the default approach, a TRCM after Bauer [22] is deployed, which takes account of the thermal capacities of the grout and therefore achieves a more accurate reproduction of the transient short-time behavior. The second approach disregards the grout capacities in a TRM. Consequently, the degrees of freedom (DoF) and thus the computing time are reduced. Both approaches contain models for Single-U, Double-U, and Coaxial BHEs. A detailed definition of the models is given by Bauer [22,25].

2.1.2. Local Heat Transport Models

The main purpose of a local model is to link the borehole wall temperature T_b of the BHE segment it is connected with, to the temperature of its corresponding global volume element T_{glo} , which is defined as the average temperature inside this ground volume. There are currently two different approaches for the local model implemented in *MoBTES*: one generally more suited for transient operation scenarios and the other one rather for more steady conditions like step-response studies. For the more transient case, an FDM is used to represent the radial symmetric process around a single BHE segment. The approach, which is already known from the DST or HSRM models [11,12], divides the local volume into concentric ring elements (see Figure 2a). Following Eskilson and Claesson’s [19] guidelines for radial meshing, the three innermost elements have an equal thickness and succeeding elements grow by a constant factor. As defined by Equation (1), the global temperature T_{glo} is calculated by the weighted average ring temperatures. C_i and T_i are the thermal capacity and temperature of a single ring element, respectively, and C_{loc} is the overall thermal capacity of the local volume.

$$T_{glo} = \sum_{i=1}^{n_{rings}} \frac{C_i}{C_{loc}} * T_i \tag{1}$$

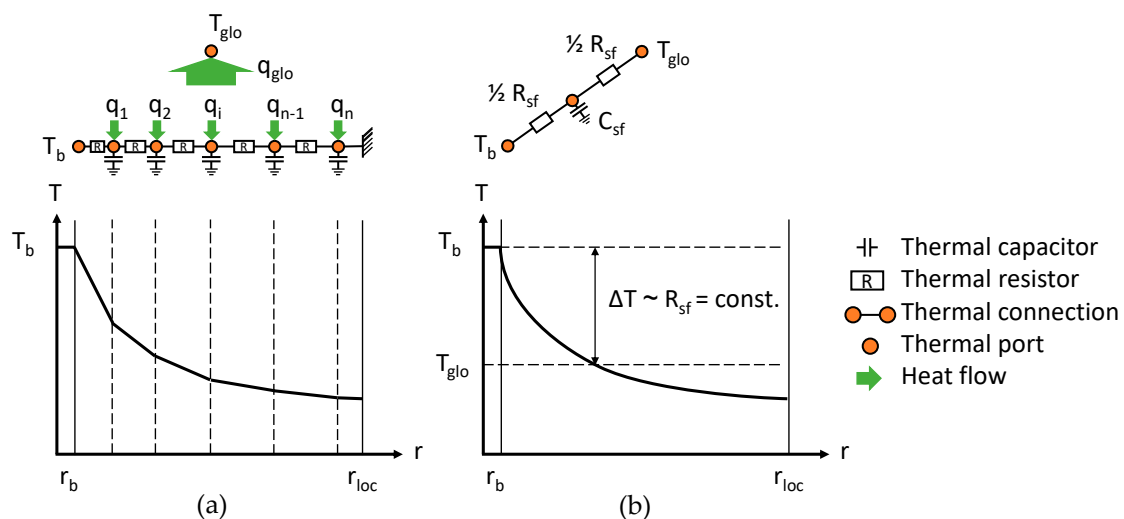


Figure 2. Local model concepts: (a) finite differences model and (b) steady flux model.

The heat flux q_{glo} to or from a volume element is defined on the global level and distributed as q_i among the n ring elements of the local model according to the weighting factors.

The second local model variant implemented in *MoBTES* is based on the steady flux part of the analytical solution for heat conduction inside a hollow cylinder with a fixed heat flow Q_{sf} at the inner boundary and no flow of heat over the outer boundary [26] (see Figure 2b). This steady flux profile describes the temperature gradient within the hollow cylinder after initial transient processes have subsided. Its shape is time-independent and can therefore be used to calculate the temperature difference between the borehole wall temperature T_b and the average volume temperature T_{glo} . The

relation between the steady flux Q_{sf} and this temperature difference can be expressed as a resistance R_{sf} . The DST model uses this resistance to calculate heat transport processes for long time-scales [11].

Carslaw and Jaeger analytically investigated the conduction of heat in a hollow cylinder for different boundary conditions [27]. Their result for the above-mentioned case of a fixed heat flow Q_{sf} over the inner boundary and no flow of heat over the outer boundary is given by Equation (2) and can be used to obtain a solution for the local volume temperature profile. It depends on time and radius and consists of three terms. The first one only depends on the energy injected over time and gives an expression for the average volume temperature T_m (Equation (3)). The second term defines a time-independent radial temperature profile T_o , which corresponds to the profile shape under steady flux conditions, where R_0 is the thermal resistance between the borehole wall radius r_b and radius r , r_{loc} the radius of the local volume and λ the thermal conductivity inside the volume (Equation (4)).

$$T(r, t) = Q_{sf} \left(\frac{1}{C_{loc}} t + R_0(r) - \sum_{i=1}^{\infty} R_i(r) e^{-\frac{t}{\tau_i}} \right) \quad (2)$$

$$T_m(t) = \frac{Q_{sf}}{C_{loc}} t = \frac{Q_{sf}}{c \rho \pi (r_{loc}^2 - r_b^2)} t \quad (3)$$

$$T_o(r) = Q_{sf} R_0(r) = \frac{Q_{sf}}{2\pi \lambda} \frac{r_{loc}^2}{r_{loc}^2 - r_b^2} \left(\ln\left(\frac{r_{loc}}{r}\right) - \frac{3}{4} + \frac{2r^2 - r_b^2}{4r_{loc}^2} + \frac{r_b^2}{r_{loc}^2 - r_b^2} \ln\left(\frac{r_{loc}}{r_b}\right) \right) \quad (4)$$

Finally, the third term describes the transition from the initially uniform temperature inside the hollow cylinder to the steady flux temperature profile. Its summands converge to zero with time. The speed of this process depends on the size of the respective time constants τ_i and is generally higher for summands with a higher index i . If this initial transition period is disregarded, Equations (5)–(8) can be used to obtain an expression for the steady flux resistance R_{sf} .

$$T(r_b, t) - T_m(t) = T_0(r_b) \quad (5)$$

$$= \frac{Q_{sf}}{2\pi\lambda} \left(\left(\frac{r_{loc}^2}{r_{loc}^2 - r_b^2} \right)^2 \ln\left(\frac{r_{loc}}{r_b}\right) - \frac{3r_{loc}^2 - r_b^2}{4(r_{loc}^2 - r_b^2)} \right) \quad (6)$$

$$= \frac{Q_{sf}}{2\pi\lambda} \left(\ln\left(\frac{r_{loc}}{r_b}\right) - \frac{3}{4} \right), r_{loc} \gg r_b \quad (7)$$

$$= Q_{sf} R_{sf} \quad (8)$$

Franke [28] introduced the idea of implementing a surrogate capacity C_{sf} to this steady flux model to approximate the initial transient behavior until steady flux conditions prevail. Equation (9) gives the definition of this capacity, where a is the thermal diffusivity of the local volume and τ_1 the first and largest time constant of Equation (2). The resulting steady flux local model is depicted in Figure 2b. It was originally designed for dynamic optimization problems. Consequently, strong emphasis was put on computational speed.

$$C_{sf} = \frac{\tau_1}{R_{sf}} \simeq \frac{r_{loc}^2}{15 a R_{sf}} \quad (9)$$

2.1.3. Global Heat Transport Model

Most BTES systems exhibit an axial symmetry. This symmetry is exploited by the global model to reduce the 3D problem to a 2D FDM model with axes in the radial and vertical directions. The subsurface domain is discretized into rectangular elements. Each of these elements represents the cross section of a ring of the modeled region. The average element temperatures, which are derived from the local model, serve as input for the calculation of the global thermal diffusion process. Furthermore, Dirichlet boundary conditions are used to define temperatures at the outer model edges. Thereby,

the temperature at the model's ground surface boundary is either set to the average annual ambient temperature or to a time-varying temperature defined by an input. To ensure a sufficient size of the modeled region, while simultaneously maintaining a low number of DoF, the size of the global elements outside of the storage region increases by a defined growth factor following the scheme of Eskilsson and Claesson [19].

2.2. Model Validation

The individual validities as well as the limitations of the sub-model approaches are demonstrated and discussed in detail in the original literature [18,25,28]. Therefore, the validation of the *MoBTES* model focuses on the functional interaction of the sub-models. To assess the accuracy of results, a parameter study was carried out for a large range of parameters, in which the energy balances of *MoBTES* models are compared to those of detailed FEM models.

In a case study, monitoring data from an existing BTES system is used to test *MoBTES'* ability to accurately reproduce real-world applications. The relative deviations δQ of the charged and discharged energy as well as the resulting energy balance are calculated according to Equation (10).

$$\delta Q = \frac{Q_{\text{model}} - Q_{\text{reference}}}{Q_{\text{reference}}} * 100\% \quad (10)$$

2.2.1. Parameter Study

To evaluate the long-term accuracy of the proposed model for both local model variants (FDM and steady flux), a parameter study is carried out, in which the average annual amounts of charged and discharged energy are compared to detailed 3D simulations. These benchmark simulations are performed in *FEFLOW* [29], a commercial finite element software tool for the simulation of groundwater flow, and mass and heat transport in porous and fractured media, which is frequently used for the simulation of BTES applications [8,30–32]. An operation period of ten years is simulated. In each year, the storage is charged for six months with a constant inlet temperature of 80 °C, and afterwards is discharged for another six months with an inlet temperature of 20 °C. All BHEs are connected in parallel and the volume flow rate is set to 2 l/s per BHE. The investigated parameter range is given in Table 1.

Table 1. Parameter range for the 3D finite element method (FEM) benchmark models.

| Parameter | Range |
|----------------------|---|
| Number of BHEs | 4, 7, 9, 16, 19, 25, 36, 37, 49, 61, 62, 64, 81, 91, 93, 100, 121, 127, 130, 144, 169, 173, 196 |
| BHE length | 50 m, 100 m |
| BHE spacing | 3 m, 5 m |
| BTES layout | circular, rectangular, hexagonal |
| Local model variants | steady flux, FDM with 10 capacity nodes |

Closely-packed and symmetric BTES designs of rectangular, circular, and hexagonal shapes of up to 196 BHEs are investigated (Figure 3). For each of the resulting layouts, models with a minimal axial spacing of 3 m and 5 m between the BHEs as well as lengths of 50 m and 100 m are created. Finally, a total of 99 corresponding benchmark simulations are carried out. Each of those benchmarks is compared to two *MoBTES* simulations, one using the steady flux local model, and the other using the FDM local model with 10 capacity nodes. Moreover, all models in this study utilize the TRM variant for Double-U BHEs, since *FEFLOW* does not provide a TRCM model. A full list of all benchmark and *MoBTES* models, their parametrization, and aggregated results can be found in the supplementary data (Table S1).

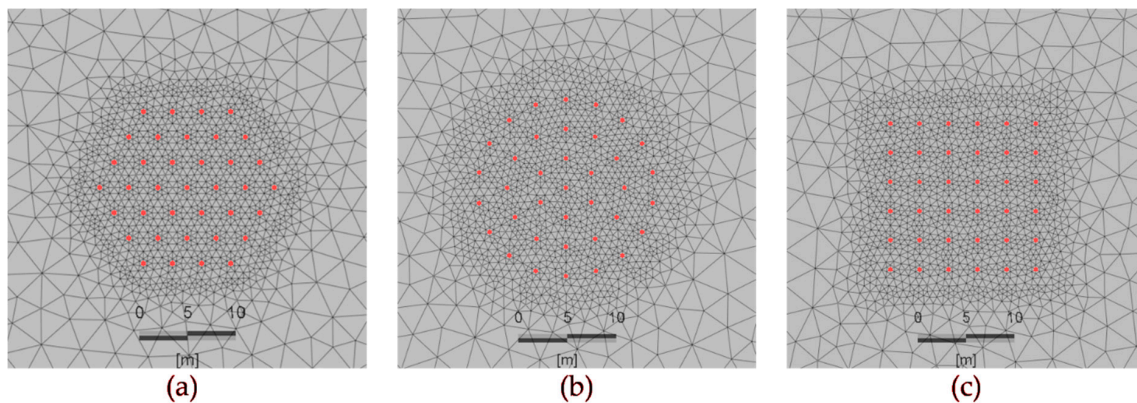


Figure 3. Top view on *FEFLOW* benchmark models with red markers for BHE positions: (a) hexagonal storage with 37 BHEs; (b) circular storage with 37 BHEs; (c) rectangular storage with 36 BHEs.

2.2.2. Case Study

To assess the predictive abilities of *MoBTES* concerning real storage operation, a BTES system installed in the Brødstrup solar district heating system (Denmark) [33] is simulated and the results are compared to monitoring data. The Brødstrup system consists of 48 BHEs with a length of 45 m each. Six BHEs are connected in series, resulting in eight strings of BHEs in parallel (see Figure 4). During charging operation, the flow through the BTES system is directed from the central BHEs to the peripheral BHEs. During discharging, the flow direction is reversed.

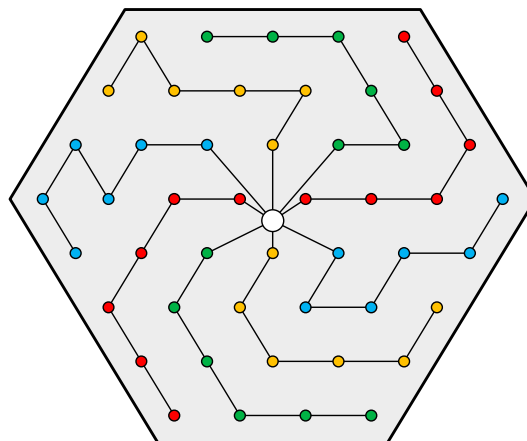


Figure 4. Brødstrup borehole thermal energy storage (BTES) system layout and serial BHE connections [33].

An important prerequisite for an accurate simulation of a real BTES system is good knowledge of the underground's thermal properties at the storage location. Tordrup et al. [31] used inverse modeling to determine thermal conductivity and volumetric heat capacity values for six geological layers at the storage site for a suitable model parametrization. Using monitoring data of the first 500 days of operation, they could reach an overall deviation between the energy balance of their fitted model and the monitoring data of 4.0%. The resulting average effective values for the thermal conductivity and the volumetric heat capacity of 1.72 W/(m K) and 1.96 MJ/(m³ K), respectively, were used for the parametrization of the *MoBTES* model. However, this study has some important limitations which have to be kept in mind for the interpretation of the case study results. For example, adiabatic boundary conditions were set at all model boundaries to reduce the computational effort of the inverse modeling process. This is a major limitation, especially for the ground surface boundary, where thermal losses of the storage are usually highest.

In contrast to Tordrup et al. [31], who used data smoothed to daily values, this study exploits the full temporal resolution of 5 min from the raw monitoring data. Although the available data covers the time from the initial storage startup until the end of 2017, Tordrup et al.'s parameter estimation only utilized data of the first 500 days of operation. Therefore, the performance evaluation of the *MoBTES* model is primarily conducted for this period as well. Nevertheless, selected *MoBTES* models are simulated over the whole range of available data and compared to the monitored energy balance.

Figure 5 shows the measured inlet and outlet temperatures of the storage system during the considered time span. It indicates that during this time span, different operation strategies were tested: In 2012, the first year of operation, charging and discharging was performed in pulses with constant volume flow rates. In contrast to that, during the second charging period in 2013, the outlet temperatures were kept constant at defined temperature levels over longer periods, presumably by regulation of the volume flow. The presence of different operational strategies and the comparably good availability of data make the Brødstrup dataset a particularly suitable test case for the validation of *MoBTES*.

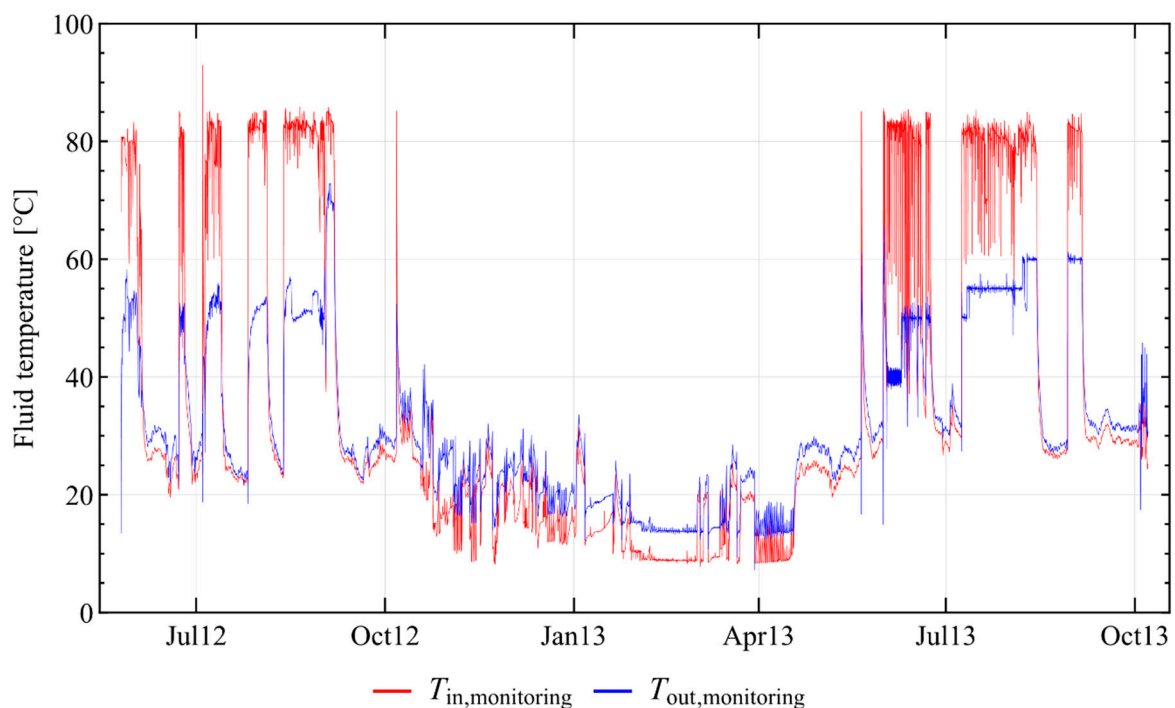


Figure 5. Measured inlet and outlet temperatures of the BTES system in Brødstrup during the first 500 days of operation.

For the comparison of the measurement data to the *MoBTES* models, all implemented modeling approaches are tested, using the monitored inlet temperature and volume flow rate time series as input. TRM and TRCM models are deployed for the BHE models and for the local model the steady flux and the FDM variants are compared. The FDM model's number of capacity nodes is varied between 2 and 16. Overall, a total of 20 simulations are carried out over the first 500 days of operation. Subsequently, the deviations between simulated and monitored values of the storage outlet temperature as well as the charged and discharged amount of energy are calculated for all models.

3. Results

3.1. Parameter Study Results

Different BTES layouts and geometries are simulated using *MoBTES* with both the FDM as well as the steady flux local model. Subsequently, the amounts of charged and discharged heat are calculated

and compared to the results of the outcome of the respective *FEFLOW* benchmark models. Figure 6 shows the individual deviations of charged and discharged energy of all simulated *MoBTES* models. For both model variants, regression lines are depicted for the deviation in charging and discharging to illustrate the impact of the storage volume.

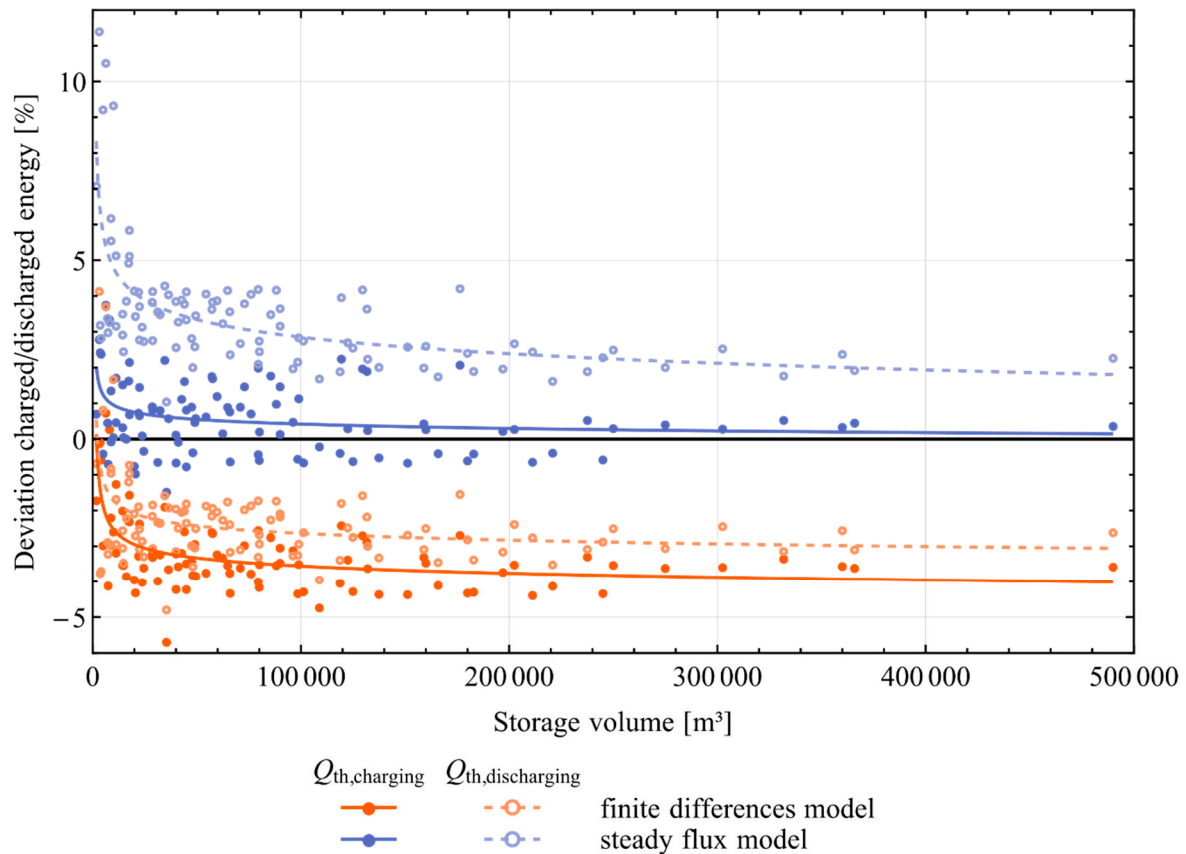


Figure 6. Relative deviation of charged and discharged thermal energy between *MoBTES* and *FEFLOW* for different storage system layouts.

Table 2 summarizes the mean results of the two local model variants. In comparison with the *FEFLOW* models, the FDM models underestimate the amount of charged energy by an average of -3.2% and discharged energy by an average of -2.3% . The similar magnitudes of deviation for both charging and discharging result in storage efficiencies close to those of the benchmark models. While the mean storage efficiency of all *FEFLOW* models is 60.9% the FDM *MoBTES* models yield an efficiency of 61.4% . In contrast to that, the deviations for charging and discharging differ significantly more for the steady flux models which achieve 62.5% storage efficiency on average. Underlying reason for this is a small deviation of $+0.6\%$ for charging in combination with an overestimation of $+3.5\%$ for the discharged energy amounts.

Table 2. Mean values of the *MoBTES* simulation results for both local model variants and deviation to *FEFLOW* benchmark models (standard deviation in brackets).

| Results | <i>MoBTES</i> FDM | <i>MoBTES</i> Steady Flux Model |
|---|--------------------------|------------------------------------|
| Mean storage efficiency <i>MoBTES</i> | 61.4% | 62.5% |
| Mean deviation from <i>FEFLOW</i> : charged energy | -3.2% ($\pm 1.1\%$) | $+0.6\%$ ($\pm 1.0\%$) |
| Mean deviation from <i>FEFLOW</i> : discharged energy | -2.3% ($\pm 1.3\%$) | $+3.5\%$ ($\pm 1.7\%$) |
| Average computation time <i>MoBTES</i> | 751.8 s | 181.1 s |

On average, running an FDM model took 752 s, whereas the steady flux-based models required less than one-quarter of this time (181 s). Most of the computation time was consumed for the preprocessing, translation, and compilation of the *Modelica* models to C-code, whereas the actual simulations required only a fraction of it. The study was carried out using *SimulationX*, but for comparison, selected models were simulated in *Dymola* [34] and *OpenModelica* [35] as well. While *OpenModelica* yielded similar computation times as *SimulationX*, the model translation and compilation in *Dymola* took significantly less time resulting in much shorter overall computation times.

Figure 7 shows the impact of different parameters on the relative deviation between the charged and discharged energy amounts of *FEFLOW* and *MoBTES* FDM models. In accordance with Figure 6, the mean deviation in charging is larger than the deviation in discharging for all models utilizing an FDM local model. Additionally, it can be observed that the choice of layout seems to have an impact on the deviation, since there is a notable difference for circular, rectangular, and hexagonal layouts. Moreover, the deviation increases for more shallow systems and for larger BHE spacings.

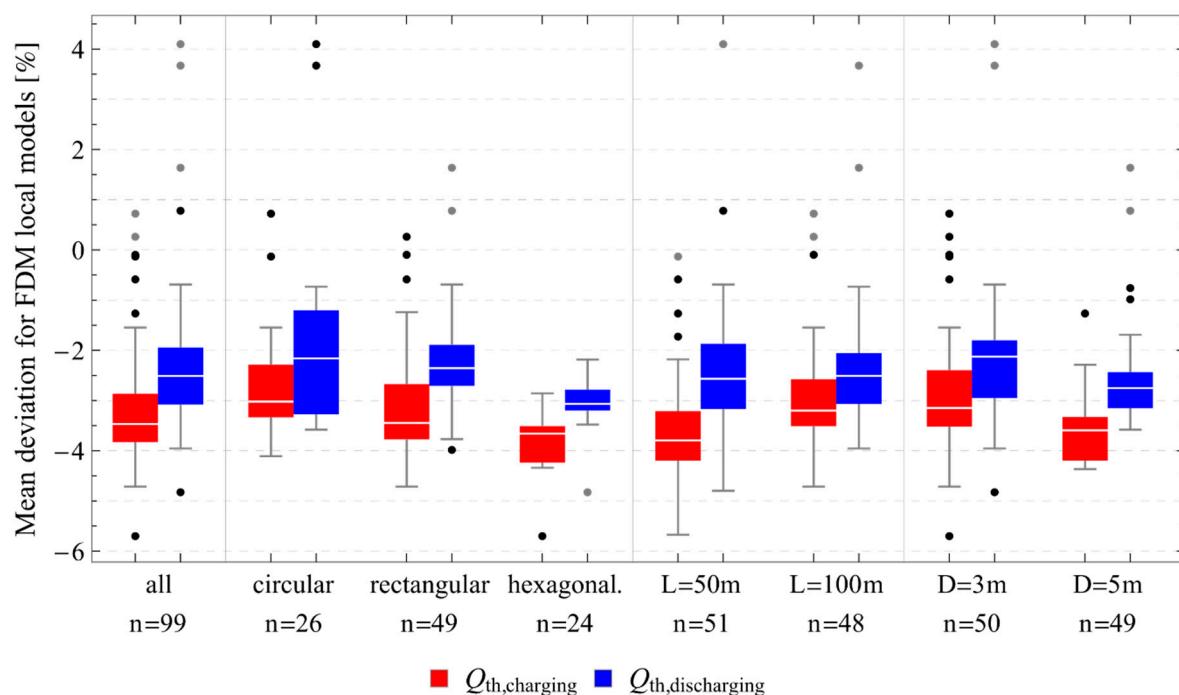


Figure 7. Impact of different parameters on the deviation of charged and discharged energy between *FEFLOW* and *MoBTES* models using an FDM local model (L = BHE length, D = minimal BHE distance).

Figure 8 illustrates the distribution of the deviations between *FEFLOW* and steady flux *MoBTES* models. During charging, the *MoBTES* models produce results very similar to *FEFLOW* and exhibit only few outliers. In contrast, the deviation is much larger during discharging and more outliers occur. The increased difference between relative deviations for charging and discharging leads to the higher discrepancy in storage efficiencies (cf. Table 2).

3.2. Case Study Results

For the case study, 20 *MoBTES* models with different modeling approaches and levels of discretization are simulated using monitoring data from the Bødstrup BTES inlet temperature as input. Subsequently, their outputs are compared to the outputs of the on-site measurements. One simulation of the considered 500-day-spanning monitoring data takes on average 12.3 min with models using the FDM approach for the local model. Compared to that, the steady flux approach reduces the computation time by more than 70% to only 3.5 min.

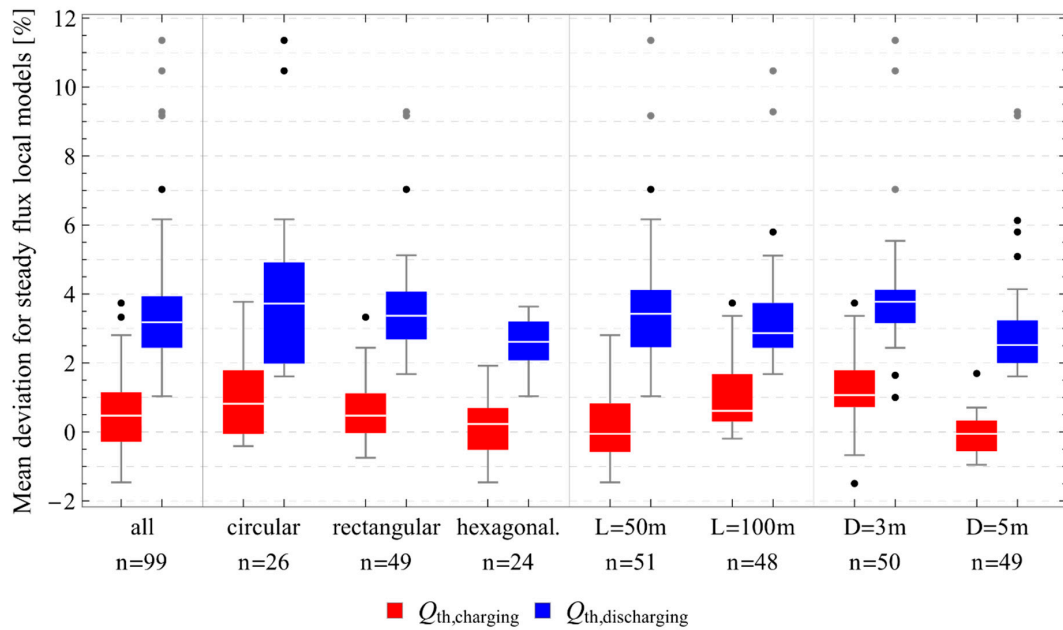


Figure 8. Impact of different parameters on the deviation of charged and discharged energy between *FEFLOW* and *MoBTES* models using a steady flux local model ($L =$ BHE length, $D =$ minimal BHE distance).

Figure 9 plots the computation times against the average temperature deviations for all individual simulation runs. In case of the FDM-based models, the computation time correlates with the level of discretization, i.e., the number of capacity nodes used. The steady flux models, which have only one capacity included, achieve a comparable computational speed to the FDM models with two capacities. This indicates that not only the absolute amount of DoFs determines the computational effort. Accordingly, model runs which utilize a TRCM BHE model do not generally take longer than their TRM counterparts, even though they have additional DoFs.

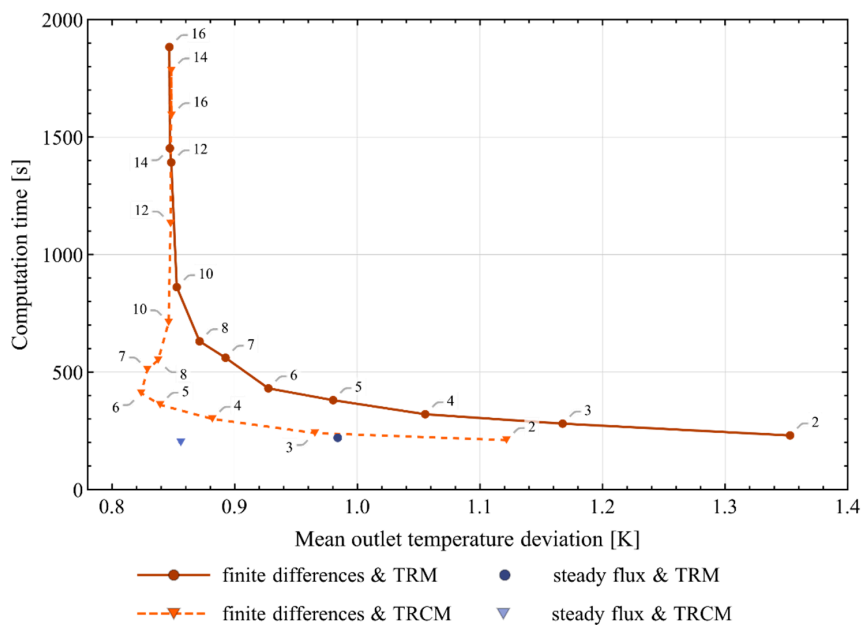


Figure 9. Computation time and mean deviation of the outlet temperature in comparison to the Brødstrup monitoring data for different local models. FDM models are labeled with their according number of used capacity nodes.

As a measure for the model accuracy, the mean outlet temperature deviation ΔT_{mean} is determined according to Equation (11), where t_{sim} is the final simulation time and $\mathbb{1}(t)$ is an indicator function being 1 for times of storage operation and 0 otherwise:

$$\Delta T_{mean} = \frac{\int_0^{t_{sim}} \mathbb{1}(t) \left| T(t)_{outlet,monitoring} - T(t)_{outlet,MoBTES} \right| dt}{\int_0^{t_{sim}} \mathbb{1}(t) dt} \quad (11)$$

Regarding the outlet temperature deviation, models using a TRCM generally perform better than their counterparts with a TRM. Only for finer capacity node meshes both approaches' accuracies converge. Notably, a minimum in the deviation of the outlet temperature can be observed for the combination of TRCM models and FDM local models with six capacity nodes. A finer discretization does not improve the model's accuracy any further.

Figure 10 shows the deviation of the energy balance of the *MoBTES* models and the monitoring data. All models exhibit an underestimation of the energy balance by -3.2 to -8.4% . The lowest deviations can be observed for the models, which use a steady flux local model, showing an underestimation of the monitored energy balance of -3.2% for the model using a TRCM BHE model and -3.9% for the TRM variant, respectively. For the simulations utilizing FDM local models, a general trend towards lower deviations can be observed for an increase in the number of capacity nodes. Variants with six capacities or more exhibit an underestimation of the energy balance by approximately 6% . Regarding the BHE models, it can again be observed that models, which use the TRCM approach, show better accuracy in comparison to their TRM counterparts.

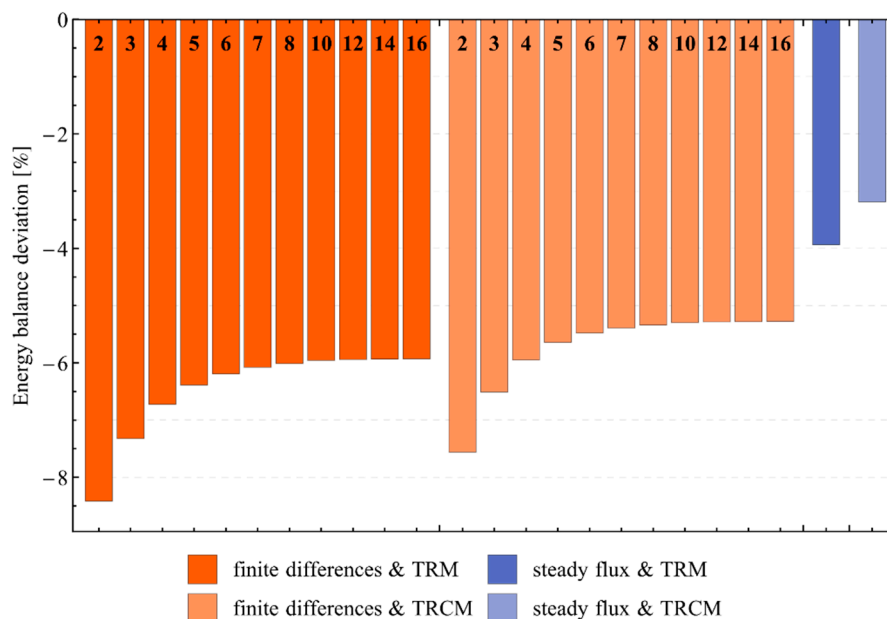


Figure 10. Relative deviation of the *MoBTES* models' energy balance in relation to the monitoring data after 500 simulated days (number of local model capacities on finite differences bars).

A more detailed insight into the model's short-time behavior can be gained by comparing the results of the different TRCM-based models to the monitored data over the first 24 h of BTES system operation (cf. Figure 11). At the initial startup of the system, the inlet temperature was kept relatively constant at a temperature of $80\text{ }^{\circ}\text{C}$, whereas the volume flow rate was adjusted over time. During the first twelve hours, models utilizing the FDM approach with two to five capacities or the steady flux model result in outlet temperatures above the monitored outlet temperature, whereas FDMs with seven or more capacities underestimate it. The model, which uses an FDM with six capacities, shows an almost perfect fit. It can be observed that the outlet temperature of the FDM variants converges to a

certain profile for an increasing number of capacity nodes. For the second half of the shown period, all models overestimate the outlet temperature, exhibiting smaller deviations for models with a finer discretization of the capacity.

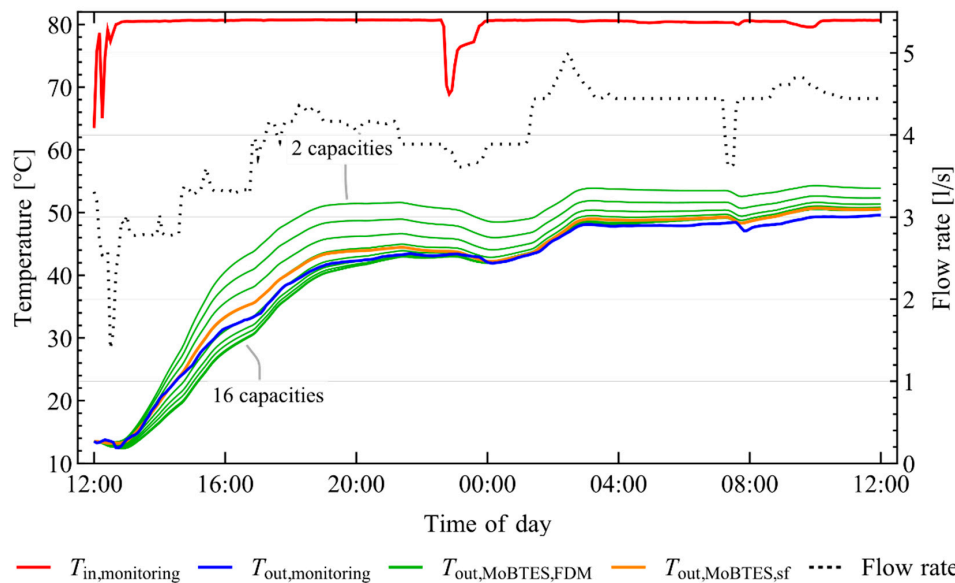


Figure 11. Comparison of monitored and simulated outlet temperatures for *MoBTES* models with Thermal Resistance and Capacity Model (TRCM) (FDM variants: number of capacity nodes increases from top to bottom).

To test the predictive abilities of *MoBTES* and the underlying parametrization of the case study over a larger time span, a steady flux model and an FDM model with six capacities (both using the TRCM BHE model) are simulated over the whole range of available monitoring data of 1680 days. Subsequently, the energy balance histories of the models are calculated and compared to the monitored energy balance history (Figure 12).

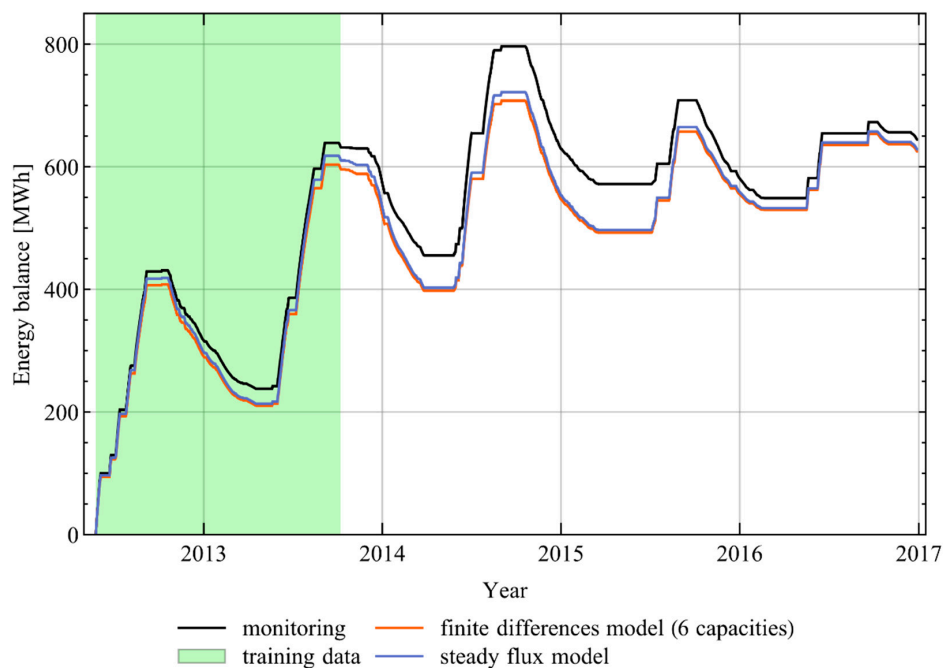


Figure 12. Energy balance from monitoring data and two selected models from startup until the end of the available data.

The final energy balance deviation after 1680 days amounts to -2.9% and -2.4% for the FDM approach and the steady flux approach, respectively. Surprisingly, these values are considerably lower than the deviations observed after 500 days of simulation (-5.5% and -3.2%). More important though is the maximum deviation which occurs during the summer of 2015 and amounts to -13.9% and -13.1% , respectively. The difference between the energy balances of the two *MoBTES* model variants is small in comparison to their deviation to the monitored data.

4. Discussion

4.1. Parameter Study

The parameter study's main purpose is to compare *MoBTES* to an established model with well-defined parameters and thereby assess its ability to accurately predict the amount of charged and discharged thermal energy over a large parameter range. However, the *FEFLOW* models, which were chosen as benchmarks, also represent a simplification of reality and are prone to the effect of geological uncertainty. Consequently, *FEFLOW*'s actual accuracy in terms of simulating real BTES systems is limited. The comparison of *FEFLOW* and *MoBTES* should therefore be regarded as validation of the new model by numerical means.

The results presented in Section 3.1 show minor deviations between the charged and discharged amount of heat for all *MoBTES* models, except for very small BTES systems (cf. Figure 6). However, BTES systems consisting only of very few BHEs are not common, as storage efficiency generally increases with size, making those small systems inefficient. Therefore, the inaccuracy for small systems does not represent a major limitation of *MoBTES*. It is most likely caused by assumptions made for the modeling approaches of *MoBTES* local models. Figure 1 illustrates that the local models exchange thermal energy with the BHEs through the borehole walls and with the global model by extracting and injecting heat to their whole volume. As a consequence, no heat is exchanged via their outer boundaries. This poses a reasonable assumption for BHEs in the center of BTES systems. However, the error is larger for BHEs at the edge of the storage volume as they are not symmetrically surrounded by neighboring BHEs. The surface-to-volume ratio increases for small systems, hence leading to larger deviations. As a consequence, the minimal possible number of BHEs in *MoBTES* was limited to seven, to avoid excessive errors.

The overall magnitude of deviation for most models is in a low single-digit percentage range, which can be regarded as adequate. Accordingly, it is not possible to identify a local model approach as more accurate for simple step-response studies like the presented parameter study. However, additional information can be drawn from it. Although, the steady flux local models exhibit comparable magnitudes of deviation as the FDM variants, they clearly outperform them regarding the computational efficiency (cf. Table 2). Consequently, the steady flux model is preferable for large parameter studies with steady operation schemes.

Interestingly, the choice of the BTES layout seems to have an impact on the deviation for both local model variants (cf. Figures 7 and 8). Circular layouts tend to higher estimates in comparison to rectangular layouts, hexagonal resulting in the lowest estimates. There are several possible underlying reasons, which have to be discussed:

The first one concerns the overall shape of the BTES systems and the global models. We have to remember that *MoBTES* itself is a circular BTES model, and therefore the actual shapes of the benchmark models differ for rectangular and hexagonal layouts (cf. Figure 3). If this geometry transformation was the root cause for the observed layout impact, the circular models would have to perform best. This is true for the FDM variants, where the magnitude of deviation is smallest for circular arrangements, but not true for the steady flux variants, where the opposite is the case. Consequently, the model reduction approach of the global model has probably only a minor effect.

A second potential cause regards the shape of the local models. These have a circular cross section, whereas none of the areas around a single BHE is circular for the actual layouts. However, this

deviation in shape is considerably smaller for hexagonal cross-sections in comparison to rectangular ones. Again, the fact that hexagonal layouts perform best for the steady flux variants, while they exhibit the largest deviations for FDM variants contradicts the assumption that this might be the major cause for the impact of the choice of layout on the deviation.

A third potential cause for the observed impact of the storage layout on the deviation could be their diverging packing densities. Equal minimal BHE distances D lead to different radii of the local model r_{loc} for rectangular, hexagonal, and circular layouts. Hexagonal layouts yield the highest packing density, resulting in smaller radii r_{loc} for the same BHE distances D . Therefore, parameter study models with equal minimal BHE distance D , but varying storage layouts, result in different radii r_{loc} . If this would be the underlying reason, the observed impact would actually have to be related to the model volume, which is directly correlated to the BHE distance D and length L . Hexagonal layouts, which have the highest packing density, i.e., smaller storage volumes in average, yield in lower estimates of charged and discharged amounts of energy for both local model variants. However, the impact of BHE distance D and length L (cf. Figures 7 and 8) suggests that a potential correlation between deviation and storage volume should be reversed.

All effects, which are implied by the presented figures, are rather small and possibly not statistically significant. Nevertheless, some useful conclusions can be drawn by analyzing the difference in deviation between charging and discharging for the steady flux models (cf. Figure 8). There is a higher number of more pronounced outliers for discharging than for charging. Referring to Figure 6, these outliers can be connected to models of small BTES systems. This indicates that steady flux models with very small storage volumes exhibit the highest deviations from the *FEFLOW* benchmarks of all simulated *MoBTES* models. Therefore, FDM local models should be preferably applied for the simulation of small BTES systems.

As an overall result of the parameter study, it can be stated that *MoBTES* can be used for the simulation of simple BTES applications, as it produces results very close to those of detailed FEM models. Still, this is limited to certain applications. For example, *MoBTES* does not consider groundwater flow or BHE arrangements that strongly diverge from axisymmetric layouts. However, BTES systems are preferably built on sites with negligible groundwater flow to reduce convective losses. In addition to that, these systems should be constructed with a low surface-to-volume ratio to ensure an efficient performance. Due to these general rules for the construction of BTES systems, the aforementioned limitations do not pose a problem for most practical purposes. These general rules do not necessarily apply for regular BHE arrays, which are only used either for extraction or for injection of heat. This underlines the importance of using *MoBTES* for its original purpose of storage applications.

4.2. Case Study

Design and operation of the Brødstrup system were investigated in great detail to achieve an accurate representation by the *MoBTES* models [31,33]. Nevertheless, there are still significant uncertainties left regarding the components' thermal properties. This has to be kept in mind in order to avoid overinterpretation when comparing the simulation results to the monitoring data. Independently, the case study is perfectly suited for a further comparison of the different *MoBTES* model variants in terms of efficiency and accuracy.

4.2.1. Computational Effort and Mean Outlet Temperature Deviation

While the simulation of BTES systems using *MoBTES* reduces the computational effort in comparison to 3D FEM models by several orders of magnitude, there are significant differences between the different *MoBTES* approaches as well: computation times for the initial 500-day period range from 200 s to 1880 s (Figure 9). As expected, the specific computation time for the simulation of one year of storage operation is considerably higher compared to the parameter study described in Section 3.1. For example, the combination of steady flux local model and TRM BHE model takes 165.1 s per simulated year for the case study. In contrast, a comparable *MoBTES* model from the parameter

study takes only 20.6 s for one year. This can probably be attributed to generally smaller time steps in the case study due to a more transient operation, on the one hand, as well as a limitation of the maximum time step size to the resolution of the monitoring data of 5 min on the other hand.

Putting the computational time and the mean outlet temperature deviation of the different models in relation to each other (Figure 9) also unveils some interesting coherencies. As expected, the computational effort generally increases with the number of capacities of the local models. Consequently, the steady flux local models, which include only one capacity reach the lowest computation times. Comparing the temperature deviation of TRM-based and TRCM-based combinations strongly emphasizes the superiority of the TRCM approach. Both the FDM-TRM as well as the FDM-TRCM model combinations' mean outlet temperature deviations decrease with an increase in the number of capacities. However, for higher capacity numbers they seem to converge to a certain minimal value, which is a common outcome for grid refinement studies. However, for all models comprising less than ten capacities, the TRCM approach achieves in some cases significantly lower deviations than the comparable TRM models, while resulting in slightly lower computation times. As stated several times, the consideration of the grout's thermal capacity is of high importance. Discretization of meshes for numerical simulation should generally be refined at model areas with steep gradients and strong transient behavior. The temperatures within the boreholes of a BTES system fulfill both aspects, which explains the good performance of the *MoBTES* variants that use TRCM BHE models.

It seems that there is a good trade-off between the computational effort and the accuracy for models with six to eight capacities: these models gain a significant reduction in the temperature deviation while they experience only a minor increase in the computational time. Surprisingly, the deviation for FDM-TRCM model combinations even exhibits a minimum for six capacities, which might be explained by a closer look at the short time performance of the models (see Section 4.2.3). In terms of a good trade-off between computational speed and accuracy, the steady flux model combined with a TRCM model seems to be a serious alternative to the FDM based models.

4.2.2. Comparison of Overall Energy Balance Deviations

Counterintuitively, the overall energy balance deviations (cf. Figure 10) of the models utilizing the steady flux approach even undercut that of the FDM based models. However, this finding does not contradict the observation that some of the FDM models perform better in terms of predicting the outlet temperature (cf. Figure 9). This is because of two reasons: First, the underlying energy balance is achieved by the summation of charged and discharged energy. Consequently, an error in charging can be compensated by an equally large error in discharging. In contrast to that, the temperature deviation considers only absolute deviation values, as defined by Equation (11). Second, the temperature deviation does not take the volume flow rate into account. Since the volume flow rate varies significantly over time, the simulated outlet temperature contributes to the energy balance with varying weights.

4.2.3. Short Time Accuracy

The presented results are values integrated over the entire simulated time span. Therefore, they are mostly defined by the long-term accuracy of the model, whereas the short-time accuracy can be investigated best at times of strong changes in the operation of the BTES. The start-up phase of the storage represents such a sudden change in operation, which can be regarded as a step-pulse with a temperature raise of almost 70 K (cf. Figure 11). Moreover, the strong variation of the volume flow rate during that time span poses an additional difficulty for the reproduction of the transient operation behavior of the system. Most likely, the model with six capacities represents the best fit to the monitored outlet temperature by coincidence. However, this could explain the minimum in the mean outlet temperature deviation for this number of capacities (cf. Figure 9). In line with the results for the average outlet temperature deviation (cf. Figure 9), the steady flux model performs equally

well as the FDM model with five capacities. As expected, the difference between the model variants decreases over time.

4.2.4. Comparison of Model Results and the Extended Monitoring Data

A successful comparison of the *MoBTES* models to the monitored data requires a good knowledge of the subsurface properties. For the Brædstrup case study, these key input parameters are gathered from a parameter estimation study conducted by Tordrup et al. [31]. With this parametrization, *MoBTES* underestimates the amount of energy after 500 days of operation by 3.2% to 6.5% disregarding models that use local FDM models with four or less capacities (cf. Figure 10). For comparison, the 3D FEM model by Tordrup et al. [31] with the best fit also resulted in an underestimation of the energy budget by 4%. This indicates that *MoBTES* is capable to reproduce the operation of the Brædstrup system during this period just as well as the 3D FEM model.

Regarding the energy balance history for the extended simulation period of 1680 days (cf. Figure 12) a maximum deviation of the *MoBTES* energy balance can be observed in 2015 before a trend reversal sets in resulting in a comparably low deviation by the end of the simulation period. The change in the model drift could indicate an insufficient size of the modeled region. However, this concern could be dispelled as a significant increase of the outer model boundaries did not result in any noticeable change in the models' energy balance.

When assessing the predictive capabilities of *MoBTES*, the limitations of the inverse modeling study by Tordrup et al. mentioned in Section 2.2.2 should be considered. Especially, the application of the adiabatic model boundaries represents an oversimplification as it corresponds to a perfect insulation on the ground surface. This is of little consequence during the initial storage operation when temperatures inside the storage volume and consequently the losses through the ground surface are naturally low. Therefore, this could explain both the good fit during the start-up period and the following increasing deviation.

The decline in the deviation towards the end of the simulation is an indication that the meaningfulness of an overall balance is limited, as different segments of the energy balance compensate each other. However, the use of the overall energy balance as evaluation value is due to the lack of more detailed data of the original simulations of Tordrup et al.

If an overall evaluation of the model quality is to be given, it must be considered that model input parameters, such as heat capacities and thermal conductivities of the soil and grout are subject to considerable uncertainties. Under this premise, the results of the FDM models with at least five capacities and the results of the steady-flux model are sufficiently accurate. As all models have some difficulties to accurately predict the storage behavior beyond the fitting period, the parameter estimation study should be repeated on the data foundation that is available now, taking thermal losses through the ground surface into account. As this goes clearly beyond the scope of this study, it should be considered as a future application of *MoBTES*.

5. Conclusions

The presented *MoBTES* model facilitates the deployment of different modeling approaches for its sub-models, allowing for an adaption to the numerical requirements of varying applications. The currently implemented variants are based on well-known and proven approaches, which exploit the physical characteristics of BTES systems. Consequently, the comparison of *MoBTES* to 3D FEM benchmark models and monitoring data from an existing plant reveals only minor deviations in their performance figures. While all variants are able to adequately reproduce the long-term system behavior, the right choice can significantly increase the computational efficiency or short-time accuracy. In addition to that, the presented model framework can be used as a test bed for new developed modeling approaches, provided they are compatible with the division of the model into a global, a local and a BHE sub-model. Other possible future applications of the developed open source *Modelica* library, could

be the rededication of the BHE models for non-storage applications or the realization of additional underground thermal energy storage technologies by reusing the available ground components.

In contrast to existing BHE models in *Modelica*, *MoBTES* is a dedicated BTES model and therefore should cover all relevant design features of such systems. Therefore, emphasis was put on the implementation of functionalities like serially connected BHEs, consideration of the stratigraphy at the storage site, flow reversal, hydraulic pressure loss, or partly insulated BHEs. To ensure an efficient operation, actual BTES systems are favorably build as compact arrays of thermally interacting BHEs on sites with negligible groundwater movement. Therefore, *MoBTES* only considers those cases and its accuracy might be impaired significantly for other applications.

The implemented model features allow for an accurate assessment of the impact of different designs on the storage performance, while maintaining a computational efficiency suitable for system simulation. Additionally, the flexibility of *MoBTES* enables the use of very fast models for extensive parameter studies or stochastic simulation. The versatile and multi-domain modeling approach of *Modelica*, allows for the integration of *MoBTES* into models of whole energy systems, including sector coupling and the combination with a wide range of other open source model libraries.

Supplementary Materials: The following are available online at <http://www.mdpi.com/1996-1073/13/9/2327/s1>, Table S1: Benchmark parameter study models and results. The *MoBTES* *Modelica* library, including an example package with the parameter study model, the case study model and all related parameters or datasets, is available online at <https://github.com/JFormhals/MoBTES>.

Author Contributions: This research was made collaboratively by all authors. Conceptualization was done by J.F., B.W., D.O.S., and I.S. Development of the methodology, software, data processing, formal analysis, and visualization was done by J.F. Validation was done by H.H., B.W., and J.F. Funding acquisition and supervision was done by D.O.S. and I.S. Review and editing was done by D.O.S., H.H., B.W., I.S., and J.F. All authors have read and agree to the published version of the manuscript.

Funding: This work was financially supported by the German Research Foundation (DFG) in the framework of the Excellence Initiative, Darmstadt Graduate School of Excellence Energy Science and Engineering (GSC 1070) and the European Research Development Fund (ERDF) by supporting the North-West Europe Interreg project DGE-Rollout.

Acknowledgments: The authors want to thank Brædstrup Fjernvaerme for sharing the monitoring data of the solar district heating plant in Brædstrup that was used for this work. Furthermore, the authors want to thank Morten Vang Bobach of Arcon-Sunmark and Jim Larsen of Brædstrup Fjernvaerme for sharing their detailed knowledge about the construction and operation of the BTES system.

Conflicts of Interest: The authors declare no conflicts of interest.

Nomenclature

| | |
|--------|--|
| BHE | borehole heat exchanger |
| BTES | borehole thermal energy storage |
| DoF | degrees of freedom |
| FDM | finite differences model |
| HSRM | hybrid step response model |
| MoBTES | Modelica borehole thermal energy storage model |
| SBM | superposition borehole model |
| TRCM | thermal resistance and capacity model |
| TRM | thermal resistance model |

Symbols

| | | |
|-----------|------------------------------|------------------------|
| a | thermal diffusivity | m^2/s |
| c | gravimetric thermal capacity | kg/m^3 |
| C | thermal capacity | J/K |
| D | borehole spacing | m |
| L | Borehole length | m |
| q | specific heat flux | W/m |
| Q | Thermal energy | J |
| \dot{Q} | heat flux | W |
| r | radius | m |
| R | thermal resistance | K/W |
| T | temperature | K |
| t | time | s |
| δ | relative deviation | - |
| ρ | density | kg/m^3 |
| λ | thermal conductivity | W/(m K) |
| τ | time constant | s |
| 1 | indicator function | - |

Subscripts

| | |
|-----|--|
| b | borehole wall |
| glo | global problem |
| loc | local problem |
| m | mean |
| min | minimum |
| sf | steady flux |
| sim | final simulation time |
| th | thermal |
| 0 | constant temperature profile under steady flux condition |

Appendix A Modelica Library

The structure of the developed *Modelica* library can be seen in Figure A1. The main component is the *BTES* model, which has one fluid port each for inlet and outlet of the storage. An additional input is available if the user chooses to define a time-varying ground surface temperature. All physical components, which are used to build the *BTES* model, are included in the *Components* package. The *Components.Ground* package includes models for the global solution and the different local solutions, whereas the *Components.BoreholeHeatExchangers* package includes the Single-U, Double-U and Coaxial BHE models. The *Builder* package includes functions and enumerations which are needed for the assembly of the *BTES* model. All parameter sets which can be used in the *BTES* model are stored in the *Parameters* package as records. There are typical data records and the records of the examples shown in this work for the location, different soil types, the heat exchangers, grouts and heat carrier fluids. All components or parameter records that can be replaced by each other share common base classes. These base classes define all common properties, like interfaces or indispensable parameters, which is especially important for the replacement of the local, global, and BHE models. New implementations should inherit from the respective base class, to be in conformity with the *MoBTES* modeling approach. *MoBTES* version 1.0 has been successfully tested for *SimulationX* and *Dymola*.

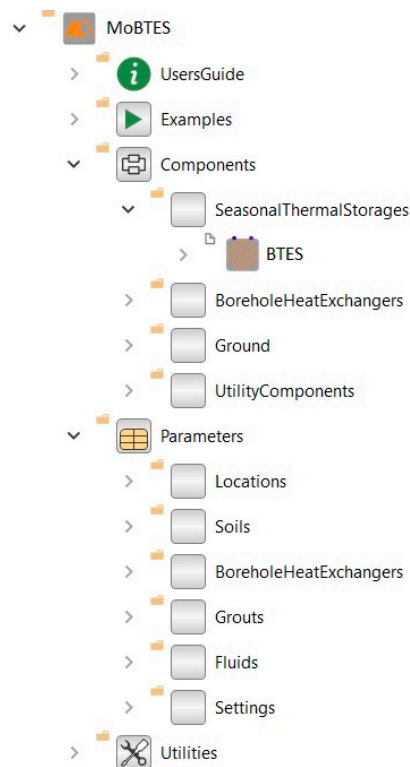


Figure A1. MoBTES Modelica library structure.

References

1. Reuss, M. The use of borehole thermal energy storage (BTES) systems. In *Advances in Thermal Energy Storage Systems: Methods and Applications*; Elsevier: Cambridge, UK, 2015; pp. 117–147. ISBN 9781782420965.
2. Gehlin, S. Borehole thermal energy storage. In *Advances in Ground-Source Heat Pump Systems*; Elsevier: Duxford, UK, 2016; pp. 295–337.
3. Welsch, B.; Göllner-Völker, L.; Schulte, D.O.; Bär, K.; Sass, I.; Schebek, L. Environmental and economic assessment of borehole thermal energy storage in district heating systems. *Appl. Energy* **2018**, *216*, 73–90. [CrossRef]
4. Olsson, H. Modelica—A unified object-oriented language for physical systems modeling; Modelica Association. Available online: <https://www.modelica.org/documents/ModelicaSpec34.pdf> (accessed on 30 April 2020).
5. Schweiger, G.; Larsson, P.O.; Magnusson, F.; Lauenburg, P.; Velut, S. District heating and cooling systems—Framework for Modelica-based simulation and dynamic optimization. *Energy* **2017**, *137*, 566–578. [CrossRef]
6. Filonenko, K.; Howard, D.; Buck, J.; Veje, C. Comparison of two simulation tools for district heating applications. In Proceedings of the 9th International Conference on Energy Reliability REMOO-2019, Hong Kong, China, 16–18 April 2019.
7. Wetter, M. Haugstetter Modelica versus TRNSYS—A Comparison between an equation-based and a procedural modeling language for building energy simulation. *Proc. SimBuild* **2006**, *2*, 262–269.
8. Diersch, H.J.G.; Bauer, D.; Heidemann, W.; Rühaak, W.; Schätzl, P. Finite element modeling of borehole heat exchanger systems. Part 2. Numerical simulation. *Comput. Geosci.* **2011**, *37*, 1136–1147. [CrossRef]
9. Schulte, D.O.; Welsch, B.; Rühaak, W.; Bär, K.; Sass, I. BASIMO—Borehole Heat Exchanger Array Simulation and Optimization Tool. In Proceedings of the European Geosciences Union General Assembly 2017, Vienna, Austria, 23–28 April 2017.
10. Blocon. *Earth Energy Designer* (version 4); Windows; Blocon: Lund, Sweden, 2016.

11. Pahud, D.; Hellström, G. The new duct ground heat model for TRNSYS. In Proceedings of the Eurotherm Seminar n°49, Physical models for Thermal Energy Stores, Eindhoven, The Netherlands, 25–27 March 1996; pp. 127–136.
12. Picard, D.; Helsen, L. A New Hybrid Model For Borefield Heat Exchangers Performance Evaluation. In Proceedings of the 2014 Ashrae Annual Conference, Seattle, WA, USA, 28 June–2 July 2014; pp. 857–866.
13. Skarphagen, H.; Banks, D.; Frengstad, B.S.; Gether, H. Design Considerations for Borehole Thermal Energy Storage (BTES): A Review with Emphasis on Convective Heat Transfer. *Geofluids* **2019**, 1–26. [[CrossRef](#)]
14. Moradi, A.; Smits, K.M.; Lu, N.; McCartney, J.S. Heat Transfer in Unsaturated Soil with Application to Borehole Thermal Energy Storage. *Vadose Zone J.* **2016**, *15*. [[CrossRef](#)]
15. Picard, D. Modeling, Optimal Control and HVAC Design of Large Buildings using Ground Source Heat Pump Systems. Ph.D. Thesis, KU Leuven, Leuven, Belgium, 2017.
16. Lanahan, M.; Tabares-Velasco, P.C. Seasonal thermal-energy storage: A critical review on BTES systems, modeling, and system design for higher system efficiency. *Energies* **2017**, *10*, 743. [[CrossRef](#)]
17. Chio, S.; Miraiillosseinabadi, S. Simulation modeling of ground source heat pump systems for the performance analysis of residential buildings. In Proceedings of the BS 2013: 13th Conference of the International Building Performance Simulation Association, Chambéry, France, 26–28 August 2013; pp. 1960–1967.
18. Hellström, G. Ground Heat Storage: Thermal Analyses of Duct Storage Systems. Ph.D. Thesis, Lund University, Lund, Sweden, 1991.
19. Eskilson, P.; Claesson, J. Simulation model for thermally interacting heat extraction boreholes. *Numer. Heat Transf.* **1988**, *13*, 149–165. [[CrossRef](#)]
20. Javed, S. Thermal Modelling and Evaluation of Borehole Heat Transfer. Ph.D. Thesis, Chalmers University of Technology, Göteborg, Sweden, 2012.
21. Solar Energy Laboratory. *TRNSYS—A Transient System Simulation Program (Version 18)*; University of Wisconsin-Madison, Solar Energy Laboratory: Madison, WI, USA, 2017.
22. Bauer, D.; Heidemann, W.; Müller-Steinhagen, H.; Diersch, H.J.G. Thermal resistance and capacity models for borehole heat exchangers. *Int. J. Energy Res.* **2011**, *35*, 312–320. [[CrossRef](#)]
23. Schulte, D.O.; Welsch, B.; Boockmeyer, A.; Rühaak, W.; Bär, K.; Bauer, S.; Sass, I. Modelling Insulated Borehole Heat Exchangers. *Environ. Earth Sci.* **2016**, *75*, 910. [[CrossRef](#)]
24. ESI ITI. *SimulationX (Version 4.1)*; ESI ITI: Dresden, Germany, 2017.
25. Bauer, D. Zur thermischen Modellierung von Erdwärmesonden und Erdsonden-Wärmespeichern. Ph.D. Thesis, Universität Stuttgart, Stuttgart, Germany, 2012.
26. Claesson, J.; Eskilson, P. Conductive heat extraction to a deep borehole: Thermal analyses and dimensioning rules. *Energy* **1988**, *13*, 509–527. [[CrossRef](#)]
27. Carslaw, H.S.; Jaeger, J.C. Conduction of Heat in Solids. *Phys. Today* **1962**, *15*, 74–76. [[CrossRef](#)]
28. Franke, R. *Integrierte Dynamische Modellierung und Optimierung von Systemen mit Saisonaler Wärmespeicherung*; Fortschrittberichte VDI: Reihe 6, Energietechnik Nr. 394; VDI-Verlag: Düsseldorf, Germany, 1998; ISBN 3-18-339406-5.
29. DHI WASY. *FEFLOW (version 7.1)*; Windows; DHI WASY: Berlin, Germany, 2017.
30. Mielke, P.; Bauer, D.; Homuth, S.; Götz, A.E.; Sass, I. Thermal effect of a borehole thermal energy store on the subsurface. *Geotherm. Energy* **2014**, *2*, 5. [[CrossRef](#)]
31. Tordrup, K.W.; Poulsen, S.E.; Bjørn, H. An improved method for upscaling borehole thermal energy storage using inverse finite element modelling. *Renew. Energy* **2017**, *105*, 13–21. [[CrossRef](#)]
32. Homuth, S.; Mikisek, P.; Götz, A.E.; Sass, I. Geothermische Langzeitmodellierung eines solargekoppelten Erdsonden-Wärmespeichers in Crailsheim. In Proceedings of the Der Geothermiekongress 2011, Bochum, Germany, 15–17 November 2011.
33. Sørensen, P.A.; Larsen, J.; Thøgersen, L.; Dannemand Andersen, J.; Østergaard, C.; Schmidt, T. Boreholes in Brødstrup. *Final Rep.* **2013**.

34. Dassault Systemes. *Dymola—Dynamic Modeling Laboratory* (version 2020); Windows; Dassault Systèmes AB: Lund, Sweden, 2020.
35. Fritzson, P.; Aronsson, P.; Lundvall, H.; Nyström, K.; Pop, A.; Saldamli, L.; Broman, D. The OpenModelica Modeling, Simulation, and Development Environment. In Proceedings of the 46th Conference on Simulation and Modelling of the Scandinavian Simulation Society (SIMS2005), Trondheim, Norway, 13–14 October 2005; pp. 83–90.



© 2020 by the authors. Licensee MDPI, Basel, Switzerland. This article is an open access article distributed under the terms and conditions of the Creative Commons Attribution (CC BY) license (<http://creativecommons.org/licenses/by/4.0/>).



Appendix C – Optimized layouts of borehole thermal energy storage systems in 4th generation grids

Published as:

Hemmatabady, H., **Formhals, J.**, Welsch, B., Schulte, D.O., and Sass, I., 2020, Optimized layouts of borehole thermal energy storage systems in 4th generation grids: *Energies*, v. 13, doi:10.3390/en13174405.

Article

Optimized Layouts of Borehole Thermal Energy Storage Systems in 4th Generation Grids

Hoofar Hemmatabady ^{1,2,*} , Julian Formhals ^{1,2}, Bastian Welsch ^{1,2} , Daniel Otto Schulte ¹ and Ingo Sass ^{1,2}

¹ Geothermal Science and Technology, Technical University of Darmstadt, Schnittspahnstraße 9, 64287 Darmstadt, Germany; formhals@geo.tu-darmstadt.de (J.F.); welsch@geo.tu-darmstadt.de (B.W.); daniel.schulte@gast.tu-darmstadt.de (D.O.S.); sass@geo.tu-darmstadt.de (I.S.)

² Graduate School of Excellence Energy Science and Engineering, Technical University of Darmstadt, Otto-Berndt-Str. 3, 64287 Darmstadt, Germany

* Correspondence: hemmatabady@geo.tu-darmstadt.de

Received: 31 July 2020; Accepted: 19 August 2020; Published: 26 August 2020



Abstract: Borehole thermal energy storage (BTES) systems are a viable option to meet the increasing cooling demand and to increase the sustainability of low-temperature district heating and cooling (DHC) grids. They are able to store the rejected heat of cooling cycles on a seasonal basis and deliver this heat during the heating season. However, their efficient practical implementation requires a thorough analysis from technical, economic and environmental points of view. In this comparative study, a dynamic exergoeconomic assessment is adopted to evaluate various options for integrating such a storage system into 4th generation DHC grids in heating dominated regions. For this purpose, different layouts are modeled and parameterized. Multi-objective optimization is conducted, varying the most important design variables in order to maximize exergetic efficiency and to minimize levelized cost of energy (LCOE). A comparison of the optimal designs of the different layouts reveals that passive cooling together with maximizing the heating temperature shift, accomplished by a heat pump, lead to optimal designs. Component-wise exergy and cost analysis of the most efficient designs highlights that heat pumps are responsible for the highest share in inefficiency while the installation of BTES has a high impact in the LCOE. BTES and buffer storage tanks have the lowest exergy destruction for all layouts and increasing the BTES volume results in more efficient DHC grids.

Keywords: district heating and cooling; borehole thermal energy storage; dynamic exergoeconomic method; TRNSYS; MATLAB; coupling; multi-objective optimization

1. Introduction

In European households, heating accounts for 78% of the total final energy use. Cooling of buildings still has a fairly small share in the energy use, but the demand during summer months is continuously rising due to climate change [1]. It is estimated that by 2025 the installed cooling capacity in Europe is likely to be 55–60% higher than in 2010 [2]. Therefore, simultaneous supply of heating and cooling needs to be considered as an important part of the future energy supply system.

By 2050, more than 80% of European residents are expected to live in urban areas [3]. This trend increases the benefits of district energy systems, which tend to be more economic for densely populated regions [4]. District heating and cooling (DHC) systems can be environmentally beneficial and pave the way toward the sustainable energy supply, if they are applied appropriately [4,5].

The 4th generation district heating (DH) concept specifies some prerequisites that need to be met for the proper application of DH systems and the fulfillment of their role in a future sustainable energy economy. The most important ones are the implementation of low-temperature DH networks,

the ability to recycle heat from low-temperature sources such as solar and geothermal heat and the implementation as an integrated part of smart energy systems [6]. A future 4th generation district cooling (DC) system can be defined as a system more interactive with the electricity, DH and gas grids [6]. Overall, a 4th generation DHC grid can be considered as a low-temperature interactive energy grid for supplying heating and cooling demands.

Every cooling process involves the rejection of excess heat to a heat sink. Lower sink temperatures generally result in a more efficient system operation. As the temperature of the ground during cooling seasons is lower and more stable than the ambient temperature, it can be used as an efficient heat sink by utilizing borehole heat exchangers (BHEs). In addition, arrays of BHEs are suitable thermal energy storage systems for waste heat and fluctuating renewable energy sources [7]. Such borehole thermal energy storage (BTES) systems exploit the high heat capacity of the underground to store large quantities of heat on a seasonal basis in the geological environment [8]. The results of analyzing the influence of design parameters on energetic performance of medium deep BTES systems showed that they can have a very high efficiency of more than 80% in large-scale applications [7,9–11].

Aforementioned benefits of BTES systems and the increasing trend of installing cooling capacity in Europe, makes the utilization of BTES-assisted 4th generation DHC grids an interesting concept for future energy supply. These benefits have been already proven by several projects (e.g., [12–14]). A review of some of these projects can be found in [15]. However, there are not enough guidelines for designing BTES systems in DHC grids. An efficient implementation of this concept requires more detailed assessments and system design from technical, economic and environmental points of view. A BTES should not be regarded in isolation, but merely as one component within a district heating and cooling network [8,16,17]. Therefore, a method needs to be selected that evaluates the optimal integration of BTES systems into DHC grids considering their interaction with other components.

An energy carrier's exergy is defined by its potential to interact with its environment [18], namely the availability of energy. Exergoeconomics is the branch of engineering that combines exergy analysis and economic principles. It can provide information to a system designer which are not available through conventional energy analysis and economic evaluations, but crucial to the design and operation of a cost-effective system [18]. Moreover, increasing exergy efficiency leads to reduced environmental impacts and a higher sustainability [19]. For environmental evaluation of BTES and energy systems, Life Cycle Assessment (LCA) has been proven to be a useful tool [20,21]. However, LCA lacks thermodynamic assessment [19]. Therefore, the exergoeconomic analysis method can be considered as a method which takes technical, economic and environmental aspects into consideration. Moreover, by adding CO₂ emission costs to the total costs, economic effects of direct environmental emissions can be considered as well.

Exergy analysis of an installed BTES system for heating and cooling applications was done by Kizilkan and Dincer [22,23]. These studies specify that a significant energy saving can be done by determining the exergy destruction of the whole system and its components. However, they have mainly used a static approach, which is suitable for high-temperature systems, e.g., power generation systems. When a system's operating temperature is close to the reference state, e.g., heating and cooling systems, the utilization of a dynamic approach is necessary [24].

In this study, a dynamic exergoeconomic assessment approach including CO₂ emission costs is adapted to BTES systems to render a comprehensive technical, economic and environmental assessment of their implementation into 4th generation DHC grids. The approach is presented on the example of a generic case study. After giving a general overview on this case study, different system layouts and scenarios are specified. Moreover, mathematical optimization is done for each scenario using the outputs of the exergoeconomic assessment approach as objective functions, varying the most sensitive system parameters. Finally, the results are compared and discussed.

2. Case Study Setup

For the case study, a notional district located in Frankfurt, Germany is chosen. Frankfurt is located in a heating-dominated region with a low cooling demand, which is mainly caused from the commercial and industrial sectors. It is assumed to consist of 100 single family houses, 100 multifamily houses and 50 office buildings. After designing 3D thermal zone models of each building type, load profiles are calculated in TRNBuild [25]. Boundary conditions are based on standard libraries for building construction types of renovated buildings [26], schedules (e.g., occupation) [27] and regime types (e.g., heating and cooling set point temperature) [27]. The weather data from Frankfurt airport is taken from Meteonorm data [28].

Figure 1 shows the calculated load profile. The total annual heating and cooling demands of the DHC grid are 8.47 GWh and 1.05 GWh, respectively, with more than 70% of the cooling demand for the office buildings. Supply and return temperatures (T_{sup} , T_{ret}) of the grid are 6 °C and 12 °C for active and 18 °C and 22 °C for passive cooling. In accordance to the 4th generation DH concept, supply and return temperatures are set to 45 °C and 35 °C during the heating season [29].

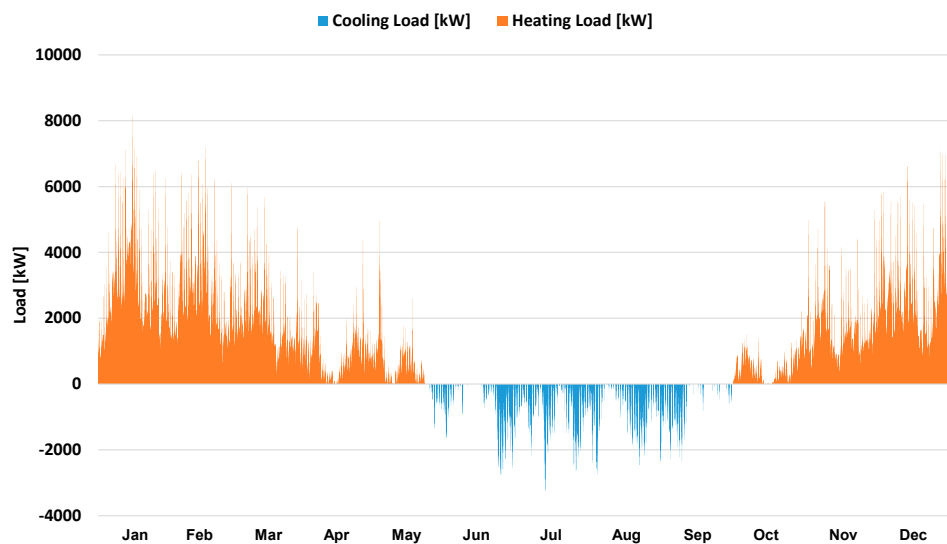


Figure 1. District heating and cooling (DHC) load profile.

3. System Design Scenarios

Four generally different designs of the case district's heating and cooling system shall be evaluated. The proposed scenarios are summarized in Table 1. All scenarios comprise a BTES system which is discharged by a heat pump (HP). Furthermore, the systems contain one or two gas boilers (GB) to cover heat demands which are not covered by the BTES system. Moreover, all scenarios include a buffer storage tank (BST) which is needed to lower the size of the BTES system, to maximize the total load supply from the ground loop and to operate the HPs more steadily by smoothening the load demands. The four scenarios generally differ by their approach of cooling (active or passive) and by the connection of the BTES system and the GB (serial or parallel). All four systems have their own characteristics during heating and cooling operation, respectively, which shall be outlined in the following.

Table 1. The proposed scenarios.

| Scenario | Cooling | GB | HPs | BST |
|----------|---------|----------|--------------|-----------------|
| ActSer | Active | Serial | Single stage | Cooling/Heating |
| ActPar | Active | Parallel | Double stage | Cooling/Heating |
| PasSer | Passive | Serial | Single stage | Cooling/Heating |
| PasPar | Passive | Parallel | Double stage | Cooling/Heating |

3.1. Cooling Operation

The DHC is located in a heating-dominated region. The two general cooling approaches are

- Active Cooling (Scenarios ActSer and ActPar): The total cooling load is supplied actively by heat pumps, which use the BTES as their heat sink (Figure 2) and
- Passive Cooling (Scenarios PasSer and PasPar): The total cooling load is supplied passively by the BTES using heat exchangers (HEX), which separate load and sink side (Figure 3).

The BTES temperature difference is taken as 5 K for active and 3 K for passive scenarios. The nominal BTES side flow rate of the HP, as well as the connected pump, are specified accordingly and at a BTES side temperature of 15 °C. The pump is turned on or off by a thermostat, which monitors the BST supply temperature.

In the active scenarios, either a single stage HP covers the whole cooling demand (ActSer), or each double stage HP module covers it partially (ActPar). Double stage HPs are selected for ActPar scenario, because of their more efficient operation in partial cooling mode. The nominal load side flow rate of the HP, as well as that of the connected pump, are selected according to the design supply and return temperatures. The BST thermostat turns on or off the pump and its flow rate is regulated considering the HP output capacity. For passive scenarios, the same on/off strategy operates the pump and the regulation is done considering the energy balance equation of the HEX.

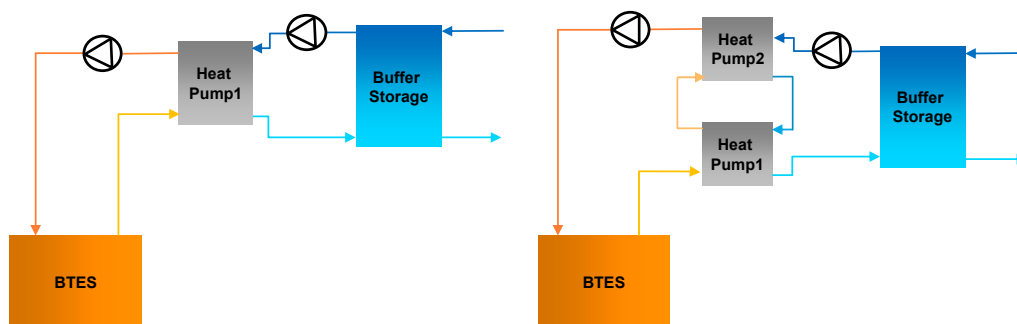


Figure 2. System layouts of the active cooling scenarios: ActPar (left) and ActSer (right).

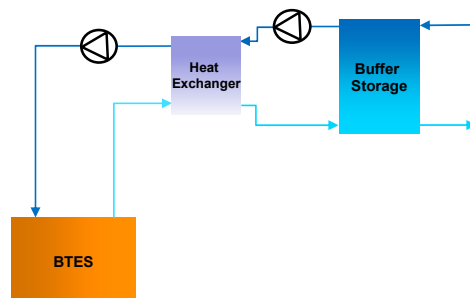


Figure 3. System layout of the passive cooling scenarios (PasSer and PasPar).

3.2. Heating Operation

The scenarios in heating mode are defined to compare the effect of the temperature shift and the maximum corresponding heating load that can be supplied efficiently by the ground loop. The design temperature difference of the BTES for heating mode is suggested to be between 3–5 K by some geothermal HP manufacturers [30]. In some practical applications this is taken as approx. 4 K [14,31]. 4 K can hardly be achieved for serially-connected HPs at full load performance (according to the manufacturer's data [32]). Therefore, to have similar boundary conditions for all scenarios, it is taken as 5 K for this study. The nominal flow rate of the HP on the source side and the connected pump are specified to meet the temperature difference at a source side temperature of 10 °C. The pump is

controlled by the BST on/off thermostat. On the load side, lower temperature shifts increase the COP of the HP but result in a lower BST efficiency [33] and a higher power consumption of the circulating pumps. Consequently, the serial and parallel scenarios are proposed to assess partial and full grid temperature shift by the ground loop, respectively. Like active cooling scenarios, the load side pump is turned on or off by the BST thermostat and its flow rate is regulated considering the HP output capacity.

3.2.1. Serial Scenarios

In serial mode (Figure 4) the HP consists of single stage modules, which heat the return water temperature from the bottom of the BST up to a specific set point temperature. The supplementary boiler GB2, which is connected to the BST in series, provides the additional heat up to the grid supply temperature of 45 °C. The maximum volume flow rate from the grid, which is sent from the diverter to the BST, is specified regarding the selected HP capacity for its continuous daily operation during the peak heating day. On the load side, the overall heat pump capacity (Cap_{HP}), the temperature shift of the BST (ΔT_{BST}) and the volume of the BST (Vol_{BST}) are selected using an optimization approach. Consequently, as the case study is located in a heating-dominated region, GB1 supplies the rest of the overall heating demand, which cannot be supplied by the HP and GB2 optimally.

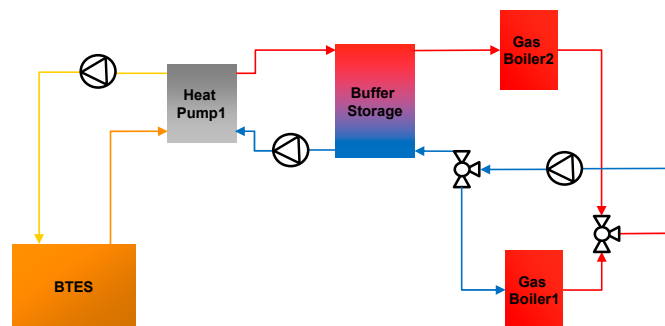


Figure 4. System layout of serial heating scenarios.

3.2.2. Parallel Scenarios

The system layout for parallel scenarios is shown in Figure 5. Two serially-connected HPs heat the return fluid from the BST up to the grid supply temperature. The amount of heat which cannot be supplied by the ground loop will be supplied by the gas boiler, which is in parallel operation with the HPs. On the load side, the maximum amount of the return fluid which is sent to the BST, Cap_{HP} and Vol_{BST} are specified with the same strategy as the serial scenario and ΔT_{BST} is fixed to the grid temperature shift.

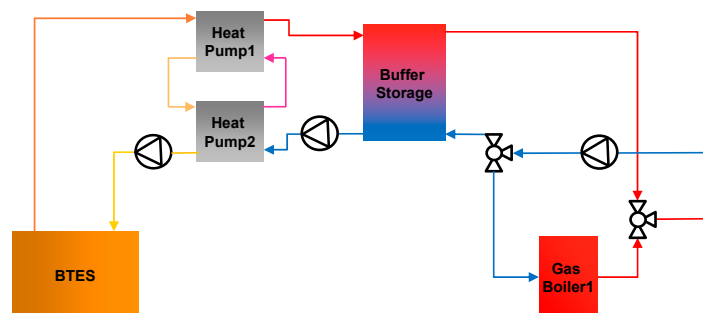


Figure 5. System layout of parallel heating scenarios.

A reference scenario is designed based on energetically-efficient conventional systems. In this reference case, the total heating demand is supplied by condensing GBs with a high energetic efficiency of 95% [34] and the whole cooling demand is covered by air-source HPs with a seasonal COP of 4 [35].

4. Evaluation Criterion

4.1. Exergy Analysis

As mentioned earlier, exergy is defined as a system's potential to interact with its environment. For thermal systems, this corresponds to the temperature difference between the heat carrier medium and a predefined reference temperature. A variation of the reference temperature does not affect the results of an exergy analysis significantly for systems with higher operating temperatures (e.g., power plants). In contrast, when operation temperatures of a system are close to the reference temperature (e.g., in heating and cooling systems), the results of an exergy analysis strongly depends on the definition of the reference environment [36]. The reference temperature for a steady-state exergy analysis must be chosen as a fixed temperature, such as the seasonal mean temperature or annual mean temperature. For the dynamic analysis, however, several possible reference temperatures like the indoor air temperature, the undisturbed ground temperature and the outdoor temperature are discussed [36]. In this study, the outdoor temperature is considered as the reference temperature. Thermal exergy of a fluid, which can be used for exergy calculations in heating and cooling systems [24], can be calculated using Equation (1). T_0 is the reference temperature and is taken as the ambient temperature in this study.

$$\dot{E} = \dot{m}c_p \times ((T - T_0) - T_0 \ln \frac{T}{T_0}) \quad (1)$$

The exergetic efficiency (η_{exergy}) of a system is the ratio of the output exergy rate (\dot{E}_{out}) to the exergy rate of the expended resources (\dot{E}_{in}) to generate this output. By integrating \dot{E}_{in} and \dot{E}_{out} into each time step over a system's lifetime (n_{end}), its overall average η_{exergy} can be calculated (Equation (2)).

$$\eta_{\text{exergy}} = \frac{\sum_{n=0}^{n_{\text{end}}} \dot{E}_{\text{out},n}}{\sum_{n=0}^{n_{\text{end}}} \dot{E}_{\text{in},n}} \times 100\% \quad (2)$$

Dynamic exergy calculation of \dot{E}_{out} and \dot{E}_{in} for the whole system in heating load (HL) and cooling load (CL) supply can be calculated using Equations (3) and (4), respectively.

$$\dot{E}_{\text{out, HL}} = \begin{cases} \dot{E}_{\text{sply}} - \dot{E}_{\text{rtn}} & T_0 \leq T_{\text{ret}} \\ \dot{E}_{\text{sply}} & T_{\text{ret}} < T_0 \leq T_{\text{sup}} \\ 0 & T_0 \geq T_{\text{sup}} \end{cases} \quad \dot{E}_{\text{in, HL}} = \dot{E}_{\text{elec}} + \dot{E}_{\text{gas}} + \dot{E}_{\text{BTES}} \quad (3)$$

$$\dot{E}_{\text{out, CL}} = \begin{cases} \dot{E}_{\text{sup}} - \dot{E}_{\text{ret}} & T_0 \geq T_{\text{ret}} \\ \dot{E}_{\text{sup}} & T_{\text{sup}} \leq T_0 < T_{\text{ret}} \\ 0 & T_0 \leq T_{\text{sup}} \end{cases} \quad \dot{E}_{\text{in, CL}} = \dot{E}_{\text{elec}} + \dot{E}_{\text{gas}} - \dot{E}_{\text{BTES}} \quad (4)$$

where \dot{E}_{BTES} is the exergy which is stored in or extracted from the BTES system during heating and cooling seasons, it can be calculate using Equation (5). T_b denotes the temperature on the boundary where heat transfer (\dot{Q}_{BTES}) occurs [9]. As BTES is considered as a component in the DHC grid, it is taken as the average storage temperature.

$$\dot{E}_{\text{BTES}} = \dot{Q}_{\text{BTES}} \times (1 - \frac{T_0}{T_b}) \quad (5)$$

\dot{E}_{gas} , the chemical exergy of natural gas, can be calculated by Equation (6) [37] using the lower heating value (LHV) of natural gas.

$$\dot{E}_{\text{gas}} \approx 1.04 \times \text{LHV} \quad (6)$$

4.2. Economic Analysis

The total expenditures to generate the output consists of capital investment costs (\dot{C}_{IC}), maintenance costs (\dot{C}_{MC}), fuel costs (\dot{C}_f) and environmental costs (\dot{C}_{env}). By dividing the net present value of the total cost by the discounted total energy output, levelized cost of energy (LCOE) can be calculated using Equation (7) [38]. The system lifetime (n_{end}) and the discount rate (i) are assumed to be 30 years and 3%, respectively.

$$LCOE = \frac{\sum_{n=0}^{n_{end}} (\dot{C}_{IC, n} + \dot{C}_{MC, n} + \dot{C}_{f, n} + \dot{C}_{env, n}) \cdot (1 + i)^{-n}}{\sum_{n=0}^{n_{end}} \dot{Q}_{out, n} (1 + i)^{-n}} \times 100\% \quad (7)$$

Investment cost (IC) and maintenance cost (MC) functions of the main components are listed in Table 2. After summing up electricity consumptions (f_{elec}) as well as gas consumptions (f_{gas}) in each time step over the system lifetime for each simulation, fuel and environmental costs are calculated using Equations (8) and (9). Electricity and gas costs (c_{elec} and c_{gas}), Global Warming Potential as a result of the consumption of electricity and gas (GWP_{elec} and GWP_{gas}) and the emission costs (c_{CO2}) as a function of the assessment year are calculated as given in Table 3.

$$\dot{C}_{f, n} = f_{elec, n} c_{elec, n} + f_{gas, n} c_{gas, n} \quad (8)$$

$$\dot{C}_{env, n} = f_{elec, n} c_{CO2, n} GWP_{elec, n} + f_{gas, n} c_{CO2, n} GWP_{gas, n} \quad (9)$$

Table 2. Cost function of different components.

| Component | Investment Cost Function (€) | Maintenance (€/yr.) | Reference |
|-----------|---|------------------------|-----------|
| BTES | $65 \times L_{BHE}$ | - | [39] |
| Property | $75.05 \times A_{Property}$ | - | [40] |
| HP | $(2053.8 \cdot Cap_{HP}^{-0.348}) \times Cap_{HP}$ | $0.0075 \times C_{IC}$ | [41] |
| BST | $(130 + 11,680 \cdot Vol_{BST}^{-0.5545}) \times Vol_{BST}$ | - | [42] |
| GB | $(11,418.60 + 64.6115 \cdot Cap_{GB}^{0.7978}) \times f_{GB}^a$ | $0.02 \times C_{IC}$ | [43] |

$$^a f_{GB} = 1.0818 - 8.2898 \cdot 10^{-7} Cap_{GB}.$$

Table 3. Fuel costs, CO2 costs and GWP.

| Parameter | Cost Function 2020–2030 | Cost Function 2030–2050 | Reference |
|----------------------------|-------------------------------------|-------------------------------------|-----------|
| $C_{elec, n}$ (€/kWh) | $0.002364n + 0.131$ | $-0.0005n + 0.1625$ | [44,45] |
| $C_{gas, n}$ (€/kWh) | $0.00216n + 0.0268$ | $0.00321n + 0.04702$ | [44,45] |
| $c_{CO2, n}$ (€/tCO2) | $-0.2083n^2 + 9.072n + 5.553$ | 80 | [46] |
| $GWP_{elec, n}$ (tCO2/kWh) | $(-20.99n + 423.89) \times 10^{-6}$ | $(-8.595n + 287.55) \times 10^{-6}$ | [47] |
| $GWP_{gas, n}$ (tCO2/kWh) | 250×10^{-6} | 250×10^{-6} | [48] |

4.3. Exergoeconomic Analysis

In every technoeconomic evaluation, the aim is to minimize cost and to maximize the efficiency. Therefore, the two objective functions, Equations (2) and (7), need to be optimized simultaneously. Setup and boundaries of the optimization variables and technical constraints are summarized in Table 4.

$$\begin{array}{ll} \max & \eta_{exergy} \\ \min & LCOE \end{array}$$

Table 4. Ranges of optimization variables and constraints.

| Subject to | Reason |
|---|--|
| $30 \text{ m} \leq L_{\text{BHE}} \leq 400 \text{ m}$ | Length range of shallow BHEs [49] |
| $30 \leq N_{\text{BHE}} \leq 1200$ | Heat transfer range of BHEs (W/m), corresponds to L_{BHE} |
| $2 \text{ m} \leq S_{\text{BHE}} \leq 25 \text{ m}$ | Maximum available surface area |
| $50 \text{ kW} \leq \text{Cap}_{\text{HP}} \leq 8150 \text{ kW}$ | Minimum capacity of each HP module/Maximum heating load |
| $25 \text{ m}^3 \leq \text{Vol}_{\text{BST}} \leq 10,000 \text{ m}^3$ | HP min. running time/continuous HP operation in peak load |
| $3 \text{ K} \leq \Delta T_{\text{BST}}^b \leq 10 \text{ K}$ | Minimum temperature shift of HPs/Grid temperature shift |
| Constraints | Reason |
| $\text{Re}_{\text{BHE}} \geq 2300$ | Minimum Reynolds number for turbulent flow in BHEs |
| $T_{\text{BHE,in}} \geq -5 \text{ }^\circ\text{C}$ | Minimum peak load BHE inlet temperature [49] |

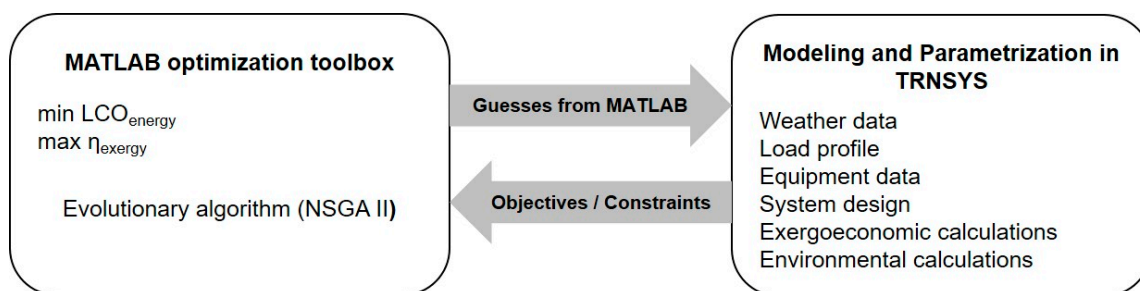
^b For ActSer and PasSer scenarios.

5. Computational Model

The proposed system layouts are modeled and parameterized in TRNSYS 18 [50]. MATLAB [51] is coupled with TRNSYS for multi-objective optimization utilizing the non-dominated sorting genetic algorithm (NSGA II) [52] toolbox.

5.1. Multi-Objective Optimization

The mentioned objective functions and constraints (Section 4.3) are specified in MATLAB. Initial guesses from MATLAB are written into a text file, which is read by TRNSYS. The corresponding values of the objective functions and constraints are calculated in TRNSYS and written into another text file, which is read by MATLAB. The coupling happens once at the beginning and once at the end of each simulation. The algorithm initially tries to find the points, which do not violate the constraints, and assesses the objectives afterwards. This procedure is repeated for each scenario until the best Pareto front, which is the loci of the most optimal solutions, is selected. Figure 6 illustrates the computational model.

**Figure 6.** Computational model.

5.2. System Simulation

The calculated load profile, as shown Figure 1, is given as a time series to TRNSYS simulation studio. Type 557, which is based on a duct storage model [53], is used for BTES modeling. It can be used to simulate thermally interacting BHEs within a cylindrical storage volume. The validity of Type 557 has already been proven in many practical projects (e.g., [54]). Design parameters (Table 5) are based on standard libraries [49] and location-specific parameters are chosen according to experimental data [55]. The BST is modelled with type 534, which divides the tank's volume into different stratified layers and solves the energy balance equation to calculate a time-dependent temperature change of the fluid inside the tank at different levels. It has also been used for the simulation and validation of similar studies [56–58]. The loss coefficient (Table 5) is based on the data from a manufacturer [59]

and matches practical investigations [54,56]. Types 927 and 1221 are used for simulating single- and double-stage HPs, respectively. According to inlet source- and load-side temperatures and flow rates, output capacity and power consumption of HPs are calculated based on the provided catalog files. The catalogs are chosen so that they can be representative of the operation of common HPs on the market [32,60]. The chosen catalogs are transformed into external files with normalized values, which are read by the HP types and a parametric study was conducted to check the compatibility of the provided files and the original manufacturers' catalogs. Type 700 was used to model the GBs, which are assumed to be condensing gas boilers with a high energetic efficiency of around 95% [34]. Important parameters of the other components including heat exchangers, pumps and thermostats were mainly selected based on manufacturer [30] or experimental [54] data and are illustrated in Table 5.

Table 5. Main TRNSYS parameters.

| Component | Parameter | Value | Component | Parameter | Value |
|-------------------------------|------------------------------|---------------------------|-------------------------------------|----------------------------|----------|
| BTES Type 557 | BHE type | 2U | HP Type 1221 ^c | 1st stage cooling capacity | 102.9 kW |
| | Boreholes in series | 6 | | 2nd stage cooling capacity | 56.1 kW |
| | Borehole radius | 0.065 m | | 1st stage cooling power | 22.9 kW |
| | Pipe outer/inner radius | 0.016/0.0131 m | | 2nd stage cooling power | 10.2 kW |
| | Pipe thermal conductivity | 0.38 W/m.K | | 1st stage heating capacity | 86.9 kW |
| | BTES thermal conductivity | 2.6 W/m.K | | 2nd stage heating capacity | 49.8 kW |
| | BTES heat capacity | 2080 kJ/m ³ .K | | 1st stage heating power | 28.9 kW |
| | Grout thermal conductivity | 2 W/m.K | | 2nd stage heating power | 15.1 kW |
| | Fluid specific heat (EG 25%) | 3.811 kJ/kg.K | | | |
| BST Type 534 | Number of tank nodes | 30 | HP Type 927 ^c | Cooling capacity | 59.8 kW |
| | Number of ports | 4 | | Cooling power | 13 kW |
| | Aspect ratio | 2.5 | | Heating capacity | 50.6 kW |
| | Loss Coefficient | 0.15 W/m ² .K | | Heating power | 18 kW |
| Pump Type 110 | Total pump efficiency | 60% | Boiler Type 700 | Efficiency | 95% |
| Thermostat 106, 113 | Dead band temperature | 0.5 K | HEX Type 91 | Effectiveness | 0.895 |

^c Values at rated conditions of the catalog and differ from normalization values.

6. Results

Figure 7 displays the area assessed by the optimization algorithm, including points that violate the constraints. As it is expected, the algorithm initially tries to find a minimum, where increasing the efficiency decreases the cost. From that point on, a further increase in efficiency results in higher costs and the algorithm searches for the loci of the points with maximum efficiencies and minimum costs.

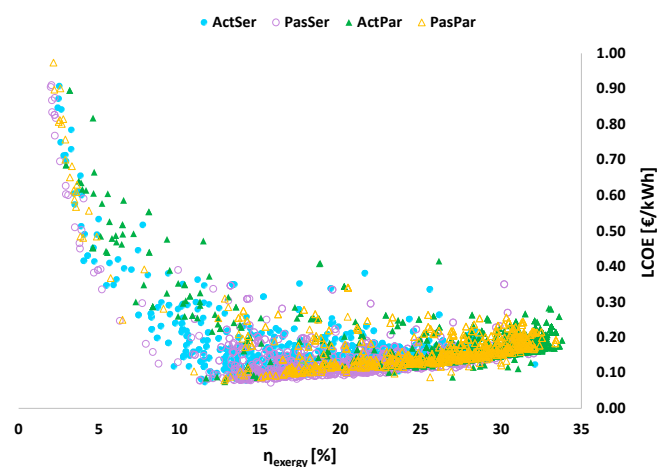


Figure 7. The assessed area by the optimization algorithm to find a minimum for each scenario.

6.1. Pareto Efficient Solutions

Figure 8 shows the local evaluations by the algorithm for finding the points which do not violate the constraints. The non-dominated points for each scenario are located on a Pareto front, which is closest to the bottom right corner (Figures 8 and 9). On the Pareto fronts LCOE ranges from aimately 8 to 20 ct/kWh and η_{exergy} from 14 to 35%. For the reference scenario those numbers are 6.5 ct/kWh and 12%, respectively.

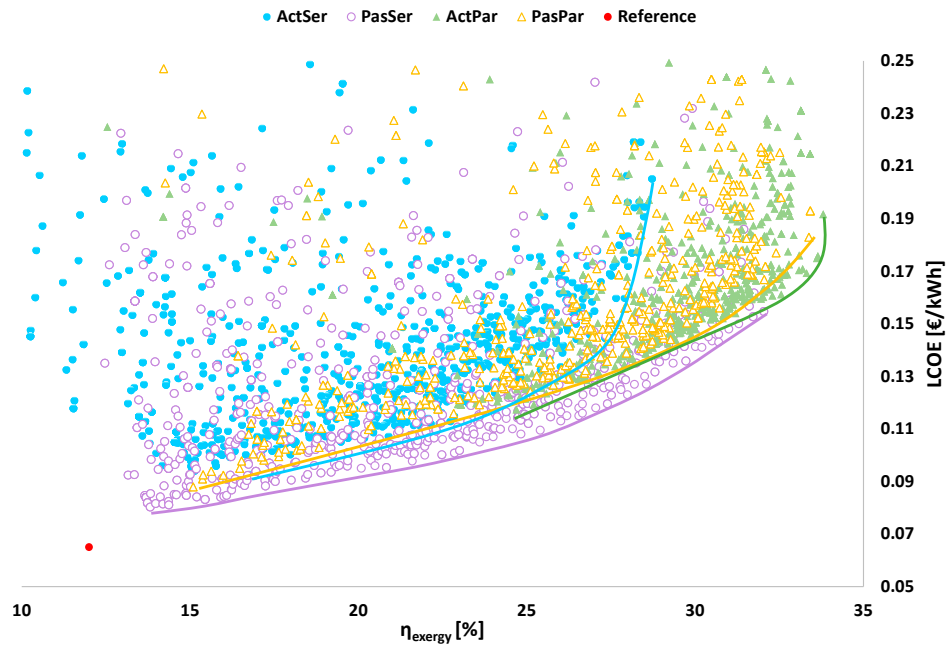


Figure 8. Results of local evaluations by the algorithm.

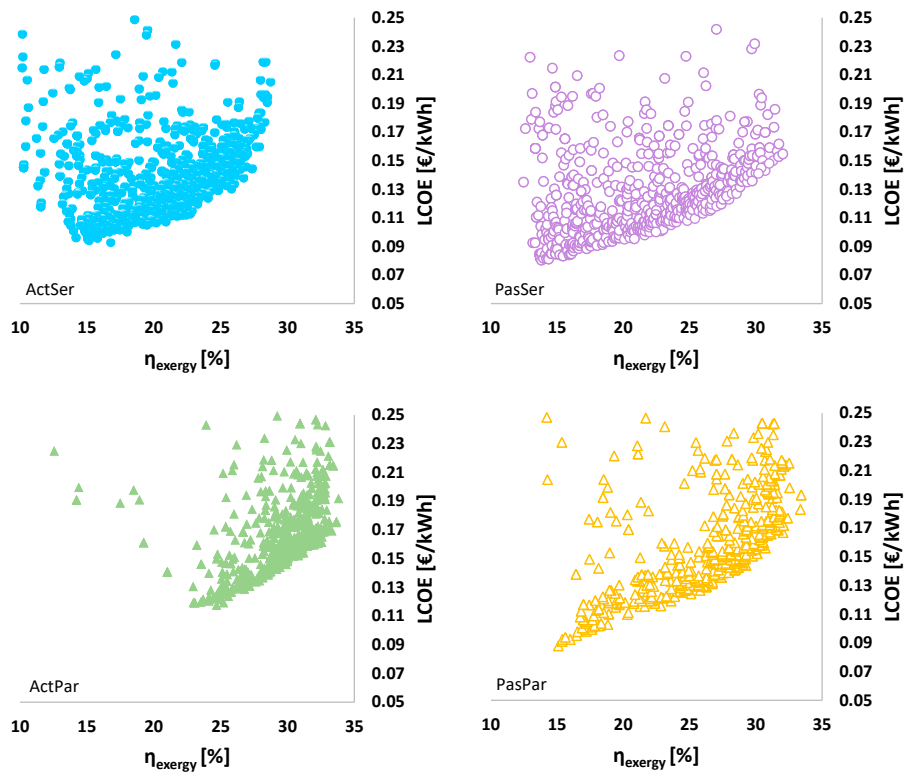


Figure 9. Results of local evaluations by the algorithm.

When HPs are designed to cover the whole ΔT_{BST} i.e., in the serial scenarios, supplying cooling load passively (PasSer) leads to more economical and more efficient designs. This means designs with equal efficiency have lower costs and designs with equal costs are more efficient for the PasSer scenario than for the ActSer scenario. Especially, when it comes to efficiencies higher than approx. 27%, costs for the ActSer scenario show a much steeper increase than the other scenarios.

In contrast, when double stage HPs are connected serially and cover almost half of ΔT_{BST} i.e., in the parallel scenarios, active cooling (ActPar) is superior to passive cooling (PasPar) for designs with efficiencies higher than approx. 25%. However, for less efficient designs, passive cooling becomes more economical again than active cooling.

When comparing the serial with the parallel connection of HP and GB in heating operation, it is obvious that the parallel scenarios generally are able to reach higher efficiencies than their parallel counterparts with equal cooling mode, while the serial systems are generally advantageous when lower efficiencies are in demand as they reach lower costs.

However, the serial scenario with passive cooling (PasSer) also reaches exergetic efficiencies up to 32% and thus shows the most economical designs for a wide efficiency range, except for the highly efficient design points with exergetic efficiencies over 32%. Here, ActPar scenario becomes beneficial, as it reaches efficiencies up to almost 34%.

The ranges of the selected optimized variables for each scenario are given in Table 6. Scattering plots showing the distribution of the volume of BTES (Vol_{BTES}) and Cap_{HP} on the pareto front of each scenario and their effect on the objective functions are illustrated in Figure 10. Vol_{BTES} (Equation (10) [53]) is selected because it gives a relation for three of the main optimization variables including N_{BHE} , L_{BHE} and S_{BHE} . Consequently, by choosing the mentioned variables from the optimized ranges in Table 6, an optimum design point with a corresponding HP capacity can be selected using Figure 10. Although there are exceptions, it can be generally implied that the increase in Vol_{BTES} as well as Cap_{HP} results in more efficient, but more expensive, design points. Figure 11a shows Vol_{BTES} for the local search of the ActSer scenario and its effect on the objective functions. η_{exergy} and LCOE have their optimum values in the middle ranges of the chosen boundaries. Moreover, a higher ΔT_{BST} (Figure 11b) mainly results in a more efficient and more economical design, with η_{exergy} showing a higher sensitivity. The objective functions of the other serial scenario, PasSer, have approx. the same sensitivity to Vol_{BTES} and ΔT_{BST} .

$$Vol_{BTES} = \pi \times N_{BHE} \times L_{BHE} \times (0.525 \times S_{BHE})^2 \quad (10)$$

Table 6. Ranges of the optimized solutions on the Pareto fronts.

| Scenario | L_{BHE} [m] | N_{BHE} | S_{BHE} [m] | Cap_{HP} [kW] | Vol_{BST} [m ³] | ΔT_{BST} [K] |
|----------|---------------|-----------|---------------|-----------------|-------------------------------|----------------------|
| ActSer | 95–155 | 294–1194 | 10.7–15.1 | 1264–4400 | 917–6847 | 7.9–9.1 |
| ActPar | 156–200 | 426–924 | 11.4–15 | 2175–4349 | 1260–5630 | - |
| PasSer | 143–169 | 222–1026 | 7.3–11.6 | 809–4097 | 795–6356 | 6.7–9.8 |
| PasPar | 159–224 | 174–1008 | 11.3–14 | 759–4046 | 1459–7045 | - |

For further analysis of the scenarios, three characteristic Pareto efficient designs (further referred to as Characteristic Designs) are chosen for each scenario. These include the most economical, the most efficient and a compromise solution, which is the closest to the corner (Figures 8 and 9). Table 7 lists their most important design parameters as well as the corresponding η_{exergy} and LCOE. Bold lines show the most economical and the most efficient layouts overall, which belong to PasSer and ActPar scenarios. The economical, the compromise and the most efficient layouts of each scenario are referred to with ECO, COMP and EFF respectively.

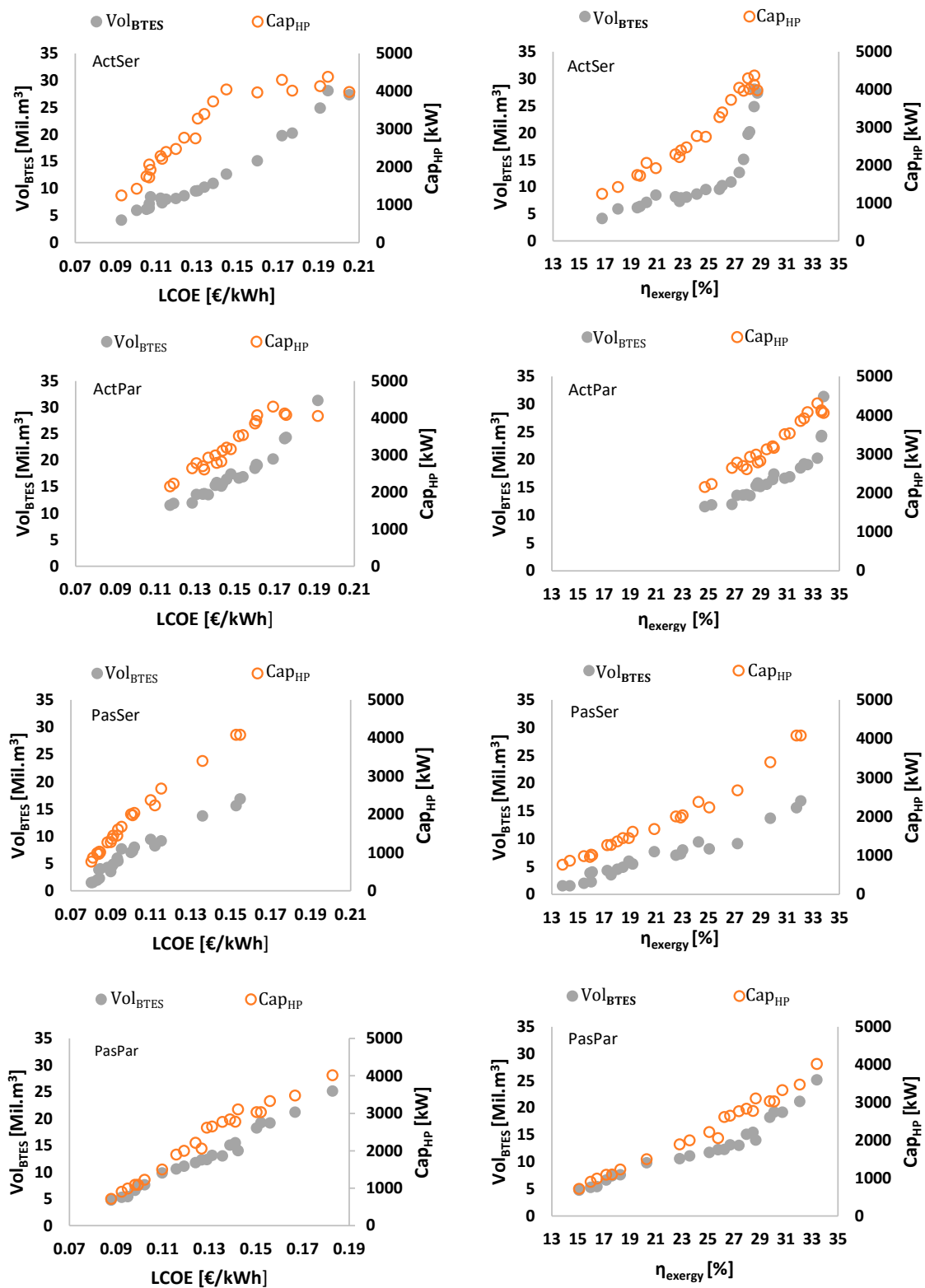


Figure 10. Scattering of the decision variables on the Pareto fronts of ActSer, ActPar, PasSer and PasPar scenarios.

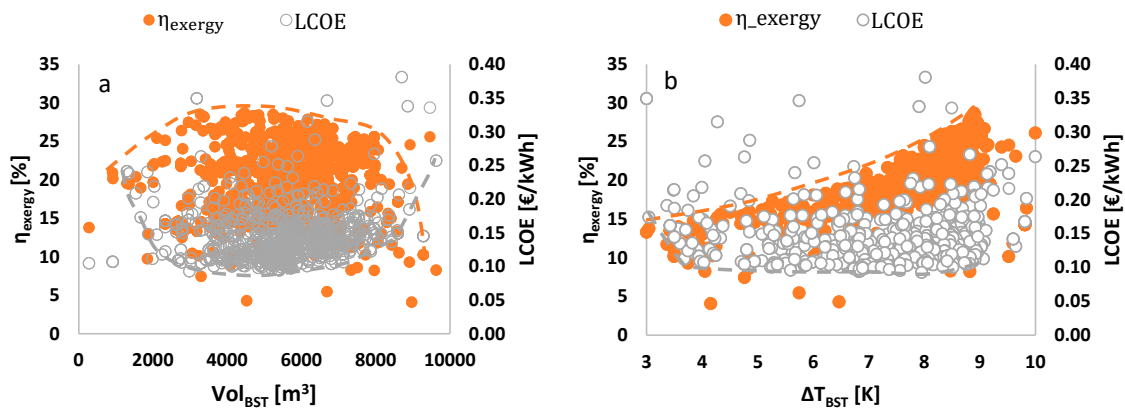


Figure 11. Local search for finding optimum ranges of (a) Vol_{BTES} and (b) ΔT_{BST} of ActSer scenario.

Table 7. The economic, the compromise and the efficient system designs of each scenario.

| Scenario | | LCOE [ct/kWh] | η_{exergy} [%] | L_{BHE} [m] | N_{BHE} | S_{BHE} [m] | Cap_{HP} [kW] | Vol_{BST} [m^3] | ΔT_{BST} [K] |
|----------|----------------|---------------|----------------------------|----------------------|------------------|----------------------|-------------------------------|--|-----------------------------|
| ActSer | Economical | 9.27 | 16.77 | 112 | 294 | 12.0 | 1264 | 2989 | 7.95 |
| | Compromise | 12.37 | 24.05 | 116 | 702 | 11.0 | 2782 | 4646 | 8.59 |
| | Most efficient | 19.45 | 28.49 | 136 | 1036 | 15.1 | 4400 | 3281 | 8.91 |
| ActPar | Economical | 11.73 | 24.69 | 190 | 426 | 12.8 | 2175 | 1260 | - |
| | Compromise | 14.37 | 29.42 | 170 | 660 | 12.6 | 3136 | 5420 | - |
| | Most efficient | 19.16 | 33.80 | 175 | 918 | 15.0 | 4097 | 4307 | - |
| PasSer | Economical | 8.02 | 13.81 | 145 | 222 | 7.4 | 809 | 3556 | 6.68 |
| | Compromise | 10.00 | 22.47 | 143 | 480 | 10.9 | 2007 | 3008 | 9.50 |
| | Most efficient | 15.47 | 32.04 | 153 | 942 | 11.6 | 4097 | 4658 | 9.65 |
| PasPar | Economical | 8.79 | 15.10 | 185 | 174 | 12.9 | 758 | 4186 | - |
| | Compromise | 12.66 | 25.78 | 164 | 636 | 11.6 | 2073 | 4007 | - |
| | Most efficient | 18.29 | 33.38 | 162 | 1008 | 13.3 | 4046 | 5128 | - |

6.2. Scenario Analysis

To gain deeper insight into the coherencies of the results and the differences for the four scenarios, the component-wise exergy destruction and loss (Figure 12) and composition of LCOE (Figures 13–16) for all 12 Characteristic Designs (cf. Section 6.1.) as well as for the reference case are presented and discussed in the following sections.

6.2.1. Reference Case

As mentioned earlier, for the reference scenario the total heating demand is supposed to be supplied by condensing GBs and the cooling demand by air-source HPs. Therefore, it has one design point and not a pareto front. Despite high energetic efficiency, condensing GBs have a very low exergetic efficiency as natural gas with its high exergy content is converted to generate low exergy heat [18]. The calculated η_{exergy} of the condensing GBs and the air-source HPs are 11% and 21%, respectively. Consequently, the calculated overall average η_{exergy} is 12% and its corresponding exergy destruction is 240 GWh/30yrs. Moreover, using the cost functions in Tables 2 and 3, the LCOE of the reference scenario is 6.5 ct/kWh. The largest exergy destruction belongs to the most economical design from PasSer scenario and is 197 GWh/30yrs (Figure 12), which is almost 22% lower than the reference case. However, its LCOE is 23.5% higher.

6.2.2. ActSer–Active Cooling and Serial Heating

The total exergy destruction is reduced significantly by moving from the economical to the most efficient point (Figure 12). For the economical design, the highest exergy destruction is from the GBs

followed by the HP. For the compromise solution, these are almost balanced and for the most efficient design, the HP dominates exergy destruction. Exergy destruction of the BST and the BTES show the lowest number compared to the other system components.

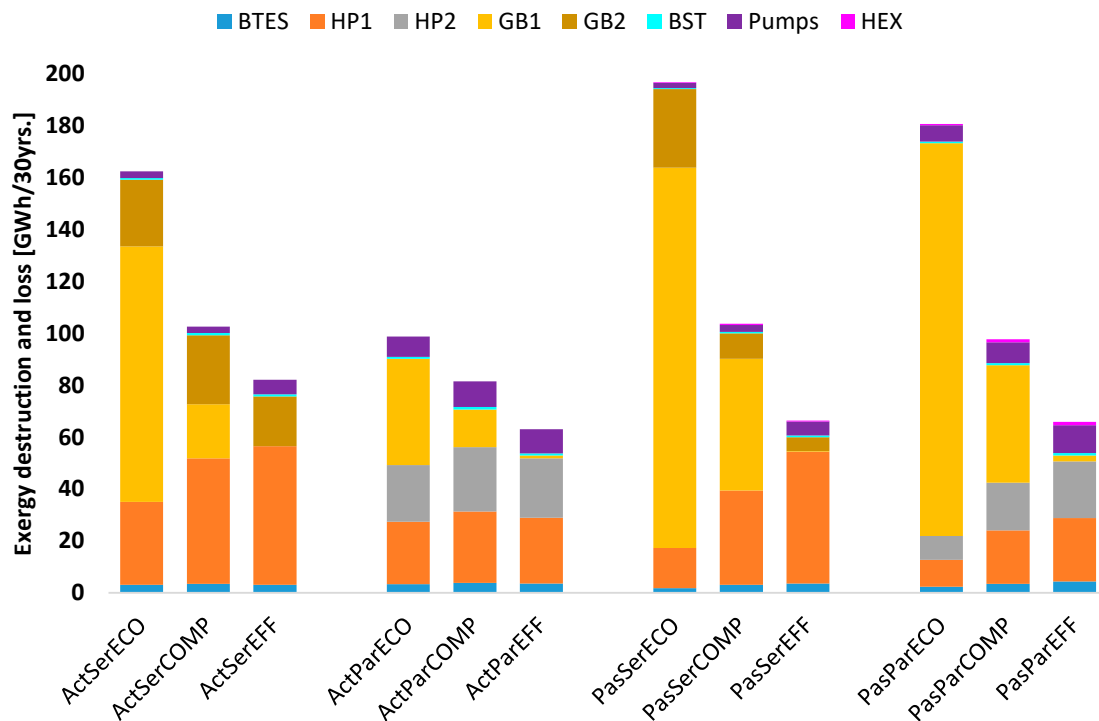


Figure 12. Component-wise exergy destruction and loss for the economical (ECO), the compromise (COMP) and the most efficient (EFF) designs in Table 7.

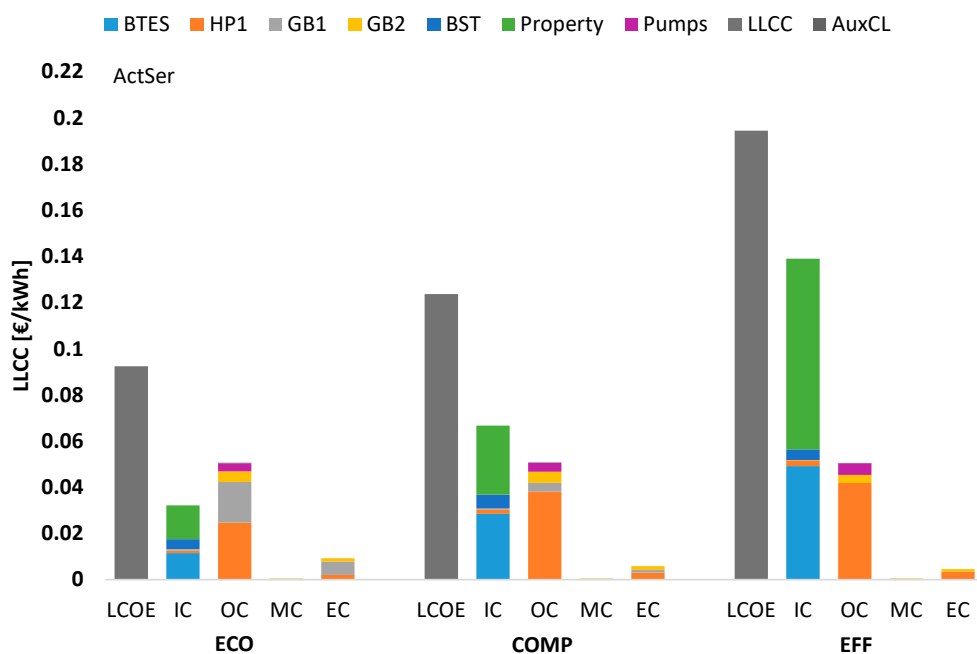


Figure 13. Total and component-wise Levelized Life Cycle Cost (LCOE) of ActSer scenario; LCOE is the summation of Initial Cost (IC), Operational Cost (OC), Maintenance Cost (MC) and Emission Cost (EC) for the economical (ECO), the compromise (COMP) and the most efficient (EFF) designs.

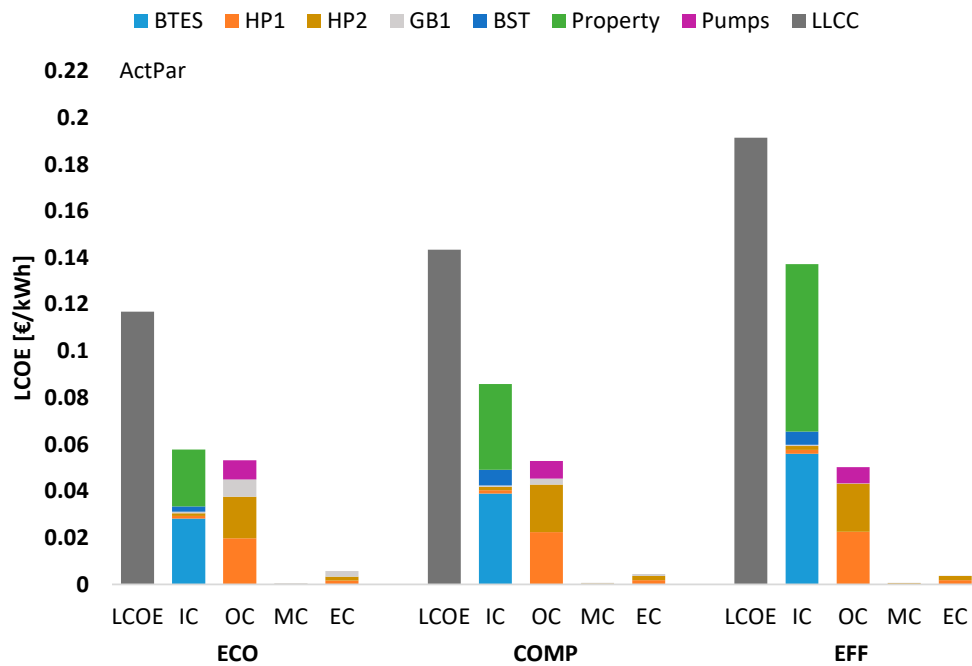


Figure 14. Total and component-wise Levelized Life Cycle Cost (LCOE) of ActPar scenario; LCOE is the summation of Initial Cost (IC), Operational Cost (OC), Maintenance Cost (MC) and Emission Cost (EC) for the economical (ECO), the compromise (COMP) and the most efficient (EFF) designs.

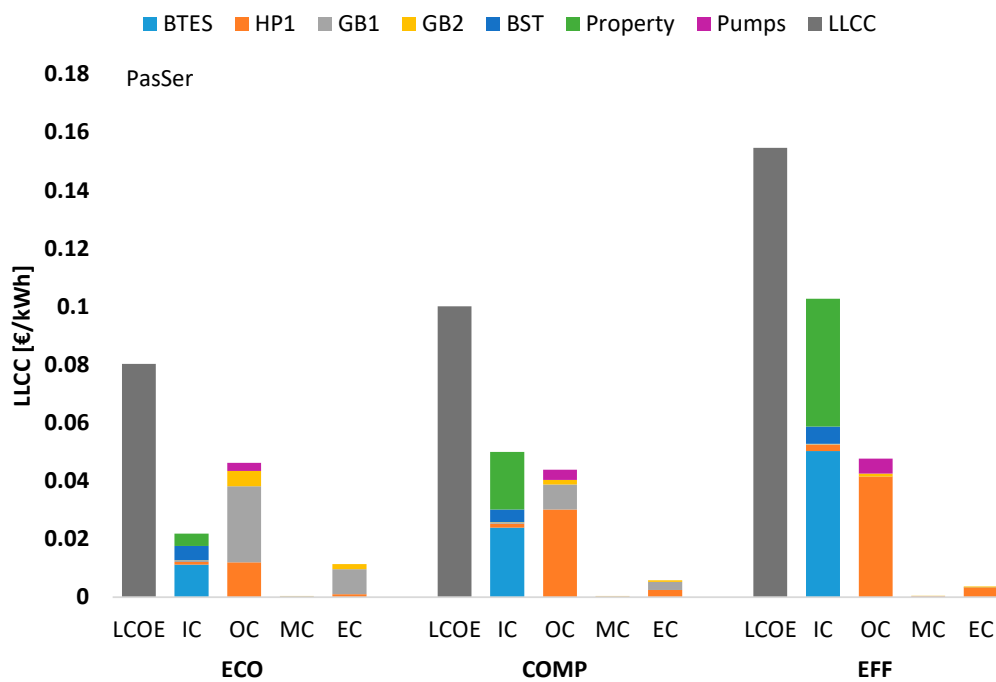


Figure 15. Total and component-wise Levelized Life Cycle Cost (LCOE) of PasSer scenario; LCOE is the summation of Initial Cost (IC), Operational Cost (OC), Maintenance Cost (MC) and Emission Cost (EC) for the economical (ECO), the compromise (COMP) and the most efficient (EFF) designs.

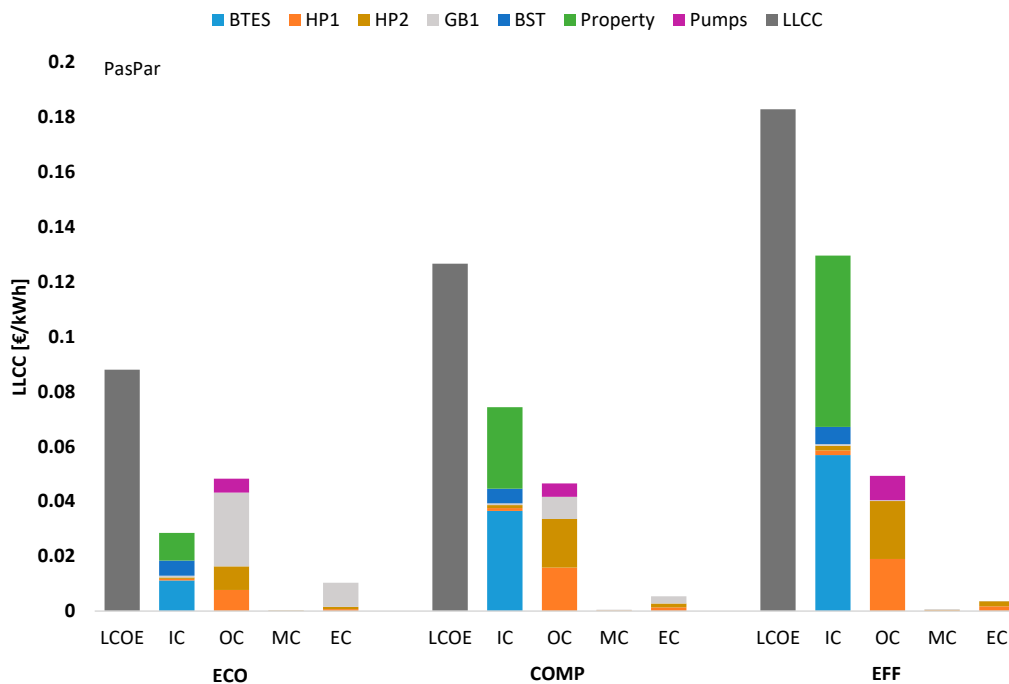


Figure 16. Total and component-wise Levelized Life Cycle Cost (LCOE) of PasPar scenario; LCOE is the summation of Initial Cost (IC), Operational Cost (OC), Maintenance Cost (MC) and Emission Cost (EC) for the economical (ECO), the compromise (COMP) and the most efficient (EFF) designs.

Figure 13 shows the LCOE of the Characteristic Designs for the ActSer scenario. For the economical design ICs are lower than OCs. This relation is reversed for the most efficient and compromise designs. It is almost three times higher for the most efficient design. GBs have the lowest share in ICs, even for the economical layout. The largest share is either from the BTES or from the property, which is used for installing the BTES. Combined, they make up more than 94% of the ICs of the most efficient layout. The OCs remain almost the same for all designs, with HPs being the major part for the compromise and the most efficient designs. The power consumption of the pumps is mainly required to circulate the fluid inside the BTES and increases with its size. However, it also depends on N_{BHE} , which specifies the design pressure drop that the pump is required to meet. MCs are very low in comparison to the other costs and increase slightly from the economical to the most efficient design point. This is mainly due to the increased HP capacity. The highest ECs can be observed for the economical design and originates from the high share of the GB.

6.2.3. ActPar–Active Cooling and Parallel Heating

ActPar scenario comprises the most efficient layout among all the layouts (Figure 8, Table 7). Like for the other scenarios, the most efficient layout has the lowest share of GBs for covering the peak demand and the highest share of HPs in heating load supply. In heating mode, entering temperatures on the BTES side of HP1 are higher than HP2 with lower load side temperatures. In cooling mode, HP1 has lower BTES side and load side temperatures. As HP2 has lower exergy destruction in heating and cooling modes, it can be concluded that the load side temperature has more effect on the exergetic performance of the HPs in the proposed system layout (Figure 12). Increased flow rates are required to maintain the same design temperature difference on both sides of the HPs in comparison to the other scenarios. This results in higher power consumption of the circulating pumps and the associated exergy destruction. Like previous scenarios, the exergy destruction of the BST and the BTES are the lowest in comparison to the other components.

As shown in Figure 14, ICs are higher than OCs for all three Characteristic Designs. The BTES and the property have the highest shares in ICs, followed by the BST. HPs contribute to a high percentage

of OCs, which increases from the economical to the most efficient one because of larger HP capacities. The higher power consumption of the circulating pumps also results in their higher share in OCs, which increases for higher efficiencies. Like previous scenarios, MCs increase and ECs decrease from the economical to the most efficient design.

6.2.4. PasSer–Passive Cooling and Serial Heating

PasSer scenario shows the most economical and least efficient design point of all Characteristic Designs (Table 7). As shown in Figure 12, the highest exergy destruction results from the GBs followed by the HP. Here, due to the passive cooling strategy, the exergy destruction of the HP in cooling mode is omitted and that of the HEX is added, which is the lowest among other components. Overall, HEX, BST and BTES show the lowest share in exergy destruction.

As for the ActSer scenario, OCs remain almost the same for the three design options. ICs are lower than OCs for the economical layout and more than double for the most efficient one. The largest share of ICs is either from the BTES or from the land use, except for the economical design, for which the property costs are much lower than the ICs of the BTES due to the lowest spacing. Like for the ActSer scenario, MCs are negligible and increase with efficiency. The highest ECs can be observed for the economical point and decrease for more efficient systems.

6.2.5. PasPar–Passive Cooling and Parallel Heating

As for all scenarios, the most economical layout has the highest exergy destruction, which decreases from the economical to the most efficient solution (Figure 12). The exergy destruction of the HP in cooling mode is replaced with that of the HEX and increases for larger BTES volumes due to higher flow rates. In accordance with the ActPar scenario, the overall exergy destruction of HP1 is higher than HP2, which implies the importance of load side temperature. The relatively high flow rates of the pumps result in a high share of the overall exergy destruction, which increases from the economical to the most efficient design.

Total and component-wise LCOE of the PasPar scenario are illustrated in Figure 16. The economical layout has a high share of GB in heating load supply. Therefore, the OCs and ECs as a result of gas consumption are approx. 55% and 12% of the LCOE, respectively. The most efficient solution has the largest number of BHEs and the largest spacing of all Characteristic Designs. Consequently, the ICs are the dominating part of the LCOE with a share of above 65%, which is again caused by high costs of the BTES and the associated property. MCs are a minor share and increase from the economical to the most efficient design. ECs make up almost 12% of the LCOE of the economical layout and decrease with increasing efficiency.

6.3. Sensitivity Analysis

6.3.1. Variation of Initial Costs and Energy Costs

In a one-at-a-time sensitivity analysis, effects of 20% variation in ICs and OCs on the LCOE of the Characteristic Designs (cf. Section 6.1.) are assessed (Figure 17). Changing the ICs has a stronger effect than changing OCs for the most efficient designs (gray lines). In contrast to that, the OCs show a higher impact on the LCOE for the economical layouts. By reducing OCs and ICs of the economical point of PasSer scenario by 20%, its LCOE decreases to 7.0 ct/kWh and 7.6 ct/kWh, respectively. Moreover, the influence of varying OCs on LCOE of different scenarios is almost the same for all of the chosen points of each scenario. This is different from varying ICs, which has a higher influence on more efficient layouts with larger BTES volumes and smaller GB capacities.

6.3.2. Changing Heat Pump Type

As mentioned earlier, HPs contribute to a high percentage of exergy destruction and LCOE. In the previous parts of the study, a commonly used standard heat pump type was considered. However,

to capture the effects of increasing HP efficiencies, the HPs of the active scenarios are replaced by a more efficient HP type [61] with a 20% higher nominal COP (Figure 18). As expected, total exergetic efficiency increases and LCOE decreases by using a more efficient HP. This is more pronounced for the most efficient scenarios because of their higher contribution of HPs. For the most efficient point of ActPar scenario, the overall exergetic efficiency increases by 11.2% and the cost decreases by 2.9%. Therefore, using HPs with higher COPs has a larger effect on the exergetic efficiency than on the cost.

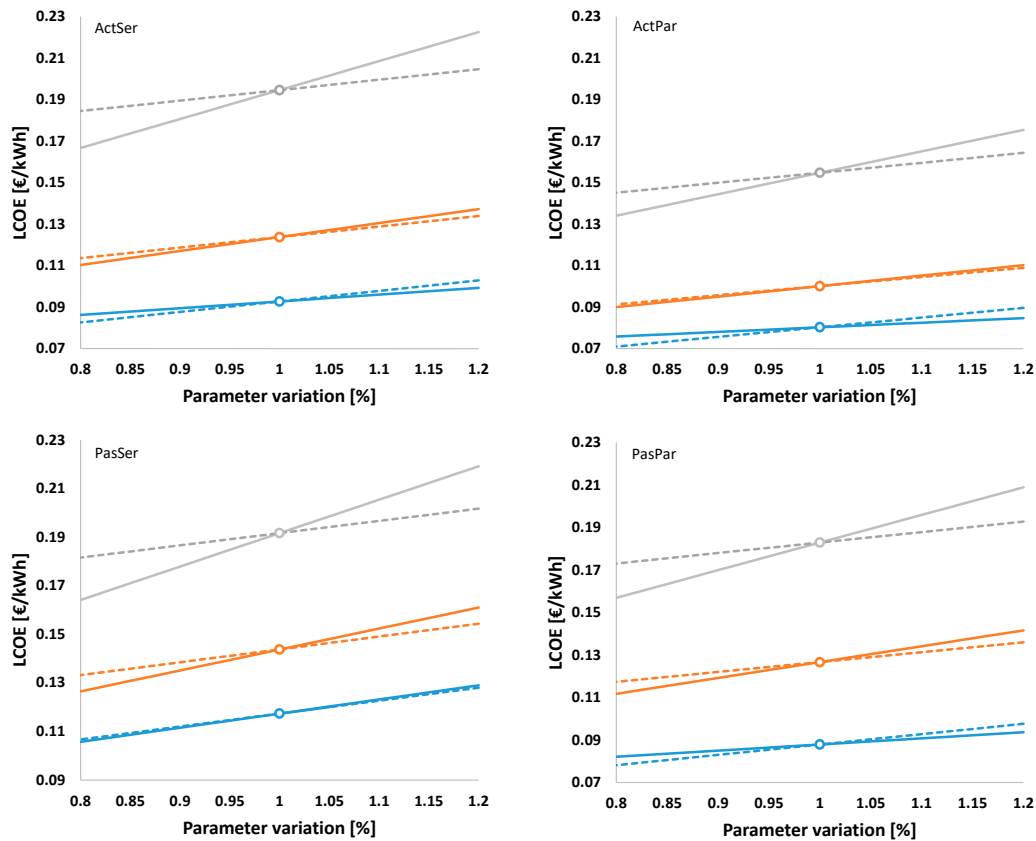


Figure 17. Effect of varying ICs (solid lines) and OCs (dash lines) for the economical (blue), the compromise (orange) and the most efficient (gray) designs of ActSer, ActPar, PasSer and PasPar.

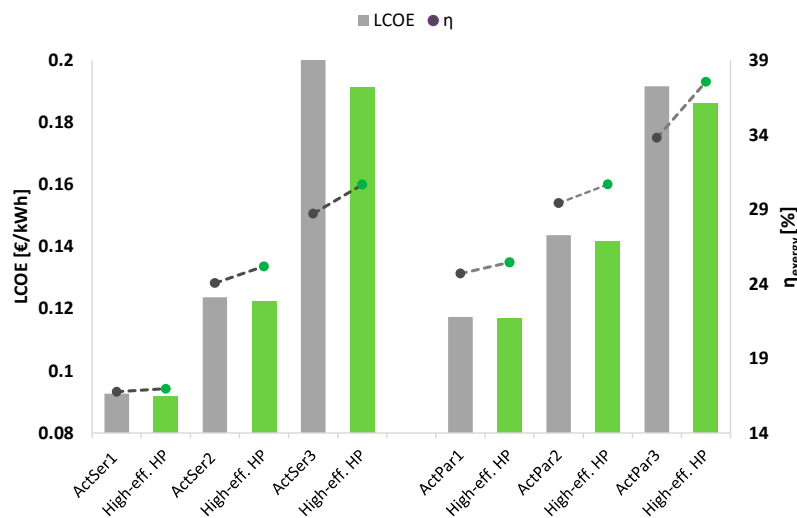


Figure 18. Effects of changing HP on LCOE and η_{exergy} on the economical (1), the compromise (2) and the most efficient (3) designs of the active scenarios.

6.4. Exergy and Global Warming Potential

Reducing environmental impacts plays a major role in global transition to renewable energies. As mentioned earlier, the LCA method lacks thermodynamic assessment. Moreover, increasing exergy efficiency reduces environmental impacts [19]. To have a rough estimation of how they are related to each other, GWPs of the evaluated system layouts were calculated parallel to the optimization procedure in each simulation run. To assess GWPs, the GWPs associated with electricity and gas consumption are calculated based on the functions in Table 3. The GWP as a result of the production of each system component ($GWP_{prod,n}$) is calculated using available online data [20,62]. Finally, Equation (11) was used for the calculation of each component's GWP and then summed up for the overall GWP of each system layout.

$$GWP = \sum_{n=0}^{n_{end}} GWP_{elec,n} + GWP_{gas,n} + GWP_{prod,n} \quad (11)$$

Results of calculating GWP for different design points of the scenarios and their corresponding exergetic efficiency are illustrated in Figure 19. As expected, an increase in exergetic efficiency leads to a decrease in environmental impacts. This trend can be expressed by a function. Therefore, the exergoeconomic optimization results in system layouts with lower GWP by taking thermodynamic inefficiencies into consideration.

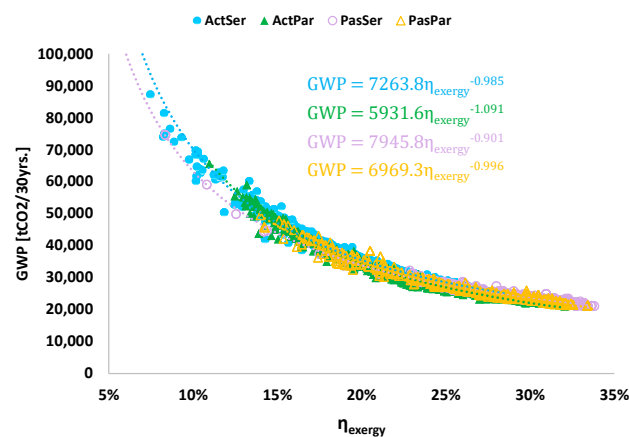


Figure 19. Relation between η_{exergy} and GWP.

7. Discussion

7.1. Limitations

On the one hand, a generic study of a complex system requires many simplifications and assumptions, which has its own drawbacks and may cause uncertainties. On the other hand, implementing too much detail is computationally expensive and may lead to unexpected results, which can prevent the definition of generic rules and guidelines. A proper approach can be conducting a generic study which is followed by detailed assessments, when it comes to practical applications. The following simplifications and assumptions were considered in this study:

- Load scenarios were calculated based on German standards for renovated buildings. Results of this study can provide design guidelines for buildings with different performances as long as they have the same temperature ranges and similar functionalities. The definition of the DHC grid temperature levels were based on the target return temperatures of low-temperature grids. However, due to simplification, the DHC grid configuration and the associated costs and exergy destruction rates are not considered in this study. Future studies, which assess different building types and grid configurations, and consider DHC pipes and circulation pumps as main components of BTES-assisted DHC grids are required for more comprehensive analysis.

- To set up an optimization algorithm according to real HP data within a wide range, it is assumed that the selected HP consists of a number of HP modules with similar performances. However, there is a maximum limit for the number of HP modules to avoid technical issues in practice. Moreover, according to an inquiry from a HP manufacturer, large-scale HPs can be ordered with desired technical specifications which are easily compatible with part-load applications.
- It is assumed that GBs cover the load which cannot be supplied by the ground loop, without considering the effect of part-load ratio on its performance. However, modulating GBs mainly have a minimum turn-down ratio, which specifies the minimum acceptable part-load ratio. For a more detailed assessment the boiler and the combustion efficiencies need to be provided as a function of entering liquid temperature and device part-load ratio.
- The selected BST volume by the optimization algorithm is allocated to one tank with an aspect ratio (the ratio of height to diameter) of 2.5, according to an estimation regarding an efficient design as well as the maximum acceptable tank height for large-scale applications. Splitting the selected volume into multiple tank units with different aspect ratios can be considered as a future study.
- The project lifetime is considered to be 30 years. Approx. 2000 evaluations, each taking around 20 min, were required for the initial convergence of the optimization algorithm. Consequently, a time step of one hour was considered for the simulations. However, a more detailed assessment required shorter time steps down to a few minutes, which also enables an application of more exact control strategies. The optimization always results in better solutions with shorter time steps and a larger number of evaluations.
- The heat transfer mechanism of the BTES is considered to be conductive. It is also assumed that BTES is installed in the ground with a uniform thermal conductivity and heat capacity. However, in real geothermal applications convective heat transfer might exist and ground thermal characteristics might not be uniform. Moreover, there are always regional limitations for the implementation of large-scale geothermal projects, e.g., unfavorable subsurface conditions or restrictions due to groundwater protection.
- The IC functions (Table 2) are based on the available literature, which are mainly defined by having data from real projects in a specific range. However, due to the large ranges of the optimization boundaries, it is assumed that extrapolation is acceptable. Regarding OCs (Table 3), energy cost functions are specified by the predicted costs from the economic studies for the years 2030 and 2050 and assuming a linear interpolation between the available data points. Similar assumptions have been made for the environmental emissions and the associated costs. Consequently, cost functions are subject to large uncertainties and the sensitivity analysis was done with the purpose of lowering these uncertainties.

7.2. Discussion of Results

The PasSer scenario shows the most economical designs for a wide efficiency range of up to 32%. This can be explained by the passive cooling strategy, which leads to an omission of HPs that are usually responsible for significant amounts of exergy destruction and high OCs. Moreover, lower pumping power, due to covering the whole heating temperature shift in serial scenarios, overcompensates higher COPs in parallel scenarios because of lower temperature shifts by HPs.

For the highly efficient designs with exergetic efficiencies over 32%, ActPar scenarios show the best results. Large values for both Cap_{HP} and Vol_{BTES} are needed to reach such high exergetic efficiencies. Consequently, higher COPs of HPs in parallel scenarios have a larger impact and overcompensate lower power consumption of circulation pumps in serial scenarios. However, in cooling mode, a higher power consumption of the pumps due to the lower temperature shift on BTES side has a slightly higher share in inefficiencies and losses.

For the serial scenarios (Figure 11), higher ΔT_{BST} mainly results in a more efficient and more economical design, with η_{exergy} showing a higher sensitivity. This indicates that the improved

performance of the BST, due to better stratification and less mixing losses, overcompensates the lower COPs of the HPs due to higher temperature shifts. Therefore, the algorithm favors scenarios with higher values for ΔT_{BST} .

The optimization of the serial layouts leads to the maximum possible temperature shift of the grid by the HPs, which makes them similar to the HPs in parallel scenarios. However, due to weaker performance of HPs for covering high temperature shifts, η_{exergy} does not exceed 28.5% with a LCOE of 19.45 ct/kWh for ActSer scenario. This corresponds to a layout in which GB1 is omitted and the supplementary load is supplied by GB2 serially. A Pareto efficient design point of the ActPar scenario with the same η_{exergy} has an LCOE of 13.86 ct/kWh. Therefore, to move towards more economical points in the serial scenarios, both GBs are required, and a splitter sends the fluid to either the HPs and GB2 or to the GB1. The GB1 has a share between 0 and 49% of the total heating demand on the Pareto front of the ActSer scenario. Similarly, for the PasSer scenario, the point with the highest η_{exergy} of 32% has LCOE of 15.5 ct/kWh with the highest share of HPs and GB2. Reducing this share on the Pareto front results in more economical and less efficient points with an increased share of GB1 up to 60%.

As mentioned earlier, HPs contribute to a high share of exergy destruction as well as OCs, especially for the most efficient scenarios. For the same design, two HPs, each of which cover parts of the heat demand, have lower exergy destruction and power consumption than one HP covering all of it. However, the pumping power that is required for circulating the fluid on both sides of the serially-connected HPs as well as the associated exergy destruction and OCs are much higher. Therefore, a suitable HP for integrating BTES systems is the one that can provide the highest temperature change with the lowest power consumption as well as the minimum possible flow rates.

The design flow rate also has a high influence on heat transfer characteristics on the BTES side. Higher flow rates lead to better convective heat transfer from the circulating fluid to the ground. Therefore, definition of the optimum flow rate on the BTES side and the characteristics of the most efficient corresponding HP is proposed as a future study.

As indicated in Figure 9, an increase of Vol_{BTES} yields in a higher η_{exergy} as well as higher LCOE. L_{BHE} and S_{BHE} are mainly selected from the middle ranges of the specified boundaries by the optimization algorithm, with maximum amounts of 220 m and 15 m, respectively. N_{BHE} has the widest range which varies between 15% and 85% of the maximum boundary from the most economical to the most efficient point. Therefore, it can be implied that N_{BHE} has the highest influence on the objective functions. The number of BHEs in series has a high effect on the distribution of BHEs in a BTES with a specific volume, the flow rate per BHE and the circulating pump's power. In this study it was taken as 6, like for many installed BTES systems [63]. Therefore, for a future study, taking it as an additional optimization variable could result in more efficient design points.

Cooling-based BTES systems recover the rejected heat from cooling cycles seasonally for an efficient design. In heating-dominated regions, the amount of extracted heat is much more than the stored heat and the dominating mechanism equals that of conventional geothermal HPs. Consequently, similar cost incentives to geothermal HPs in the household sector [64] need to be considered for DHC grids of such regions, in order to be more cost-competitive with fossil-based systems with low exergetic efficiencies and high GWPs.

8. Conclusions

A dynamic exergoeconomic optimization method is used for detailed evaluation of the proposed layouts for integrating BTES systems into 4th generation DHC grids in heating-dominated regions. Based on the results of this study, the following general conclusions can be drawn:

- In cooling mode, passive strategy yields to a high share of the optimized designs from the most economical up to highly efficient ones. Active cooling with serially-connected heat pumps results in a small share of the optimized designs, which are the most efficient but the most expensive ones.
- In heating mode, maximizing the heating temperature shift by single HPs and supplying the remaining shift up to the grid supply temperature by serially-connected GBs yields to a high

percentage of the optimized designs. However, in the most economical design, the maximum 40% of the overall heating share are supplied by this configuration and the rest is met by parallel-operating GBs. The share increases up to 100% for more efficient designs.

- The most efficient but most expensive designs are resulted from covering nearly the overall heating demand on the grid temperature shift by serially-connected HPs and supplying only the peak loads by GBs.
- Larger BTES volumes and corresponding HP capacities mainly result in more efficient designs with higher costs. However, less efficient and more economical designs have higher capacities of GBs. The highest share of exergy destruction comes from HPs for the most efficient and from GBs for the least efficient designs. BTES, BST and HEX have the lowest exergy destruction for all Pareto efficient layouts.
- For the most efficient designs ICs significantly exceed OCs. While the largest share of ICs arises either from the BTES itself or from the property, which is used for building it, the highest share in OCs originates from the HPs. Nevertheless, for the most economical designs, OCs usually exceed ICs. For all layouts, ECs decrease from the most economical to the most efficient designs while MCs increase.
- GWPs decrease with increasing exergetic efficiency and their relation can be expressed with a function. Therefore, by conducting exergoeconomic analysis, thermodynamic inefficiencies as well as environmental impacts are improved. By considering GWPs and LCOE as objective functions and comparing the results with the optimized results of this study, further relations between LCA and exergoeconomic analysis and their application for optimization problems can be specified.

The results of this study can be used to design 4th generation DHC grids and to assess the transition of old generation to low-temperature grids utilizing BTES systems. In future, the same method will be used for the evaluation of integrating BTES systems into 4th generation solar DHC grids.

Author Contributions: Conceptualization, H.H., J.F., B.W., D.O.S. and I.S.; methodology, H.H.; original draft preparation, H.H.; review and editing, B.W., J.F., I.S., D.O.S. and H.H.; visualization, H.H.; supervision, D.O.S., B.W. and I.S.; funding acquisition, I.S. All authors have read and agreed to the published version of the manuscript.

Funding: This work was financially supported by the German Research Foundation (DFG) in the framework of the Excellence Initiative, Darmstadt Graduate School of Excellence Energy Science and Engineering (GSC 1070) and the Open Access Publishing Fund of Technical University of Darmstadt.

Conflicts of Interest: The authors declare no conflict of interest.

Nomenclature

| | |
|--------|---|
| ActSet | active serial |
| ActPar | active parallel |
| BHE | borehole heat exchanger |
| BST | buffer storage tank |
| BTES | borehole thermal energy storage |
| COMP | compromise |
| DC | district cooling |
| DH | district heating |
| DHC | district heating and cooling |
| ECO | economical |
| EFF | efficient |
| GB | gas boiler |
| HP | heat pump |
| NSGA | non-dominated sorting genetic algorithm |
| PasSer | passive serial |
| PasPar | passive parallel |

Symbols

| | | |
|-----------|--------------------------|----------------------------|
| A | area | m ² |
| c | specific heat capacity | kJ/(kg K) |
| c | specific cost | €/tCO ₂ , €/kWh |
| \dot{C} | cost rate | €/yr. |
| Cap | capacity | kW |
| EC | emission cost | €/kWh |
| \dot{E} | thermal exergy rate | kW |
| GWP | global warming potential | CO ₂ /kWh |
| i | discount rate | % |
| IC | initial cost | €/kWh |
| L | length | m |
| LHV | lower heating value | kW |
| LCOE | levelized cost of energy | €/kWh |
| \dot{m} | flow rate | kg/s |
| MC | maintenance cost | €/kWh |
| OC | operational cost | €/kWh |
| n | year | |
| N | number | |
| Rey | Reynolds number | |
| S | spacing | m |
| T | temperature | °C |
| Vol | Volume | m ³ |
| f | fuel consumption | kWh |
| \dot{Q} | heat flux | kW |
| η | efficiency | % |

Subscripts

| | |
|------|---------------------------------|
| BHE | borehole heat exchanger |
| BST | buffer storage tank |
| BTES | borehole thermal energy storage |
| CL | cooling load |
| elec | electricity |
| env | environmental |
| f | fuel |
| HL | heating load |
| IC | initial cost |
| MC | maintenance cost |
| prod | production |
| ret | return |
| sup | supply |
| 0 | reference |
| b | boundary |

References

1. Fleiter, T.; Steinbach, J.; Ragwitz, M.; Dengler, J.; Köhler, B.; Reitze, F.; Tuille, F.; Hartner, M.; Kranzl, L.; Forthuber, S. *Mapping and Analyses of the Current and Future (2020–2030) Heating/Cooling Fuel Deployment (Fossil/Renewables)*; European Commission, Directorate-General for Energy: Brussel, Belgium, 2016.
2. Werner, S. European space cooling demands. *Energy* **2016**, *110*, 148–156. [[CrossRef](#)]
3. United Nations Department of Economics and Social Affairs, Population Division. *World Urbanization Prospects: The 2014 Revision*; United Nations Department of Economics and Social Affairs, Population Division: New York, NY, USA, 2015; p. 41.
4. Rezaie, B.; Rosen, M.A. District heating and cooling: Review of technology and potential enhancements. *Appl. Energy* **2012**, *93*, 2–10. [[CrossRef](#)]
5. Werner, S. International review of district heating and cooling. *Energy* **2017**, *137*, 617–631. [[CrossRef](#)]

6. Lund, H.; Werner, S.; Wiltshire, R.; Svendsen, S.; Thorsen, J.E.; Hvelplund, F.; Mathiesen, B.V. 4th Generation District Heating (4GDH): Integrating smart thermal grids into future sustainable energy systems. *Energy* **2014**, *68*, 1–11. [[CrossRef](#)]
7. Schulte, D.O.; Rühaak, W.; Oladyshkin, S.; Welsch, B.; Sass, I. Optimization of medium-deep borehole thermal energy storage systems. *Energy Technol.* **2016**, *4*, 104–113. [[CrossRef](#)]
8. Skarphagen, H.; Banks, D.; Frengstad, B.S.; Gether, H. Design considerations for Borehole Thermal Energy Storage (BTES): A review with emphasis on convective heat transfer. *Geofluids* **2019**, *2019*, 4961781. [[CrossRef](#)]
9. Welsch, B.; Ruehaak, W.; Schulte, D.O.; Baer, K.; Sass, I. Characteristics of medium deep borehole thermal energy storage. *Int. J. Energy Res.* **2016**, *40*, 1855–1868. [[CrossRef](#)]
10. Schulte, D.O.; Welsch, B.; Boockmeyer, A.; Rühaak, W.; Bär, K.; Bauer, S.; Sass, I. Modeling insulated borehole heat exchangers. *Environ. Earth Sci.* **2016**, *75*, 910. [[CrossRef](#)]
11. Bär, K.; Rühaak, W.; Welsch, B.; Schulte, D.; Homuth, S.; Sass, I. Seasonal high temperature heat storage with medium deep borehole heat exchangers. *Energy Procedia* **2015**, *76*, 351–360. [[CrossRef](#)]
12. Sibbitt, B.; McClenahan, D.; Djebbar, R.; Thornton, J.; Wong, B.; Carriere, J.; Kokko, J. The performance of a high solar fraction seasonal storage district heating system—five years of operation. *Energy Procedia* **2012**, *30*, 856–865. [[CrossRef](#)]
13. Bauer, D.; Marx, R.; Nußbicker-Lux, J.; Ochs, F.; Heidemann, W.; Müller-Steinhagen, H. German central solar heating plants with seasonal heat storage. *Sol. Energy* **2010**, *84*, 612–623. [[CrossRef](#)]
14. Dincer, I.; Rosen, M. A unique borehole thermal storage system at University of Ontario Institute of Technology. In *Thermal Energy Storage for Sustainable Energy Consumption*; Springer: Dordrecht, The Netherlands, 2007; pp. 221–228.
15. Lanahan, M.; Tabares-Velasco, P.C. Seasonal thermal-energy storage: A critical review on BTES systems, modeling, and system design for higher system efficiency. *Energies* **2017**, *10*, 743. [[CrossRef](#)]
16. Formhals, J.; Hemmatabady, H.; Welsch, B.; Schulte, D.O.; Sass, I. A modelica toolbox for the simulation of borehole thermal energy storage systems. *Energies* **2020**, *13*, 2327. [[CrossRef](#)]
17. Welsch, B.; Rühaak, W.; Schulte, D.O.; Formhals, J.; Bär, K.; Sass, I. Co-simulation of geothermal applications and HVAC systems. *Energy Procedia* **2017**, *125*, 345–352. [[CrossRef](#)]
18. Bejan, A.; Tsatsaronis, G.; Moran, M.J. *Thermal Design and Optimization*; John Wiley & Sons: New York, NY, USA, 1995.
19. Nuss, P. *Life Cycle Assessment Handbook: A Guide for Environmentally Sustainable Products*; Curran, A.M., Ed.; John Wiley & Sons, Inc.: Hoboken, NJ, USA; Scrivener Publishing LLC: Salem, MA, USA, 2015.
20. Welsch, B.; Göllner-Völker, L.; Schulte, D.O.; Bär, K.; Sass, I.; Schebek, L. Environmental and economic assessment of borehole thermal energy storage in district heating systems. *Appl. Energy* **2018**, *216*, 73–90. [[CrossRef](#)]
21. Karasu, H.; Dincer, I. Life cycle assessment of integrated thermal energy storage systems in buildings: A case study in Canada. *Energy Build.* **2020**, *217*, 109940. [[CrossRef](#)]
22. Kizilkan, O.; Dincer, I. Borehole thermal energy storage system for heating applications: Thermodynamic performance assessment. *Energy Convers. Manag.* **2015**, *90*, 53–61. [[CrossRef](#)]
23. Kizilkan, O.; Dincer, I. Exergy analysis of borehole thermal energy storage system for building cooling applications. *Energy Build.* **2012**, *49*, 568–574. [[CrossRef](#)]
24. Sayadi, S.; Tsatsaronis, G.; Morosuk, T. Dynamic exergetic assessment of heating and cooling systems in a complex building. *Energy Convers. Manag.* **2019**, *183*, 561–576. [[CrossRef](#)]
25. Klein, S.; Beckman, W.; Mitchell, J.; Duffie, J.; Duffie, N.; Freeman, T.; Mitchell, J.; Braun, J.; Evans, B.; Kummer, J. *Trnsys 18—Volume 6 Multizone Building Modeling with Type 56 and Trnbuild*; Solar Energy Laboratory, University of Wisconsin: Madison, WI, USA, 2017; p. 199.
26. DIN4108. *Thermal Protection and Energy Economy in Buildings-Part 2: Minimum Requirements to Thermal Insulation*; Beuth Verlag: Berlin, Germany, 2013.
27. Merkblatt, S. *Raumnutzungsdaten für die Energie-und Gebäudetechnik*; SIA: Zürich, Switzerland, 2015.
28. Meteotest. *Meteonorm: Irradiation Data for Every Place on Earth*. Available online: <http://www.meteonorm.com/> (accessed on 12 August 2020).
29. Nussbaumer, T. *Planungshandbuch Fernwärme*; EnergieSchweiz, Bundesamt für Energie: Bern, Switzerland, 2017.
30. Viessmann GmbH. Available online: www.viessmann.de (accessed on 12 August 2020).

31. Gautschi, T. *Anergienetze in Betrieb*; Städtische Wärmewende: Wien, Austria, 2015.
32. Waterfurnace Co. Available online: <https://www.waterfurnace.com/commercial/products/water-source-geothermal-heat-pumps/> (accessed on 12 August 2020).
33. Karim, A.; Burnett, A.; Fawzia, S. Investigation of stratified thermal storage tank performance for heating and cooling applications. *Energies* **2018**, *11*, 1049. [CrossRef]
34. Viessmann GmbH. Available online: <https://www.viessmann.de/de/wohngebaeude/gasheizung/vitocrossal.html> (accessed on 12 August 2020).
35. Viessmann GmbH. Available online: <https://www.viessmann.de/de/wohngebaeude/hybridheizung/gas-hybridgeraete/vitocal-250-s.html> (accessed on 12 August 2020).
36. Sayadi, S.; Tsatsaronis, G.; Morosuk, T. A New Approach for Applying Dynamic Exergy Analysis and Exergoeconomics to a Building Envelope. Available online: <https://pdfs.semanticscholar.org/e5d6/e5929d68b7d153f590d8d8e113ee1e86993b.pdf> (accessed on 24 August 2020).
37. Bargel, S. Entwicklung eines exergiebasierten Analysemodells zum umfassenden Technologievergleich von Wärmeversorgungssystemen unter Berücksichtigung des Einflusses einer veränderlichen Außentemperatur. Ph.D. Thesis, Ruhr-Universität Bochum, Universitätsbibliothek, Bochum, Germany, 2011.
38. Short, W.; Packey, D.J.; Holt, T. *A Manual for the Economic Evaluation of Energy Efficiency and Renewable Energy Technologies*; National Renewable Energy Lab.: Golden, CO, USA, 1995.
39. Luo, J.; Rohn, J.; Bayer, M.; Priess, A. Thermal performance and economic evaluation of double U-tube borehole heat exchanger with three different borehole diameters. *Energy Build.* **2013**, *67*, 217–224. [CrossRef]
40. Statistisches Bundesamt. Available online: https://www.destatis.de/DE/Home/_inhalt.html (accessed on 12 August 2020).
41. Croteau, R.; Gosselin, L. Correlations for cost of ground-source heat pumps and for the effect of temperature on their performance. *Int. J. Energy Res.* **2015**, *39*, 433–438. [CrossRef]
42. Mauthner, F.; Herkel, S. Technology and Demonstrators-Technical Report Subtask C–Part C1-C1: Classification and Benchmarking of Solar Thermal Systems in Urban Environments. Available online: <http://task52.iea-shc.org/data/sites/1/publications/IEA-SHC-Task52-STC1-Classification-and-benchmarking-Report-2016-03-31.pdf> (accessed on 24 August 2020).
43. Gebhardt, M.; Kohl, H.; Steinrötter, T. *Preisatlas, Ableitung von Kostenfunktionen für Komponenten der rationellen Energienutzung*; Institut für Energie und Umwelttechnik eV (IUTA): Duisburg-Rheinhausen, Germany, 2002; pp. 1–356.
44. Bundesamt, S. Preise–Daten zur Energiepreisentwicklung. Available online: https://www.destatis.de/DE/Themen/Wirtschaft/Preise/Publikationen/Energiepreise/energiepreisentwicklung-pdf-5619001.pdf?__blob=publicationFile (accessed on 24 August 2020).
45. Schlesinger, M.; Hofer, P.; Kemmler, A.; Kirchner, A.; Koziel, S.; Ley, A.; Piégsa, A.; Seefeldt, F.; Straßburg, S.; Weinert, K. Entwicklung der Energiemärkte-Energierferenzprognose: Studie im Auftrag des Bundesministeriums für Wirtschaft und Technologie. Available online: <https://www.bmwi.de/Redaktion/DE/Publikationen/Studien/entwicklung-der-energiemaerkte-energierferenzprognose-endbericht.html> (accessed on 24 August 2020).
46. German Federal Government. *German Federal Government (2019): Climate Action Programme 2030*; German Federal Government: Berlin, Germany, 2019.
47. Fritsche, U.R.; Greß, H.-W. *Der nicht erneuerbare kumulierte Energieverbrauch und THG-Emissionen des deutschen Strommix im Jahr 2016 sowie Ausblicke auf 2020 bis 2050*; Internationales Institut für Nachhaltigkeitsanalysen und-strategien GmbH (IINAS): Darmstadt, Germany, 2018.
48. IINAS (2017): *GEMIS-Globales Emissions-Modell Integrierter Systeme-Model and Database*; International Institute for Sustainability Analysis and Strategy: Darmstadt, Germany, 2017.
49. VDI. *VDI 4640 Thermal Use of the Underground*. VDI-Gesellschaft Energie und Umwelt (GEU); Beuth Verlag: Berlin, Germany, 2019.
50. Klein, S.; Beckman, W.; Mitchell, J.; Duffie, J.; Duffie, N.; Freeman, T.; Mitchell, J.; Braun, J.; Evans, B.; Kummer, J. *TRNSYS 18–A TRaNsient System Simulation Program, User Manual*; Solar Energy Laboratory, University of Wisconsin-Madison: Madison, WI, USA, 2017.
51. MATLAB. 9.2.0.556344 (R2017a), The MathWorks Inc.: Natick, MA, USA, 2017.
52. Deb, K.; Pratap, A.; Agarwal, S.; Meyarivan, T. A fast and elitist multiobjective genetic algorithm: NSGA-II. *IEEE Trans. Evol. Comput.* **2002**, *6*, 182–197. [CrossRef]

53. Hellstrom, G. Ground Heat Storage: Thermal Analyses of Duct Storage Systems. Ph.D. Thesis, Lund University, Lund, Sweden, 1991.
54. Mesquita, L.; McClenahan, D.; Thornton, J.; Carriere, J.; Wong, B. Drake Landing Solar Community: 10 Years of Operation. In Proceedings of the ISES Conference Proceedings, Abu Dhabi, UAE, 11 February 2017; pp. 1–12.
55. Bär, K.; Arndt, D.; Fritsche, J.-G.; Götz, A.E.; Kracht, M.; Hoppe, A.; Sass, I. 3D-Modellierung der tiefeingeothermischen Potenziale von Hessen–Eingangsdaten und Potenzialausweisung [3D modelling of the deep geothermal potential of the Federal State of Hesse (Germany)–input data and identification of potential. *Z. Dtsch. Ges. Geowiss.* **2011**, *162*, 371–388.
56. Renaldi, R.; Friedrich, D. Techno-economic analysis of a solar district heating system with seasonal thermal storage in the UK. *Appl. Energy* **2019**, *236*, 388–400. [[CrossRef](#)]
57. Allard, Y.; Kummert, M.; Bernier, M.; Moreau, A. Intermodel comparison and experimental validation of electrical water heater models in TRNSYS. In Proceedings of the Building Simulation, Sydney, Australia, 14 November 2011; pp. 688–695.
58. Baldwin, C.; Cruickshank, C.A. Using TRNSYS types 4, 60, and 534 to model residential cold thermal storage using water and water/glycol solutions. In Proceedings of the IBPSA-Canada’s eSim Conference, Hamilton, ON, Canada, 3–6 May 2016; pp. 335–348.
59. LIPP GmbH. Available online: <https://www.lipp-system.de/tanks/thermal-storage-tanks> (accessed on 12 August 2020).
60. Trane Co. Available online: <https://www.trane.com/commercial/north-america/us/en/products-systems/equipment/unitary/water-source-heat-pumps.html> (accessed on 12 August 2020).
61. Viessmann GmbH. Available online: <https://www.viessmann.de/de/wohngebaeude/waermepumpe/sole-wasser-waermepumpen/vitocal-350-g.html> (accessed on 12 August 2020).
62. Ökobaudat–Sustainable Construction Information Portal. Available online: <https://www.oekobaudat.de/OEKOBAU.DAT/> (accessed on 12 August 2020).
63. Miedaner, O.; Mangold, D.; Sørensen, P.A. Borehole thermal energy storage systems in Germany and Denmark–Construction and operation experiences. In Proceedings of the 13th International Conference on Energy Storage, Beijing, China, 19–21 May 2015; pp. 1–8.
64. BMWi–This Is How Germans Heat Their Homes. Available online: <https://www.bmwi-energiewende.de/EWD/Redaktion/EN/Newsletter/2015/09/Meldung/infografik-heizsysteme.html> (accessed on 12 August 2020).

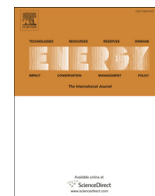


© 2020 by the authors. Licensee MDPI, Basel, Switzerland. This article is an open access article distributed under the terms and conditions of the Creative Commons Attribution (CC BY) license (<http://creativecommons.org/licenses/by/4.0/>).

Appendix D – Strategies for a transition towards a solar district heating grid with integrated seasonal geothermal energy storage

Published as:

Formhals, J., Feike, F., Hemmatabady, H., Welsch, B., and Sass, I., 2021, Strategies for a transition towards a solar district heating grid with integrated seasonal geothermal energy storage: Energy, v. 228, p. 120662, doi:10.1016/j.energy.2021.120662.



Strategies for a transition towards a solar district heating grid with integrated seasonal geothermal energy storage

Julian Formhals^{a, b, *}, Frederik Feike^{b, c}, Hoofar Hemmatabady^{a, b}, Bastian Welsch^{a, b}, Ingo Sass^{a, b}

^a Geothermal Science and Technology, Technical University of Darmstadt, 64287, Darmstadt, Schnittspahnstraße 9, Germany

^b Graduate School of Excellence Energy Science and Engineering, Technical University of Darmstadt, 64287, Darmstadt, Otto-Berndt-Str. 3, Germany

^c Institute for Technical Thermodynamics, Technical University of Darmstadt, 64287, Darmstadt, Alarich-Weiss-Str. 10, Germany



ARTICLE INFO

Article history:

Received 1 December 2020

Received in revised form

12 March 2021

Accepted 14 April 2021

Available online 19 April 2021

Keywords:

4GDH

Solar district heating

Borehole thermal energy storage

Transition strategies

Modelica

Life cycle assessment

ABSTRACT

District heating plays a key role in achieving the TU Darmstadt's emission reduction target for 2050. A combination of efficiency measures, integration of solar thermal collectors, waste heat utilization and seasonal storage is being considered to achieve these targets. However, the existing campus building infrastructure does not allow for an efficient immediate transition to a low-temperature solar district heating grid. Therefore, a stepwise transition with a successive reduction of the grid temperatures is investigated. Dynamic system simulations serve to compare transition strategies until 2050 with regard to their environmental performance and economic efficiency. The proposed strategies differ in dimensions of components as well as the timing of construction or decommissioning. Results indicate that the emission reduction target can be met most economically by a strategy with a gradual construction of 42,000 m² of solar thermal collectors and a seasonal storage consisting of 37 boreholes of 750 m each, accompanied by a concurrent scaling-down of the existing CHP capacity. Compared to a strategy with an immediate construction of a full-sized system, the levelized cost of heat can be reduced from 7.6 ct/kWh to 6.3 ct/kWh, as projected renovation rates, energy prices and emission factors are taken into account better.

© 2021 Elsevier Ltd. All rights reserved.

1. Introduction

Recent studies suggest district heating (DH) as a viable option for supplying large amounts of renewable energy for space heating [1]. Particularly fourth generation district heating (4GDH) systems [2], which operate on supply temperatures down to 50 °C or lower, facilitate the efficient integration of renewable energies [3,4] and waste heat sources [5]. However, a prerequisite for the rollout of 4GDH is a building stock suitable for low temperature heating [6]. Slow replacement and renovation rates of existing buildings impede a fast transition toward this technology [7]. Transition strategies specially tailored to existing building and grid infrastructure [8,9], as well as the utilization of locally available renewable and waste heat potentials [10], can help to overcome these hurdles.

The Technical University of Darmstadt is currently investigating concepts to reduce its energy demand [11], in order to support national targets for global warming potential (GWP) reduction [12]. Even though several synergy and efficiency related measures can bring the university one step closer to its emission saving goals, it has become evident that a large-scale integration of renewable heat sources is imperative [11,13].

Solar district heating (SDH) [14] with underground thermal energy storage (UTES) [15] has proven to be a promising technology in this context. Although solar thermal systems on their own have a very high potential to provide the annual required thermal energy, they have the inherent drawback of their heat supply not corresponding to the temporal course of the heat demand. This mismatch can be overcome by storing excess heat for periods of several months into UTES systems [16]. Borehole thermal energy storage (BTES) systems are a common type of UTES, as they are comparably cheap and site requirements are low [17]. Arrays of borehole heat exchangers (BHE) are used to access the underground's vast thermal capacity for sensible heat storage [18].

* Corresponding author. Geothermal Science and Technology, Technical University of Darmstadt, 64287, Darmstadt, Schnittspahnstraße 9, Germany.

E-mail address: julian.formhals@tu-darmstadt.de (J. Formhals).

The amount of discharged energy from such systems increases for lower discharge temperatures [19] and is usually raised to grid supply temperatures by heat pumps (HP), whose efficiency in turn depends to a large extent on the temperature raise they must provide. Consequently, the efficiency of BTES-assisted systems is highest for systems with low supply temperatures [21,51], i.e. 4GDH systems. A novel concept of BTES are medium deep (MD-BTES) systems, which consist of fewer BHEs of several hundred meters of length [19]. They have the advantage over conventional shallow systems of a much smaller thermal impact on shallow groundwater resources [22]. Moreover, MD-BTES systems utilize naturally higher undisturbed ground temperatures in larger depths. Consequently, they can be operated efficiently on higher temperature levels than their shallow counterparts [23].

A transformation into a campus SDH system with an integrated MD-BTES seems to be a promising option to achieve the university's emission reduction targets. However, such a transformation can be performed in several ways and at different rates. Which strategy is the most favorable in terms of costs and emissions strongly depends on local conditions and is still unclear at this stage.

1.1. State of the art and scope

A general definition of the concept of 4GDH and its advantages over systems of the 3rd generation (3GDH) is given by Lund et al. [2]. Sorknæs et al. [4] investigate the transition to a 100% renewable municipal energy system and find it beneficial both from an economic as well as an energetic point of view. Their scenario comprises a transition towards 4GDH, including solar thermal collectors (STC) and seasonal storage. Welsch et al. [24] conduct a life cycle assessment of different combinations of STC, BTES and combined heat and power (CHP). They identify a combined utilization of those technologies as most efficient solution. This result is supported by Elhashmi et al. [25], who investigate the integration of STCs and BTES into an existing DH system and find a combined system to be superior as well. Rämä et al. [26] investigate the integration of HPs or STCs into an existing 3GDH system over the period of 2014–2030 in three steps. Different combinations of technologies are compared, for integration into 3GDH or 4GDH, respectively. They conclude that an integration of HPs is most favorable in the existing 3GDH system, but STCs could be profitable as well, if grid temperatures were lowered. Several further studies assess the integration of renewable energies into DH systems on different temperature levels and conclude that a transition to 4GDH seems to be favorable [3,27–29]. However, all those studies compare 3GDH to 4GDH in a static manner, in which the transition process itself is excluded. Volkova et al. [6] evaluate the process dynamics of a transition towards 4GDH and identify retrofitting of consumer equipment as a main barrier. Accordingly, Oltmanns [13] focuses on identifying buildings which impede transition of the *Lichtwiese* DH system most. He states that these should be improved first, as they provide the highest leverage, while buildings with a lower impact should be renovated in the upcoming decades. Hence, a gradual transition is to be expected. Studies investigating such a process should therefore take long-term projections of expected renovation rates, required grid temperatures and energy prices into account.

This study presents a new methodology, which facilitates the assessment of strategies for the transition of an existing 3GDH system towards 4GDH. It considers a step-wise integration of STC, MD-BTES and waste heat sources. Strategies for integrating new components and decommissioning existing infrastructure are compared by energetic, economic and environmental means. The time frame of the study extends from 2025 to 2050 and is divided into three periods, enabling changes in the system design at the

start of each period. Dynamic system simulations are carried out to assess the DH system performance, using long-term projections for energy prices, weather conditions and EFs. To account for high uncertainties in projected prices, a sensitivity analysis is appended.

1.2. Campus *Lichtwiese* district heating grid

The *Lichtwiese* is located on an old airfield on the outskirts of Darmstadt and one of four main campuses of the university. It comprises 40 buildings, consisting of offices, lecture halls, laboratories, large test halls, a library and a cafeteria, with a net floor area of about 150,000 m². The annual heat demand is approximately 25 GWh, which corresponds to 43% of the university's overall heat demand. Most of the campus was erected in the seventies and several of its buildings are under monumental protection, complicating energetic refurbishment. Since the *Lichtwiese* still has large open space, it is currently the main expansion area of the university, resulting in brisk construction work in recent years. A DH grid of 3.8 km length is supplying heat from a central CHP plant (Fig. 1), located on site. It consists of three CHP units with a total thermal power of 7 MW_{th} and six gas boilers of 9.3 MW_{th} each, providing heat to all university buildings. Grid supply temperatures range from 80 to 110 °C, depending on the ambient temperature, and the return temperature is 60 °C.

A recent study examined the present potential for reducing the temperature level of the grid. The authors concluded, that the current building stock would allow for a reduction of grid temperatures by at least 10 K [50]. The project *EnEff:Stadt Campus Lichtwiese*, which is currently running in its second phase, has identified components of the grid, which are most critical for further lowering of the grid temperature level down to temperatures of a 4GDH system [11]. As one of the first practical implementations from this project, waste heat from a high-performance computer (HPC) is fed into the return line of the grid by a heat pump [5]. In 2017, a cooling grid was constructed to cope with the increasing cooling demand on the campus. It is fed by three compression and one absorption chiller with a combined cooling power of 3 MW_{th}. However, the cooling grid is outside of the scope of this study and should be considered in future studies.

In order to achieve the German national climate protection goals, the university aims to reduce the specific GWP by 80% until 2050 compared to the level of 1990. As part of this plan, the area-specific final energy demand is to be reduced by 50% compared to 2015 [11]. Considering the aforementioned campus building stock, this might be an ambitious goal, but initial studies have deemed it feasible [11]. However, the campus net floor area is projected to double until 2050. Consequently, the total heat demand is expected to remain approximately constant.

As a complement to the *EnEff* project, the upcoming project *SKEWS* includes the construction of a MD-BTES demonstrator on campus [31]. It will consist of four BHEs, each 750 m deep, using the crystalline bedrock as heat storage medium, which is located only a few tens of meters below ground surface. A thermal insulation of the upper BHE sections shall preserve potential aquifers and lower thermal losses [32,55].

2. Methods

The study examines the period from 2025 to 2050, which is divided into three transition stages. Within each stage, the grid temperature range and system design are fixed. Different transition strategies are compared to identify the most economical way to satisfy the university's emission saving goals.

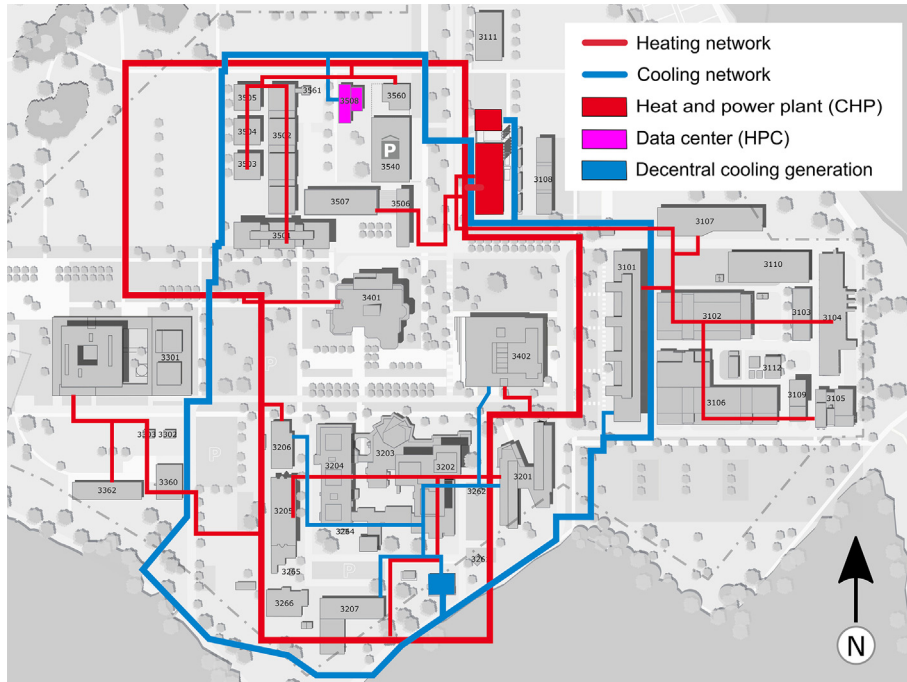


Fig. 1. TU Darmstadt campus Lichtwiese district heating and cooling network in 2018 (changed after [13]).

2.1. Study design

Five strategies are defined, which differ in final dimensioning of the renewable system components as well as the timing of construction and decommissioning of components. Additionally, a reference scenario is used for comparison to status quo.

2.1.1. Assumptions and boundary conditions

It is assumed that the grid supply temperatures will decrease stage by stage from the current level of 80–110 °C to 50–60 °C (Table 1). Correspondingly, the return temperatures are expected to decrease from 60 °C down to 30 °C. Moreover, the amount of waste heat output from HPC cooling is expected to double. Projections of the net heated floor area suggest a continuation of the vigorous construction activities on campus in recent years, resulting in a doubling to 300,000 m². A regression analysis of the current weather dependent heat demand has predicted a lowering of the final heat demand, due to the impact of climate change, from 24.9 GWh to 22.7 GWh. The increase in net heated floor area is assumed to be compensated by efficiency related measures.

2.1.2. Energy saving goals

In accordance with national climate protection goals, the university's goals use the year 1990 as a reference [11]. This makes an exact calculation of the reference EF difficult, as information on heat supply and demand for this period is incomplete. According to the envisaged reduction pathway, the EF in 2025 should amount to 50% of its 1990 value, which already constitutes a significant

reduction. And there is no doubt that the university has already been able to significantly reduce its EF during this period through measures such as increased deployment of CHP and new buildings with a significantly lower specific heat demand. Therefore, for the purposes of this study, it is assumed that the 2025 energy saving goals will be achieved and further reductions are specified in relation to that year. Table 2 shows the resulting target EFs for each transition stage. The energy saving goals are considered satisfied if the system attains an average EF equal to or lower than that of the saving goals pathway of 85.3 gCO₂-equiv/kWh.

2.1.3. Definition of transition strategies

The construction and decommissioning of the system components is classified into five transition levels, where level 0 corresponds to the current status and level IV to the most advanced state (see Fig. 2). For the STC area, a reference value is indicated (i.e. 100%), which is varied from 50% to 200% in a parametric study.

Approximately 43% of the university's final heat demand can be attributed to campus Lichtwiese. Consequently, the same share of the overall thermal power of the CHP units can be assigned to the Lichtwiese, which amounts to 3 MW_{th}.

The BHEs of the MD-BTES are planned in a hexagonal arrangement, limiting the possible number of BHEs to 19 or 37. While systems with only seven BHEs are considered inefficient, the next larger arrangement of 61 BHEs is excluded in advance as being oversized.

As mentioned in chapter 2.1.1, the HPC cooling capacity is expected to double. The flow temperature range of the existing HPC

Table 1 Assumptions for the three transition stages.

| Parameter | Status quo | Stage I | Stage II | Stage III |
|-------------------------------|----------------------|----------------------|----------------------|----------------------|
| Period | 2021 | 2025–2030 | 2030–2040 | 2040–2050 |
| Grid supply temperature level | 80–110 °C | 70–100 °C | 60–80 °C | 50–60 °C |
| Grid return temperature | 60 °C | 50 °C | 40 °C | 30 °C |
| HPC cooling power | 350 kW _{th} | 350 kW _{th} | 500 kW _{th} | 700 kW _{th} |

Table 2
Energy saving goals for the end of each transition stage used for this study.

| Target/Projection | Unit | Status quo | Stage I | Stage II | Stage III |
|---|-------------------------------|--------------------|---------|----------|-----------|
| Net heated floor area | [m ²] | 150,000 | 180,000 | 240,000 | 300,000 |
| Total final heat demand | [GWh/a] | 24.9 | 24.9 | 22.7 | 22.7 |
| Specific final heat demand | [kWh/(m ² a)] | 165.3 | 133.3 | 91.4 | 73.1 |
| Specific EF compared to 2025 ^a | [%] | 100 | 86 | 60 | 40 |
| Specific EF | [gCO ₂ -equiv/kWh] | 125.7 ^b | 108.1 | 75.4 | 50.3 |

^a Hanson et al. [13].

^b Reference scenario simulation result.

| Transition Level | 0 | I | II | III | IV |
|-----------------------|--------|--------|---------|--------|---------|
| STC [m ²] | 0 | 10,000 | 20,000 | 30,000 | 40,000 |
| CHP [MW] | 3 | - | 1,5 | 0,5 | 0 |
| BTES [BHEs] | 0 | - | 19 | - | 37 |
| HPC [kW] | 350 | 350 | 500 | 500 | 700 |
| | HP/ret | HP/sup | dir/ret | HP/sup | dir/sup |

Fig. 2. Transition levels of system components ("–": level not used/defined).

high temperature cooling is 45–50 °C. Currently the waste heat is fed into the return line of the grid by a HP (HP/ret). With the assumed lowering of the grid temperatures, a direct feed into the return line (dir/ret), a supply line feed by HP (HP/sup) or direct feed into the supply line (dir/sup) become viable options.

Fig. 3 shows the planned transition levels of each of the DH components during the three transition stages for each proposed strategy. The *Immediate* strategy is characterized by maximum deployment of renewable energies and decommissioning of all CHP units in transition stage I. A bit less abrupt, but still aiming at a fast transition, the *Progressive* scenario starts with the implementation of SDH in stage I, but keeps the existing CHP units running during this stage. To avoid costs for repeated construction work, the *Step* scenario maintains the existing system design until 2030 and implements the final SDH system in one step. In contrast to the first two scenarios, the *Step* scenario does not require a HP for the HPC in addition to the currently existing one, since waste heat continues to be fed into the return line of the grid during transition stage II. To take the step-wise lowering of the grid temperatures into account, the *Gradual* scenario expands the STC field and the MD-BTES accordingly. At the same time the CHP capacity is reduced step-wise down to level III. The *Conservative* scenario keeps the system unchanged in stage I and results in the smallest SDH system (i.e. STC and BTES). Additionally, a *Reference* scenario is defined for comparison, using only CHP, gas boilers and waste heat utilization with their dimensions corresponding to the existing infrastructure (level 0). In contrast to the five transition strategies, grid temperatures are left unchanged from the current level.

For each proposed strategy, the reference STC field size is varied between 50% and 200% in steps of 10% in relation to the area given in Fig. 2. Thus, including the *Reference* scenario, a total of 81 systems is investigated.

2.2. Model implementation

The system is modeled with *Modelica* [34] and simulation runs are carried out using *SimulationX* [35] as simulation environment. Dynamic simulations of the thermo-hydraulic system are carried out over the period of 25 years. Within each stage the component

| | | 2025-2030 | 2030-2040 | 2040-2050 |
|--------------|------|-----------|-----------|-----------|
| Immediate | STC | IV | IV | IV |
| | CHP | IV | IV | IV |
| | BTES | IV | IV | IV |
| Progressive | STC | I | III | IV |
| | CHP | II | IV | IV |
| | BTES | II | IV | IV |
| Step | STC | II | IV | IV |
| | CHP | II | IV | IV |
| | BTES | II | IV | IV |
| Gradual | STC | I | II | III |
| | CHP | II | II | III |
| | BTES | II | III | IV |
| Conservative | STC | I | II | II |
| | CHP | II | II | II |
| | BTES | II | IV | IV |

Fig. 3. Component transition levels within each transition stage for the defined strategies.

dimensions, DH grid conditions and ambient conditions are adapted according to the scenario design.

2.2.1. Model library, model components and their setup

The DH system was modeled using the in-house developed *MoSDH* (Modelica Solar District Heating) library (Fig. 4). *MoSDH* is based on low level components of the *Modelica Standard Library's Thermal* package. The defining variables for DH system simulations with *MoSDH* are fluid temperature (i.e., enthalpy), pressure and mass flow rate. Heat transfer and pressure loss calculations are mostly based on the *VDI Heat Atlas* [36].

In the following sections the components of the library and their specific setup for this study are described.

Solar Thermal: The flat plate collector model uses a quadratic loss term for efficiency calculation and the isotropic sky model after Liu and Jordan [37,38]. It considers multiple collector modules connected in parallel and in series as well as mutual shadowing of

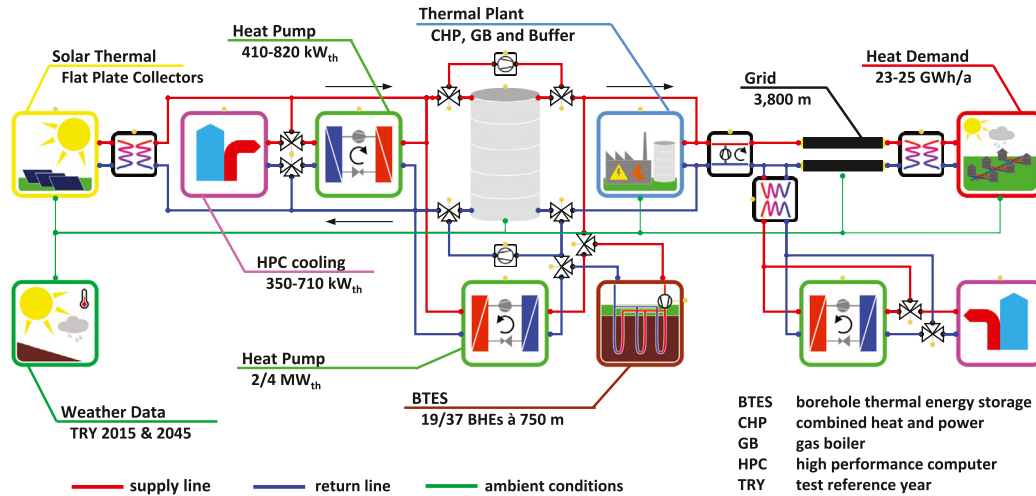


Fig. 4. Model of the SDH system in Modelica.

collector rows. Efficiency parameters are obtained from data sheets of large-scale STCs [52]. Validation was carried out against an established model from TRNSYS [40] for the locations Tehran, Sydney and Reykjavik. The deviation of the annual solar yield was below 5% for all locations.

Weather: The weather component reads hourly ambient temperature as well as direct and diffuse solar irradiation data from text files. Test reference years (TRY) for the campus location are used from the German Weather Service [41]. For transition stage I the TRY 2015 is used, which represents a typical year derived from measured data during the period from 1995 to 2012. At the start of transition stage II, the weather data switches to TRY 2045, which constitutes a typical year for climate projections in the period from 2031 to 2060. Average ambient temperatures and annual solar irradiation amount to 10.6 °C and 1085 kWh/m² for TRY 2015 as well as 11.3 °C and 1162 kWh/m² for TRY 2045, respectively.

BTES: A BTES consisting of 19 or 37 BHEs of 750 m in a hexagonal layout is modeled using the MoBTES model. The design of the modeled coaxial BHEs was carried out according to the planned demonstrator, where the upper section is thermally insulated by the use of a backfill material with low thermal conductivity [31]. A detailed description of the MoBTES model and its validation can be found in Formhals et al. [42].

Buffer storage: The model consists of several volume elements to account for thermal stratification. It was developed in the course of a master thesis and validated against an existing model [43]. Since the volume of the buffer storage tank should be adapted according to the size of the STC aperture area, its size is defined by a ratio of 0.25 m³_{buffer}/m²_{collector}.

Thermal power plant: This model combines a CHP model with several units and a gas boiler for auxiliary heating. In both models, the fuel consumption is derived from efficiency curves. In addition to that, the CHP model uses a curve for its power to heat ratio. For the underlying case study, data sheets of the existing components at campus Lichtwiese are used. According to the existing system at campus Lichtwiese, a smaller buffer storage with a volume of 125 m³ is used to increase the running times of the CHP units.

Heat pumps: The HPs are modeled using efficiency maps for the maximum heating power and the coefficient of performance, which are derived from manufacturer datasheets of high temperature HP [53]. Since the availability for high temperature HPs data in the required heating power range is limited, the maximum

heating power was scaled. This was done under the assumption that larger HPs have an efficiency at least as high as smaller units.

Grid: The campus DH grid has a length of approximately 3.8 km, represented by two segmented pipes of this length, one for the supply and one for the return line. Since the weighted average diameter of the campus grid is close to the diameter of a DN250 DH pipe [54], the pipe model was parametrized accordingly. The pre-insulated pipes are modeled by reusing sub-models from the MoBTES model: DH pipe segments are represented by BHE segments. Moreover, the ground surrounding the pipes is modeled by a thermal resistance and capacity model, which was initially implemented to consider the heat transport in the immediate vicinity of BHE segments. The thermal resistance between this circular region and the ground surface is derived from the VDI Heat Atlas [36].

Heat Demand: In accordance with the simplified representation of the campus DH grid, the demand side is combined into one consumer. The heat load curve was generated by applying a regression model, derived by monitoring data over the period between November 2016 and July 2019, on the used TRY datasets [13].

2.2.2. Control strategy

The control strategy is based on system states, which define respective component behaviors. Transitions between states are triggered by conditional expressions. According to the active state, components receive set values for thermal power, supply temperature or mass flow rate via a central bus system. STC, HPC and BTES are activated and deactivated in the given order depending on the state of charge of the buffer storage tank. The single HPC in the grid is represented by two separate model blocks, one of which is connected to the supply line of the grid and the other to the return line. As in the existing system, HPC cooling is only fed into the grid during the heating period, while cooling fans are used in summer [5].

In summer operation heat is transferred to the BTES, if the buffer's state of charge exceeds a certain threshold. During heating season, the BTES is discharged into the buffer storage directly or via HP. Discharging is enabled if half of the buffer storage volume is below the reference grid temperature, which is the case almost all winter and carries on until BTES flow temperatures fall below 10 °C.

The thermal plant satisfies the heat demand, which cannot be covered by the SDH system. CHP units are switched on and off according to the charging state of the small buffer. If CHP units are active, a direct feed can be used to bypass the buffer. If the required

heat demand exceeds the limits of the CHP and the buffer, the gas boiler covers the residual load. The temperatures that enter the grid are regulated according to a heating curve, which relates the supply temperature to the 24 h average ambient temperature. Up to a certain level, the temperature level of the heat supplied by the SDH part is raised by mixing with volume flow from the thermal plant, if necessary.

2.3. Analysis

An economic and environmental assessment of the systems under investigation is carried out after Mauthner et al. [14] and Welsch et al. [24]. It is expected that both the energy prices and the EF of the electricity purchased from the grid will change over time, as assumed in the EVO scenario by Welsch et al. [24]. For this reason, the EVO scenario was applied in this study as well. To account for uncertainties in fuel and investment costs, a sensitivity analysis is carried out for selected systems.

2.3.1. Economic assessment

A common figure for comparing the economic efficiency of thermal energy systems is the LCOH (Equation (1)) [46]. To allow for an annual resolution of costs, attributed to the heat delivered over the span of one year Q_a , the concept of annuities A is used [47]. In this concept, repayments of an initial investment are evenly distributed over its lifetime of n years. Functions and data for investment costs I_0 , annual maintenance costs M_a , fuel costs F_a , revenues R_a and expected lifetimes a_{life} for the system components are adopted from Mauthner et al. [14] and Welsch et al. [24]. For each of the components, annuities AN are calculated by multiplying the initial investment costs by the annuity factor AF [48] (Equation (2)). An interest rate r of 3% was assumed. Residual values of existing components are factored in by their age and expected remaining lifetime. Annuities are paid accordingly. In the case of early decommissioned components (e.g., existing CHP units), no resale was considered. Investment costs were further repaid over the remaining depreciation period, but no further maintenance costs were charged.

$$LCOH_a = \frac{AN + M_a + F_a - R_a}{Q_a} \quad (1)$$

$$AN = I_0 AF = I_0 \frac{(1+r)^{a_{life}} r}{(1+r)^{a_{life}} - 1} \quad (2)$$

2.3.2. Environmental assessment

The environmental impact of the delivered heat Q_{th} was calculated using an LCA approach, taking into account emissions caused by operation (GWP_{op}) and production (GWP_{prod}). In the case of CHP, the production of electricity was included in the evaluation, to avoid allocation of emissions. As a result, the economic and environmental differences of the investigated systems due to a change in produced electricity, are considered as well. The total EF of each system was calculated according to Equation (3), where i stands for the different components of the system [24]. However, in order to allow for a comparison between annual EFs and energy saving goals, Equation (3) had to be adapted. Emissions attributed to the production of components are distributed evenly over the lifetime a_{life} of each component as given in Equation (4).

$$EF = \frac{GWP}{Q_{th,tot}} = \frac{1}{Q_{th,tot}} \sum_{i=1}^n (GWP_{prod,i} + \sum_{a=1}^{a_{life}} GWP_{a,op,i}) \quad (3)$$

$$EF_a = \frac{GWP_a}{Q_{th,a}} = \frac{1}{Q_{th,a}} \sum_{i=1}^n \left(\frac{GWP_{prod,i}}{a_{life}} + GWP_{a,op,i} \right) \quad (4)$$

2.3.3. System performance figures

Equation (5) defines the solar fraction of a system, where the amount of energy stored into the BTES $Q_{BTES,charged}$ is subtracted from the overall energy supplied by the STC field Q_{solar} to achieve the direct delivered solar energy. The amount of energy discharged from the storage $Q_{BTES,discharged}$ is included into the solar fraction. The storage utilization factor η_{BTES} is defined by Equation (6).

$$f_s = \frac{Q_{solar} - Q_{BTES,charged} + Q_{BTES,discharged}}{Q_{grid,feed}} \quad (5)$$

$$\eta_{BTES} = \frac{Q_{BTES,discharged}}{Q_{BTES,charged}} \quad (6)$$

2.4. Limitations

Due to the necessity of several simplifications and assumptions, the presented study has certain limitations that should be kept in mind. In accordance with the mentioned *EnEff* project, the focus of this study was put on a single campus of the university. Even though a separate supply of heat is generally possible and the different campus grids are already operating on various temperature levels, technical and economical interdependencies of the connected grids are strong. This could result both in synergetic as well as adverse effects. Furthermore, the district cooling grid of the university was not within the system boundaries of this study. A coupling of the two grids will most certainly be implemented in the future and improve energetic efficiency. The assumed measures and costs for the conversion of the DH grid into a 4GDH, especially concerning consumers and distribution, need to be considered as a part of separate studies. Another limitation concerns the underlying input data for the development of energy prices and climate as well as the used cost relations, since these are subject to significant uncertainties. Moreover, the design of the study introduces several simplifications, using discrete system transition stages, a limited number of parameter variations and a fixed set of technologies. This was caused by numerical limitations on the one hand, and the case study character of the study on the other hand, focusing on a certain system and a certain possible technology. A widening of this scope would have been hard to handle as thoroughly as the presented work.

3. Results

3.1. Parameter study

3.1.1. Annual supplied thermal energy

As expected, in each transition scenario the amount of directly provided solar thermal energy increases with an increase in the STC field size (Fig. 5). The BTES system covers up to 38.5% of the total heat demand. It can be observed that this share increases with STC size up to a maximum and decreases hereafter, which is in line with the feed-in order mentioned in Chapter 2.2.2. Accordingly, the

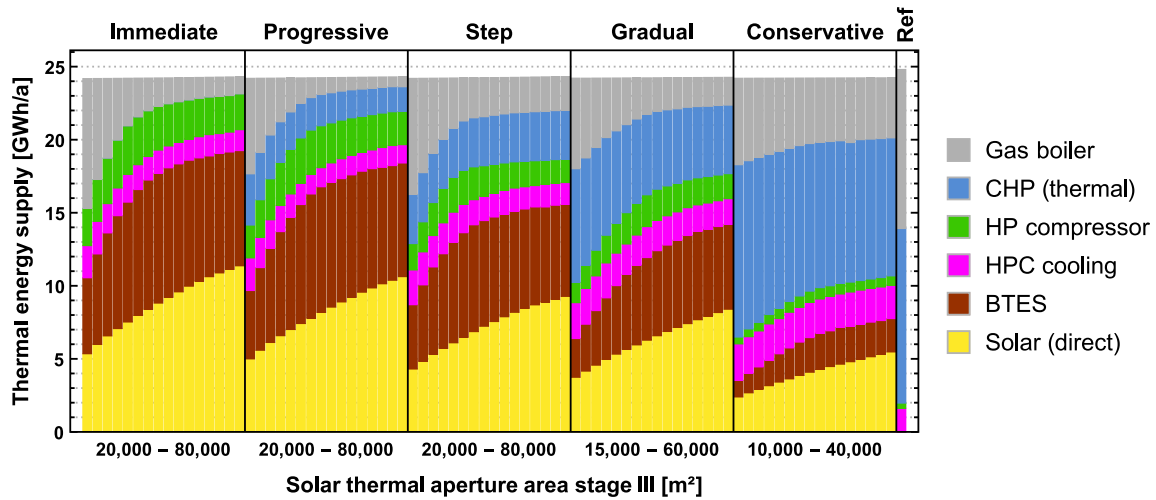


Fig. 5. Average annual thermal energy supply of each simulated system. Direct solar delivery is calculated by subtracting the energy stored into the BTES from the total solar production.

amount of HPC waste heat, reduces for systems with high solar shares, since priority is given to STCs. An early integration of BTES into the grid generally results in higher demands of electricity, since the HPs need to raise discharged energy to higher temperatures (*Immediate & Progressive*). Finally, the share of CHP increases for slow transition strategies and almost reaches the level of the *Reference* system for *Conservative* strategies. The *Reference* system yields a CHP share of 51.7%, which is close to the actual share of 55% in 2018 [13]. This deviation can be partly explained by the integration of HPC cooling, which was only installed in 2021.

3.1.2. Economic and environmental performance

Even without further modifications, the existing heating system can reach a comparatively low EF at moderate heating costs (*Reference* scenario, Fig. 6). This can be attributed to the high share of CHP, which leads to considerable enhancements in the GWP balance due to emission credits for the replacement of grid electricity with CHP electricity.

Within each strategy, an increase of the STC area results in a lowering of the EF. Below a certain point however, further

reductions lead to a disproportional increase in the LCOH. Counterintuitively, it is not the *Immediate* but the *Progressive* strategy that provides the system design with the lowest overall EF. In contrast, the overall lowest LCOH is obtained by the *Conservative* strategy, which cannot compete with the other strategies in terms of emission reduction. Among the other four strategies that gain similarly low EFs, the *Gradual* strategy achieves the lowest LCOH. Most importantly, both the *Conservative*, as well as the *Gradual* strategy are even more economic than the *Reference* scenario.

3.1.3. Selection of efficient system designs

Table 3 specifies several performance figures for three characteristic system designs per transition strategy: the ones with the lowest EF, lowest LCOH and lowest LCOH that attains the EF target.

The solar yield of all characteristic systems lies in the range of 306–518 kWh/(m² a), which is plausible for SDH systems [14]. It generally decreases for systems with larger aperture areas indicating a saturation effect. Furthermore, the solar fraction f_{sol} varies between 27.9% for the LCOH_{min} *Conservative* scenario and 83.3% for the EF_{min} *Immediate* scenario system. The storage utilization η_{BTES}

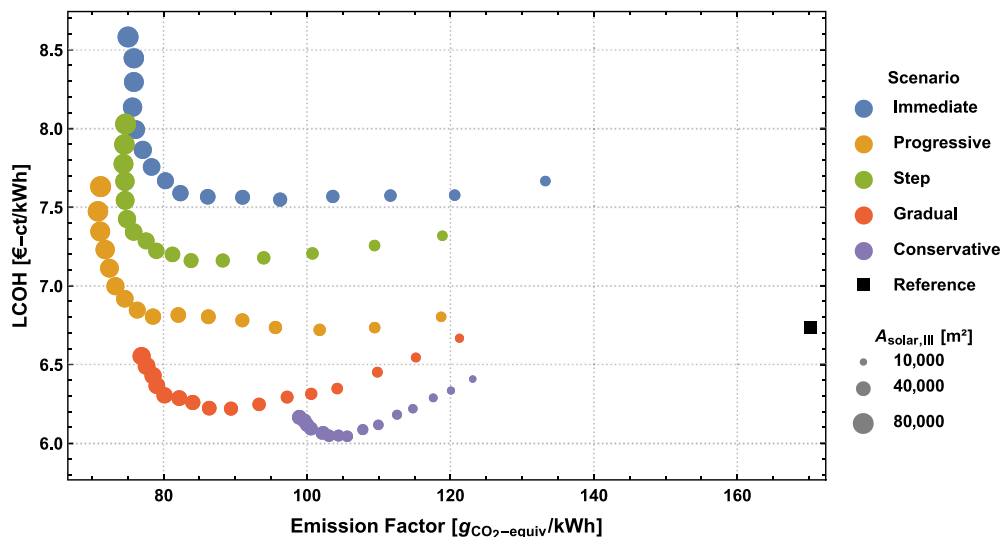


Fig. 6. LCOH and EF for the systems under investigation.

of the characteristic systems reaches a maximum of 92.4%. For the comparison of the total GWP from 2025 to 2050, it should be considered that the *Reference* system already includes a reduction of the specific heat demand in 2050 by 50%. Consequently, the actual GWP of a completely unchanged DH system would be significantly higher.

Apparently, none of the system designs which use the *Conservative* transition strategy reaches the target EF. In contrast, several of the selected system designs of the four more ambitious strategies do so. An abrupt transformation of the *Lichtwiese* into an SDH system however, as represented by the *Immediate* scenario, is not advisable under the given circumstances as well. Those systems result in higher LCOHs, particularly in comparison to the *Gradual* and *Progressive* transition strategies, without a significant additional emission reduction. For further analysis, the EF_{target} systems of each scenario are selected. In the case of the *Conservative* scenario the EF_{min} system is chosen instead.

With an LCOH of 6.3 ct/kWh, the most economic system to reach the target EF belongs to the *Gradual* strategy. Even for an increase of all energy prices and investment costs by 20%, it would result in an LCOH below the expected value of the *Immediate* system (cf. **Table 3 Cost variation**).

Fig. 7 depicts the composition of the specific costs per transition phase of the selected systems as well as the revenues from the sale of excess electricity to the grid. The composition of the LCOH for the *Immediate* system reveals that the integration of a BTES in Phase I results in a high LCOH, if the HP's electricity demand is not covered by self-production of the CHP.

The *Gradual* system, which does not use a BTES within stage I and reduces the CHP capacity beginning from stage II onwards, results in a total LCOH which is 0.5 ct/kWh lower than for the second most economic system (*Progressive*). This cost advantage can be attributed mostly to transition stage II (cf. **Fig. 7**). While the *Progressive* strategy comprises a simultaneous full-scale integration of an SDH system with integrated BTES and the phase out of CHP technology in stage II, the CHP units maintain half capacity for the *Gradual* strategy. Consequently, there is still enough self-produced cogenerated electricity available to supply circulation pumps and HPs.

However, since the economic and environmental performance of the CHP is projected to continuously decrease, a successive increase of STC area and BTES capacity within stage II and III, with a

simultaneous reduction of the CHP capacity down to minimum, as included in the *Gradual* strategy, is advisable.

According to the results of the study, a reasonable transition strategy for the *Lichtwiese* campus could be as follows: The STC area should be enlarged from 14,000 m² in 2025 to 28,000 m² in 2030, and to a final size of 42,000 m² in 2040. At the same time, the CHP capacity should be reduced from 3 MW_{th}, to 1.5 MW_{th} and finally to 0.5 MW_{th}. An expansion to the maximum sized MD-BTES with 37 BHEs is recommended in 2040, with an initial size of 19 BHEs in 2030.

These findings, however, assume that no subsidies are considered, as they are difficult to predict. Current subsidies could favor earlier construction as they significantly reduce investment costs of BTES systems and STCs [24].

3.1.4. Energy saving goals

Fig. 8 shows emission targets as well as the temporal development of the annual EFs for the selected systems in relation to the emissions of the *Reference* scenario in 2025. It is quite clear, that the *Reference* system loses attractiveness over time. As already pointed out by Welsch et al. [24], a decrease in the EF of grid electricity is very likely, due to a higher share of renewables in the future. Subsequently, emission credits caused by the substitution of grid electricity with CHP electricity, will diminish. Accordingly, EFs increase within all transition stages in which CHP is used. As a result, the target trajectory is exceeded by all systems before 2030. In addition to that, the *Immediate* scenario system, which does not use CHP at all, even starts with an EF higher than the *Reference* case, highlighting the currently prevailing advantage of the CHP technology. While the *Immediate*, *Progressive*, *Step* and *Gradual* scenario systems surpass the cumulated emission reduction goal, they narrowly miss the final target value in 2050.

Overall, the development of specific emissions over time illustrates that CHP is an efficient technology for several years to come, not only from an economic but also from an ecological perspective. The investigated transition scenarios comprise cost-effective ways to reduce the total emissions of DH systems. However, the final emission target in 2050 was missed, even for systems with a large SDH dimensioning (cf. **Fig. 8**). This indicates the importance of the integration of additional renewable technologies or the expansion of waste heat utilization. Latter one should be a feasible option, since projections of the waste heat potential were very

Table 3

Performance figures for the most economic system that attains the EF target, the system with the lowest EF and the system with the lowest LCOH within each transition strategy.

| Scenario | System | Final A _{solar} [m ²] | Solar yield [kWh/(m ² a)] | Solar fraction f _s [%] | BTES utilization η _{BTES} [%] | Total GWP [tCO ₂] | Total EF [gCO ₂ /kWh] | Final EF [gCO ₂ /kWh] | Total LCOH [ct/kWh] | 20% cost variation [ct/kWh] | Final LCOH [ct/kWh] |
|---------------|----------------------|--|--------------------------------------|-----------------------------------|--|-------------------------------|----------------------------------|----------------------------------|---------------------|-----------------------------|---------------------|
| Reference | — | 0 | 0 | 0 | 0 | 98,301 | 170.2 | 188.8 | 6.7 | 5.4–8.1 | 7.3 |
| Immediate | EF _{target} | 48,000 | 431 | 76.6 | 74.9 | 47,601 | 82.4 | 58. | 7.6 | 6.1–9.1 | 6.9 |
| | EF _{min} | 80,000 | 306 | 83.3 | 60.2 | 43,392 | 75.1 | 56.6 | 8.6 | 6.9–10.3 | 8.1 |
| | LCOH _{min} | 36,000 | 475 | 68.0 | 85.7 | 55,615 | 96.2 | 71.1 | 7.6 | 6.0–9.1 | 6.9 |
| Progressive | EF _{target} | 48,000 | 449 | 72.6 | 77.7 | 45,386 | 78.5 | 60.4 | 6.8 | 5.5–8.2 | 6.5 |
| | EF _{min} | 76,000 | 349 | 78.9 | 61.2 | 40,935 | 70.8 | 57.3 | 7.5 | 6.0–9.0 | 7.5 |
| | LCOH _{min} | 28,000 | 518 | 54.4 | 92.4 | 58,811 | 101.8 | 89.8 | 6.7 | 5.4–8.1 | 6.5 |
| Step | EF _{target} | 40,000 | 476 | 59.0 | 81.6 | 48,459 | 83.9 | 62.6 | 7.2 | 5.7–8.6 | 6.7 |
| | EF _{min} | 72,000 | 348 | 66.6 | 58.2 | 43,011 | 74.4 | 57.2 | 7.8 | 6.2–9.3 | 7.8 |
| | LCOH _{min} | 36,000 | 494 | 56.1 | 84.7 | 50,987 | 88.2 | 67.9 | 7.2 | 5.7–8.6 | 6.7 |
| Gradual | EF _{target} | 42,000 | 452 | 55.3 | 79.4 | 48,584 | 84.1 | 62.7 | 6.3 | 5.0–7.5 | 6.4 |
| | EF _{min} | 60,000 | 396 | 61.5 | 60.9 | 44,441 | 76.9 | 56.7 | 6.6 | 5.3–7.9 | 6.9 |
| | LCOH _{min} | 36,000 | 474 | 51.6 | 85.7 | 51,653 | 89.4 | 70.1 | 6.2 | 5.0–7.5 | 6.3 |
| Conservative | EF _{target} | — | — | — | — | — | — | — | — | — | — |
| | EF _{min} | 40,000 | 364 | 33.5 | 56.7 | 57,185 | 99.0 | 75.4 | 6.2 | 4.9–7.4 | 6.0 |
| | LCOH _{min} | 24,000 | 438 | 27.9 | 87.1 | 61,020 | 105.6 | 84.7 | 6.1 | 4.8–7.3 | 5.8 |
| Target | | | | | | 50,135 | 85.3 | 50.3 | | | |

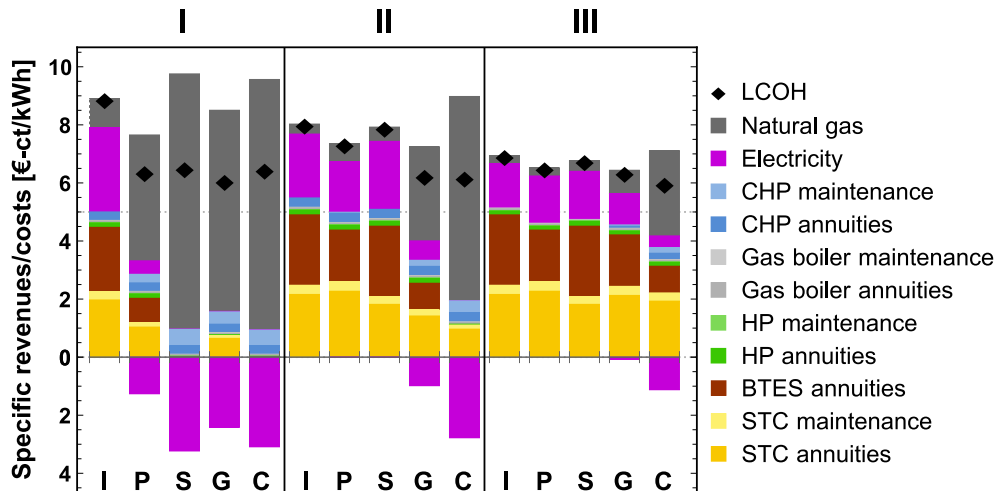


Fig. 7. Specific revenues (bottom) and costs (top) for the EF_{target} system of Immediate (I), Progressive (P), Step (S) and Gradual (G) transition strategies and the EF_{min} system of Conservative (C) allocated to the different transition stages.

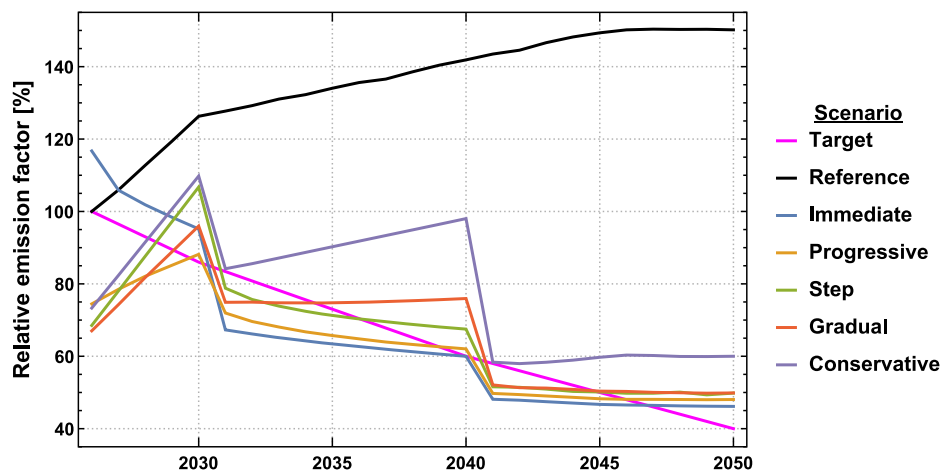


Fig. 8. Relative annual emission factor of the EF_{min} system for the Conservative scenario and EF_{target} systems else.

conservative. The remaining emissions in 2050 are mostly due to gas consumption of boiler and CHP units, which could be reduced by the utilization of biomass. However, a total carbon-neutrality in 2050 seems hard to attain. For one thing, the used LCA approach considers emissions during production phase, which cannot be avoided completely and would have to be compensated by carbon sinks. Secondly, the used projections do not anticipate carbon neutrality of the grid electricity in 2050. Nevertheless, if this goal were to be achieved, it would contribute significantly to the goal of a carbon-neutral campus DH system.

3.2. Sensitivity analysis

Both the energy prices as well as the investment costs are varied for the selected system designs (cf. Table 3) in order to assess the sensitivity of the heat costs incurred to changes in the economic input data (Fig. 9). It can be observed that the Reference and Conservative scenarios, which have the highest share of CHP heat, are especially sensitive to changes in energy prices. For scenarios with an increasing share of SDH, the sensitivity shifts from a high impact of energy prices towards a high impact of investment costs, which is due to the generally high investment costs of STC and BTES.

4. Conclusion

The presented study investigates different strategies and technological pathways for the transition of an existing campus district heating grid towards a low-temperature SDH system. It emphasizes the importance of considering the projected development of existing infrastructure and boundary conditions. If such temporal developments are excluded during system engineering, it can lead to considerably higher costs. In contrast, a dynamic study design, as presented in this study, allows economic and ecological advantages of certain technologies at certain transition phases to be identified and included in the planning process. While studies of 4GDH systems with fixed system design make a compelling point for the utilization of 4GDH in general, operators of existing DH systems could argue that a transition of their system is not possible due to practical reasons. The presented study demonstrates the feasibility of a step-wise transition of such a system, which comprises several old buildings under monumental protection and a relatively new CHP plant. Hence, the proposed methodology of numerical simulations with dynamic boundary conditions and system design represents a reasonable extension to existing approaches. However, due to the higher computational effort of such a transient simulation approach, it does not provide the ability of a completely

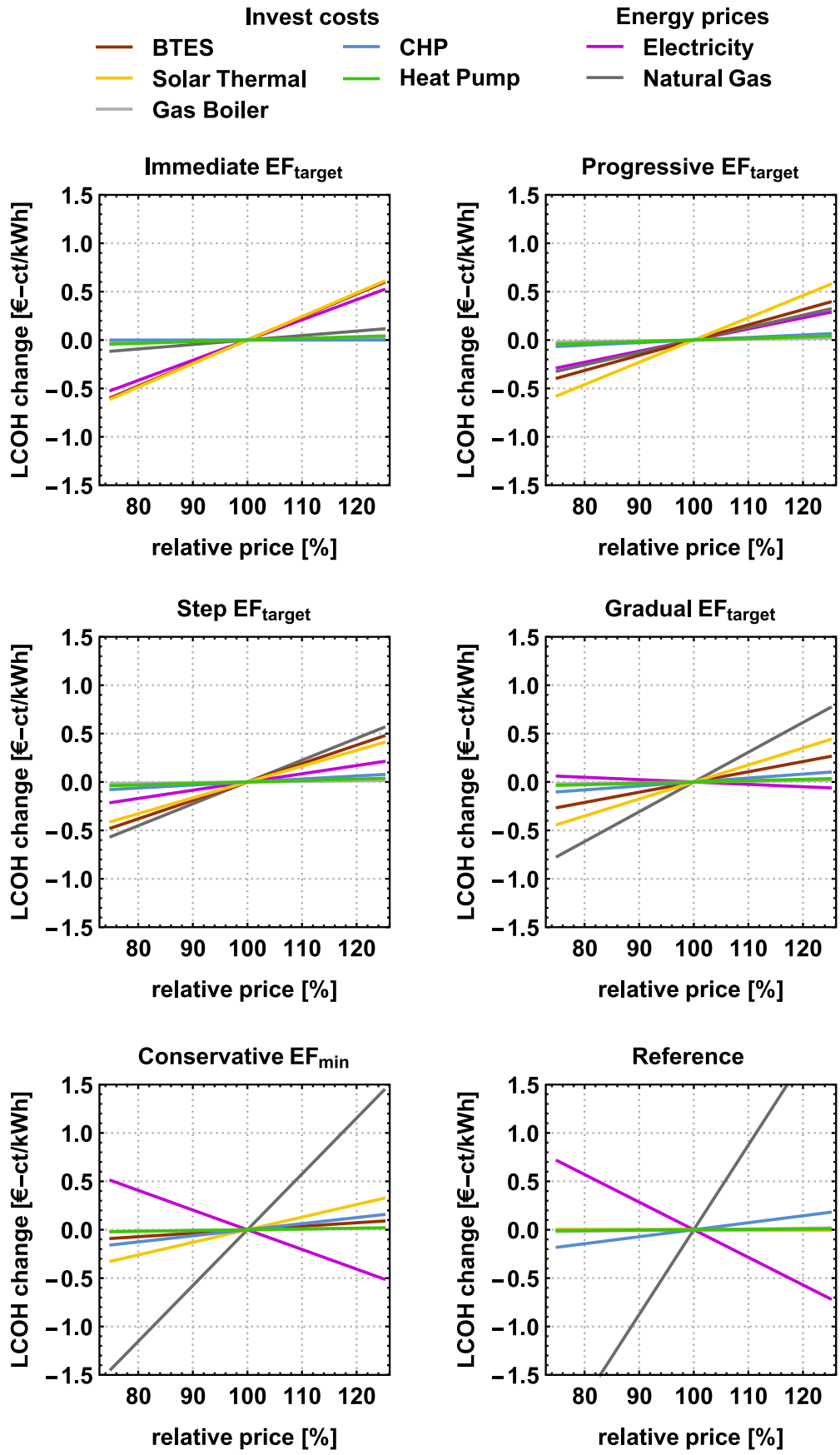


Fig. 9. Variation of energy prices and invest costs for the selected systems.

technology-open analysis, as it can be achieved e.g., by energy budget tools [49]. Nevertheless, the developed model library efficiently exploits the possibilities of equation-based modeling with *Modelica* and facilitates a detailed representation of specific existing systems.

The approach was used to conduct a parametric study, which demonstrates that MD-BTES systems facilitate high solar fractions and thus enable the provision of a significant share of renewable energies in the heat demand of SDH systems. In the case study of the campus *Lichtwiese* DH grid, the BTES-assisted systems under consideration appear to be very promising options for taking a major step towards achieving the TU Darmstadt's emission reduction targets. Even LCOHs below the reference case are possible, but for a definite conclusion costs of transition measures, such as adjustments to building heating systems and the grid, should be included.

Furthermore, results indicate that unambitious transition strategies similar to the *Conservative* scenario will ultimately fail to attain the emission targets. However, an abrupt transformation of the *Lichtwiese* into a SDH system, as represented by the *Immediate* scenario, is also not advisable under the given circumstances. Such hasty transitions result in higher LCOH, compared to *Gradual* and *Progressive* transition strategies, without achieving any significant additional emission reductions.

Consequently, in the case of the *Lichtwiese* DH system, it is advisable to gradually integrate SDH from 2025 with a final STC area of 42,000 m² and an MD-BTES consisting of 37 BHEs. The existing CHP units are to be operated at full capacity until 2030 and afterwards reduced in steps to a final capacity of 500 kW in 2040.

While cumulative emission saving goals in 2050 could be satisfied by the proposed systems, the final target in 2050 is missed narrowly and carbon-neutrality cannot be achieved. Consequently, future studies should include additional measures like a switch from natural gas to biomass combustion or power-to-heat technology. Furthermore, necessary transformation measures on the consumer side and subsidies should be considered and included in cost calculation. Finally, the proposed concept of MD-BTES, which so far has only been evaluated numerically, should be validated by experimental data, to verify the identified energetic and economic potentials.

Declaration of competing interest

The authors declare that they have no known competing financial interests or personal relationships that could have appeared to influence the work reported in this paper.

Nomenclature

| | |
|------|------------------------------------|
| 3GDH | Third generation district heating |
| 4GDH | Fourth generation district heating |
| BHE | borehole heat exchanger |
| BTES | borehole thermal energy storage |
| CHP | combined heat and power |
| DH | district heating |
| EF | emission factor |
| GB | gas boiler |
| GWP | global warming potential |
| HP | heat pump |
| HPC | high-performance computer |
| LCOH | levelized cost of heat |
| MD | medium deep |
| SDH | solar district heating |
| STC | solar thermal collector |
| TRY | test reference year |

UTES underground thermal energy storage

Symbols

| | |
|----|-------------------------------|
| A | Area m ² |
| AN | Annuities € |
| AF | Annuity factor |
| F | Fuel costs € |
| f | Fraction % |
| M | Maintenance costs € |
| I | Investment costs € |
| Q | Thermal energy J |
| r | Interest rate % |
| R | Revenues € |
| η | Efficiency/utilization rate % |

Subscripts

| | |
|------|---------------------------------|
| a | Index of specific year |
| i | Index of a specific component |
| life | Component lifetime |
| min | Minimum |
| op | Concerning component operation |
| prod | Concerning component production |
| sol | Solar |
| th | Thermal |
| tot | Total |

Author contribution

Julian Formhals: Conceptualization, Methodology, Software, Validation, Formal analysis, Investigation, Data curation, Writing – original draft, Visualization, Frederik Feike: Conceptualization, Validation, Investigation, Data curation, Writing – review & editing, Hoofar Hemmatbady: Conceptualization, Validation, Investigation, Writing – review & editing, Bastian Welsch: Conceptualization, Methodology, Investigation, Writing – review & editing, Supervision, Project administration, Ingo Sass: Conceptualization, Resources, Writing – review & editing, Supervision, Project administration, Funding acquisition

Funding

This work was financially supported by the European Regional Development Fund (ERDF) by supporting the North-West Europe Interreg project *DGE-Rollout* (NWE 892), the German Federal Ministry of Economic Affairs and Energy (BMWi) in the project *EnEff-Stadt Campus Lichtwiese II* (03ET1638) as well as the German Research Foundation (DFG) in the framework of the Excellence Initiative, *Darmstadt Graduate School of Excellence Energy Science and Engineering* (GSC 1070).

References

- [1] Connolly D, Lund H, Mathiesen BV, Werner S, Möller B, Persson U, et al. Heat Roadmap Europe: combining district heating with heat savings to decarbonise the EU energy system. *Energy Pol* 2014;65:475–89. <https://doi.org/10.1016/j.enpol.2013.10.035>.
- [2] Lund H, Werner S, Wiltshire R, Svendsen S, Thorsen JE, Hvelplund F, et al. 4th Generation District Heating (4GDH). Integrating smart thermal grids into future sustainable energy systems. *Energy* 2014;68:1–11. <https://doi.org/10.1016/j.energy.2014.02.089>.
- [3] Averfalk H, Werner S. Economic benefits of fourth generation district heating. *Energy* 2020;193. <https://doi.org/10.1016/j.energy.2019.116727>.
- [4] Sorknæs P, Østergaard PA, Thellufsen JZ, Lund H, Nielsen S, Djørup S, et al. The benefits of 4th generation district heating in a 100% renewable energy system. *Energy* 2020;213. <https://doi.org/10.1016/j.energy.2020.119030>.
- [5] Oltmanns J, Sauerwein D, Dammel F, Stephan P, Kuhn C. Potential for waste heat utilization of hot-water-cooled data centers: a case study. *Energy Sci Eng* 2020;8:1793–810. <https://doi.org/10.1002/ese3.633>.
- [6] Volkova A, Mašatin V, Siirde A. Methodology for evaluating the transition

- process dynamics towards 4th generation district heating networks. *Energy* 2018;150. <https://doi.org/10.1016/j.energy.2018.02.123>.
- [7] Esser A, Dunne A, Meeusen T, Quaschnig S, Wegge D, Hermelink A, et al. Comprehensive study of building energy renovation activities and the uptake of nearly zero-energy buildings in the EU. Brussel, Belgium. European Commission; 2019.
- [8] Volkova A, Krupenski I, Ledvanov A, Hlebnikov A, Lepiksaar K, Latšov E, et al. Energy cascade connection of a low-temperature district heating network to the return line of a high-temperature district heating network. *Energy* 2020;198. <https://doi.org/10.1016/j.energy.2020.117304>.
- [9] Kleinertz B, Brühl G, Veitengruber F, Pellinger C, Roon S Von. Transformation of an existing into a fourth generation heating network. *Energy Procedia* 2018;149. <https://doi.org/10.1016/j.egypro.2018.08.212>.
- [10] Pelda J, Stelter F, Holler S. Potential of integrating industrial waste heat and solar thermal energy into district heating networks in Germany. *Energy* 2020;203. <https://doi.org/10.1016/j.energy.2020.117812>.
- [11] Hanson J, Plößer T, Maihöfner D, Kuhn C, Sauerwein D, Stein T, et al. EnEff: Stadt Campus Lichtwiese: energieeffiziente Weiterentwicklung des Campus Lichtwiese durch intelligente Systemvernetzung (Abschlussbericht zum Fkz: 03ET1356 A). Darmstadt, Germany. Technical University of Darmstadt; 2019.
- [12] BMUB. Climate Action Plan 2050 - principles and goals of the German government's climate policy. Berlin. Federal Ministry for the Environment, Nature Conservation, Building and Nuclear Safety (BMUB); 2016.
- [13] Oltmanns J. Analysis and Improvement of an existing university district energy system. Technical University of Darmstadt; 2021. <https://doi.org/10.26083/tuprints-00017367>.
- [14] Mauthner F, Herkel S. Task 52 - solar heat and energy economics in Urban Environments - technical Report Subtask C1 - technology and demonstrators. Solar Heating and Cooling Programme. Gleisdorf, Austria: International Energy Agency; 2016.
- [15] Reed AL, Novelli AP, Doran KL, Ge S, Lu N, McCartney JS. Solar district heating with underground thermal energy storage: pathways to commercial viability in North America. *Renew Energy* 2018;126:1–13. <https://doi.org/10.1016/j.renene.2018.03.019>.
- [16] Sibbitt B, McClenahan D, Djebbar R, Thornton J, Wong B, Carriere J, et al. The performance of a high solar fraction seasonal storage district heating system—five years of operation. *Energy Procedia* 2012;30:856–65. <https://doi.org/10.1016/j.egypro.2012.11.097>.
- [17] Mangold D, Miedaner O, Tziggili EP, Schmidt T, Unterberger M, Zeh B. Technische-wirtschaftliche Analyse und Weiterentwicklung der solaren Langzeit-Wärmespeicherung. Stuttgart. Stuttgart: Solites - Steinbeis Research Institute for Solar and Sustainable Thermal Energy Systems; 2012.
- [18] Gehlin S. Borehole thermal energy storage. In: Rees S, editor. *Adv. Ground-source heat pump syst.* Elsevier; 2016. p. 295–327.
- [19] Welsch B, Rühaak W, Schulte DO, Bär K, Sass I. Characteristics of medium deep borehole thermal energy storage. *Int J Energy Res* 2016;40:1855–68. <https://doi.org/10.1002/er.3570>.
- [20] Gabrielli P, Acquilino A, Siri S, Bracco S, Sansavini G, Mazzotti M. Optimization of low-carbon multi-energy systems with seasonal geothermal energy storage: the Anergy Grid of ETH Zurich. *Energy Convers Manag X* 2020;8. <https://doi.org/10.1016/j.ecmx.2020.100052>.
- [21] Welsch B. Technical, environmental and economic assessment of medium deep borehole thermal energy storage systems, Dissertation. Darmstadt: Technical University of Darmstadt; 2019.
- [22] Sass I, Heldmann C-D, Lehr C. Erschließung eines Marmorarkstorkommens als mitteltiefer Erdwärmesondenspeicher im Tuxertal, Tirol. *Grundwasser* 2016;21:137–45.
- [23] Welsch B, Göllner-Völker L, Schulte DO, Bär K, Sass I, Schebek L. Environmental and economic assessment of borehole thermal energy storage in district heating systems. *Appl Energy* 2018;216:73–90. <https://doi.org/10.1016/j.apenergy.2018.02.011>.
- [24] Elhashmi R, Hallinan KP, Chiasson AD. Low-energy opportunity for multi-family residences: a review and simulation-based study of a solar borehole thermal energy storage system. *Energy* 2020;204. <https://doi.org/10.1016/j.energy.2020.117870>.
- [25] Rämä M, Wahlroos M. Introduction of new decentralised renewable heat supply in an existing district heating system. *Energy* 2018;154. <https://doi.org/10.1016/j.energy.2018.03.105>.
- [26] Hemmatbady H, Formhals J, Welsch B, Schulte DO, Sass I. Optimized layouts of borehole thermal energy storage systems in 4th generation grids. *Energies* 2020;13. <https://doi.org/10.3390/en13174405>.
- [27] Rehman H ur, Hirvonen J, Jokisalo J, Kosonen R, Sirén K. EU emission targets of 2050: costs and CO2 emissions comparison of three different solar and heat pump-based community-level district heating systems in nordic conditions. *Energies* 2020;13. <https://doi.org/10.3390/en13164167>.
- [28] Behzadi A, Arabkoohsar A. Comparative performance assessment of a novel cogeneration solar-driven building energy system integrating with various district heating designs. *Energy Convers Manag* 2020;220. <https://doi.org/10.1016/j.enconman.2020.113101>.
- [29] Sass I, Bär K, Schulte DO, Welsch B, Formhals J, Hornich W, et al. SKEWS (Solargekoppelter kristalliner Erdwärmesondenspeicher): Wärmespeicherprojekt der TU Darmstadt am Campus Lichtwiese. Darmstadt: 11 Tiefengeothermie-Forum; 2016.
- [30] Schulte DO, Welsch B, Boockmeyer A, Rühaak W, Bär K, Bauer S, et al. Modeling insulated borehole heat exchangers. *Environ Earth Sci* 2016;75:910. <https://doi.org/10.1007/s12665-016-5638-x>.
- [31] Modelica. Modelica Association. Version 3.4 [Software]. 2017. Available from: <https://modelica.org/>.
- [32] SimulationX. Version 4.1 [Software]. ESI ITI; 2020. Available from: <https://www.simulationx.de/>.
- [33] Kabelac S, Kind M, Martin H, Mewes D, Schaber K, Stephan P. VDI Heat Atlas. In: VDI e V. 11th. Berlin, Heidelberg, Germany: Springer-Verlag; 2013. 978-3-540-77876-9.
- [34] Duffie JA, Beckman WA. *Solar Engineering of Thermal Processes*. In: *Solar Energy Laboratory University of Wisconsin-Madison*. 4th. New Jersey: John Wiley & Sons, Inc.; 2013. ISBN 978-0-470-87366-3.
- [35] Liu BYH, Jordan RC. The long-term average performance of flat-plate solar-energy collectors. *Sol Energy* 1963;7. [https://doi.org/10.1016/0038-092x\(63\)90006-9](https://doi.org/10.1016/0038-092x(63)90006-9).
- [36] TRNSYS. Version 18 [Software]. Thermal Energy System Specialists; 2020. Available from: <http://www.trnsys.com>.
- [37] BBR. Updated and enhanced test reference years (TRY) of Germany for medium and extreme weather conditions. Germany: Federal Office for Building and Regional Planning (BBR); 2017.
- [38] Formhals J, Hemmatbady H, Welsch B, Schulte DO, Sass I. A modelica toolbox for the simulation of borehole thermal energy storage systems. *Energies* 2020;13. <https://doi.org/10.3390/en13092327>.
- [39] Kirschstein X. Modelling, simulation and analysis of the integration of seasonal underground thermal energy storages into Campus Lichtwiese district heating grid, Master thesis. Darmstadt: Technical University of Darmstadt; 2020.
- [40] Louvet Y, Fischer S, Furbo S, Giovanetti F, Köhl M, Mauthner F, et al. Task 54 - price reduction in solar thermal systems - LCOH for solar thermal Applications. Solar Heating and Cooling Programme. International Energy Agency; 2017.
- [41] Fish JCL. *Engineering economics: first principles*. second ed. New York: McGraw-Hill; 1923.
- [42] Whitman DL, Terry R. *Fundamentals of engineering economics and decision analysis*. Barrett SF, editor. Synthesis lectures on engineering, vol. 18. Williston, VT, USA: Morgan & Claypool; 2012. <https://doi.org/10.2200/S00410ED1V01Y201203ENG018>.
- [43] Lund H. *The EnergyPLAN energy system Analysis model*. Renewable Energy Systems. 2nd. London: Academic Press; 2014. p. 53–78. ISBN: 9780124095953.
- [44] Oltmanns J, Frey Stein M, Dammel F, Stephan P. Improving the operation of a district heating and a district cooling network. *Energy Procedia* 2018;149: 539–48. <https://doi.org/10.1016/j.egypro.2018.08.218>.
- [45] Formhals J, Welsch B, Schulte DO, Sass I. Effects of the district heating supply temperature on the efficiency of borehole thermal energy storage systems. 3rd international conference on smart energy systems and 4th generation district heating 2017.
- [46] Solar Collector Factsheet - Arcon-Sunmark HT-SolarBoost 35/10. 2018. Accessed 20 April 2021.
- [47] Planungsanleitung VITOCAL 350-HT PRO. 2019. Accessed 20 April 2021.
- [48] Isoplus - Design manual rigid compound systems. 2020. Accessed 20 April 2021.
- [49] Welsch B, Schulte DO, Rühaak W, Bär K, Sass I. Thermal impact of medium deep borehole thermal energy storage on the shallow subsurface. Vienna: European Geosciences Union General Assembly; 2017.

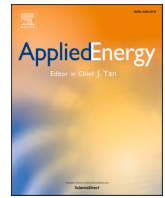
Appendix E – Co-Simulation of District Heating Systems and Borehole Heat Exchanger Arrays using 3D Finite Element Method Subsurface Models

Formhals, J., Welsch, B., Hemmatabady, H., Schulte, D.O., Seib, L., and Sass, I., 2021, Co-Simulation of District Heating Systems and Borehole Heat Exchanger Arrays using 3D Finite Element Method Subsurface Models. *Journal of Building Performance Simulation*, doi: 10.1080/19401493.2022.2058088.

Appendix F – AI-based Enviro-economic Optimization of Solar-coupled and Standalone Geothermal Systems for Heating and Cooling

Published as:

Hemmatabady, H., Welsch, B., **Formhals, J.**, and Sass, I., 2022, AI-based Enviro-economic Optimization of Solar-coupled and Standalone Geothermal Systems for Heating and Cooling. *Applied Energy*, doi:10.1016/j.apenergy.2022.118652.



AI-based enviro-economic optimization of solar-coupled and standalone geothermal systems for heating and cooling

Hoofar Hemmatabady^{*}, Bastian Welsch, Julian Formhals, Ingo Sass

Geothermal Science and Technology, Technical University of Darmstadt, Schnittspahnstraße 9, 64287 Darmstadt, Germany

Graduate School of Excellence Energy Science and Engineering, Technical University of Darmstadt, Otto-Berndt-Str. 3, 64287 Darmstadt, Germany

HIGHLIGHTS

- Long-term enviro-economic optimizations of shallow geothermal layouts are conducted.
- Solar-coupled layouts with heat pumps are the most favorable option for heating.
- Standalone layouts are reasonable options for combined heating and cooling.
- The combination of ANN and multi-objective optimization methods is an accurate approach.

ARTICLE INFO

Keywords:

District heating and cooling
Borehole thermal energy storage
Enviro-economic method
Artificial neural network
TRNSYS
Multi-objective optimization

ABSTRACT

Borehole heat exchanger (BHE) arrays represent a key technology for the future provision of sustainable building heating and cooling energy. They are either used as pure geothermal systems only extracting heating energy from the subsurface or they are also used to store excess heat from solar thermal collectors or waste heat from cooling applications in summer. The diversity of the systems makes it difficult to identify the optimal system in terms of emission reduction and economic efficiency. In this study, we assess the most relevant BHE system layouts for heating-only as well as combined heating and cooling purposes using dynamic simulations of the overall heating system in combination with an enviro-economic analysis method. The assessment routine is used in a multi-objective optimization approach to minimize the different system layouts' emission factor (EF) and their levelized cost of energy (LCOE). In order to cope with the high computational cost of the required long-term considerations, an artificial neural network (ANN) has been used to generate a proxy model in an intermediate step of the multi-objective optimization procedure. This approach delivers reliable optimization results, which reveal, that the lowest emissions for heating and cooling systems are realized by solar-assisted layouts. Comparison with a fossil-based reference layout shows that the most economical BHE layout accomplishes a 60% reduction in the EF with a moderate increase in the LCOE of only 13%. If, however, emission penalty costs are taken into account, the evaluated layouts also become economically advantageous compared to fossil-based systems.

1. Introduction

Climate change is a serious issue that the world is confronted with. Greenhouse gases (GHG) emitted by energy use from fossil fuels are the main reason for climate change [1]. In Europe, buildings require 40% of the overall energy and emit 36% of the GHG [2]. Heating and hot water consume 79% of the final energy demand in European households [3]. Cooling of buildings still has small share, but the demand is expected to

increase considerably as the climate warms on average [4]. It is estimated that by 2025 the installed cooling capacity in Europe is likely to be 55–60% higher than in 2010 [5]. Statistics show that approximately 75% of heating and cooling is generated from fossil fuels [6]. Consequently, simultaneous supply of heating and cooling with higher sustainability needs to be considered as an important part of future energy systems.

By 2050, more than 80% of European residents are expected to live in urban areas [7]. This trend increases the benefits of district energy

^{*} Corresponding author at: Geothermal Science and Technology, Technical University of Darmstadt, Schnittspahnstraße 9, 64287 Darmstadt, Germany.

E-mail addresses: hemmatabady@geo.tu-darmstadt.de (H. Hemmatabady), welsch@geo.tu-darmstadt.de (B. Welsch), formhals@geo.tu-darmstadt.de (J. Formhals), sass@geo.tu-darmstadt.de (I. Sass).

<https://doi.org/10.1016/j.apenergy.2022.118652>

Received 11 June 2021; Received in revised form 5 December 2021; Accepted 25 January 2022

Available online 4 February 2022

0306-2619/© 2022 Elsevier Ltd. All rights reserved.

| Nomenclature | |
|-------------------|--|
| ANN | artificial neural network |
| ASHP | air-source heat pump |
| BHE | borehole heat exchanger |
| BST | buffer storage tank |
| BTES | borehole thermal energy storage |
| COMP | compromise |
| DC | district cooling |
| DH | district heating |
| DHC | district heating and cooling |
| Eco | economical |
| EF | emission factor |
| Env | environmentally-friendly |
| GB | gas boiler |
| GHG | greenhouse gases |
| GSHP | ground-source heat pump |
| HEX | heat exchanger |
| HP | heat pump |
| LCA | life cycle assessment |
| LCC | life cycle cost |
| LCOE | levelized cost of energy |
| NG | natural gas |
| NSGA | non-dominated sorting genetic algorithm |
| Op | operation |
| STC | solar thermal collector |
| Symbols | |
| A | area of solar collector m^2 |
| a | year |
| a_0 | intercept efficiency |
| a_1 | efficiency slope $kJ/hr.m^2.K$ |
| a_2 | efficiency curvature $kJ/hr.m^2.K^2$ |
| Cap | capacity kW |
| f | fuel consumption kWh |
| GWP | global warming potential $g CO_2 eq /kWh$ |
| i | component number |
| I | incident radiation on solar collectors $kJ/hr.m^2$ |
| IC | initial cost $€/kWh$ |
| L | Length m |
| LCC | the present value of total life cycle cost $€$ |
| LCOE | levelized cost of energy $€/kWh$ |
| MC | maintenance cost $€/kWh$ |
| n | number of systems components |
| N | number |
| OC | operational cost $€/kWh$ |
| Q | thermal out put kWh |
| r | discount rate % |
| T | Temperature $°C$ |
| Vol | Volume m^3 |
| Q' | heat flux kW |
| η | Efficiency % |
| Subscripts | |
| BHE | borehole heat exchanger |
| BST | buffer storage tank |
| BTES | borehole thermal energy storage |
| CL | cooling load |
| Elec | electricity |
| F | fuel |
| GB | gas boiler |
| HP | heat pump |
| IC | initial cost |
| MC NG | maintenance cost natural gas |
| Prod | production |
| ret | return |
| sup | supply |
| tot | total |

systems, which tend to be more economic for densely populated regions [8]. 4th generation district heating (4GDH) networks, with supply temperatures of less than $50\text{ }^\circ\text{C}$, are suitable for recycling heat from low-temperature sources such as solar and geothermal [9]. A future district cooling (DC) system, can be defined as a system more interactive with the electricity, DH and gas grids [9]. Overall, a 4th generation DHC grid can be considered as an interactive low-temperature energy grid to satisfy both heating and cooling demands [9,10]. The significant share of heating in final energy demand of European households as well as the increasing trend towards smart energy systems has made district heating (DH) a viable option for future energy supply [7,11].

As one of the main renewable energy sources, solar energy can have a major contribution in sustainable heating supply. Flat plate solar thermal collectors (STC), which are the most common type for heating applications, operate more efficiently at lower temperature levels [12]. Therefore, they are suitable options for low-temperature DH networks. However, the temporal mismatch between solar thermal supply and heat demand is a major drawback of such systems. To overcome this problem, seasonal energy storage technologies are essential. They can also be utilized in cooling cycles, where the rejected waste heat is stored seasonally for further use in the heating season.

Thermal energy storage (TES) technologies can be categorized to sensible, latent and chemical heat storage, from which chemical and latent TES solutions are not competitive for large-scale (district) applications [13]. Only some sensible heat storage technologies are appropriate for large-scale TES, which can be classified to large aboveground water tanks and underground TES (UTES) systems [14]. The most common types of UTES systems include tank TES, pit TES, aquifer TES

and borehole TES (BTES) [15,16]. The main concentration of this study is on shallow BTES systems, with depths usually less than 100 m, but partly also in excess of 200 m [17]. BHEs with depths of more than 400 m are not dealt with shallow geothermal standards [17]. BTES systems exploit the high underground thermal capacity, to store large quantities of fluctuating renewable or waste energy on a seasonal basis [18,19]. In general, a BTES system consists of an array of boreholes, each fitted with a BHE, which is a closed-loop pipe system placed in a borehole. The number of BHEs, their radial distance and their length define the size of the storage [20]. The BHEs are backfilled with a cement-based grouting material, which stabilizes the borehole, provides hydraulic sealing and improves thermal contact with the underground. The heat transfer process starts by circulating a heat transfer fluid (usually a water-glycol mixture) in the pipes [21].

The high efficiency of BTES systems, especially in lower temperature levels [22,23], makes them a promising option for integration into low-temperature solar DH networks, to fill the temporal mismatch between solar thermal supply and heat demand. Moreover, BTES systems can be utilized to shift the excess heat from cooling seasons to be used in heating seasons for combined heating and cooling applications. The underground has higher/lower temperatures in heating/cooling seasons, compared to the ambient temperature. Higher source temperatures lead to more efficient operation of heating cycles. On the other hand, lower sink temperatures result in enhanced performance of cooling cycles. Consequently, in addition to its utilization for TES on a long-term basis, the underground is an efficient heat source/sink of conventional ground-source HP (GSHP) systems for heating-/cooling-only purposes.

Various implementation projects have already proven the

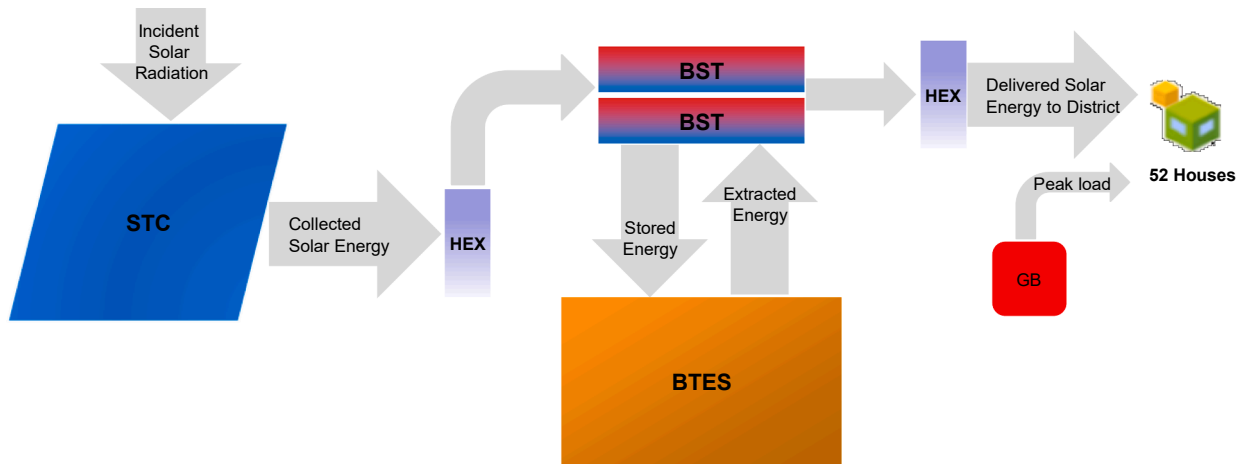


Fig. 1. Energy flow diagram of the reference case, modified after [33].

practicability of geothermal heating and cooling systems, for examples refer to [24,25]. However, the main issue that may lead to reduced efficiency of these systems is their inappropriate design and dimensioning considering their interaction with other components of the energy system. An exemplary system in Germany, consists of a BTES that is charged by STCs and discharged by a HP, which are connected to two buffer storage tanks (BSTs) [26,27]. The low HP capacity of this system led to its inefficient operation and caused a large capacity of the BTES to be remained unused as it is discharged less than planned [27]. Moreover, stagnation occurred in STCs due to smaller dimensions of the BTES, BST and HP, compared with design values [27]. A BTES should not be regarded in isolation, but merely as one component within a district heating and cooling network [18]. Guidelines are required for design and optimization of the BTES systems in DHC networks, considering their integration with other system components.

Considering the experience from demonstration and pilot projects, different configurations of BTES-assisted systems represent viable options. These need to be evaluated from a technical, economic and environmental point of view in order to increase their share in a sustainable thermal load supply. With this goal in mind, many studies have been conducted in recent years. Life cycle assessment (LCA) studies demonstrate that the integration of BTES systems yields a large reduction in global warming potential (GWP) [28,29]. Furthermore, the results of a parametric study on a BTES-assisted solar DH system show that, besides reducing GWP, they are economically more favorable than GSHPs [30]. Multi-objective optimization to simultaneously minimize the life cycle cost (LCC) and CO₂ emissions of a BTES-assisted central heating system in different cold climate locations depicts its viability [31]. Moreover, the results of energetic and LCC analysis of a small-scale BTES-assisted solar DH system for several locations in the UK show the technical feasibility of these systems. However, encouraging financial policies are required for a faster rollout [32].

Nevertheless, none of the aforementioned and other similar studies have compared possible layouts of BTES-assisted systems for heating as well as cooling from environmental and economic points of view. In addition, as the operation of BTES systems and their temperature level are strongly dependent on the stored and extracted energy as well as the number of charging and discharging cycles, they should be evaluated on a long-term basis such as the project life time. Since such a long-term assessment entails high computational costs, though, optimization approaches for minimizing GWP and LCC are mainly based either on simplified parametric studies or on multi-objective optimizations with a limited number of variables or simulation years. This in turn is associated with lower accuracies. Moreover, due to computational costs the optimizations are mainly conducted with a limited number of evaluations, which rarely leads to final convergence of optimization

algorithms. Therefore, an optimization study for comparing possible heating and cooling layouts of the BTES systems to specify decisive optimization variables, with less restrictions to the number of the variables, is needed. This should be done during project lifetime with unlimited number of evaluations until real convergence of the optimization problem.

In this study, solar-assisted and standalone geothermal layouts for heating as well as combined heating and cooling applications are compared using an environ-economic analysis method to minimize emission factor (EF) and Levelized Cost of Energy (LCOE). Initially, a model of a well-known reference system from Canada [33] is created, which is validated against real operational data. Subsequently, the boundary conditions are adapted to a case study in Germany. Based on the reference scenario and other studies, alternative layouts and their control strategies are then proposed. For modeling the different system layouts, the Software TRNSYS [34] is used. To evaluate the proposed designs, a combination of artificial neural network (ANN) and multi-objective optimization methods is utilized for predicting and minimizing the objective functions in MATLAB [35]. The ANN approach is required to reduce the optimization time. It is used as an intermediate stage to predict and validate the objective functions after initial evaluations of the objectives by a genetic algorithm. This leads to higher accuracy of the predicted functions for the optimization purposes with less input data, in comparison with similar studies which normally utilize uniform distribution functions to generate data in the evaluated space, e. g. [36]. As the final stage of the computational procedure, the validated objective functions are optimized until the final convergence of the optimization algorithm. Finally, a sensitivity analysis is conducted to assess the effect of changing cost functions.

Optimization results of this study define dimensions of the most important components of geothermal layouts by taking their required long-term evaluations into consideration. Utilizing the proposed computational model, it is assured that the results are converged to the best solutions. Consequently, design guidelines for geothermal systems, considering their transient interaction with other system components during project lifetime can be presented, which has not been done so far.

2. Reference case selection and validation

The selected reference case, Fig. 1, is the BTES system in Drake Landing Solar Community [37]. In summer, nearly 2,300 m² roof-mounted flat plate STCs store solar energy in 144 single U-tube bore-hole heat exchangers (BHE) with a length of 35 m each. During winter operation, the recovered energy from the BTES and the collected energy from the STCs provide most of the required heating load for 52 single-family homes, supported only by a gas boiler (GB) to supply peak

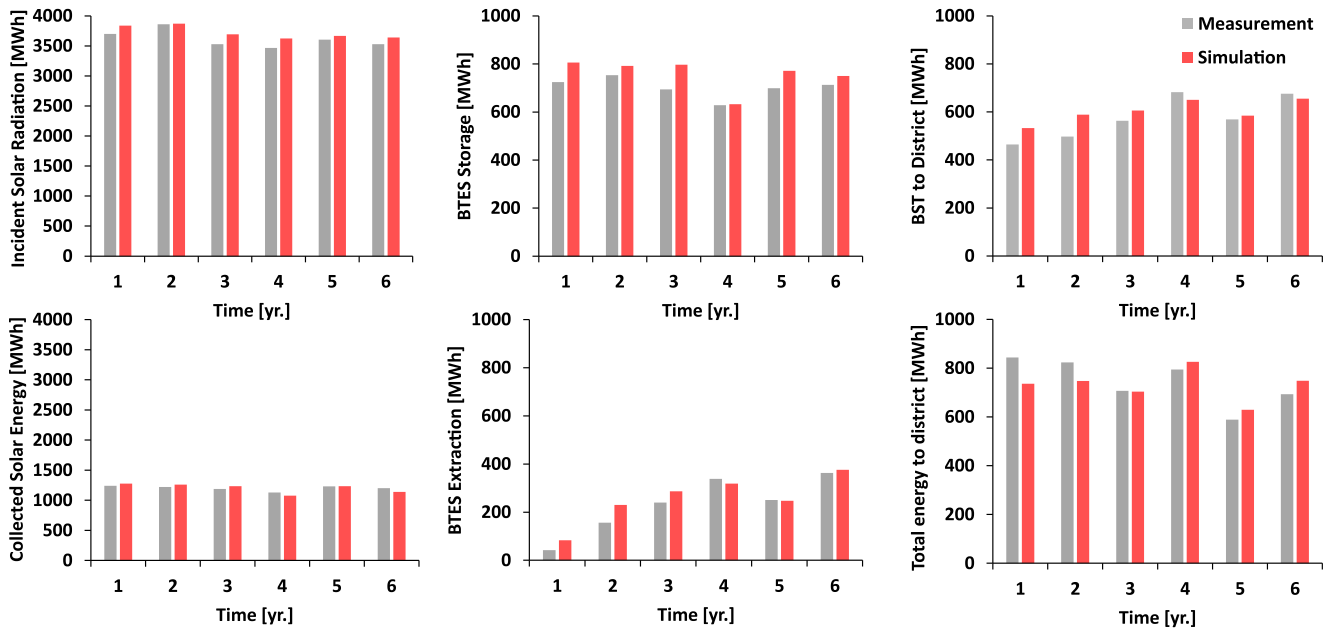


Fig. 2. Simulation results (orange) vs. measurement data (blue) of the reference case.

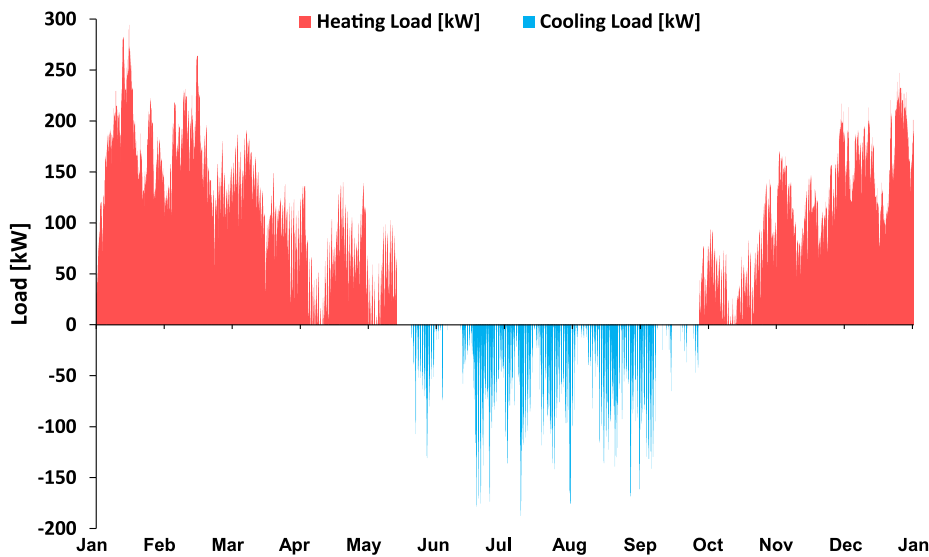


Fig. 3. District load profile.

demand. Two horizontal BSTs, each having a volume of 120 m³, are used for diurnal storage of solar energy and the thermal connection of solar, ground and district loops. Two heat exchangers (HEXs) separate solar and district loops from BSTs and ground loop.

In case of the validation of reference model, data from the annual report [33], calibrated parameter values from the designers [38–40], a regression model for calculating load profile as a function of ambient temperature [40] and the weather data of 6 years of operation [41] serve as model inputs. Fig. 2 shows the simulation results in TRNSYS against the measured numbers as given in the annual report. It can be seen that the simulation can represent the performance of the system in operation. The deviations between the measurement and the simulation results are mainly due to differences in the operational strategies used in the simulation (cf. Chapter 4.1.1.) in comparison with the ones applied in reality [33,42]. Moreover, to enhance system’s performance, modifications have been implemented to the system during years of operation [33]. Overall, it can be concluded that the system can be used as a

validated reference case for a generic study to compare different layouts of geothermal systems.

3. Case study

3.1. Case study setup

A notional urban quarter in Frankfurt, Germany, consisting of 31 single-family homes and 4 office buildings is considered in a generic case study. Load profiles of each building topology are calculated using 3D thermal zone models in TRNBuild, taking into account weather data from Frankfurt [10,43,44]. Construction materials, occupation schedules and set point temperatures are based on standard libraries [44,45].

Fig. 3 shows the total calculated load profile of the quarter. The overall annual heating and cooling demands are 523 MWh and 62 MWh, respectively, with most of the cooling demand attributed to the office buildings. In heating mode, the supply temperature (T_{sup}) to the

Table 1
The proposed scenarios for heating-only mode.

| Scenario | Heating | Cooling | STC | GHE | BST | GB |
|----------|----------------|---------|------------|---------|----------|------|
| H1 | Passive (BTES) | — | Flat plate | 2U-tube | Vertical | Peak |
| H2 | Active (BTES) | — | Flat plate | 2U-tube | Vertical | Peak |
| H3 | Active (GSHP) | — | — | 2U-tube | Vertical | Peak |

Table 2
The proposed scenarios for combined heating and cooling mode.

| Scenario | Heating | Cooling | STC | GHE | BST | GB |
|----------|----------------|----------------|------------|---------|----------|------|
| HC1 | Passive (BTES) | Active (ASHP) | Flat plate | 2U-tube | Vertical | Peak |
| HC2 | Active (BTES) | Active (ASHP) | Flat plate | 2U-tube | Vertical | Peak |
| HC3 | Active (BTES) | Passive (BTES) | — | 2U-tube | Vertical | Peak |

buildings is a function of the ambient temperature with gliding-constant operation [30] and minimum and maximum values of 37 °C and 41 °C, respectively. The return temperature (T_{ret}) is approximately 7 °C lower. These values are compatible with the temperature level of low-energy buildings, 4GDH grids and the reference case. In cooling mode, T_{sup} and T_{ret} are 18 °C and 22 °C, respectively, which are reasonable values for passive geothermal cooling operation [46].

3.2. Adapting the reference case to the case study

In a next step, the validated reference case model is adapted to the case study. This includes the adjustment of different location-dependent parameters such as the solar irradiation and BTES thermophysical properties. Moreover, the reference BHE type is replaced by double U-tube BHEs, which are the most popular type of BHEs in Germany [21]. Furthermore, the horizontal BSTs from the reference system are

substituted by vertical BSTs, which are commonly used in central solar heating plants in Germany [26]. The main advantage of vertical BSTs is reduced mixing and heat loss due to smaller relative contact area between water temperature layers. This advantage is more in tanks with higher aspect ratios [33], which can be reached easier by using two (multiple) BSTs, especially when there is a limitation for maximum allowable installation heights. Moreover, using two (multiple) BSTs, as the center of a thermal plant, ensures more sustainable and consistent load supply. Therefore, in this study, as in the reference case and other similar plants like [47], two BSTs are considered. Definition of the optimum number and length of the BHEs and volume of the BSTs is part of this study.

4. System design scenarios

Two different operational scenarios are considered: heating-only mode (H) and combined heating and cooling mode (HC). For each of these, three different system designs are compared.

In heating-only mode (Table 1), two system layouts (H1 and H2) contain a BTES systems, which is charged by STCs during summer season. In winter, system H1 supplies the heating load passively without the use of HPs, while system H2 uses HPs. The third system option H3 represents a conventional GSHP system without storage or regeneration.

In combined heating and cooling mode (Table 2), the solar-assisted BTES systems (HC1 and HC2) are heated up by STCs during the summer seasons as well. Therefore, they cannot be used as heat sink for cooling purposes efficiently. In both cases, the cooling load is supplied by an air-source HP (ASHP). As for the heating-only scenario, the heating load in winter is either provided without (H1) or with (H2) HPs. Again, the third system layout (HC3) lacks STCs. Instead, the rejected waste heat from the cooling cycle is passively stored in the BTES system, which renders the air-source heat pump obsolete. When the BTES temperature is not low enough for passive cooling load supply, HPs meet the load actively. In the heating season, the BTES is once more discharged actively with the use of the HPs.

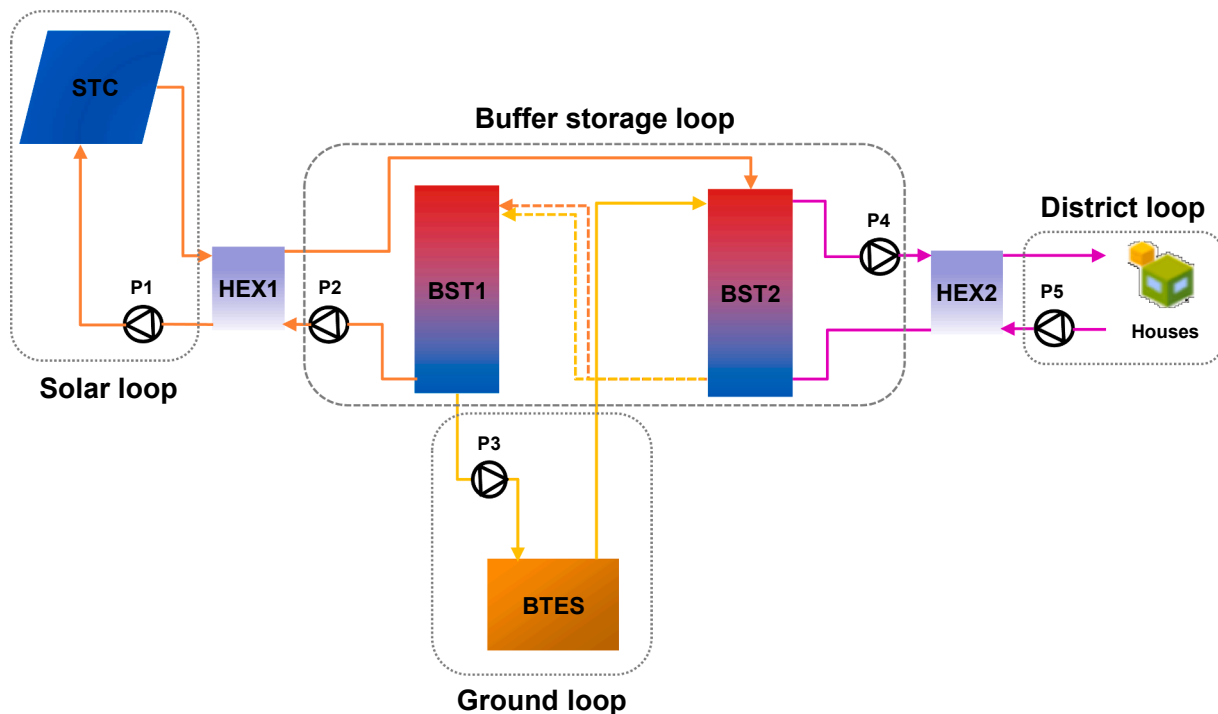


Fig. 4. System layout of the passive heating (BTES).

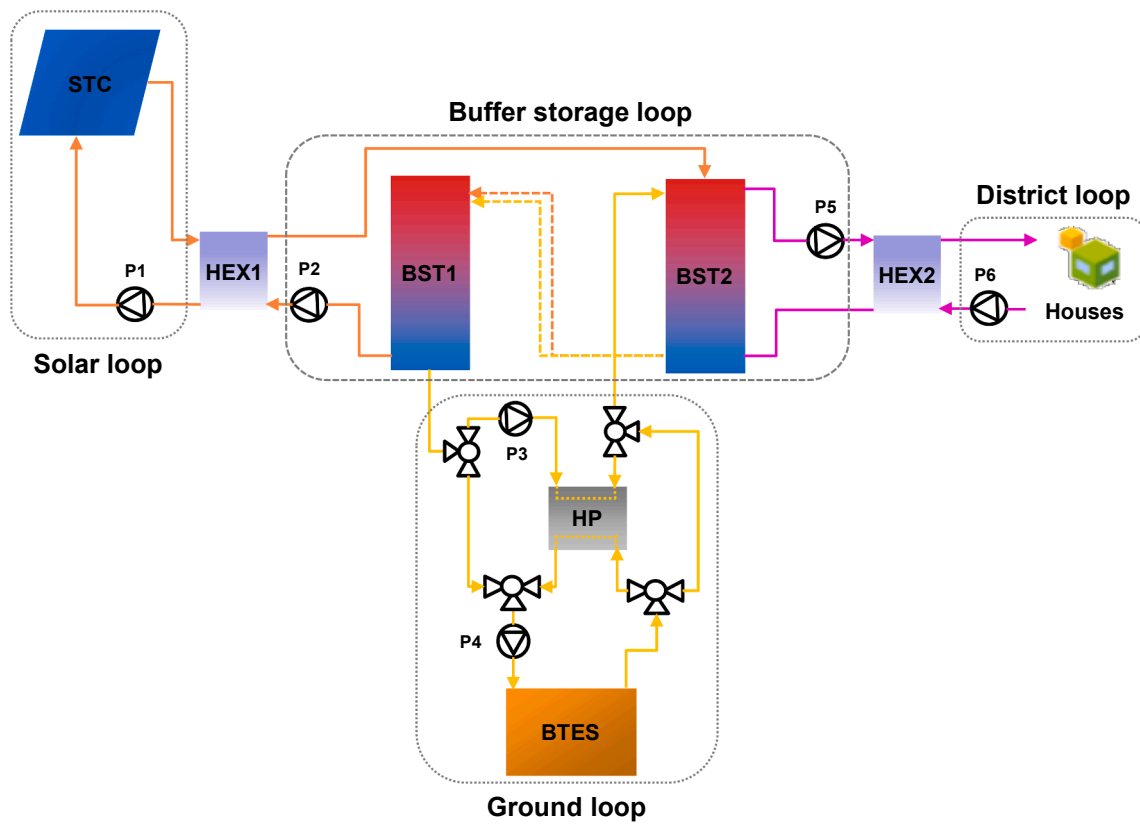


Fig. 5. System layout of the active heating (BTES).

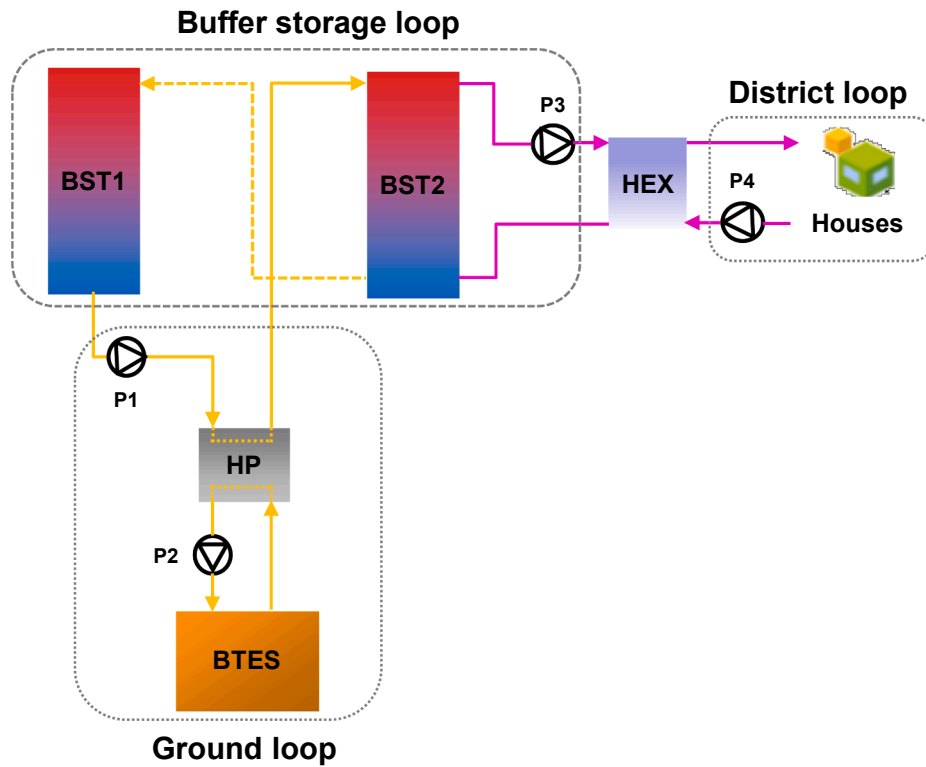


Fig. 6. System layout of the active heating (GSHP).

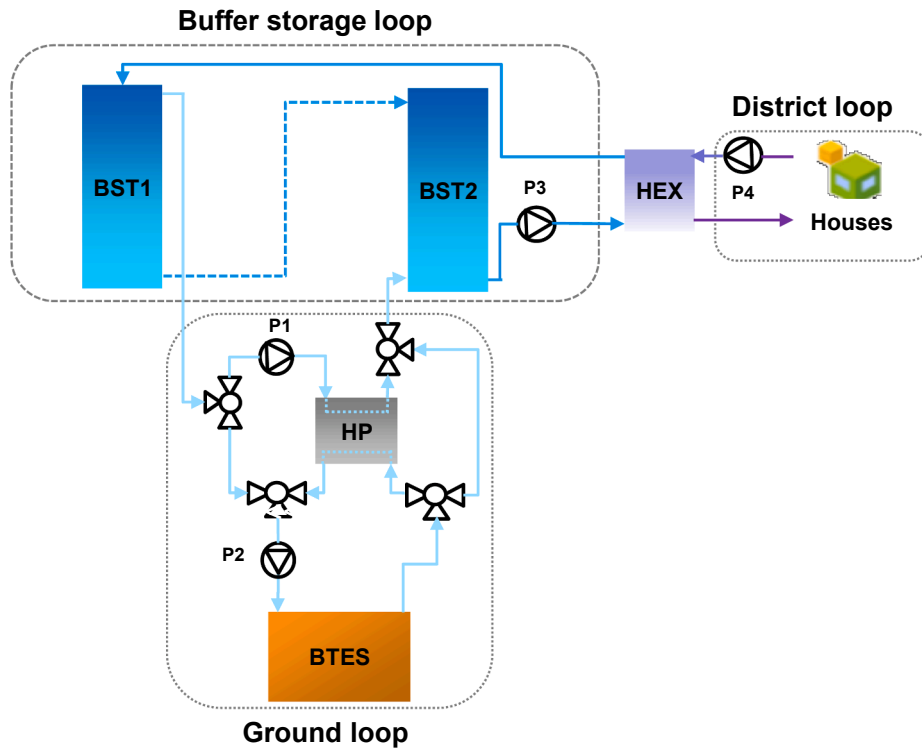


Fig. 7. System layout of the BTES in cooling mode.

4.1. Heating operation

4.1.1. Passive heating (BTES)

A simplified representation of system layout H1 in discharging mode is illustrated in Fig. 4. During summer operation, the collected solar energy is delivered to the BSTs via the solar loop HEX (HEX1). The control strategy is adapted from [48]. A variable-speed STC pump (P1) is activated by a differential controller, which monitors the outlet temperature of the STCs, the top temperature of the warmer BST and the bottom temperature of the colder BST. The design temperature difference (ΔT) of STCs is taken as 15 K [42]. The variable-speed pump that delivers the solar energy to the BSTs (P2) has the same flow rate as the solar loop pump, with the nominal flow rate slightly lower than the solar loop, as in the reference case [42].

Charging of the BTES is controlled by a differential controller, which monitors the temperature difference ΔT between the BTES center and the top of the warmer BST (BST2). Similarly, ΔT between the BTES center and the bottom of the colder BST (BST1) is used for BTES discharging control. In both modes, a high limit cut-out prevents the BTES and BST2 from overheating. A supplementary charging mode is also possible in parallel with the discharging mode, especially during transition seasons, when the solar yield exceeds the heating demand.

Another variable-speed pump (P4) is placed in the loop that delivers BSTs energy to the district HEX (HEX2). Its flow rate is controlled by the HEX's energy balance equation and the supply temperature in the district loop T_{sup} so that the fluid of the district loop is heated up to set point. The variable-speed pump of the district loop (P5) is also controlled to meet the district design ΔT (cf. Chapter 3.1.).

4.1.2. Active heating (BTES)

For the H2 layout (Fig. 5) the control strategies of solar, buffer storage and district loops are the same as for H1. A HP, which is chosen based on the operational data from a manufacturer [49], discharges the BTES actively and is bypassed when the BTES temperature is high enough to supply the load passively. The HP and the BTES pumps (P3

and P4) start working when the BSTs are not hot enough to supply the demand. For this purpose, the ΔT between the district T_{sup} and the bottom of the colder BST (BST1) is monitored as the dead band for filling the BSTs. Moreover, the top of the warmer BST (BST2) is monitored as high limit cut-out. The flow rate on the load side of the HP is modulated considering its capacity and the design ΔT of the BST side of the district HEX.

4.1.3. Active heating (Geothermal)

In the H3 scenario (Fig. 6) a GSHP actively supplies the heating load. The control strategies of the buffer storage and the district loops are similar to the H1 layout. For the BTES loop, the control strategy is similar to the active mode of the H2 layout, where the temperatures of the district and the BSTs are monitored to control the filling level of tanks. The load side flow rate of the GSHP is also modulated considering its capacity and the design ΔT of the BST side of the district HEX.

4.2. Cooling operation

In the combined heating and cooling scenarios, the operational data of the ASHP used for cooling in the layouts HC1 and HC2 is selected based on a manufacturer's catalog [50]. The control strategy for the BTES when used as the heat sink for passive cooling in layout HC3 (Fig. 7) is set by a differential controller. It monitors ΔT between the BTES center and the top of the BST1, which is the entering node of the return fluid from the district loop HEX. Active cooling mode is activated as soon as the passive cooling controller turns off due to high BTES temperatures and the T_{sup} of the district exceeds the design value.

5. Evaluation criterion

5.1. Environmental analysis

For the environmental assessment of the proposed system layouts their EF is calculated by dividing their overall GWP by total thermal

Table 3
Objective functions and optimization variables.

| Objective functions | Definition |
|---|--------------------------|
| min EF | Emission Factor |
| min LCOE | Levelized Cost of Energy |
| Subject to | |
| $30 \text{ m} \leq L_{\text{BHE}} \leq 400 \text{ m}$ | Length of BHEs |
| $6 \leq N_{\text{BHE}} \leq 300$ | Number of BHEs |
| $56.6 \text{ kW} \leq \text{Cap}_{\text{HP}}^a \leq 300 \text{ kW}$ | Capacity of HP |
| $13.57 \text{ m}^2 \leq A_{\text{STC}} \leq 5000 \text{ m}^2$ | Area of STCs |
| $10 \text{ m}^3 \leq \text{Vol}_{\text{BST}} \leq 1000 \text{ m}^3$ | Volume of BSTs |

^a for active scenarios.

Table 4
Main TRNSYS parameters.

| Component | Parameter | Value | Component | Parameter | Value |
|-----------------|----------------------------|-----------------------------|------------------|------------------------|-----------------|
| BTES | BHE type | 2U | STC | Fluid specific heat | 3.798 kJ/(kg·K) |
| Type 557 | Boreholes in series | 3,6 | Type 1a | Efficiency mode | 2 |
| | Borehole radius | 0.065 m | | Tested flow rate | 25 l/min |
| | Pipe outer/inner radius | 0.016/0.013 m | | Intercept efficiency | 0.778 |
| | BTES thermal conductivity | 2.6 W/(m·K) | | Efficiency curvature | 0 |
| | BTES heat capacity | 2080 kJ/(m ³ ·K) | HEX | | |
| | Grout thermal conductivity | 2 W/(m·K) | Type 91 | Effectiveness | 0.80 |
| | Fluid specific heat | 4.182 kJ/(kg·K) | Type 512 | Effectiveness | 0.95 |
| BST | Number of tank nodes | 30 | HP | Rated heating capacity | 56.6 kW |
| Type 534 | Number of ports | 4 | Type 927c | Rated power | 13.2 kW |
| | Aspect ratio | 3.916 | | Rated cooling capacity | 43.4 kW |
| | Loss coefficient | 0.15 W/(m ² ·K) | Boiler | Efficiency | 95% |
| Pump | Total pump efficiency | 60% | Type 700 | | |

^c Values at entering load-side and source-side temperatures of 30 °C and 0 °C [36].

output (Q_{tot}), Eq. (1) [28]. The overall GWP is calculated using Eq. (2). It adds up the GWP associated with the production of n system components ($\text{GWP}_{\text{Prod},i}$), cf. Table A1, and the GWP associated with the emissions caused during the operation of the evaluated layout ($\text{GWP}_{\text{Op},a}$) for the whole project lifetime (a_{life}). Q_{tot} is the summation of thermal output at each year (Q_a) during project lifetime.

$$\text{EF} = \frac{\text{GWP}}{Q_{\text{tot}}} \quad (1)$$

$$\text{GWP} = \sum_{i=1}^n \text{GWP}_{\text{Prod},i} + \sum_{a=1}^{a_{\text{life}}} \text{GWP}_{\text{Op},a} \quad (2)$$

After calculating the yearly consumption of electricity ($f_{\text{elec},a}$) and natural gas ($f_{\text{gas},a}$), $\text{GWP}_{\text{Op},a}$ can be calculated using Eq. (3). The EFs

associated with electricity and natural gas consumption as functions of the assessment year ($\text{EF}_{\text{elec},a}$ and $\text{EF}_{\text{gas},a}$) are calculated based on available data for Germany as given by IINAS [51,52]. They are projected into the future using the evolutionary scenario by Welsch et al. [28], Table A.2.

$$\text{GWP}_{\text{Op},a} = f_{\text{elec},a} \text{EF}_{\text{elec},a} + f_{\text{gas},a} \text{EF}_{\text{gas},a} \quad (3)$$

5.2. Economic analysis

The economics of the various system layouts are compared on the basis of the achieved LCOE. These can be calculated by dividing the present value of total LCC of an overall system layout by the discounted total energy using Eq. (4) [53]. $C_{\text{IC},a}$ are the capital investment costs, $C_{\text{MC},a}$ are the maintenance costs and $C_{\text{F},a}$ are fuel costs. a_{life} and the discount rate (r) are assumed as 30 years and 3%, respectively.

$$\text{LCOE} = \frac{\sum_{a=1}^{a_{\text{life}}} (C_{\text{IC},a} + C_{\text{MC},a} + C_{\text{F},a}) \cdot (1+r)^{-a}}{\sum_{a=1}^{a_{\text{life}}} Q_a (1+r)^{-a}} \quad (4)$$

Investment cost (IC) and maintenance cost (MC) of the main components are based on benchmark functions, c.f. Tables A.3. Based on the annual consumption values $f_{\text{elec},a}$ and $f_{\text{gas},a}$, $C_{\text{F},a}$ is calculated using Eq. (5). Electricity and natural gas costs are defined as functions of the assessment year ($c_{\text{elec},a}$ and $c_{\text{gas},a}$) by linearly projecting the estimated values by economic reports, cf. Table A.4 and Table A.5.

$$C_{\text{F},a} = f_{\text{elec},a} c_{\text{elec},a} + f_{\text{gas},a} c_{\text{gas},a} \quad (5)$$

5.3. Enviro-economic optimization

The aim of an enviro-economic optimization is to simultaneously minimize the LCOE and the EF. However, both target functions compete with each other. Systems with a lower EF usually cost more. Therefore, multi-objective optimization is required to find the best solutions for both. The objective functions, optimization variables and their boundaries are listed in Table 3. The optimization variables are chosen to define dimensions of important components of a geothermal layout, including BTES (L_{BHE} and N_{BHE}), HP (Cap_{HP}), STCs (A_{STC}) and BSTs (Vol_{BST}).

6. Computational model

6.1. Modeling and simulation

In the following section, the main components (TRNSYS types) used for the modeling of the proposed layouts are discussed. Moreover, the most important parameters of each type can be found in Table 4.

Type 1a is used for the simulation of STCs, which is based on a quadratic efficiency performance model (Eq. (6)) [34] for the calculation of STC efficiency η_{STC} . Coefficients a_0 , a_1 and a_2 are obtained from standardized collector performance tests, ΔT is the difference between the mean fluid temperature and ambient temperature and I is the incident radiation on STCs. Initial values for the validation of the reference case were taken from benchmark values given in [54].

$$\eta_{\text{STC}} = a_0 - a_1 \frac{\Delta T}{I} - a_2 \frac{(\Delta T)^2}{I} \quad (6)$$

The BTES is modeled using the duct storage model (Type 557) [55]. As mentioned in Chapter 3.2., double U-tube BHEs are chosen. The BHE-related design parameters, e.g. pipe material and dimensions, are selected based on standard libraries [46] and location-specific parameters. Furthermore, the storage thermal conductivity and heat capacity are taken from experimental data [56].

Type 534 is used for the modelling of the BST. It divides the tank into a series of isothermal layers to account for stratification. The number of layers is chosen in accordance with benchmark studies [39] and a manual refinement study. Data from a manufacturer [57] and installed

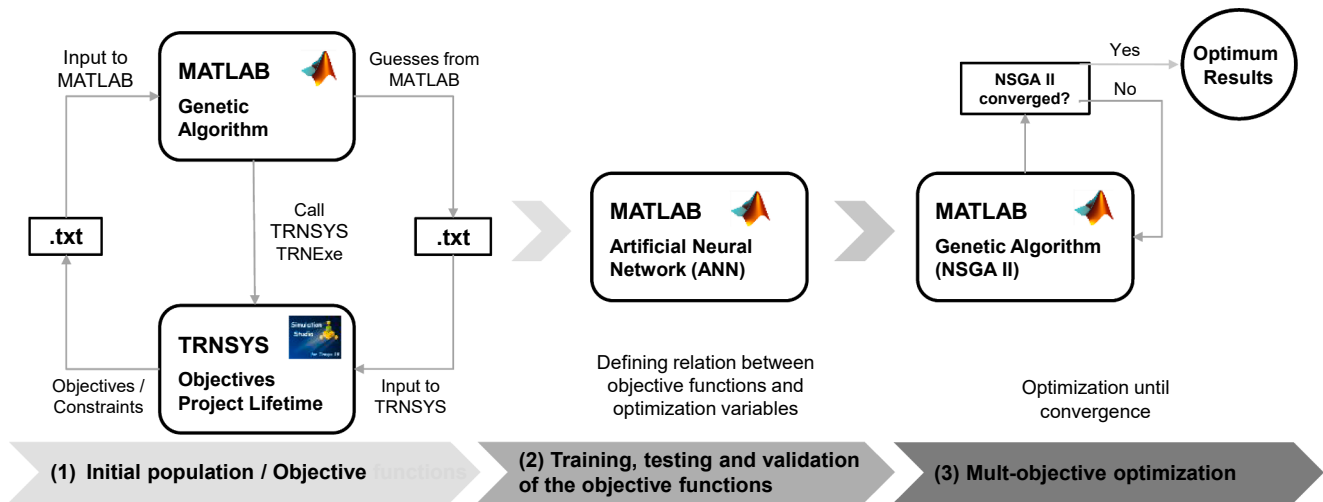


Fig. 8. Optimization procedure.

systems (e.g. [58]) are used for specifying loss coefficient and aspect ratio.

Type 927 is used for simulating HPs. It works based on interpolation with four independent variables: Output capacity, corresponding outlet source and load side temperatures as well as flow rates are read based on inlet temperatures and flow rates from a provided catalog file [49]. After preparing the catalog data files, their validity was checked against the manufacturers' catalogs at various operating conditions.

Peak demands are covered by a condensing GB with an energetic efficiency of 95% [59]. It is modelled using Type 700.

The HEX of the solar loop is modelled by Type 91b. The district HEX is modelled by Type 512, which sends a control signal to the variable-speed pump on the BST side according to the required T_{sup} . The effectiveness of the HEXs is chosen from the benchmark values in [33]. Moreover, as Type 512 is just capable of controlling the set-point temperature on the cold-side of the HEX, as required for the heating mode, the HEX type is improved and adapted to control the operation of the variable speed pump in cooling mode using the Fortran compiler inside TRNSYS.

Several variable speed pumps are used to force the flow in the different fluid loops. These are modeled with Type 110.

Finally, to implement the control strategies discussed in Chapter 4, the controllers of STCs, BSTs and BTES are modelled with a differential controller with hysteresis (Type 2b), while for controlling the operation of the GB a simple aquastat (Type 106) is used. More details about Type 2b function can be found in Appendix B.

6.2. Coupling multi-objective optimization and system simulation

The general optimization procedure for a system layout is illustrated in Fig. 8. It is divided into three sequential stages. In the first stage, an initial direct optimization based on TRNSYS system simulations is performed. Such a direct optimization method is suitable, when the simulation time is low and convergence of the optimization can be reached fast. However, since simulating the operation of geothermal-based heating and cooling systems is computationally intensive, it is not possible to achieve convergence of the direct optimization approach in an acceptable time frame. For this reason, the optimization is terminated after a certain acceptable duration before the final convergence is reached. The results gained so far are then used in the second stage to create a proxy model, which approximates the shape of the objective function in the region defined by the parameter boundaries. In the third stage, the proxy model is used to minimize LCOE and EF in a multi-objective optimization.

As the creation of the proxy model requires a much smaller

computational effort than the numerous simulations of the TRNSYS model, this approach is much more time efficient. Comparable approaches have already been presented for geothermal applications and have proven to facilitate optimization for systems that are too complex for direct optimization [19].

6.2.1. Initial direct optimization

For the direct optimization, TRNSYS is coupled with MATLAB, which allows for the utilization of the available MATLAB optimization tools. Genetic algorithm is used, which is a common method for nonlinear optimization [60]. Estimates of the algorithm for the systems design parameters under consideration are written to a text file, from which they are read by TRNSYS as input parameters for the system simulations. After a 30-year simulation is finished, the resulting LCOE and EF of 30-year simulations in TRNSYS are sent back and evaluated by the optimization algorithm in MATLAB.

6.2.2. Training, testing and validation of the proxy model

The results from the first stage direct optimization are given as input data to the artificial neural network toolbox in MATLAB, which is used here to create the proxy model. ANNs are powerful tools to identify input–output relations of nonlinear and complex systems [61]. Application of ANNs for modeling and performance predication of energy systems has already been proven by other studies [36,62]. Sample points are used for training, testing and validation of the output as a function of inputs. The sample points can be chosen randomly by uniform distribution functions that generate data points in the evaluated space. In this study, to increase the accuracy and further reduce the computational effort, the sample points are chosen based on the study's objective to minimize LCOE and EF, defined in the initial optimization in the first stage.

The Levenberg-Marquardt algorithm [63] is used as training algorithm as it resulted in lower estimation errors for the proxy model. In specifying the proxy model, the first step is defining the percentage of the fed data that are used for training, testing and validation of the ANN. Thereafter, number of hidden layers and their hidden neurons, which are used to specify relation between input data and outputs, need to be defined. Finally, the training procedure starts and the regression value R is calculated, which measures the correlation between outputs of the ANN proxy models and the actual simulation results. An R value of 1 means a close match between the guessed values and the actual values. It is calculated by the overall mean of training, testing and validation R values of the ANN, which are taken as 70%, 15% and 15% of the fed data respectively. Neural networks consist of at least 3 layers, the input layer, a hidden layer and the output layer [35]. Some adjustments, e.g.

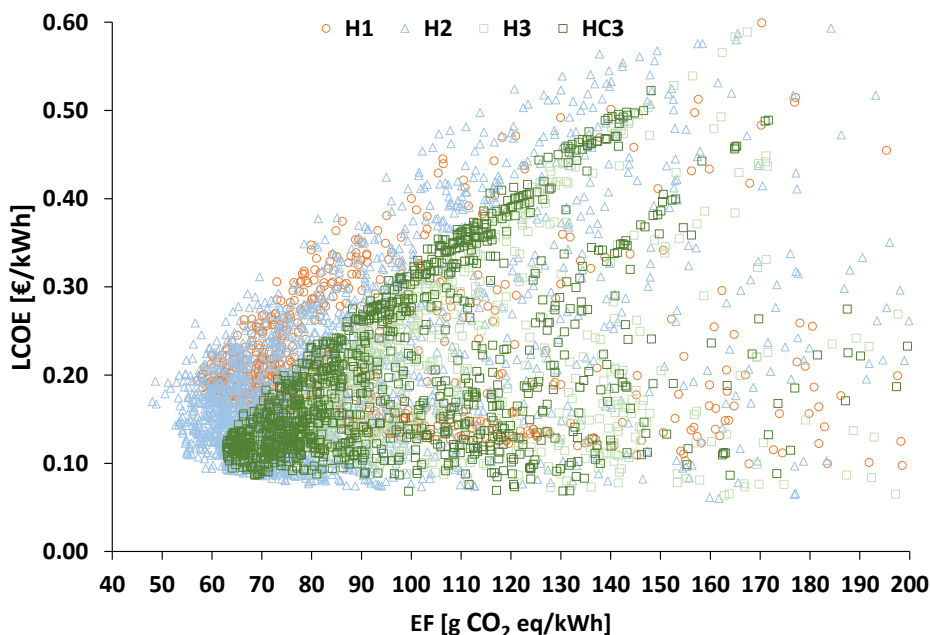


Fig. 9. Initial search by genetic algorithm to train the ANN.

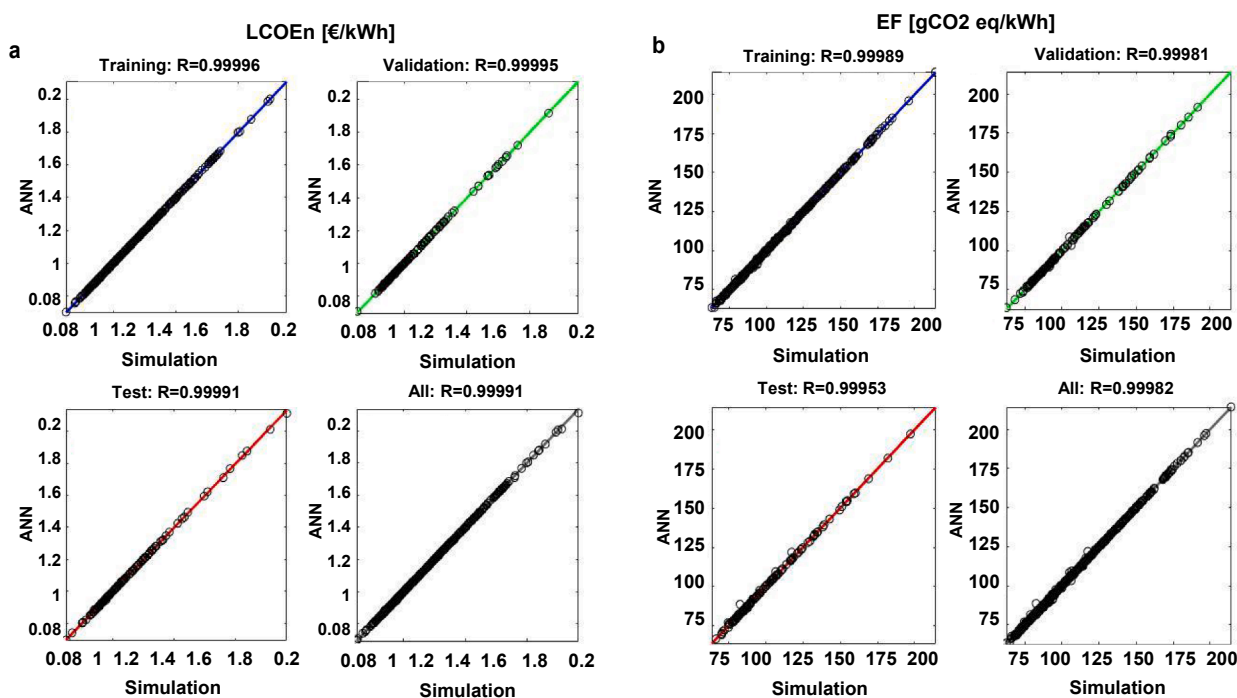


Fig. 10. Estimation error of the ANN for Scenario H1: LCOE (left), EF (right).

increasing the number of hidden layers, may be required to improve the accuracy. Multiple layers of neurons with nonlinear transfer functions allow the network to learn nonlinear relationships between input and output vectors [35]. The number of hidden layers is chosen as 1, which has 10–15 hidden neurons, depending on the investigated layout. The aforementioned numbers are chosen by running the training algorithm several times with different numbers of input data for each layout to have the lowest estimation errors (cf. Chapter 6.2.3). In this study, nearly 5% of the data is also used for validation after the proxy model is trained and the selected results of the last stage of the optimization are again compared with simulation results.

6.2.3. Verification of the objective functions

Fig. 9 shows the results of EF and LCOE for all conducted optimization iterations during the direct optimization carried out in the first stage of the optimization procedure (Fig. 8). The algorithm generally seeks in the entire parameter space, increasing the search density at loci where it comes closer to the objective of the optimization, i.e. minimum EF and LCOE.

Fig. 10 illustrates the estimation error exemplary for the H1 scenario. As it can be seen in the figure, the overall R value is 0.99996 for predicting LCOE and 0.99982 for EF, which proves the accuracy of the utilized method for estimating the objective functions. The required

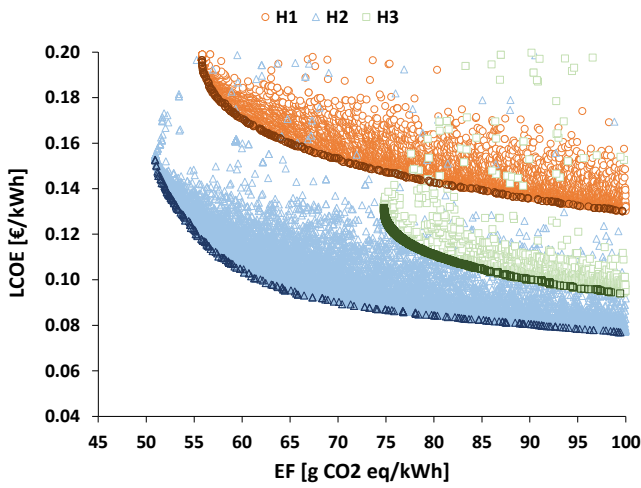


Fig. 11. Optimization results of scenarios H1, H2 and H3.

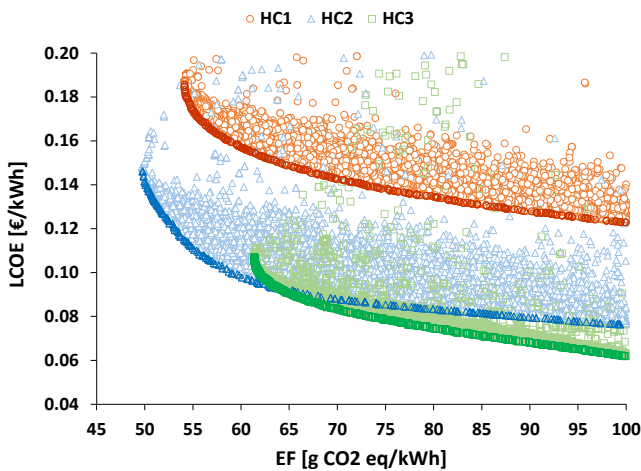


Fig. 12. Optimization results of scenarios HC1, HC2 and HC3.

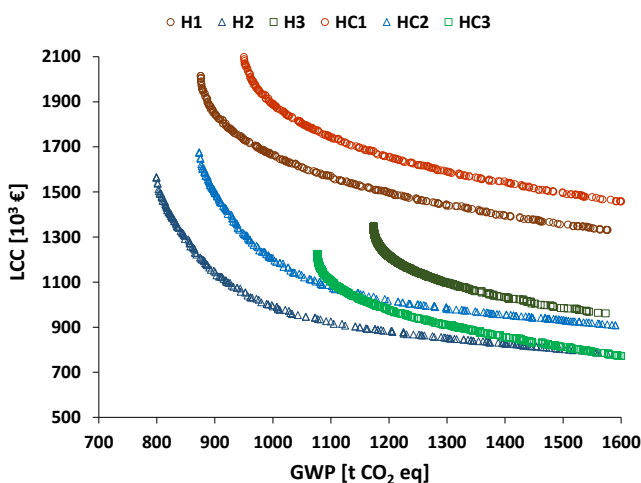


Fig. 13. Optimization results of all layouts.

number of evaluations for reaching low estimation errors is dependent on the layout and the number of optimization variables. Larger numbers of variables require more data for training. Consequently, the H2 scenario with 5 optimization variables required approximately 2000 runs,

while the H1 and H3 scenarios which have 4 optimization variables required 1400 and 1200 points.

6.2.4. Final multi-Objective optimization

Finally, in the third stage, the trained and validated proxy models are given to the non-dominated sorting genetic algorithm (NSGA II) [64] toolbox in MATLAB. The multi-objective optimization continues until the algorithm converges. The number of evaluations in this stage depends on the optimization settings. However, due to the application of the proxy model, the optimization algorithm converges within a few minutes, even for strict tolerance settings. Table C1 shows the most important NSGA II optimization settings that are used in this study, which are mainly based on recommended settings in MATLAB considering the optimization problem and number of optimization variables [65]. Results of the final multi-objective optimization of each layout specify values of the optimization variables and are located on a Pareto front, which is locus of the points with the lowest amounts of EF and LCOE. Moreover, characteristic designs on the Pareto front are selected and their component-wise EF and LCOE are discussed. Finally, a sensitivity analysis is done to consider the effects of uncertainties on the characteristic points.

7. Results and discussion

7.1. Pareto efficient solutions

After verification of the objective functions, the final stage of the computational model is conducted using the NSGA II algorithm to identify Pareto efficient solutions of each scenario, closest to the bottom left corner. Assuming a maximum of 2000 simulations for training of the ANN, and 20,000 points for the final convergence of NSGA II, the proposed computational model can reduce the computational time by approximately 90% in the present case.

Fig. 11 presents the results for the three heating-only system layouts (H1–H3). Among these, H2 (i.e. the layout with seasonal storage and active discharging via an HP) shows the best results. Moreover, for the solutions with equal EFs, H3 (i.e. the GSHP layout without storage) results in much lower LCOEs than the scenario with passive discharging of the BTES (H1). However, in terms of EF reductions, both layouts utilizing STCs and seasonal storage (H1 and H2) outperform H3 by a wide margin.

For HC1 and HC2 (i.e. the layouts including seasonal storage of solar energy and cooling via an ASHP), no separate training simulations are carried out, as the ASHPs are simulated using the same boundary conditions (Chapter 3.1 and Chapter 4.2). Moreover, it is assumed that there is no interaction between ASHPs and other system components. The calculated EF and LCOE for the ASHPs are 40 g CO₂ eq and 0.0912 € per kWh of cooling load supply. The overall EF and LCOE per kWh of the combined heating and cooling load (Fig. 12) for HC1 and HC2 are then calculated using the results of H1 and H2. However, for HC3 (i.e. the layout using the BTES as heat sink for cooling), a separate optimization is carried out.

A comparison of the optimization results of the three HC layouts reveals that HC3 achieves the lowest LCOE for EFs of more than approximately 65 g CO₂ eq/kWh. However, like for the heating-only scenarios, system 3 without STCs cannot reach EF values as low as in the solar-assisted layouts HC1 and HC2. Again, the systems with active discharging of the BTES via HP (HC2) outperform the passive layouts (HC1) in terms of EF slightly and in terms of LCOE significantly.

Finally, the heating-only scenarios and the combined heating and cooling scenarios shall be compared: For the solar-assisted layouts (H1/H2 and HC1/HC2) the specific cost and emissions per kWh of provided energy (i.e. LCOE and EF) decrease when cooling is included (Fig. 11 vs. Fig. 12). This is mainly attributed to the fact, that significantly more use energy is delivered in the cooling scenarios and that the generation of cooling energy with ASHP is comparably efficient. However, when

Table 5
Ranges of the optimized solutions on the Pareto fronts.

| Scenario | A _{STC} [m ²] | L _{BHE} [m] | N _{BHE} | Cap _{HP} [kW] | Vol _{BST} [m ³] |
|----------|------------------------------------|----------------------|------------------|------------------------|--------------------------------------|
| H1 (HC1) | 2080–2650 | 50–65 | 42–66 | | 310–690 |
| H2 (HC2) | 410–1260 | 30–85 | 30–66 | 113.2 | 30–490 |
| H3 | — | 65–170 | 42–63 | 169.8 | 95–165 |
| HC3 | — | 100–220 | 21–33 | 113.2 | 70–100 |

regarding cumulative energy costs and emissions (i.e. LCC and GWP, Fig. 13) it becomes obvious that cooling in this cases causes additional costs as well as additional emissions. In contrast to that, for the stand-alone scenarios (H3 and HC3), cooling improves both the specific and the cumulative evaluation criteria. This highlights the advantage of

recharging the underground to supply both heating and cooling load in comparison with conventional GSHP systems for heating-only purposes.

If, as a reference, it is assumed that the heating load was supplied by GBs and the cooling load by the ASHPs, the overall EF and LCOE would be roughly 250 g CO₂ eq/kWh and 0.046 €/kWh. Therefore, the investigated layouts can decrease the EF by 79%, while they increase the LCOE by more than 44%, even though increasing gas and electricity costs are considered. However, it should be mentioned that the existing national subsidies to support renewable energies as well as the CO₂ emission costs have not been included in LCOE calculations so far. These are evaluated in Chapter 6.4.

The range of the optimized variables on the Pareto front of each scenario is given in Table 5. As mentioned earlier, HC1 and HC2 are the

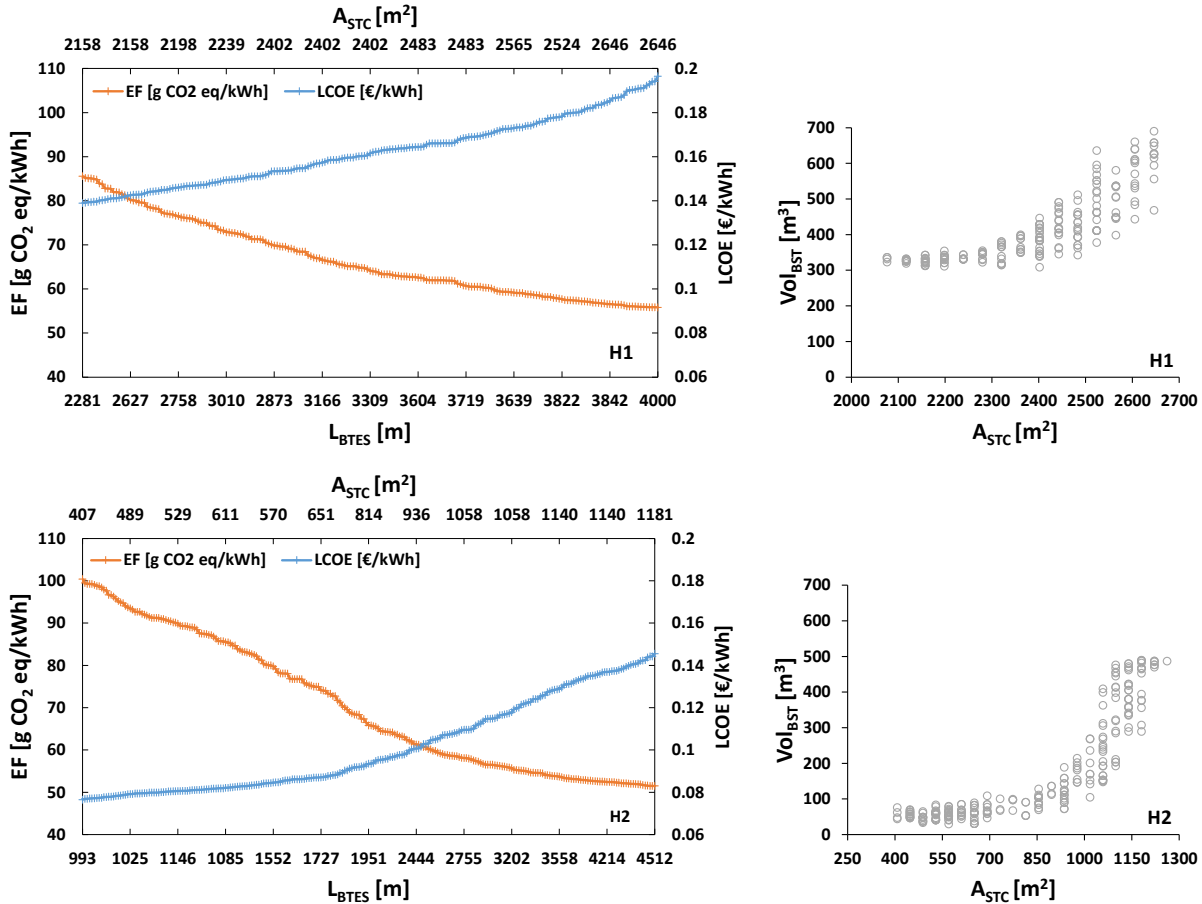


Fig. 14. Range of the optimization variables on the Pareto fronts of the solar-assisted scenarios.

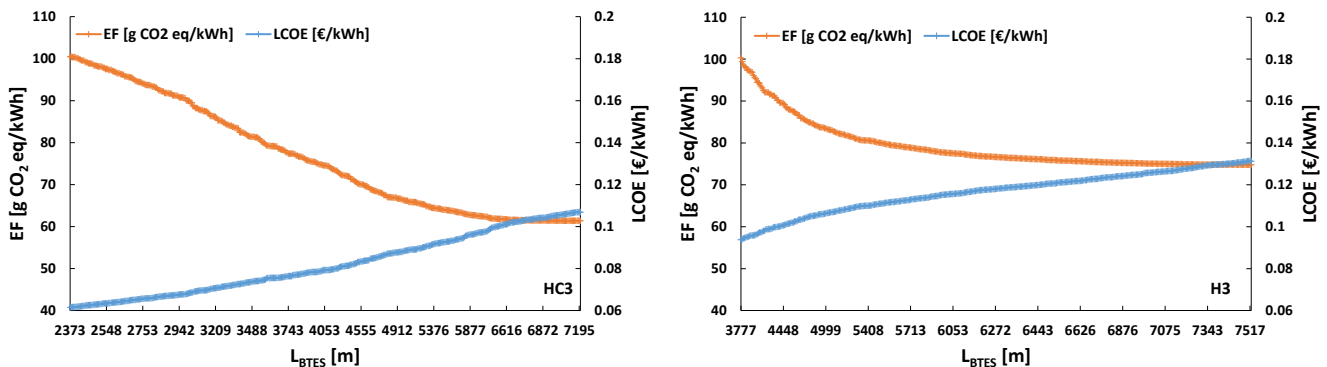


Fig. 15. Range of the optimization variables on the Pareto fronts of the standalone scenarios.

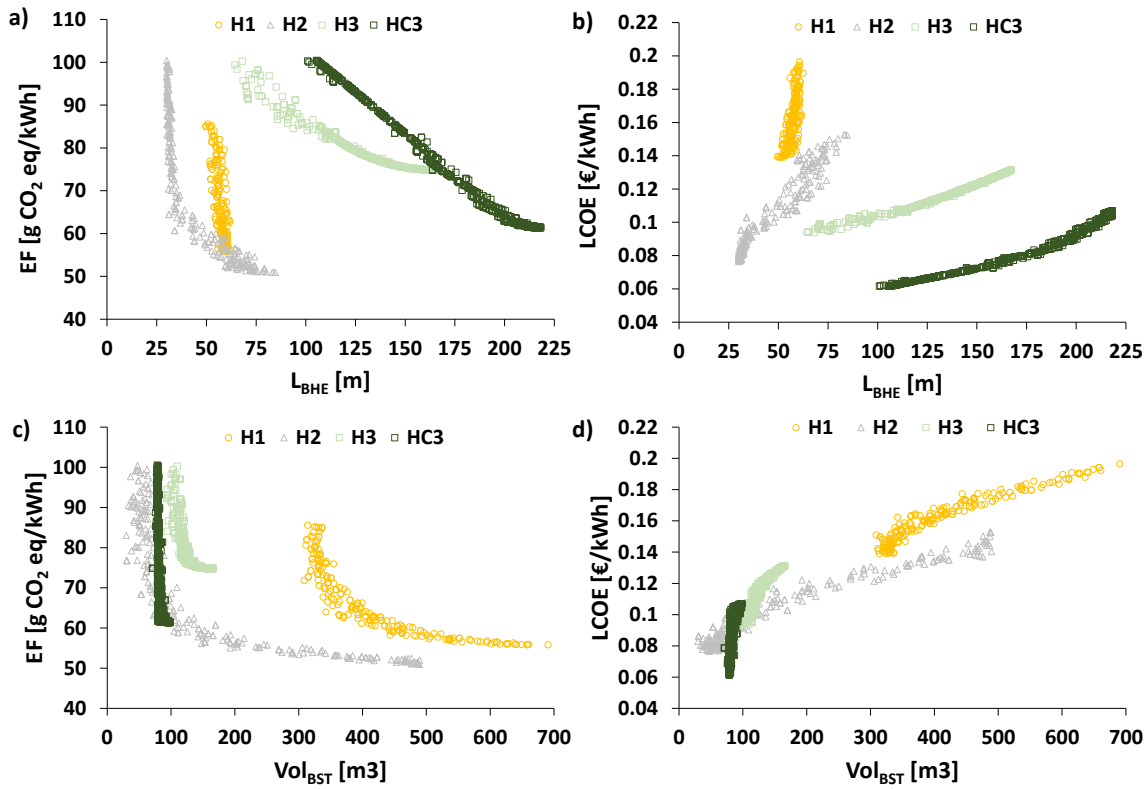


Fig. 16. Change in EF and LCOE with L_{BHE} (a and b) and with Vol_{BST} (c and d) for the optimized layouts on the Pareto front.

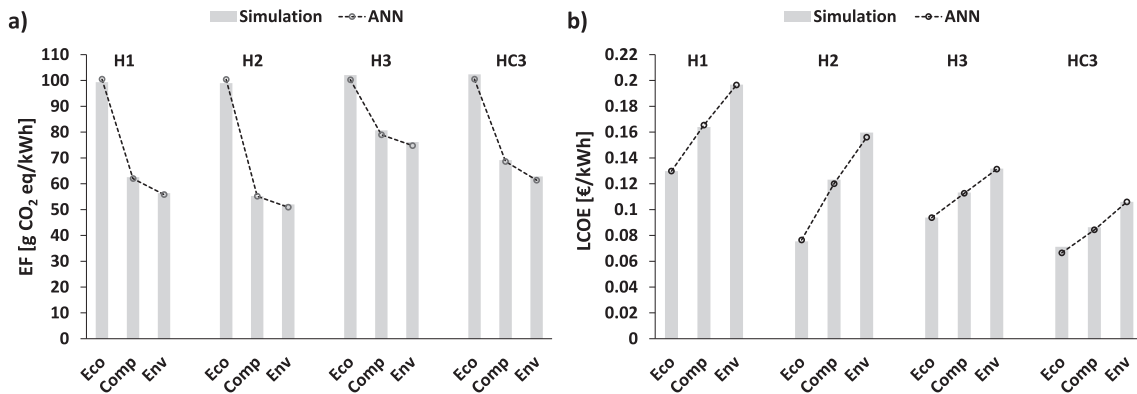


Fig. 17. Simulation vs. ANN results of EF (a) and LCOE (b) for the characteristic designs H1-H3 and HC3.

results of adding an ASHP to H1 and H2 to supply the cooling demand. Therefore, the ranges of their optimized variables are the same. For the solar-assisted scenarios, supplying the heating load passively results in larger STC areas, which requires also larger BTES and BST for seasonal and diurnal storage of the collected solar energy. The H3 and HC3 scenarios result in higher lengths than the other scenarios which is favorable because it leads to lower surface areas as larger amounts of spacing are recommended for more efficient operations of the standalone scenarios [10,46]. The H3 scenario results in lower source temperatures for the HP in comparison with the HC3 scenario, as the ground is only discharged. Hence, higher HP capacities are required to supply the same heating demand. This also results in larger Vol_{BST} for scenario H3. It should be mentioned that the capacities of the HPs on Table 5 are nominal numbers. The real capacities are dependent on the ground-side temperatures, which vary for different scenarios and simulation time.

The relation between the optimized variables of the sample points on the Pareto fronts and their corresponding outputs is shown in Figs. 14

and 15. As it is expected, for all scenarios the EF decreases and LCOE increases by increasing the total drilling length ($L_{BTES} = L_{BHE}N_{BHE}$) for installing double U-tube BHEs. Similarly, an increase in A_{STC} decreases EF and increases LCOE. Figs. 14 and 15 can be used to determine an optimal layout of the STC and the BTES, depending on a project's constraints and the envisaged layout, by choosing a value for the objectives. For a chosen total drilling length L_{BTES} , optimal ratios for L_{BHE} and N_{BHE} can be derived from Table 3, considering that higher L_{BHE} results in lower EF and higher LCOE (cf. Fig. 16). Likewise, higher Vol_{BST} also results in lower EF and higher LCOE for the solar-assisted scenarios. On the other hand, for the standalone scenarios Vol_{BST} is mainly related to the HP capacity and remains within a limited boundary for different designs on the Pareto front. The more nonlinear behavior of the objective functions with changing L_{BHE} in H1 and H2 is the result of the influence of STCs on the objectives.

For further analysis, three characteristic designs on the Pareto front of each layout are chosen. These include the most economical the most

Table 6
The economical, the compromise and the ecological system designs of each scenario.

| Scenario | | LCOE [ct/kWh] | GWP [gCO ₂ /kWh] | L _{BHE} [m] | N _{BHE} | Cap _{HP,nom} [kW] | A _{STC} [m ²] | Vol _{BST} [m ³] |
|----------|---------------|---------------|-----------------------------|----------------------|------------------|----------------------------|------------------------------------|--------------------------------------|
| H1 (HC1) | Economical | 12.98 (12.57) | 99 (93) | 50 | 42 | | 1954 | 308 |
| | Compromise | 16.39 (15.62) | 62 (60) | 58 | 60 | | 2443 | 419 |
| | Environmental | 19.67 (18.56) | 56 (55) | 61 | 66 | | 2646 | 690 |
| H2 (HC2) | Economical | 7.54 (7.65) | 99 (93) | 30 | 36 | 113.2 | 407 | 47 |
| | Compromise | 12.32 (11.92) | 55 (54) | 62 | 60 | 113.2 | 1058 | 239 |
| | Environmental | 15.96 (15.19) | 52 (51) | 83 | 60 | 113.2 | 1221 | 487 |
| H3 | Economical | 9.38 | 102 | 68 | 57 | 169.8 | – | 109 |
| | Compromise | 11.32 | 81 | 127 | 45 | 169.8 | – | 116 |
| | Environmental | 13.17 | 76 | 167 | 45 | 168.8 | – | 165 |
| HC3 | Economical | 7.12 | 102 | 105 | 24 | 113.2 | – | 79 |
| | Compromise | 8.63 | 69 | 184 | 27 | 113.2 | – | 79 |
| | Environmental | 10.60 | 63 | 218 | 33 | 113.2 | – | 98 |

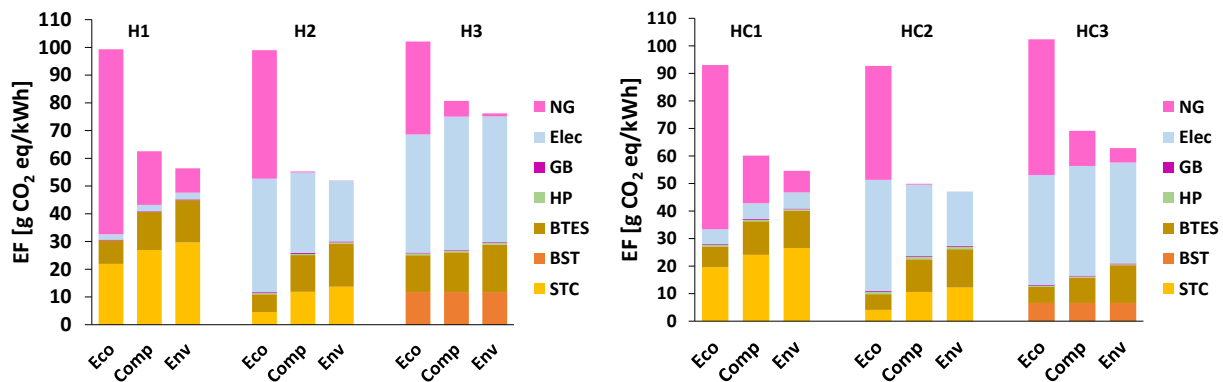


Fig. 18. Component-wise EF of the characteristic designs of Table 4.

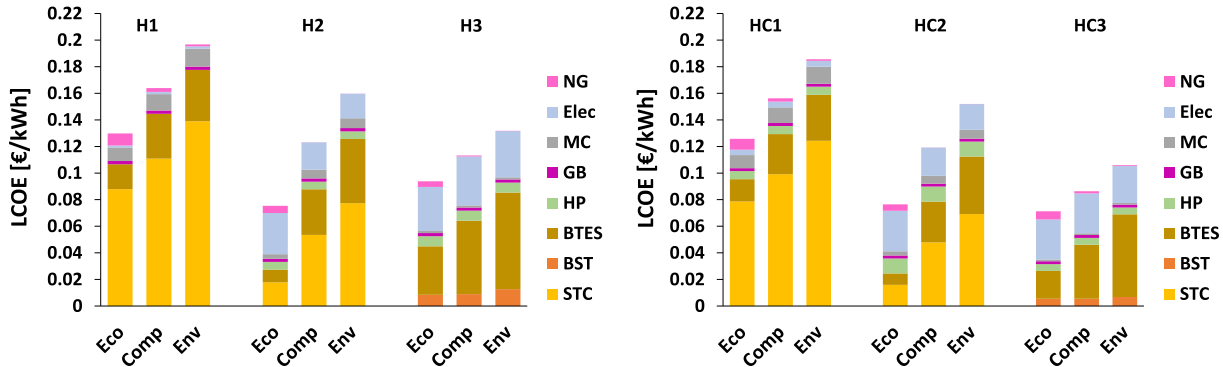


Fig. 19. Component-wise LCOE of the characteristic designs of Table 4.

environmentally-friendly and the compromise solutions. The compromise solution is the point with the minimum distance from the notional ideal point with the lowest possible EF and LCOE resulted from the optimization algorithm. These points are simulated with the TRNSYS models. The results are then compared with the outputs from the ANN, for the scenarios which were trained and optimized (H1-H3 and HC3, cf. Chapter 6.2). As illustrated in Fig. 17, the simulation results closely match the outputs from the ANN proxy model, which again proves the validity of the ANN method for predicting the objective functions. As not separate training was conducted for HC1 and HC2 scenarios. The simulation results of the characteristic designs and their corresponding optimized variables are given in Table 6 as well. The HC3 scenario yields the lowest LCOE and scenario HC2 has the lowest EF among the combined heating and cooling scenarios, while H2 always gives the best results for both objectives for the heating scenarios.

7.2. Environmental and economic analysis

To gain deeper insight into the coherencies of the results, the composition of EF and LCOE for the characteristic designs of Table 6 is shown in Figs. 18 and 19. For all scenarios, the overall EF and the EF during the operational phase decrease while the emissions during the production phase increase from the economical to the ecological designs. This is the result of more efficient operation of the layouts with higher renewable share and consequently higher LCOE. Adding ASHPs to the solar-assisted scenarios to supply cooling demand increases the IC, the overall electricity consumption, and the associated EF during the production and the operation of ASHPs. However, a comparison of H1 with HC1 and H2 with HC2 reveals that the overall specific values slightly decrease. Finally, for the standalone scenarios, utilizing the underground to supply both heating and cooling reduces both LCOE and EF considerably.

For H1 and HC1 layouts, STCs (including their diurnal BSTs) and

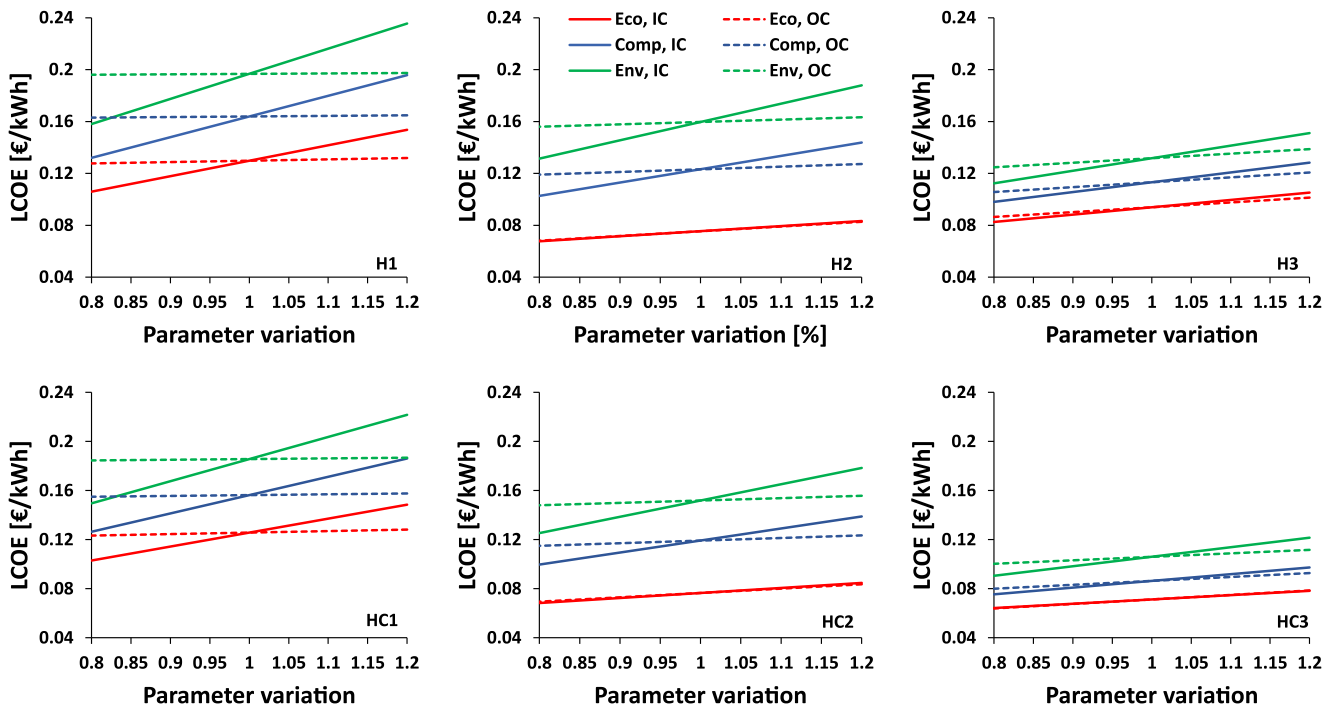


Fig. 20. Effect of varying initial costs (IC) and operational costs (OC) for the designs of Table 4.

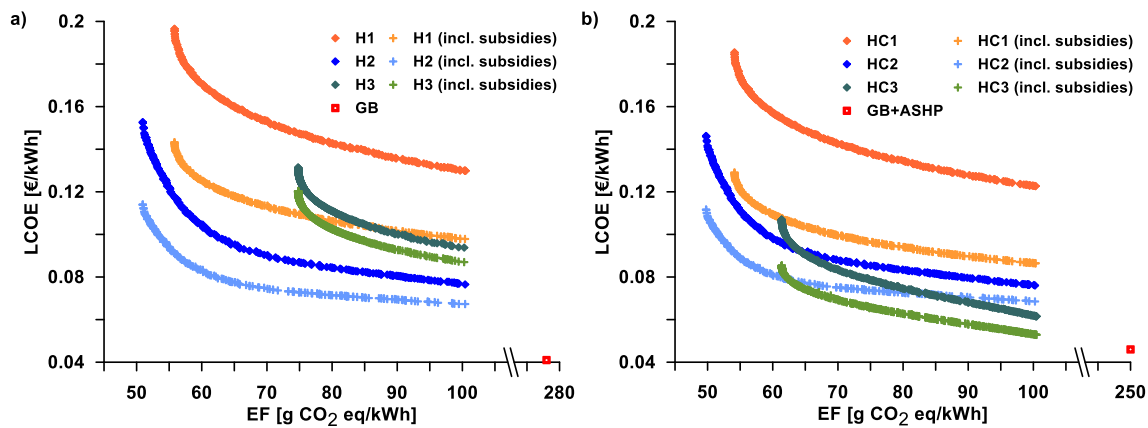


Fig. 21. Influence of considering national subsidies on the Pareto fronts of a) Heating and b) Heating and cooling layouts.

BTES have the highest shares in both EF and LCOE for the Env and Comp systems. In contrast to this, emissions from natural gas (NG) have the major share in the overall EF for the Eco system. This is the consequence of smaller BTES dimensions which results in higher NG consumption not only during the initial charging years, but also after the temperature of the BTES has reached its appropriate limit for passive load supply.

In H2 and HC2 layouts, the electricity consumption by the HPs has an important share in the EF as well as in the LCOE, which decreases from the economical to the ecological layouts due to more efficient operation of larger systems. STCs and BTES have major shares in both objectives, which are, however, comparatively lower than in the passive scenarios. This demonstrates the importance of utilizing efficient HPs for improving the performance of solar-assisted BTES systems, which almost leads to the omission of the GB operation for the compromise and the ecological solutions. Even when comparing active and passive BTES discharging for the most economical scenarios, the integration of a HP also results in a lower share of GB. But, the high electricity demand of the HP almost completely cancels out the reduction in EF due to lower gas consumption, resulting in an almost equal total EF as in the passive

scenarios. In terms of LCOE, however, the active scenarios perform significantly better than the passive ones.

For the standalone layouts without solar system (H3 and HC3), the heating-only layout H3 has significantly lower gas consumptions than the combined heating and cooling equivalent HC3. However, emissions savings due to a lower gas consumption are equalized (Eco design) or even overshoot again (Comp and Env designs) by two effects: on the one hand H3 has a higher electricity consumption of HPs due to the lower source temperatures especially after a few years of heat extraction and, on the other hand, in H3 the BTES system and BST are generally larger, which adds significant amounts of emission in the production phase. The combined heating and cooling load supply in HC3 increases the efficiency of the BTES due to recharging of the underground, which results in lower L_{BTES} and consequently reduces its impact on both objectives.

7.3. Sensitivity analysis

7.3.1. Effect of varying initial and energy costs

In a sensitivity analysis, effects of 20% variation in IC and OC on

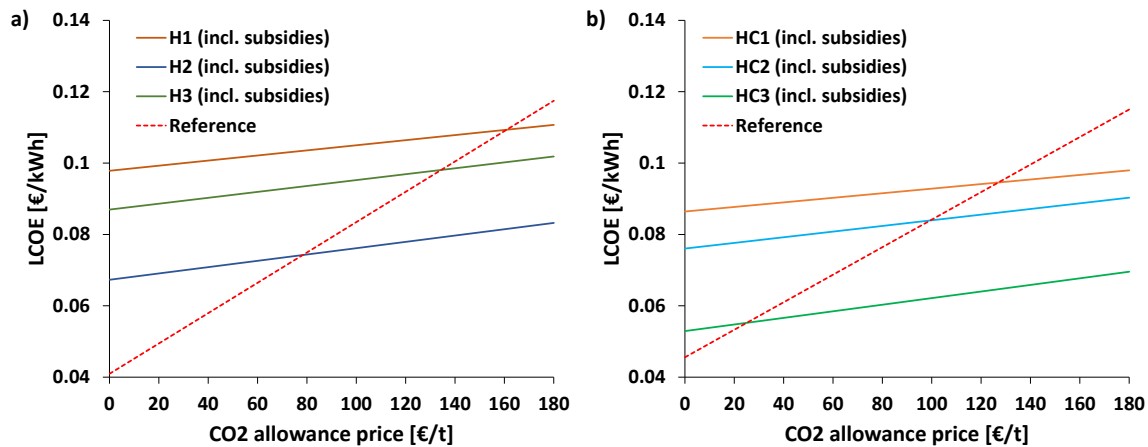


Fig. 22. Influence of considering national subsidies and emission costs on the economical designs of a) Heating and b) Heating and cooling layouts.

the LCOE of the characteristic designs of Table 6 are assessed (Fig. 20).

Varying the IC has a stronger effect than OC for the ecological and the compromise layouts. For the economical layouts, the impact of changing the OC is approximately similar to changing the IC, except for the passive scenarios. By reducing OC and IC of the economical point of HC3 scenario by 20%, its LCOE decreases from 7.12 to 6.42 ct/kWh and 6.39 ct/kWh, respectively, which corresponds to a reduction of 9.8 and 10.2%. For the different characteristic points of each layout, varying the IC has a smaller influence on more economical solutions, which are characterized by generally lower IC due to smaller L_{BTES} and A_{STC} .

While the influence of varying OC is rather small for all systems, it can be observed that passive systems (H1&HC1) are especially robust to changes in fuel costs. Since the gas price is still comparably low, even with the considered rise over time, it generally makes up only a minor share in the overall costs of all the systems (cf. Fig. 19). Layouts, including a heat pump, suffer slightly more from changes in the OC as the electricity price is higher than the gas price. However, as the Comp and Env solutions of these layouts also comprise large production cost for BTES and solar, the impact of changing IC is still much larger than that of changing the OC.

7.3.2. National subsidies

As already explained, the investigated layouts reduce the EF substantially in comparison with conventional fossil-based systems. However, EF reduction is also associated with an increase in LCOE, which is mainly due to IC of STCs and BTES. One option to make renewable energy systems competitive to conventional ones is to financially support such systems by subsidies. In Germany, subsidies are currently paid by the government for the installation of solar thermal collectors, heat storage facilities and efficient heat pump [66]. The influence of considering these national subsidies on the Pareto fronts of the optimized layouts is illustrated in Fig. 21.

It must be mentioned that due to time constraints, the subsidies were not already included in a separate optimization study, but were added later to the existing optimized layouts. It is expected that the inclusion of the subsidies would also change the optimal layouts, leading to even better system designs than presented here.

As all layouts comprise components that receive subsidies, all Pareto fronts are shifted downwards to lower LCOE. These include the subsidies that are considered for solar thermal collectors, heat storage facilities and efficient heat pumps. The cost reduction decreases for the systems with higher EFs. Moreover, the solar-assisted scenarios take the most advantage of subsidies. Consequently, the passive layouts having the largest STC areas exhibit the highest reduction in LCOE of all.

After implementing the national subsidies, a layout with an EF of 100 g CO₂ eq/kWh results in a LCOE of 0.052 €/kWh for the HC3 scenario. Therefore, compared with the reference layout with a EF and

LCOE of 250 g CO₂ eq/kWh and 0.046 €/kWh (cf. chapter 6.2) an increase of 13% in LCOE results in a reduction of 60% in EF. Overall, it can be concluded that national subsidies pave the way towards the utilization of the environmental benefits of geothermal layouts even on small-scale by making them more economically attractive. However, to reach the lowest EFs for easily-implementable small-scale systems, more supports are needed.

7.3.3. National subsidies and emission costs

Other than environmental effects of using fossil fuels, penalty costs that need to be paid for emitting environmental pollutants further decrease the economic attractiveness of fossil-based systems and will be a major barrier for their further application. Fig. 22 shows the influence of considering CO₂ emission costs as well as national subsidies on the economical designs of the layouts. As the cheapest design of HC scenarios, HC3 is preferred to the reference case by considering a CO₂ emission cost of only 30 €/t. This means 60% EF reduction with the same LCOE. For the most economical layout of the heating-only scenarios, an emission cost of approx. 80 €/t is required to have the same LCOE as fossil-based systems. It needs to be mentioned that having more environmentally-friendly solutions is associated with higher costs and the supporting policies are required to support these systems economically. Overall, it can be concluded that the simultaneous consideration of the national subsidies and the emission cost will make small-scale geothermal layouts economically comparable with fossil-based energy systems.

7.4. Limitations and future work

A generic study of a complex system requires simplifications and assumptions, which has its own drawbacks and may cause uncertainties. It has been tried to lower the uncertainties by choosing a system in operation as the reference case and simulating and validating the simulation against experimental results. In this part, the considered assumptions and simplifications as well as the proposed future works are explained.

- ANN is utilized as a proxy model for estimating the objective functions and convergence of the optimization with larger numbers of evaluations. However, estimation is always associated with uncertainties. Nevertheless, efforts were made to control these uncertainties by checking the functions from the training algorithm as well as by post-simulation of the selected final points. These measures have shown that the approach via the proxy model is very accurate.
- For the project lifetime of 30 years, every simulation with a time step of 1 h takes around 40 min. Moreover, an appropriate training of

ANN with low estimation errors, requires between 1,000 to 2,000 evaluations depending on the layout and number of variables. In dynamic simulation of energy systems, shorter time steps always result in more exact results but longer simulations, which is impracticable due to computation limits in this study.

- These computational limitations make it necessary to keep certain boundary conditions fixed. The results might for example be strongly dependent on system size and local climate conditions. The notional system located in Germany identifies optimal system layouts for central European locations and comparable regions. However, the presented methodology can generally be applied to any location and climate.
- The selected STC module has a gross area of 13.57 m². It is assumed that three STC modules are in series and, for pump selection, the pressure loss inside STCs is calculated accordingly. However, the number of STCs in series or parallel is dependent on the available area for installing the collectors and requires separate analyses considering the project site specifications.
- It is assumed that the BTES is installed in the ground with a uniform thermal conductivity and heat capacity and the only heat transfer mechanism is conductive. However, in real applications convective heat transfer might exist and ground thermal characteristics might not be uniform.
- For the calculation of OC, the energy cost functions taken from the economic studies are mainly based on predictions assuming that a linear interpolation between the available data points is acceptable. The IC functions are based on the available literature and are mainly defined by having data from real projects in a specific range. Consequently, cost functions are subject to uncertainties. The sensitivity analysis in chapter 6.4.1 is done with the purpose of considering these uncertainties.
- It is assumed that GBs cover the load that cannot be supplied by solar and/or ground loop, which is typical in many existing district heating grids. Using biomass boilers for peak load supply will result in further EF reduction. However, for a comparison with bio-fueled systems, other environmental impacts such as land consumption and fine particulate air pollution must be considered as well. Therefore, environmental and economic assessment of combined biomass boilers and the geothermal layouts is suggested as a future work.
- As mentioned earlier, for the solar-assisted HC scenarios (HC1 and HC2), BTES systems are heated up by STCs during the summer seasons and cannot be used as an efficient heat sink for cooling purposes. The utilization of two BTES systems, one for the storage of solar energy and the other for the rejection of the waste heat from cooling cycles, and possible configurations for performance improvement of the combined model is suggested as a future work.
- Although enviro-economic evaluations are initially used by decision-makers to evaluate a renewable energy project, they lack thermodynamic assessment [67]. Therefore, in practical applications, an enviro-economical optimization needs to be supplemented by a detailed thermo-economic assessment method to define the parameters which are kept constant during the optimization.

8. Conclusion

A combination of direct optimization, an ANN proxy and the NSGA II method is utilized for enviro-economic multi-objective optimization of solar-assisted and standalone geothermal layouts for heating as well as combined heating and cooling applications. The initial design and control strategies are adapted from a validated reference case to a notional case study in Germany. The following conclusions can be drawn from the results of this study:

- Utilizing the ANN as a mid-stage in the optimization procedure results in a proper verification and validation of the objective functions

in several steps and is recommended for long-term evaluation of geothermal applications.

- For heating applications, active load supply by the solar-assisted geothermal layouts results in the lowest LCOE and EF, and passive load supply leads to the most expensive solutions. The lowest EFs can only be reached by solar-assisted scenarios. Moreover, the stand-alone scenario without solar is only suggested if higher EFs are acceptable and utilizing STCs is not possible.
- The utilization of BTES for the seasonal storage of the waste heat from cooling cycle leads to the most economical layouts, which still reach reasonably low EFs. However, like in the heating-only scenarios, reaching the lowest EFs is merely possible by utilizing STCs.
- When comparing heating-only scenarios and combined heating and cooling scenarios, it is found that in the case of solar-assisted systems, the inclusion of cooling with an ASHP slightly reduces the EF and LCOE. However, the GWP and LCC increase. Consequently, in these cases, the comfort gain from cooling comes at a cost to consumers and causes additional emissions. In contrast, for the stand-alone scenarios without solar collectors, the inclusion of cooling results in a real cost reduction for the consumer and a reduction in emissions.
- Increasing the total drilling length or the area of STCs decreases the EF and increases LCOE. The relation between the optimized variables and the outputs of the multi-objective optimization from this study can be used by designers for an initial evaluation of system's dimensions and its effect on the enviro-economic objectives (Table 5 and Figs. 14-16).
- In the passive solar-assisted layout, STCs and BTES have the highest shares in both EF and LCOE. In contrast, in the active design, the electricity consumption of the HPs has important shares in both objectives.
- Utilizing efficient HPs for improving the performance of solar-assisted BTES systems leads to much smaller dimensions of STCs and BTES in comparison to passive systems. This almost leads to the omission of the GB operation in the compromise and the ecological solutions.
- The geothermal standalone heating-only layouts result in the highest EF and larger L_{BTES}, which increases the LCOE significantly. Recharging of the underground with waste heat in combined heating and cooling results in lower L_{BTES} and thus a lower impact on both the objectives.
- National subsidies can increase the economic attractiveness of the proposed layouts. By considering national subsidies, a 60% decrease in EF can be achieved if an increase in the LCOE of only 13% is accepted for the most economical layout compared to a fossil-based reference case. However, to reach the lowest EFs more supporting policies are needed.
- Considering CO₂ emission costs in addition to the national subsidies can make the geothermal layouts economically more attractive than the fossil-based reference layout while decreasing EFs substantially.

Funding

This work was financially supported by the German Research Foundation (DFG) in the framework of the Excellence Initiative, Darmstadt Graduate School of Excellence Energy Science and Engineering (GSC 1070).

CRediT authorship contribution statement

Hoofar Hemmatbady: Conceptualization, Methodology, Investigation, Visualization, Writing. **Bastian Welsch:** Conceptualization, Supervision, Visualization, Writing. **Julian Formhals:** Conceptualization, Investigation, Writing. **Ingo Sass:** Conceptualization, Supervision, Funding acquisition.

Declaration of Competing Interest

The authors declare that they have no known competing financial

interests or personal relationships that could have appeared to influence the work reported in this paper.

Appendix A. Calculations of costs and emissions

See Tables A.1–A.5.

Table A.1
Emissions caused during the production of each system component ($GWP_{Prod,i}$).

| Component | $GWP_{Prod,i}$ (kg CO ₂ eq) | Reference |
|-----------|--|-----------|
| BTES | $(4.105 \times L_{BHE} + 63.25 \times t_{drill}^a) \times N_{BHE}$ | [28] |
| HP | $58.5 \times Cap_{HP}$ | [68] |
| STC & BST | $176 \times A_{STC}$ | [28] |
| GB | $78.1 \times Cap_{GB}^{0.729}$ | [69] |

$$a \ t_{drill} = 19.8 \times (2.71828^{0.0036 \times L_{BHE}}).$$

Table A.2
EF associated with electricity ($EF_{elec,a}$) and natural gas ($EF_{gas,a}$) consumption as function of the operation year.

| Parameter | 2020–2030 | 2030–2050 | Reference |
|--|-------------------------------------|-------------------------------------|-----------|
| $EF_{elec,a}$ (kgCO ₂ /kWh) | $(-20.99a + 423.89) \times 10^{-3}$ | $(-8.595a + 287.55) \times 10^{-3}$ | [51] |
| $EF_{gas,a}$ (kgCO ₂ /kWh) | 250×10^{-3} | 250×10^{-3} | [52] |

Table A.3
Investment and maintenance cost functions of different components.

| Component | Investment cost (€) | Maintenance cost (€/yr.) | Reference |
|-----------|---|--------------------------|-----------|
| BTES | $65 \times L_{BHE}$ | – | [70] |
| HP | $(2053.8 \times Cap_{HP}^{-0.348}) \times Cap_{HP}$ | $0.0075 \times C_{IC}$ | [71] |
| STC | $(335 \times A_{STC}) + 7500$ | $0.0075 \times C_{IC}$ | [54,72] |
| BST | $(403.5 \times Vol_{BST}^{-0.4676} + 750) \times Vol_{BST}$ | – | [54] |
| GB | $(11418.60 + 64.6115 \times Cap_{GB}^{0.7978}) \times f_{GB}^a$ | $0.02 \times C_{IC}$ | [69] |

$$a \ f_{GB} = 1.0818 - (8.2898 \times 10^{-7} \times Cap_{GB}).$$

Table A.4
Electricity cost ($c_{elec,a}$) as function of the operation year.

| Parameter | 2020–2026 | 2027–2011 | 2012–2050 | Reference |
|----------------------|---------------------|-----------------------|----------------------|-----------|
| $c_{elec,n}$ (€/kWh) | $0.00302n + 0.1304$ | $-0.003356n + 0.1686$ | $-0.00042n + 0.1363$ | [73,74] |




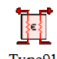





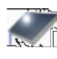





Table A.5
Natural gas cost ($c_{gas,a}$) as function of the operation year.

| Parameter | 2020–2030 | 2030–2050 | Reference |
|---------------------|----------------------|-----------------------|-----------|
| $c_{gas,n}$ (€/kWh) | $0.000432n + 0.0285$ | $0.000212n + 0.03095$ | [73,74] |

Appendix B. TRNSYS models

In this part different TRNSYS layouts and their control strategies are explained and discussed. Initially, main TRNSYS components that are used for modelling the proposed layout are shown (cf. Table B.1.1). Moreover, mathematical description of the main controllers is explained (cf. Table B.1.2). Finally, TRNSYS models of the layouts and their control parameters are discussed.

Table B.1.1
Main TRNSYS components.

| | | |
|---|---|--|
| <p>Variable Speed Pump</p>  <p>Type110</p> | <p>Flow Diverter</p>  <p>Type11f</p> | <p>Flow Mixer</p>  <p>Type11h</p> |
| <p>Heat Exchangers Constant Effectiveness</p>  <p>Type91</p> | <p>Heat Exchanger Hot-side Modulation</p>  <p>Type512</p> | |
| <p>Ground Heat Exchangers</p>  <p>Type557a</p> | <p>Buried Horizontal Single-pipe Systems</p>  <p>Type952</p> | |
| <p>GSHP</p>  <p>Type927</p> | <p>ASHP</p>  <p>Type118</p> | |
| <p>Solar Thermal Collectors</p>  <p>Type1a</p> | <p>Buffer Storage Tank</p>  <p>Type534</p> | |
| <p>Differential Controller</p>  <p>Type2b</p> | <p>Aquastat</p>  <p>Type106 Type113</p> | |
| <p>Weather Data</p>  <p>Type15</p> | <p>Load</p>  <p>Type9c Type682</p> | |

B.1. TRNSYS components (Types)

As the main control strategies of the layouts are specified by differential controllers (Type 2b), the controller function is discussed in this part. To give a hysteresis effect, the controller is normally used with the output control signal (γ_o) connected to the input control signal (γ_i) [34]. Table B.1.2 shows the controller function and how it defines γ_o based on γ_i . If the controller is already on ($\gamma_i = 1$), it remains on ($\gamma_o = 1$) if the difference between upper input temperature (T_H) and lower input temperature (T_L) is greater than or equal to lower dead band temperature difference (ΔT_L), otherwise it will be switched off ($\gamma_o = 0$). If the controller is already off ($\gamma_i = 0$), it remains off ($\gamma_o = 0$) if the difference between T_H and T_L is lower than the upper dead band temperature difference (ΔT_H), otherwise it will be switched on ($\gamma_o = 1$). Regardless of the value of γ_i , the controller switches off ($\gamma_o = 0$), if temperature for high limit monitoring (T_{in}) is higher than maximum input temperature (T_{max}).

B.2. TRNSYS model of passive heating (BTES)

TRNSYS model of H1 scenario is shown in Fig. B.2.1 As it can be seen in the figure, there are mainly four loops in the model including solar loop (SL), buffer storage loop (BSL), ground loop (GL) and district loop (DL). The solar energy that is collected in the SL is transferred to the BSL for diurnal storage. In charging mode, the energy is delivered from the BSL to the GL, to be stored in the BTES. In discharging mode, the stored energy in the BTES is then extracted and delivered from the GL to the BSL. The extracted energy from the BTES together with the collected solar energy in the SL is then transferred from the BSL to the DL to supply the heating demand.

STCs (Type1a) collect the solar energy and transfer it to the return fluid, from the underground pipes (Type952) of the solar loop (SL). The circulation is done by a variable-speed pump, P-SL, (Type 110), which is activated using a differential controller (Type2b). The controller functions are specified using Table B.1.2 with the values of the monitored temperatures, ΔT_L , ΔT_H and T_{max} from Table B.2.1. Moreover, its flow rate is controlled so that a design ΔT of 15 K for STCs is assured [42]. Using the SL HEX (Type 91b), the collected solar energy is transferred to the fluid from the bottom of the colder BST (BST2) on the BST side. This is done by another variable-speed pump, P-BST-SL, with the same flow rate as P-SL [42]. The temperature of the fluid is then increased and delivered to the top of the warmer BST (BST1), until the circulating pumps on both sides are turned off by the SL differential controller.

The return fluid from the BTES is diverted using flow diverter (Type 11f) to the bottom of the colder BST in the charging mode or to the top of the warmer BST in discharging mode. In charging mode, the stored solar energy in the BSTs is transferred to the BTES. This is done by the ground loop pump, P-GL, which is controlled by two differential controllers, one for heating and one for non-heating seasons, cf. Table B12 and Table B.2.1. In charging mode of the non-heating seasons, the controller turns off the pump when the BSTs do not contain enough energy or the BTES reaches its maximum temperature limit. In charging mode of the heating seasons, the controller turns on the pump when the bottom temperature of the colder BST (BST2) exceeds the design supply temperature on the load side. These strategies are specified by upper and lower dead band as well as maximum input temperatures, cf. Table B.3. In discharging mode, the BSTs are filled by P-GL, which is controlled by a differential controller considering the temperature level of the BTES center and BSTs, cf. Table B.1.2 and Table B.2.1.

In heating seasons, the collected energy in the BSTs, from the BTES and the STCs, is delivered to the DL using P-BST-DL. It is a variable-speed pump that is controlled by a control signal, which is an output of the district loop HEX (Type 512). It assures that the supply temperature in the district loop T_{sup} is heated up to its set point. On the load side, P-DL circulates the fluid in the underground pipes (Type952) of the DL. Its flow rate is controlled considering the heat demand of the cased study (given as input to the model by Type 9c) to meet design ΔT of the DL. Moreover, a GB (Type 700) assures that the fluid is heated up to its set point temperature before it is delivered to the final consumer. It is controlled by a simple aquastat (Type 106), which turns on the GB considering the outlet temperature of the district HEX and the design T_{sup} of the grid. Finally, Type 683 represents the simplified final consumer.

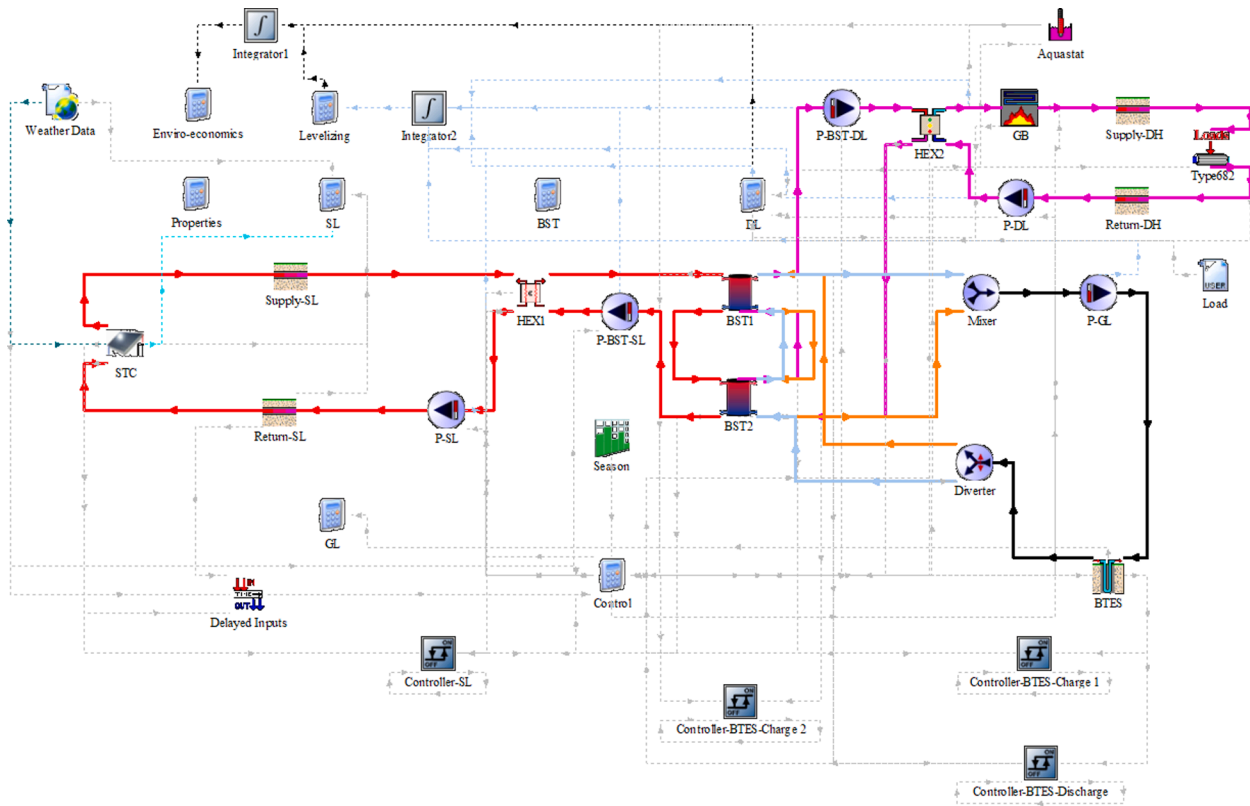


Fig. B.2.1. TRNSYS model of H1 scenario.

Table B.1.2
Differential controller (Type 2b) controller function [34].

If the controller was previously on ($\gamma_i = 1$)
 If $\Delta T_L \leq (T_H - T_L)$ then $\gamma_o = 1$
 If $\Delta T_L > (T_H - T_L)$ then $\gamma_o = 0$

If the controller was previously off ($\gamma_i = 0$)
 If $\Delta T_H \leq (T_H - T_L)$ then $\gamma_o = 1$
 If $\Delta T_H > (T_H - T_L)$ then $\gamma_o = 0$

If $T_{in} > T_{max}$ then $\gamma_o = 0$

Table B.2.1
Controller parameters of type 2b for the solar loop and BTES (charge and discharge) (slightly modified after [48]).

| | |
|--|--|
| Solar loop controller | $\Delta T_L = 2, \Delta T_H = 10, T_{max} = 90^\circ \text{C}$ T_H : outlet temperature of STCs T_L : bottom temperature of the colder BST (BST2) T_{in} : top temperature of the warmer BST (BST1) |
| BTES controller (charge) non-heating seasons | $\Delta T_L = 3, \Delta T_H = 10, T_{max} = 90^\circ \text{C}$ T_H : top temperature of the warmer BST (BST1) T_L : average soil temperature near boreholes (center) T_{in} : average storage temperature |
| BTES controller (charge) heating seasons | $\Delta T_L = 2, \Delta T_H = 10, T_{max} = \text{toptemperatureofBST1}$ T_H : load-side supply temperature T_L : bottom temperature of the colder BST (BST2) T_{in} : average soil temperature near boreholes (center) |
| BTES controller (passive discharge) heating seasons | $\Delta T_L = 3, \Delta T_H = 10, T_{max} = 45^\circ \text{C}$ T_H : average soil temperature near boreholes (center) T_L : bottom temperature of the colder BST (BST2) T_{in} : top temperature of the warmer BST (BST1) |

B.3. TRNSYS model of active heating (BTES)

TRNSYS model of H2 scenario is shown in Fig. B.3.1. The control strategies of the GL in charging mode, the SL, the BSL and the DL are the same as H1, cf. Chapter B2. For the GL in discharging mode, a HP (Type 927), based on a manufacturer’s data [49], discharges the BTES actively when its temperature is not high enough for direct heating load supply. This is done by an active discharge controller, which can be switched on only when the passive discharge controller is off. It monitors the load-side supply temperature T_{sup} and compares it with the bottom temperature of the colder BST (BST2), cf. Table B.3.1. When T_{sup} falls below the designed value, specified by ΔT_H and ΔT_L , the controller sends the return fluid from the bottom of BST2 to the HP using diverter1 and the return fluid from the BTES to the HP using diverter2. Moreover, it switches on the HP as well as its source- and load-side circulation pumps (P-GL and P-HP). P-HP is also modulated considering HP’s capacity to assure a ΔT of 7 K.

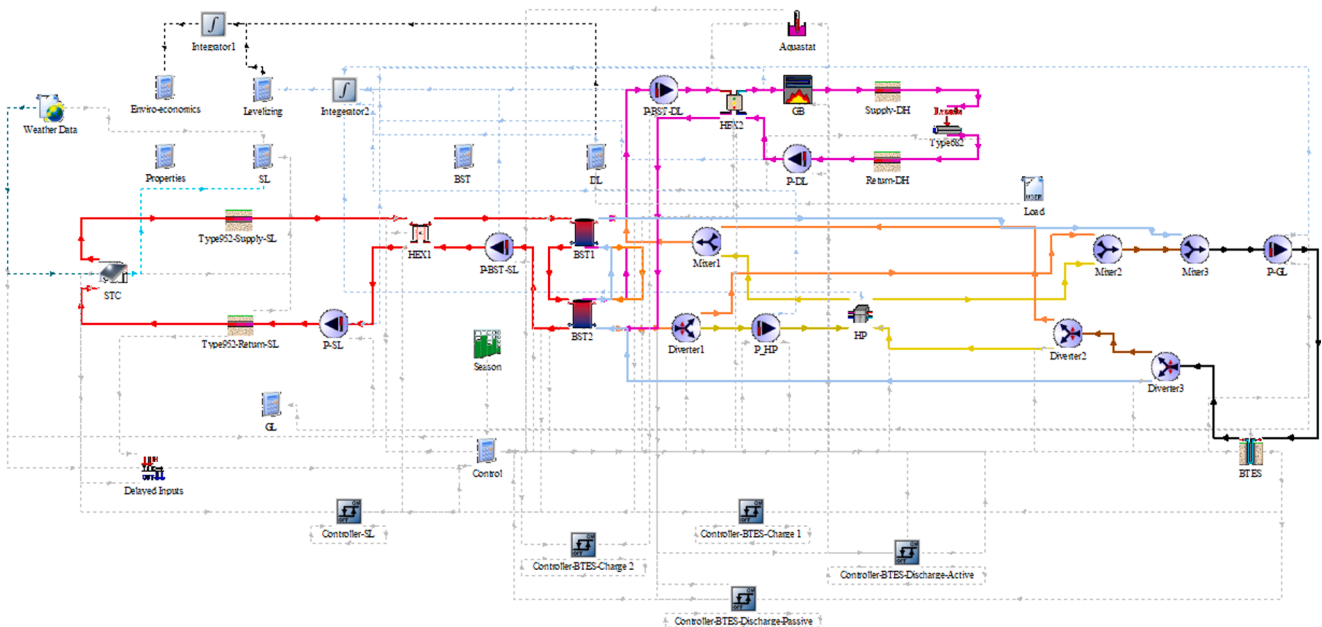


Fig. B.3.1. TRNSYS model of H2 scenario.

Table B.3.1
Controller parameters of type 2b for the ground loop in active discharge mode.

| | |
|---|--|
| BTES controller (active discharge) heating seasons | $\Delta T_L = 2, \Delta T_H = 6, T_{max} = 45^\circ C$ T_H : load-side supply temperature T_L : bottom temperature of the colder BST (BST2) T_{in} : top temperature of the warmer BST (BST1) |
|---|--|

B.4. TRNSYS model of active heating (GSHP)

TRNSYS model of H3 scenario is shown in Fig. B.4.1. The underground, without charging or regeneration, is utilized as an efficient heat source for the GSHPs. The control strategy is of the differential controller of the GL is similar to the active mode of H2 scenario, cf. Table B.3.1, which switches on the HP, P-HP and P-GL. P-HP is also modulated considering HP’s capacity to assure a design ΔT of 7 K. Like previous scenarios, P-BST-DL, is controlled by output control signals from the district loop HEX (Type 512) to assure that the DL design T_{sup} is met. The GB, which is turned on or off by an aquastat supplies the load that cannot be delivered by the BSTs.

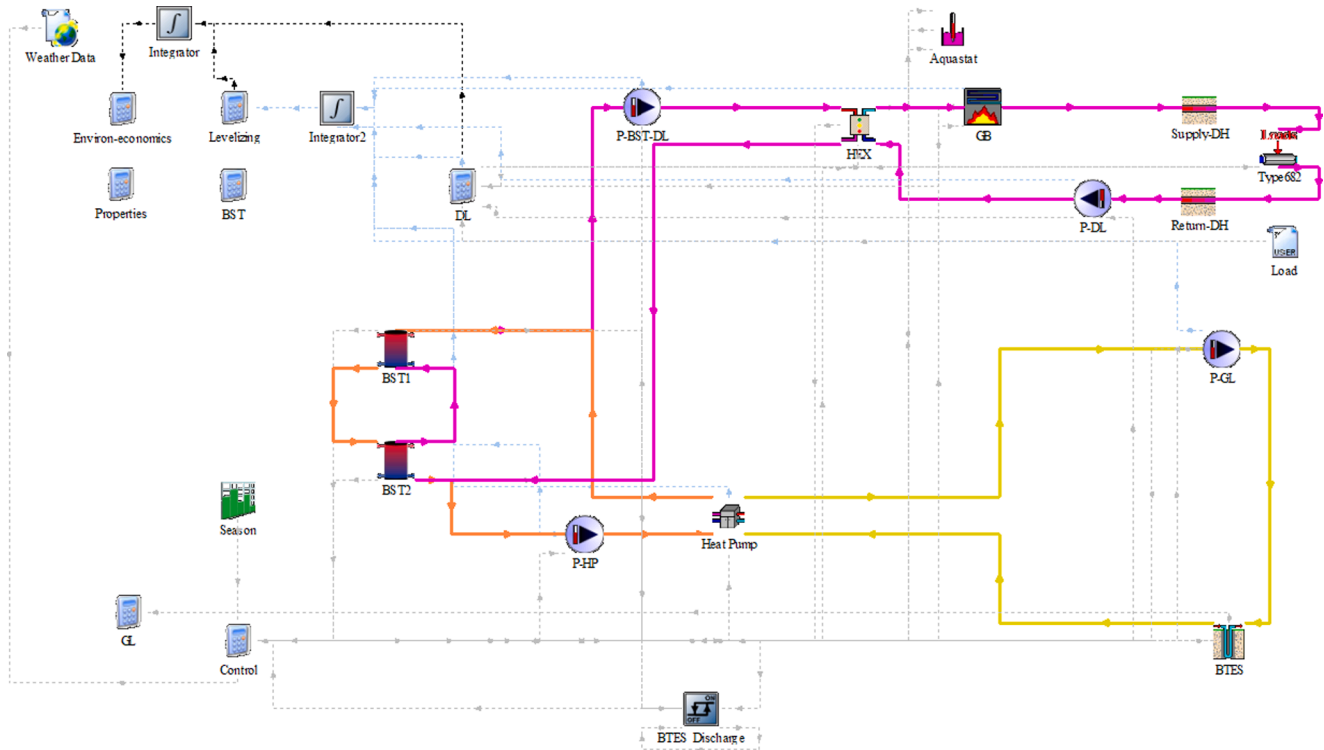


Fig. B.4.1. TRNSYS model of H3 scenario.

B.5. TRNSYS model of passive cooling (BTES)

TRNSYS model of HC3 scenario is shown in Fig. B.5.1. The heating load is supplied actively with the same strategy as H3. Controller parameters of the GL differential controller in active heating and passive cooling modes can be found Table B.5.1. In cooling season, the return fluid from the underground district pipes (Type 952) is delivered to the HEX-CL (based on Type 512 adapted to cooling operation, cf. Chapter 6.1). The output control signal of the HEX controls the operation of P-BST-DL so that the design load-side T_{sup} of 18 °C is assured. The cold fluid from bottom of BST2 is delivered to HEX-CL through diverter3, which has one control value in each season. This results in an increase in its temperature when it leaves the HEX. It then enters the top of the BST1, from where it is directly transferred through diverter1 to the GL, for passive cooling, or to the HP, for active cooling. The active cooling occurs when the passive discharge controller is off and district T_{sup} exceeds 18 °C. When the active cooling is activated, it turns on the HP and P-HP, which is modulated to supply the design cooling ΔT . Active or passive cooling strategy on the GL side is defined by diverter4, which diverts the return fluid from the GL to the bottom of BST2 or to the source side of the HP. As the load profile shows (Fig. 3), switching between heating and cooling is done once per year. Therefore, the BSTs are cooled down with the same cooling strategy, before the start of the cooling season.

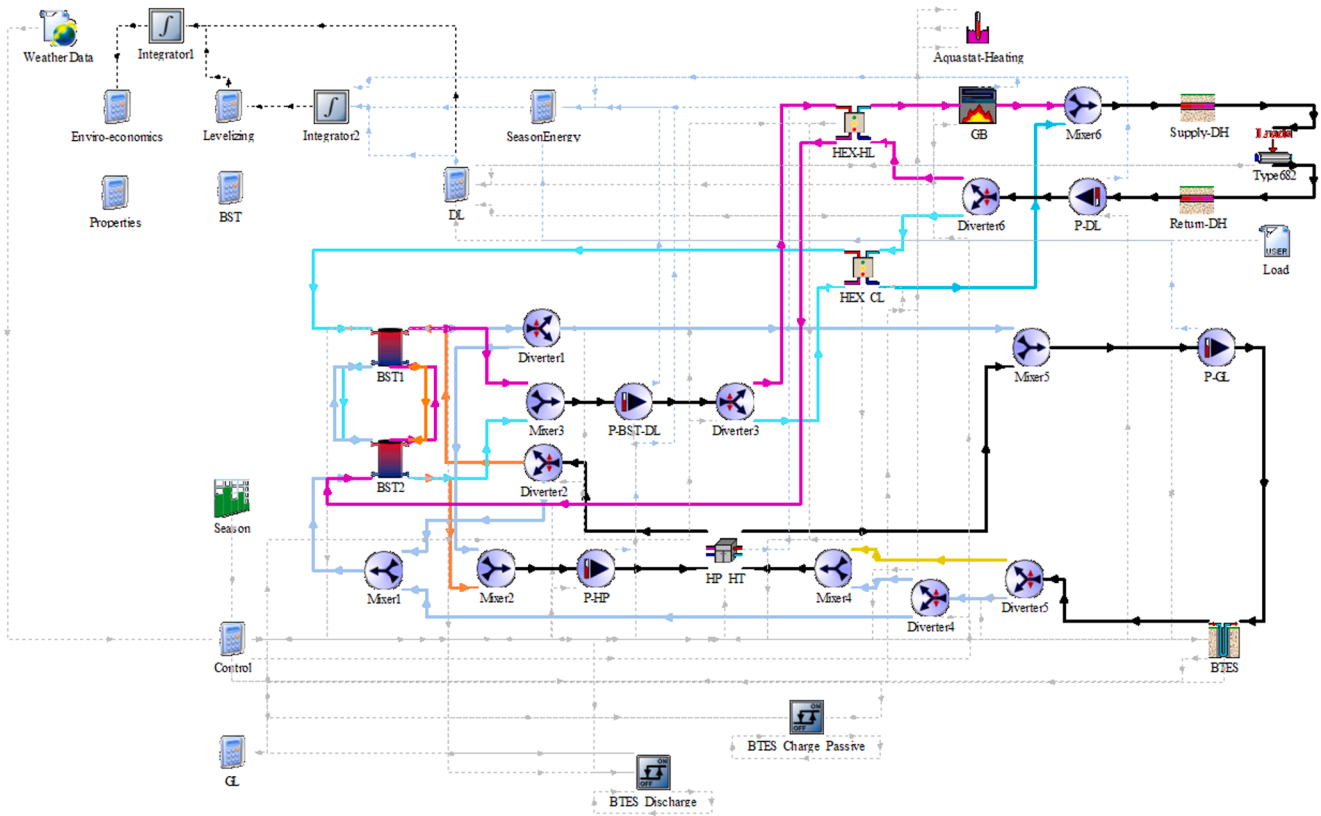


Fig. B.5.1. TRNSYS model of HC3 scenario.

Table B.5.1

Controller parameters of type 2b for the BTES in charge and discharge mode.

| | |
|---|---|
| BTES controller (passive charge) cooling seasons | $\Delta T_L = 1, \Delta T_H = 4, T_{max} = 22^\circ C$ T_H : top temperature of the warmer BST (BST1) T_L : average soil temperature near boreholes (edges) T_{in} : average soil temperature near boreholes (edges) |
| BTES controller (active discharge) heating seasons | $\Delta T_L = 2, \Delta T_H = 6, T_{max} = 45^\circ C$ T_H : load-side supply temperature T_L : bottom temperature of the colder BST (BST2) T_{in} : top temperature of the warmer BST (BST1) |

B.6. TRNSYS model of ASHP

TRNSYS model of ASHPs is shown in Fig. B.6.1. Two ASHPs (Type 118) are considered to supply the cooling demand of a single family house and an office building locally. The calculations are then expanded to the number of each building type, cf. chapter 3.1. The operational data of the ASHPs are selected based on a manufacturer's catalog [50] and given as an input file to Type 118. The HPs are inverter type that use a variable-speed compressor to meet the design temperature at each time step. Chilled water temperature (22 °C), chilled water flow rate and ambient temperature are given as inputs to the ASHPs to meet the cooling load, with a chilled water supply temperature of 18 °C, which is a design parameter.

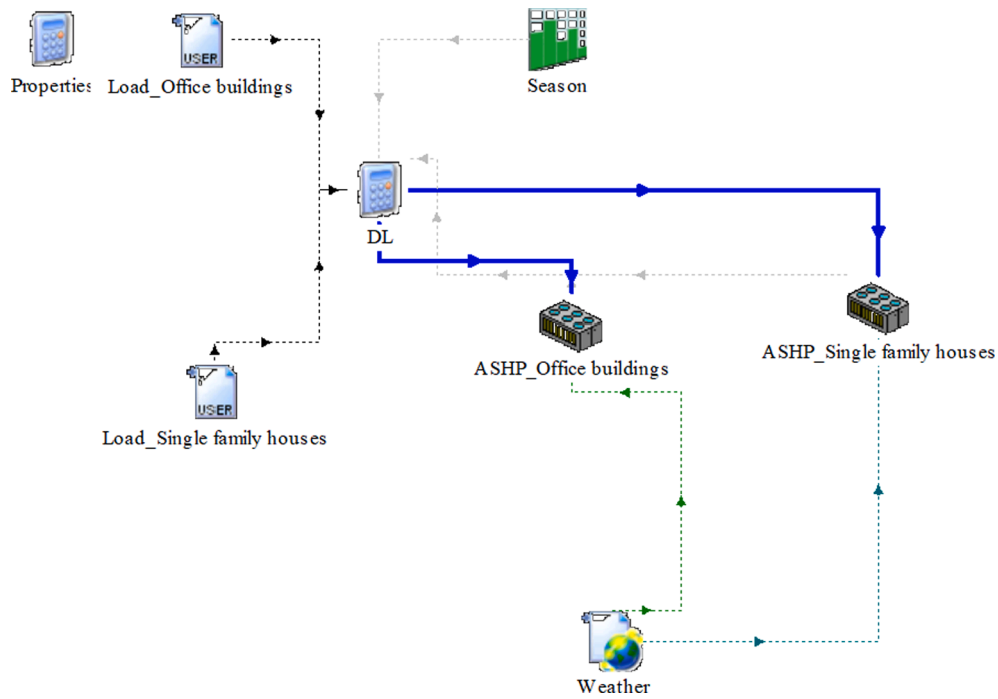


Fig. B.6.1. TRNSYS model of ASHPs.

Appendix C. . MATLAB settings

See Table C.1.

Table C.1
NSGA II optimization settings [65].

| Parameter | Definition | Value |
|---------------------|--|----------------------------------|
| CrossoverFcn | The fraction of the population at the next generation, not including elite children, that the crossover function creates. | 0.8 |
| FunctionTolerance | The algorithm stops if the average relative change in the best fitness function value over MaxStallGenerations generations is less than or equal to FunctionTolerance. | 1e-4 |
| MaxStallGenerations | | 100 |
| MaxGenerations | Maximum number of iterations before the algorithm halts. | 200 × number of variables |
| PopulationSize | Size of the population. | 50 |
| ParetoFraction | Sets the fraction of individuals to keep on the first Pareto front while the solver selects individuals from higher fronts | 0.35 |
| SelectionFcn | Function that selects parents of crossover and mutation children. | Selectiontournament ^a |

a) Tournament selection chooses each parent by choosing size players at random and then choosing the best individual out of that set to be a parent.

References

- [1] Ritchie H. Sector by sector: where do global greenhouse gas emissions come from?, <https://ourworldindata.org/ghg-emissions-by-sector>; 2021 [accessed 02 December 2021].
- [2] European Commission. Energy performance of buildings directive, https://ec.europa.eu/energy/topics/energy-efficiency/energy-efficient-buildings/energy-performance-buildings-directive_en; 2021 [accessed on 02 December 2021].
- [3] European Commission. Heating and Cooling, https://ec.europa.eu/energy/topics/energy-efficiency/heating-and-cooling_en; 2021 [accessed on 02 December 2021].
- [4] Mutschler R, Rüdissimi M, Heer P, Eggimann S. Benchmarking cooling and heating energy demands considering climate change, population growth and cooling device uptake. *Applied Energy*. 2021;288:116636. . 10.1016/j.apenergy.2021.116636.
- [5] Werner S. European space cooling demands. *Energy*. 2016;110:148–56. <https://doi.org/10.1016/j.energy.2015.11.028>.
- [6] Eurostat. <https://ec.europa.eu/eurostat>; 2019 [accessed on 02 December 2021].
- [7] UN. World urbanization prospects: The 2014 revision. United Nations Department of Economics and Social Affairs, Population Division: New York, NY, USA. 2015; 41.
- [8] Rezaie B, Rosen MA. District heating and cooling: Review of technology and potential enhancements. *Appl Energy* 2012;93:2–10. <https://doi.org/10.1016/j.apenergy.2011.04.020>.
- [9] Lund H, Werner S, Wiltshire R, Svendsen S, Thorsen JE, Hvelplund F, et al. 4th Generation District Heating (4GDH): Integrating smart thermal grids into future sustainable energy systems. *Energy*. 2014;68:1–11. <https://doi.org/10.1016/j.energy.2014.02.089>.
- [10] Hemmatbady H, Formhals J, Welsch B, Schulte DO, Sass I. Optimized Layouts of Borehole Thermal Energy Storage Systems in 4th Generation Grids. *Energies*. 2020; 13:4405. 10.3390/en13174405.
- [11] Connolly D, Lund H, Mathiesen BV, Werner S, Möller B, Persson U, et al. Heat Roadmap Europe: Combining district heating with heat savings to decarbonise the EU energy system. *Energy policy*. 2014;65:475–89. <https://doi.org/10.1016/j.enpol.2013.10.035>.
- [12] Duffie JA, Beckman WA. *Solar engineering of thermal processes*. John Wiley & Sons 2013.
- [13] Pinel P, Cruickshank CA, Beausoleil-Morrison I, Wills A. A review of available methods for seasonal storage of solar thermal energy in residential applications. *Renew Sustain Energy Rev* 2011;15(7):3341–59. <https://doi.org/10.1016/j.rser.2011.04.013>.
- [14] Welsch B. Technical, Environmental and Economic Assessment of Medium Deep Borehole Thermal Energy Storage Systems. 2019.
- [15] Dincer I, Rosen MA. *Thermal energy storage systems and applications*: John Wiley & Sons; 2021.
- [16] Mangold D, Miedaner O, Tziggili EP, Schmidt T, Unterberger M, Zeh B. Technisch-wirtschaftliche Analyse und Weiterentwicklung der solaren Langzeit-Wärmespeicherung. Schlussbericht zum BMU-Forschungsvorhaben N. 2012; 329607.
- [17] VDI. VDI 4640 Thermal Use of the Underground. VDI-Gesellschaft Energie und Umwelt (GEU), Berlin; 2019.
- [18] Skarphagen H, Banks D, Frengstad BS, Gether H. Design Considerations for Borehole Thermal Energy Storage (BTES): A Review with Emphasis on Convective Heat Transfer. *Geofluids* 2019;2019:1–26. <https://doi.org/10.1155/2019/4961781>.
- [19] Schulte DO, Rühaak W, Oladyskhin S, Welsch B, Sass I. Optimization of Medium-Deep Borehole Thermal Energy Storage Systems. *Energy Technology*. 2016;4(1): 104–13. <https://doi.org/10.1002/ente.201500254>.
- [20] Reuss M. The use of borehole thermal energy storage (BTES) systems. *Advances in thermal energy storage systems*. Elsevier 2015:117–47.
- [21] Geothermie A. Shallow Geothermal Systems-Recommendations on Design, Construction, Operation and Monitoring: Ernst et Sohn; 2016.
- [22] Welsch B, Rühaak W, Schulte DO, Bär K, Sass I. Characteristics of medium deep borehole thermal energy storage. *Int J Energy Res* 2016;40(13):1855–68. <https://doi.org/10.1002/er.3570>.
- [23] Formhals J, Hemmatbady H, Welsch B, Schulte DO, Sass I. A Modelica Toolbox for the Simulation of Borehole Thermal Energy Storage Systems. *Energies*. 2020;13: 2327. <https://doi.org/10.3390/en13092327>.
- [24] Lanahan M, Tabares-Velasco PC. Seasonal thermal-energy storage: A critical review on BTES systems, modeling, and system design for higher system efficiency. *Energies*. 2017;10:743. <https://doi.org/10.3390/en10060743>.
- [25] Rees S. *Advances in ground-source heat pump systems*. Woodhead Publishing 2016.
- [26] Bauer D, Marx R, Nußbicker-Lux J, Ochs F, Heidemann W, Müller-Steinhagen H. German central solar heating plants with seasonal heat storage. *Sol Energy* 2010;84 (4):612–23. <https://doi.org/10.1016/j.solener.2009.05.013>.
- [27] Bauer D, Drück H, Lang S, Marx R, Platz T. Weiterentwicklung innovativer Technologien zur solaren Nahwärme und saisonale Wärmespeicherung. Forschungsbericht zum BMWi-Vorhaben A. 2016;325998.
- [28] Welsch B, Göllner-Völker L, Schulte DO, Bär K, Sass I, Schebek L. Environmental and economic assessment of borehole thermal energy storage in district heating systems. *Appl Energy* 2018;216:73–90. <https://doi.org/10.1016/j.apenergy.2018.02.011>.
- [29] Formhals J, Feike F, Hemmatbady H, Welsch B, Sass I. Strategies for a transition towards a solar district heating grid with integrated seasonal geothermal energy storage. *Energy*. 2021;228:120662. <https://doi.org/10.1016/j.energy.2021.120662>.
- [30] Elhashmi R, Hallinan KP, Chiasson AD. Low-energy opportunity for multi-family residences: A review and simulation-based study of a solar borehole thermal energy storage system. *Energy*. 2020;204:117870. <https://doi.org/10.1016/j.energy.2020.117870>.
- [31] Shah SK, Aye Lu, Rismanchi B. Multi-objective optimisation of a seasonal solar thermal energy storage system for space heating in cold climate. *Appl Energy* 2020; 268:115047. <https://doi.org/10.1016/j.apenergy.2020.115047>.
- [32] Renaldi R, Friedrich D. Techno-economic analysis of a solar district heating system with seasonal thermal storage in the UK. *Appl Energy* 2019;236:388–400. <https://doi.org/10.1016/j.apenergy.2018.11.030>.
- [33] Leidos Canada, <https://www.dlsc.ca/reports/JUL2015/2012-2013%20Annual%20Report%20v07%20FINAL.pdf>; 2014 [accessed on 02 December 2021].
- [34] Klein S, Beckman W, Mitchell J, Duffie J, Duffie N, Freeman T, et al. TRNSYS 18 – A TRNSient system simulation program, user manual. Solar Energy Laboratory Madison: University of Wisconsin-Madison. 2017.
- [35] MATLAB. 9.2.0.556344 (R2017a). Natick, Massachusetts: The MathWorks Inc.; 2017.
- [36] Razmi AR, Arabkoohsar A, Nami H. Thermoeconomic analysis and multi-objective optimization of a novel hybrid absorption/recompression refrigeration system. *Energy*. 2020;210:118559. <https://doi.org/10.1016/j.energy.2020.118559>.
- [37] Mesquita L, McClenahan D, Thornton J, Carriere J, Wong B. Drake landing solar community: 10 years of operation. Proceedings of the ISES Conference Proceedings, Abu Dhabi; 02.11.2017; 2017.
- [38] Sibbitt B, McClenahan D, Djebbar R, Thornton J, Wong B, Carriere J, et al. The performance of a high solar fraction seasonal storage district heating system—five years of operation. *Energy Procedia* 2012;30:856–65. <https://doi.org/10.1016/j.egypro.2012.11.097>.
- [39] McDowell TP, Thornton JW. Simulation and model calibration of a large-scale solar seasonal storage system. *Proceedings of SimBuild*. 2008;3:174–81.
- [40] Verstraete A. Étude d'une communauté solaire avec stockage thermique saisonnier par puits géothermiques. École Polytechnique de Montréal 2013.
- [41] Government of Canada. Environment and natural resources, https://climate.weath.gc.ca/historical_data/search_historic_data_e.html; 2021 [accessed on 02 December 2021].
- [42] Saloux E, Candanedo JA. Control-oriented model of a solar community with seasonal thermal energy storage: development, calibration and validation. *J Build Perform Simul* 2019;12(5):523–45. <https://doi.org/10.1080/19401493.2018.1523950>.
- [43] Klein S, Beckman W, Mitchell J, Duffie J, Duffie N, Freeman T, et al. Trnsys 18—Volume 6 Multizone Building Modeling with Type 56 and Trnbuild. Solar Energy Laboratory, University of Wisconsin: Madison, WI, USA. 2017:199.
- [44] Meteotest. Meteotest: Irradiation data for every place on Earth, <http://www.meteotest.com/>; 2020.
- [45] DIN4108. Thermal protection and energy economy in buildings - Part 2: Minimum requirements to thermal insulation. Beuth, Berlin. 2013.
- [46] VDI. VDI 4640 Thermal Use of the Underground. VDI-Gesellschaft Energie und Umwelt (GEU), Berlin; 2010.
- [47] Nußbicker J, Mangold D, Heidemann W, Müller-Steinhagen H. *Bau und Betrieb des Erdsonden-Wärmespeichers in Neckarsulm-Amorbach*, 8. Geothermische Fachtagung & . 2004;5.
- [48] Yang L, Entchev E, Rosato A, Sibilio S. Smart thermal grid with integration of distributed and centralized solar energy systems. *Energy*. 2017;122:471–81. <https://doi.org/10.1016/j.energy.2017.01.114>.
- [49] Viessmann GmbH, <https://www.viessmann.de/de/gewerbe/waermepumpe/groswaermepumpen/vitocal-350-ht-pro.html>; 2020 [accessed on 02.12.2021].
- [50] Viessmann GmbH, <http://www.energas.co.za/wp-content/uploads/2019/02/A12-Heat-Pumps.pdf> 2020 [accessed on 22.02.2021].
- [51] Fritsche UR, Greß H-W. “Der nicht erneuerbare kumulierte Energieverbrauch und THG-Emissionen des deutschen Strommix im Jahr 2016 sowie Ausblicke auf 2020 bis 2050,“. Internationales Institut für Nachhaltigkeitsanalysen und-strategien GmbH (IINAS), Darmstadt. 2018.
- [52] IINAS. IINAS (2017): GEMIS - Globales Emissions-Modell Integrierter Systeme - model and database, version 4.95, in International Institute for Sustainability Analysis and Strategy, ed., Darmstadt. . 2017.
- [53] Short W, Packey DJ, Holt T. *A manual for the economic evaluation of energy efficiency and renewable energy technologies*. Golden, CO (United States): National Renewable Energy Lab; 1995.
- [54] Mauthner F, Herkel S. Technology and demonstrators-Technical Report Subtask C-Part C1: Classification and benchmarking of solar thermal systems in urban environments. Gleisdorf: IEA Solar Heating & Cooling Technology Collaboration Programme; 2016.
- [55] Hellstrom G. Ground heat storage: Thermal analyses of duct storage systems. I. Theory, PhD thesis, Lund University. 1992.
- [56] Bär K, Arndt D, Fritsche J-G, Götz AE, Kracht M, Hoppe A, et al. 3D-Modellierung der tiefeingetragenen Potenziale von Hesses-Eingangsdaten und Potenzialausweisung. *Zeitschrift der Deutschen Gesellschaft für Geowissenschaften* 2011;162(4):371–88.
- [57] LIPP GmbH, <https://www.lipp-system.de/tanks/thermal-storage-tanks>; 2019 [accessed on 02 December 2021].
- [58] Bauer D, Heidemann W, Müller-Steinhagen H. *Der Erdsonden-Wärmespeicher in Crailsheim*. Bad Staffelstein, Germany: Kloster Banz; 2007.
- [59] Viessmann GmbH, <https://www.viessmann.de/de/wohngebaude/gasheizng/vitocrossal.html>; 2020 [accessed on 02 December 2021].
- [60] Gallagher K, Sambridge M. Genetic algorithms: a powerful tool for large-scale nonlinear optimization problems. *Comput Geosci* 1994;20(7-8):1229–36. [https://doi.org/10.1016/0098-3004\(94\)90072-8](https://doi.org/10.1016/0098-3004(94)90072-8).

- [61] Kalogirou SA. Artificial neural networks in renewable energy systems applications: a review. *Renew Sustain Energy Rev* 2001;5(4):373–401. [https://doi.org/10.1016/S1364-0321\(01\)00006-5](https://doi.org/10.1016/S1364-0321(01)00006-5).
- [62] Jiang H, Xi Z, A. Rahman A, Zhang X. Prediction of output power with artificial neural network using extended datasets for Stirling engines. *Appl Energy* 2020; 271:115123. <https://doi.org/10.1016/j.apenergy.2020.115123>.
- [63] Moré JJ. *The Levenberg-Marquardt algorithm: implementation and theory*. Numerical analysis; Springer; 1978. p. 105–16.
- [64] Deb K, Pratap A, Agarwal S, Meyarivan T. A fast and elitist multiobjective genetic algorithm: NSGA-II. *IEEE Trans Evol Comput* 2002;6(2):182–97.
- [65] The MathWorks Inc., <https://www.mathworks.com/help/gads/gamultiobj.html>; 2021 [accessed on 02 December 2021].
- [66] KfW. Erneuerbare Energien – Premium, [https://www.kfw.de/inlandsfoerderung/Unternehmen/Energie-Umwelt/Finanzierungsangebote/Erneuerbare-Energien-Premium-\(271-281\)/#](https://www.kfw.de/inlandsfoerderung/Unternehmen/Energie-Umwelt/Finanzierungsangebote/Erneuerbare-Energien-Premium-(271-281)/#); 2021 [accessed on 02 December 2021].
- [67] Nuss P. *Life Cycle Assessment Handbook: A Guide for Environmentally Sustainable Products*; Curran, A.M., Ed.; John Wiley & Sons, Inc.: Hoboken, NJ, USA; Scrivener Publishing LLC: Salem, MA, USA. 2015.
- [68] Greening B, Azapagic A. Domestic heat pumps: Life cycle environmental impacts and potential implications for the UK. *Energy*. 2012;39(1):205–17. <https://doi.org/10.1016/j.energy.2012.01.028>.
- [69] Gebhardt M, Kohl H, Preisatlas ST. *Ableitung von Kostenfunktionen für Komponenten der rationellen Energienutzung*. Institut für Energie und Umwelttechnik eV (IUTA). Duisburg-Rheinhausen. 2002:1–356.
- [70] Luo J, Rohn J, Bayer M, Priess A. Thermal performance and economic evaluation of double U-tube borehole heat exchanger with three different borehole diameters. *Energy Build* 2013;67:217–24. <https://doi.org/10.1016/j.enbuild.2013.08.030>.
- [71] Croteau R, Gosselin L. Correlations for cost of ground-source heat pumps and for the effect of temperature on their performance. *Int J Energy Res* 2015;39(3):433–8.
- [72] Lizana J, Ortiz C, Soltero VM, Chacartegui R. District heating systems based on low-carbon energy technologies in Mediterranean areas. *Energy*. 2017;120: 397–416. <https://doi.org/10.1016/j.energy.2016.11.096>.
- [73] Statistisches Bundesamt. Preise–Daten zur Energiepreisentwicklung, https://www.destatis.de/DE/Themen/Wirtschaft/Preise/Publikationen/Energiepreise/energiepreisentwicklung-pdf-5619001.pdf?__blob=publicationFile; 2020 [accessed on 02 December 2021].
- [74] Schlesinger M, Hofer P, Kemmler A, Kirchner A, Koziel S, Ley A, et al. *Entwicklung der Energiemarkte–Energierferenzprognose: Studie im Auftrag des Bundesministeriums für Wirtschaft und Technologie*, <https://www.bmwi.de/Redaktion/DE/Publikationen/Studien/entwicklung-der-energiemaerkte-energiereferenzprognose-endorbericht.html>; 2014 [accessed on 02 December 2021].

Appendix G – Example model summaries

Chapter 7.1 example model – Brædstrup SDH system

| Model “MoSDH – Brædstrup validation” | | |
|---|-----------------------------|---|
| SolarThermalCollectorField newSolarField | | |
| Parameter | Value | Remarks |
| Aperture area | 10,637.8 m ² | 847 collectors in 70.58 rows of 12 (average) with 12.56 m ² each (Bava et al., 2015) |
| Collector row distance | 5.5 m | (Sørensen et al., 2013) |
| Efficiency data | datasheet | Type ARCON-SUNMARK HT-SA 28/8 |
| Heat carrier medium | Glycol 34/64 | (Sørensen et al., 2013) |
| SolarThermalCollectorField oldSolarField | | |
| Parameter | Value | Remarks |
| Aperture area | 8000.7 m ² | 637 collectors in 91 rows of 7 (average) with 12.56 m ² each (Bava et al., 2015) |
| Collector row distance | 5.5 m | (Sørensen et al., 2013) |
| Efficiency data | datasheet | Type ARCON-SUNMARK HT-SA 28/8 |
| Heat carrier medium | Glycol 34/64 | (Sørensen et al., 2013) |
| DistrictHeatingPipes newFiledLine | | |
| Parameter | Value | Remarks |
| Dimensions | DN200/355 | PI diagram & (isoplus, 2020) |
| Length | 650 m | Estimated with satellite image |
| DistrictHeatingPipes oldFiledLine | | |
| Parameter | Value | Remarks |
| Dimensions | DN200/355 | PI diagram & (isoplus, 2020) |
| Length | 160 m | Estimated with satellite image |
| GasBoiler gasBoiler | | |
| Parameter | Value | Remarks |
| Thermal power | 13.5 MW | (Jensen et al., 2016) |
| Rated efficiency | 104% | (Jensen et al., 2016) |
| CHP chp | | |
| Parameter | Value | Remarks |
| Thermal power | 2 x 4.1 MW _{th} | (Jensen et al., 2016) |
| Fuel efficiency | 89% | (Jensen et al., 2016) |
| Power to heat ratio | 0.89 | (Jensen et al., 2016) |
| ElectricHeatingRod electricBoiler | | |
| Parameter | Value | Remarks |
| Thermal power | 10 MW _{th} | (Jensen et al., 2016) |
| Efficiency | 99% | Assumed |
| HeatPump heatPump | | |
| Parameter | Value | Remarks |
| Thermal power & COP | monitoring | see Chapter 7.1 |
| BTES btes | | |
| Parameter | Value | Remarks |
| Boreholes | 48 x 45 m | (Sørensen et al., 2013) |
| BHEs | 6 x 2U serially | DN32; grout thermal conductivity of 1.44 W/m/K after (Sørensen et al., 2013) |
| Ground thermal conductivity | 1.72 W/(m.K) | Effective value after (Tordrup et al., 2017) |
| Ground thermal capacity | 1.96 MJ/(m ³ .K) | Effective value after (Tordrup et al., 2017) |

| TTES hotBuffer | | |
|-----------------------------------|----------------------|---|
| Parameter | Value | Remarks |
| Volume | 5,500 m ³ | (Sørensen et al., 2013) |
| Height | 17.5 m | Calculated with diameter from satellite image |
| TTES coldBuffer | | |
| Parameter | Value | Remarks |
| Volume | 2,000 m ³ | PI diagram |
| Height | 15 m | Calculated with diameter from satellite image |
| DistrictHeatingTwinPipes btesLine | | |
| Parameter | Value | Remarks |
| Dimensions | DN100 | PI diagram & (isoplus, 2020) |
| Length | 600 m | (Sørensen et al., 2013) |

Chapter 6.4 7.1 example model – BHE design and operation optimization

| Model "MoSDH – exergetic optimization" | | |
|--|------------------|---|
| BTES btes | | |
| Parameter | Value | Remarks |
| Layout | hexagonal | |
| Number of BHEs | 19 | |
| BHE length | 750 m | |
| Depth of BHE heads | 5 m | |
| BHE spacing | 5 m | |
| Location | 2 layers | Average temperature: 10 °C; Geothermal gradient: 0.003 K/m |
| Layer 1 | Top 50 m | lamda= 1.5 W/(m.K), rho=2500 kg/m ³ , cp=800 J/(kg K) |
| Layer 2 | Below 50 m | lamda= 2.65 W/(m.K), rho=2500 kg/m ³ , cp=800 J/(kg K) |
| Borehole heat exchanger | coaxial | Outer pipe:: Inner pipe: |
| Steel casing | 6 5/8" x 7.35 mm | Thermal conductivity steel: 54 W/(m.K) |
| Steel tubing | 4 1/2" x 5.7 mm | Thermal conductivity steel: 54 W/(m.K); TC PP: 0.23 W/(m.K) |
| Grout upper section | 0.5 W/(m.K) | Borehole diameter: 270 mm |
| Grout lower section | 1.5 W/(m.K) | Borehole diameter: 216 mm |